

Characterization of Pyrolysis Products from Fast Pyrolysis of Live
and Dead Vegetation

Mohammad Saeed Safdari

A dissertation submitted to the faculty of
Brigham Young University
in partial fulfillment of the requirements for the degree of

Doctor of Philosophy

Thomas H. Fletcher, Chair
Morris D. Argyle
John N. Harb
John D. Hedengren
David O. Lignell

Department of Chemical Engineering
Brigham Young University

Copyright © 2018 Mohammad Saeed Safdari

All Rights Reserved

ABSTRACT

Characterization of Pyrolysis Products from Fast Pyrolysis Products of Live and Dead Vegetation

Mohammad Saeed Safdari
Department of Chemical Engineering, BYU
Doctor of Philosophy

Wildland fire, which includes both planned (prescribed fire) and unplanned (wildfire) fires, is an important component of many ecosystems. Prescribed burning (controlled burning) is used as an effective tool in managing a variety of ecosystems in the United States to reduce accumulation of hazardous fuels, manage wildlife habitats, mimic natural fire occurrence, manage traditional native foods, and provide other ecological and societal benefits. During wildland fires, both live and dead (biomass) plants undergo a two-step thermal degradation process (pyrolysis and combustion) when exposed to high temperatures. Pyrolysis is the thermal decomposition of organic material, which does not require the presence of oxygen. Pyrolysis products may later react with oxygen at high temperatures, and form flames in the presence of an ignition source. In order to improve prescribed fire application, accomplish desired fire effects, and limit potential runaway fires, an improved understanding of the fundamental processes related to the pyrolysis and ignition of heterogeneous fuel beds of live and dead plants is needed.

In this research, fast pyrolysis of 14 plant species native to the forests of the southern United States has been studied using a flat-flame burner (FFB) apparatus. The results of fast pyrolysis experiments were then compared to the results of slow pyrolysis experiments. The plant species were selected, which represent a range of common plants in the region where the prescribed burning has been performed. The fast pyrolysis experiments were performed on both live and dead (biomass) plants using three heating modes: (1) convection-only, where the FFB apparatus was operated at a high heating rate of $180\text{ }^{\circ}\text{C s}^{-1}$ (convective heat flux of 100 kW m^{-2}) and a maximum fuel surface temperature of $750\text{ }^{\circ}\text{C}$; (2) radiation-only, where the plants were pyrolyzed under a moderate heating rate of $4\text{ }^{\circ}\text{C s}^{-1}$ (radiative heat flux of 50 kW m^{-2}), and (3) a combination of radiation and convection, where the plants were exposed to both convective and radiative heat transfer mechanisms. During the experiments, pyrolysis products were collected and analyzed using a gas chromatograph equipped with a mass spectrometer (GC-MS) for the analysis of tars and a gas chromatograph equipped with a thermal conductivity detector (GC-TCD) for the analysis of light gases.

The results showed that pyrolysis temperature, heating rate, and fuel type, have significant impacts on the yields and the compositions of pyrolysis products. These experiments were part of a large project to determine heat release rates and model reactions that occur during slow and fast pyrolysis of live and dead vegetation. Understanding the reactions that occur during pyrolysis then can be used to develop more accurate models, improve the prediction of the conditions of prescribed burning, and improve the prediction of fire propagation.

Keywords: fast pyrolysis, slow pyrolysis, live vegetation, biomass, light gas, tar, char, convection, radiation, heat transfer, pyrolysis temperature, heating rate, fuel type

ACKNOWLEDGEMENTS

I would like to give my appreciation to all of those who have been influential in helping me with this dissertation. First, my advisor, Dr. Thomas H. Fletcher, for all of his support intellectually, technically, financially, and for guiding me with patience to complete this project. I would like to express my appreciation for my committee members, Dr. Hedengren, Dr. Lignell, Dr. Argyle, and Dr. Harb, for their advice and encouragement during this project.

I also express my appreciation to the U.S. Forest Service, especially Dr. David Weise for the technical and financial support. I want to thank the undergraduate students, Joel E. Howarth and Jansen P. Berryhill for helping me during the experiments and data analysis. I would like to thank Dr. Mark Dietenberger, Dr. Milton Lee, Dr. Xiaofeng Xie, Kevin Cole, and Nick Hawkins for providing precious advice and materials to construct the setup as well as their technical support.

Finally, I would also like to thank the most important thing in my life, my family, especially my parents, for the way they raised me, stood by me, and encouraged me to pursue my dreams.

This research was supported by DOD/EPA/DOE Strategic Environmental Research and Development Program, Project RC-2640, funded through contract 16-JV-11272167-024, administered by the USDA Forest Service PSW Research Station.

TABLE OF CONTENTS

List of Tables	vi
List of Figures	viii
1 Introduction	1
2 Literature Review	5
2.1 Plant Structure	5
2.2 Pyrolysis of Biomass	8
2.3 Characterization of Pyrolysis Products	12
2.3.1 Effects of Temperature and Heating Rate on Product Yields	12
2.3.2 Tar Analysis	14
2.3.3 Light Gas Analysis	17
2.4 Differences between Live and Dead Plants	18
2.5 Heat Transfer Mechanisms in Wildland Fires	21
2.6 Summary of Literature Review	24
3 Objective and Tasks	26
3.1 Objective	26
3.2 Tasks	26
4 Description of Experiments	29
4.1 Plants Tested	29
4.2 Proximate and Ultimate Analysis	29
4.3 Physical Measurement	33
4.4 Experimental Setup and Procedure	35
4.4.1 Flat-Flame Burner (FFB) Apparatus	35
4.4.2 Pyrolyzer Apparatus	43
4.5 Statistical Analysis	44
5 Fast Pyrolysis of Plants by Convective Heat Transfer	45
5.1 Pyrolysis Product Yields	45
5.2 Light Gas Analysis	49
5.3 Tar Analysis	52
5.4 Distribution of Functional Groups in Tar	60
5.5 Mass Loss over Time	62
5.6 Fuel Surface Temperature	63
5.7 Summary and Conclusions	63
6 Comparison of Slow and Fast Pyrolysis of Live and Dead Vegetation	68

6.1	Pyrolysis Product Yields	68
6.2	Light Gas Analysis	75
6.3	Tar Analysis	83
6.4	Summary and Conclusions.....	89
7	The Effect of Heating Mode on Distribution of Pyrolysis Products	91
7.1	Fuel Surface Temperature	92
7.2	Pyrolysis Product Yields	94
7.3	Light Gas Analysis	98
7.4	Tar Analysis	106
7.5	Summary and Conclusions.....	113
8	Summary and Conclusions	117
8.1	Pyrolysis Product Yield.....	117
8.2	Light Gas Analysis	118
8.3	Tar Analysis	119
8.4	Recommended Future Work	119
	References.....	121
	Appendix A. Plants Tested	136
	Appendix B. Temperature Correction for Radiation Losses	142
	Appendix C. Calculations of Mass Flow rates and Gas Velocity.....	145
	Appendix D. Identified Tar Compounds	149
	Appendix E. Mass Loss vs. time.....	157
	Appendix F. Results of Slow and Fast Pyrolysis Experiments.....	161
	Appendix G. Results of Different Heating Modes.....	165

LIST OF TABLES

Table 4-1. List of plants used in pyrolysis experiments	30
Table 4-2. Proximate and ultimate analysis of plant species	32
Table 4-3. Physical measurements of samples	34
Table 5-1. Summary of pyrolysis product yields for convection-only experiments.....	47
Table 5-2. Summary of light gas analysis for convection-only experiments	52
Table 6-1. Pyrolysis product yields of live and dead plant species	70
Table 6-2. Summary of pyrolysis product yields for slow and fast pyrolysis experiments.....	73
Table 6-3. Light gas analysis from pyrolysis of live and dead samples	81
Table 6-4. Summary of light gas analysis for slow and fast pyrolysis experiments.....	82
Table 7-1. Operating temperature and heat flux in the experiments.....	92
Table 7-2. Summary of pyrolysis product yields for three heating modes	98
Table 7-3. Summary of light gas analysis for three heating modes.....	105
Table A-1. List of plants used in pyrolysis experiments	138
Table C-1. Mass flow rates of the reactant entered the burner	146
Table D-1. Identified tar compounds using GC-MS in high heating rate pyrolysis	149
Table D-2. Identified tar compounds using GC-MS in slow heating rate pyrolysis.....	155

LIST OF FIGURES

Figure 1-1. Prescribed burning of the forests of the southern U.S.	2
Figure 2-1. Plant structure.....	6
Figure 2-2. Structure of lignocellulosic biomass	9
Figure 2-3. Mechanism of primary and secondary pyrolysis of biomass	11
Figure 2-4. Tar classification	15
Figure 2-5. Lignin decomposition mechanism and formation of tar compounds.....	16
Figure 2-6. Heat transfer mechanisms in wildland fires	22
Figure 4-1. Proximate analysis of plants.....	31
Figure 4-2. Leaf length and width measurements.....	33
Figure 4-3. Flat-flame burner apparatus	36
Figure 4-4. The flat-flame burner apparatus with flame and pyrolyzing sample	39
Figure 4-5. Schematic of the FFB.....	42
Figure 4-6. Pyrolyzer apparatus.....	43
Figure 5-1. Product yields of live plant species	46
Figure 5-2. Product yields of dead plant species	46
Figure 5-3. Light gas analysis for live plant species.....	51
Figure 5-4. Light gas analysis for dead plant species	51
Figure 5-5. GC-MS chromatogram of tar from fast pyrolysis of live inkberry	53
Figure 5-6. Analysis of tar compounds for convection-only experiments.....	57
Figure 5-7. Mechanisms of PAH precursor formation from lignin decomposition.....	59
Figure 5-8. Mechanism of formation of naphthalene from benzene	59
Figure 5-9. Distribution of functional groups in tar for live and dead plants	61
Figure 5-10. Mass loss over time during fast pyrolysis of live and dead inkberry.....	62
Figure 5-11. Fuel surface temperature over time for convection-only experiments.....	64
Figure 6-1. Gas yield of live plant species.....	69
Figure 6-2. Tar yield of live plant species	71
Figure 6-3. Char yield of live plant species	72
Figure 6-4. Pyrolysis product yields from pyrolysis of longleaf pine litter.....	75
Figure 6-5. The yield of CO wt% obtained from pyrolysis of live plant species	76

Figure 6-6. The yield of CO ₂ wt% obtained from pyrolysis of live plant species	78
Figure 6-7. The yield of CH ₄ wt% obtained from pyrolysis of live plant species	79
Figure 6-8. The yield of H ₂ wt% obtained from pyrolysis of live plant species.....	80
Figure 6-9. GC-MS chromatogram of tar from slow pyrolysis of live longleaf pine	84
Figure 6-10. GC-MS chromatogram of tar from fast pyrolysis of live longleaf pine.....	84
Figure 6-11. Distribution of tar compounds for the slow pyrolysis of longleaf pine	85
Figure 6-12. Distribution of tar compounds for the fast pyrolysis of longleaf pine	85
Figure 6-13. Mole% of phenol in tar during pyrolysis of live plant species	87
Figure 6-14. Mole% of 1,2-benzenediol in tar during pyrolysis of live plant species.....	88
Figure 6-15. Mole% of 4-methyl phenol in tar during pyrolysis of live plant species	88
Figure 7-1. Fuel surface temperature changes over time for the radiation-only experiments	93
Figure 7-2. Fuel surface temperature changes over time for the combined mode.....	93
Figure 7-3. Gas yield of live plant species.....	95
Figure 7-4. Tar yield of live plant species	96
Figure 7-5. Char yield of live plant species	97
Figure 7-6. The yield of CO wt% from pyrolysis of live plant species	100
Figure 7-7. The yield of CO ₂ wt% from pyrolysis of live plant species.....	100
Figure 7-8. The yield of CH ₄ wt% rom pyrolysis of live plant species	102
Figure 7-9. The yield of H ₂ wt% from pyrolysis of live plant species	102
Figure 7-10. Distribution of pyrolysis products from pyrolysis of live longleaf pine	104
Figure 7-11. Analysis of tar compounds from longleaf pine in the radiation-only mode	107
Figure 7-12. Analysis of tar compounds from longleaf pine in the convection-only mode	108
Figure 7-13. Analysis of tar compounds from longleaf pine in the combined mode	109
Figure 7-14. Distribution of functional groups in tar for pyrolysis of live longleaf pine	110
Figure 7-15. Mole% of phenol in tar during pyrolysis of live plant species	112
Figure 7-16. Mole% of 1,2-benzenediol in tar during pyrolysis of live plant species.....	113
Figure B-1. Schematic of the flat-flame burner and the location of radiation.....	144
Figure C-1. Schematic of gas flow direction in the flat-flame burner apparatus.....	145
Figure E-1. Mass loss over time for live plant species in the convection-only experiments.....	158
Figure E-2. Mass loss over time for live plant species in the combined mode.....	160
Figure F-1. Gas yield of dead plant species	161

Figure F-2. Tar yield of live plant species	162
Figure F-3. Char yield of dead plant species	162
Figure F-4. The yield of CO wt% obtained from pyrolysis of dead plant species	163
Figure F-5. The yield of CO ₂ wt% obtained from pyrolysis of dead plant species	163
Figure F-6. The yield of CH ₄ wt% obtained from pyrolysis of dead plant species	164
Figure F-7. The yield of H ₂ wt% obtained from pyrolysis of dead plant species.....	164
Figure G-1. Gas yield of dead plant species	165
Figure G-2. Tar yield of dead plant species.....	166
Figure G-3. Char yield of dead plant species.....	166
Figure G-4. The yield of CO wt% from pyrolysis of dead plant species.....	167
Figure G-5. The yield of CO ₂ wt% from pyrolysis of dead plant species	167
Figure G-6. The yield of CH ₄ wt% from pyrolysis of dead plant species	168
Figure G-7. The yield of H ₂ wt% from pyrolysis of dead plant species.....	168
Figure G-8. Analysis of tar compounds for radiation-only experiments	172
Figure G-9. Analysis of tar compounds for the combined mode.....	176

1 INTRODUCTION

Wildland fire, which includes both planned (prescribed fire) and unplanned (wildfire) fires, is an important component of many ecosystems. Wildland fires often occur in highly dense live fuel forests, burn live and dead plants, and have significant ecological and economic impacts (McAllister et al., 2012). In 2000, an estimated 3.5 million km² of forest land were burned by wildland fires worldwide (Tansey et al., 2004).

Prescribed burning (controlled burning) is one way to remove smaller plants in order to decrease the accumulation of combustible materials and reduce the impact of uncontrolled wildland fires (Ferguson et al., 2013). Land managers use prescribed fire to manage a variety of ecosystems in the United States to reduce the accumulation of hazardous fuels, manage wildlife habitats, and protect ecological forests and infrastructures (Hartman, 2005). In 2014 in the United States, an estimated 9 million acres of forest land were treated with prescribed fire; in the southern U.S., 6 million acres of forest land were treated (Melvin, 2015). Prescribed fires (as shown in Figure 1-1) are often used to burn undergrowth in the forests of the southern United States.

During wildland fires, both live and dead (biomass) plants undergo a two-step thermal degradation process (pyrolysis and combustion) when exposed to high temperatures (Biagini and Tognotti, 2014). In order to improve prescribed fire application, accomplish desired fire effects, and limit potential runaway fires, an improved understanding of the fundamental processes related to pyrolysis and ignition of heterogeneous fuel beds of live and dead plants is needed.

Determining whether or not to initiate prescribed fires depends on several factors such as heat transfer mechanisms, distribution of the plants in the area, and environmental conditions (e.g. relative humidity, wind speed, air temperature, etc.).



Figure 1-1. Prescribed burning of the forests of the southern U.S.¹ (Safdari et al., 2018b)

This research helps to improve the understanding of the fundamental processes related to pyrolysis in heterogeneous fuel beds of live and dead plants. Pyrolysis is the thermal decomposition process of organic material, such as coal, wood, paper, and plants. Pyrolysis occurs following the evaporation of moisture in the burning of fuels without requiring the presence of oxygen. As volatiles leave the surface of the solid fuel, the mass transfer pushes the surrounding gas (presumably air) out of the way, creating a fuel-rich zone near the surface or in the interior of a flame. Pyrolysis products may later react with O₂ at high temperatures, and form

¹ This picture was taken by David R. Weise (USDA Forest Service) at Ft. Jackson in 2011.

flames in the presence of an ignition source. For example, by increasing temperature, lignocellulosic materials start to pyrolyze, releasing gaseous products which react with oxygen and may result in a flame (Safdari et al., 2018b).

This project was completed by the collaboration of 12 governmental and academic organizations. Analysis of the pyrolysis products of 14 live and dead plant species was performed at three scales: (1) bench-scale measurements at Brigham Young University (BYU) and the Forest Products Laboratory (FPL); (2) laboratory burn-scale in a wind tunnel at Riverside Fire Laboratory (RFL); and (3) small field-scale burns (100 m²) at Fort Jackson in South Carolina using intact fuels from living plants.

During this research, the fast pyrolysis of 14 plant species native to the forests of the southern United States was studied using a flat-flame burner (FFB) apparatus. The FFB apparatus enabled fast pyrolysis experiments at high heating rates and high temperatures to imitate pyrolysis during typical wildland fires. The fast pyrolysis experiments were operated under three heating modes. The heating modes were: (1) convection-only, where the FFB apparatus was operated at a high heating rate of 180 °C s⁻¹ (convective heat flux of 100 kW m⁻²) and a maximum fuel surface temperature of 750 °C; (2) radiation-only, where the plants were pyrolyzed under a moderate heating rate of 4 °C s⁻¹ (radiative heat flux of 50 kW m⁻²) and a maximum fuel surface temperature of 550 °C; and (3) a combination of radiation and convection, where the plants were pyrolyzed at a heating rate of 195 °C s⁻¹ under a combination of convective and radiative heat transfer mechanisms. These heat fluxes were selected to imitate pyrolysis of live and dead plants under the radiant and convective heat fluxes of approximately 100 kW m⁻² typical of wildland brush fires (Frankman et al., 2012). During the experiments, the yields and the compositions of pyrolysis products were studied using a gas chromatograph equipped with a mass spectrometer

(GC-MS) for the analysis of tars, and a gas chromatograph equipped with a thermal conductivity detector (GC-TCD) for the analysis of light gases (non-condensable gases).

The results from this research are being used by other members of the team (Weise et al., 2018) to determine the heat release rates and model reactions that occur during slow and fast pyrolysis of live and dead vegetation. Understanding the reactions that occur during pyrolysis then can be used to develop more accurate combustion and fire spread models to predict the best conditions to properly perform prescribed burning, predict fire propagation, and limit fire runaway.

This dissertation includes: first, a literature review which discusses plant structure, pyrolysis of biomass, characterization of pyrolysis products, differences between live and dead plants, and heat transfer mechanisms in wildland fires (Chapter 2). Following the literature review, the objective and tasks of the project are described (Chapter 3). Next, the description of the experiments is explained (Chapter 4). Then the results and discussions of slow and fast pyrolysis experiments are presented (Chapters 5-7). Finally, the summary and conclusions of the project are explained (Chapter 8).

2 LITERATURE REVIEW

This literature review is classified into five main sections: (1) plant structure; (2) pyrolysis of biomass; (3) characterization of pyrolysis products; (4) differences between live and dead plants; and (5) heat transfer mechanisms in wildland fires.

2.1 Plant Structure

To better understand the pyrolysis of plants, a review of plant cellular structure on a microscopic scale is required. The plant cell wall (as shown in Figure 2-1) has a complex and dynamic structure comprised of polysaccharides and other polymers around the membrane of the plant cell. The plant cell wall provides rigidity but also flexibility to the plant cell and is vital to the growth, development, and protection of the plant (Turumtay, 2015). Cell wall morphology and composition vary greatly with plant species. The plant cell wall includes both the primary and secondary cell walls. The primary cell wall consists of three polysaccharides (cellulose, hemicellulose, and pectin) and some proteins. Middle lamella, which contains pectin and proteins, connects the adjacent cell walls together. Secondary cell walls develop after the cell has stopped growing and provide additional strength to support the plant (Cosgrove, 1997; Alonso et al., 2012). Secondary cell walls consist of cellulose, hemicelluloses, and lignin (Cosgrove, 2005). The composition of cell walls varies between species and depends on the plant characteristics (Bradbury et al., 1979).

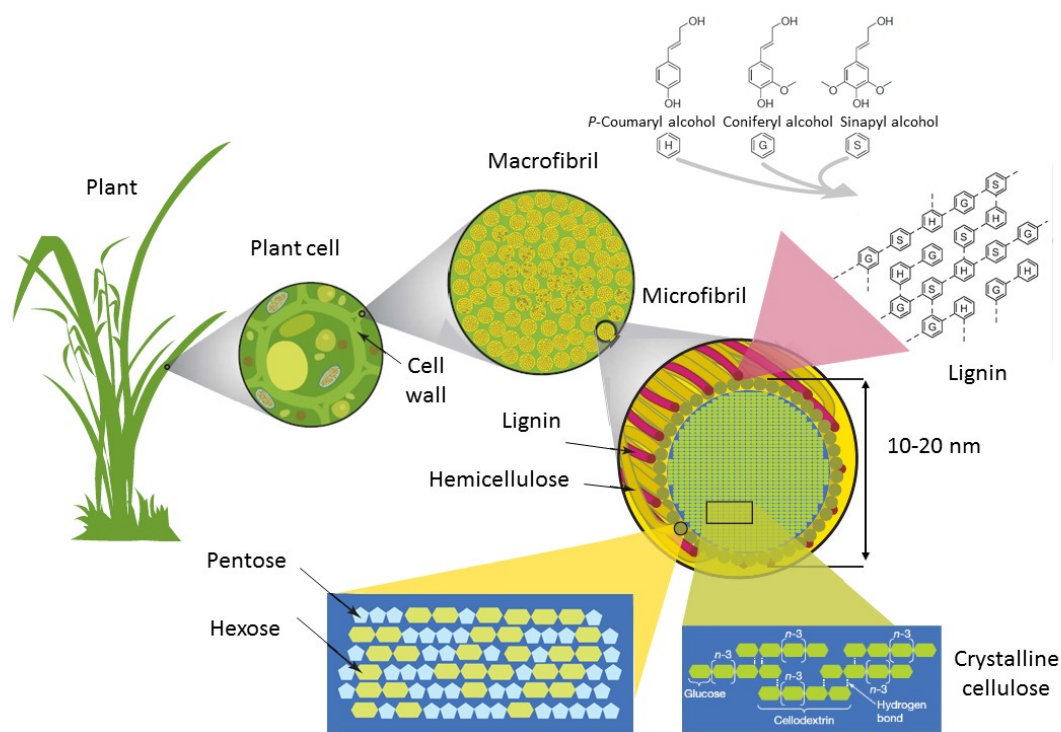


Figure 2-1. Plant structure (Rubin, 2008)

Cellulose, hemicellulose, and lignin normally comprise 90% of the dry ash-free weight of a dead plant (i.e., biomass). Extractives account for almost 10% of the entire biomass weight (Bradbury et al., 1979; Debiagi et al., 2015). Cellulose is a high molecular weight linear polymer which consists of β -1, 4-coupled glucose molecules that are non-covalently linked by hydrogen bonds into microfibrils (Turumtay, 2015). Glucose molecules bind to each other and form a crystalline structure. Crystalline domains then connect together and form an amorphous region that supports the cell wall by enhancing chemical stability, resistance to hydrolysis, strength against osmotic pressure, and water insolubility (Cosgrove, 1997).

In contrast with cellulose, hemicellulose is a lower molecular weight branched polymer which bridges cellulose fibers. Hemicellulose, in combination with cellulose, provides support for the plant by forming a strong but flexible network located in a matrix composed of pectin.

Hemicellulose structure consists of different types of hexoses or pentoses. These polysaccharides are delivered to the cell membrane via vesicles after being made in the Golgi apparatus. Once the vesicles reach the membrane, the hemicellulose can combine with the cell wall (Rubin, 2008; Turumtay, 2015).

Lignin is an aromatic polymer that is a product of polymerization of hydroxycinnamyl alcohol monomers with three degrees of methoxylation: *p*-coumaryl, coniferyl, and sinapyl alcohols. When these monomers undergo polymerization, they are called *p*-hydroxyphenyl (H), guaiacyl (G), and syringyl (S) units, respectively (Elder, 2010). Lignin is responsible for the structural integrity of the secondary cell wall and the protection of the plant against pathogens (Cesarino et al., 2012). Lignin's hydrophobic nature enhances the impermeability of the cell wall and supports water and nutrient transport through the vascular system over longer distances (Boerjan et al., 2003).

Pectin regulates intercellular adhesion, which is integral in various processes such as growth, development, defense, seed hydration, leaf shedding, and fruit development. Pectin is synthesized through the use of at least 67 enzymes in the Golgi apparatus, delivered to the cell membrane in the same manner via small vesicles, and then released to the apoplast (Mohnen, 2008). The majority of pectin polysaccharides are located in the middle lamella and primary cell wall, with a small amount found in the secondary cell wall. Even though pectin is not found in abundance in the secondary cell wall, it still plays an important part in its structure (Xiao and Anderson, 2013).

Extractives include thousands of non-structural materials within plants that have huge varieties in composition, structure, and biological function. Extractives include organic and inorganic compounds such as resins, sugars, fatty acids, proteins, terpenes, and tannins that can

be extracted by polar and non-polar solvents (Thammasouk et al., 1997; Biagini and Tognotti, 2014; Debiagi et al., 2015). Extractives can be distributed in different ways throughout the framework of the plant, and they are found most abundantly in leaves and barks. (Debiagi et al., 2015). Lipophilic extractive compounds are soluble in non-polar solvents like hexane, and hydrophilic extractive compounds are soluble in polar solvents like water or ethanol (Thammasouk et al., 1997). The presence of extractives in a sample of biomass increases its heating value, enhances the decomposition of lignin, influences the products of pyrolysis, and catalyzes the formation of acidic compounds (Guo et al., 2010).

Although the structures of live and dead plants are similar, there are some differences in their characteristics, which may lead to different compositions of their pyrolysis products. For example, live plants, in addition to lignocellulosic materials, contain significant fractions of proteins, starches, sugars, and lipids (Fourty et al., 1996; Jolly et al., 2014; Jolly and Butler, 2015; Jolly and Johnson, 2018).

2.2 Pyrolysis of Biomass

Pyrolysis of live plants has not been extensively studied. However, pyrolysis of biomass (dead and dried plants) and wood as a promising technology for bio-char, bio-oil, and bio-gas production has been explored in detail during the past few decades (Bradbury et al., 1979; DiBlasi, 1994; Diebold, 1994; Rao and Sharma, 1998; Putun et al., 2007). Recently, the use of a renewable, affordable, and prevalent energy resource such as biomass has attracted attention due to the fact that biomass conversion has low environmental impact since it does not contribute as extensively to CO₂ emissions and helps meet the rising demand for energy in the world (Xiao and Yang, 2013; Aysu and Kucuk, 2014).

Biomass can be derived from biological sources such as wood, agricultural and forest residue, and industrial and municipal solid wastes (Aysu and Kucuk, 2014). Biomass is composed of a mixture of carbon and other organic molecules containing oxygen, hydrogen, nitrogen, and small quantities of other elements such as alkali, alkaline earth, and heavy metals (Shen et al., 2016). Cellulose, hemicellulose, lignin, and extractives generally comprise about 40-50, 25-30, 15-25, and 5-10 wt% of biomass on a dry ash-free basis, respectively. However, the weight fractions may change slightly based on the characteristics of the biomass (Bradbury et al., 1979). The structure of these biomass constituents is shown in Figure 2-2.

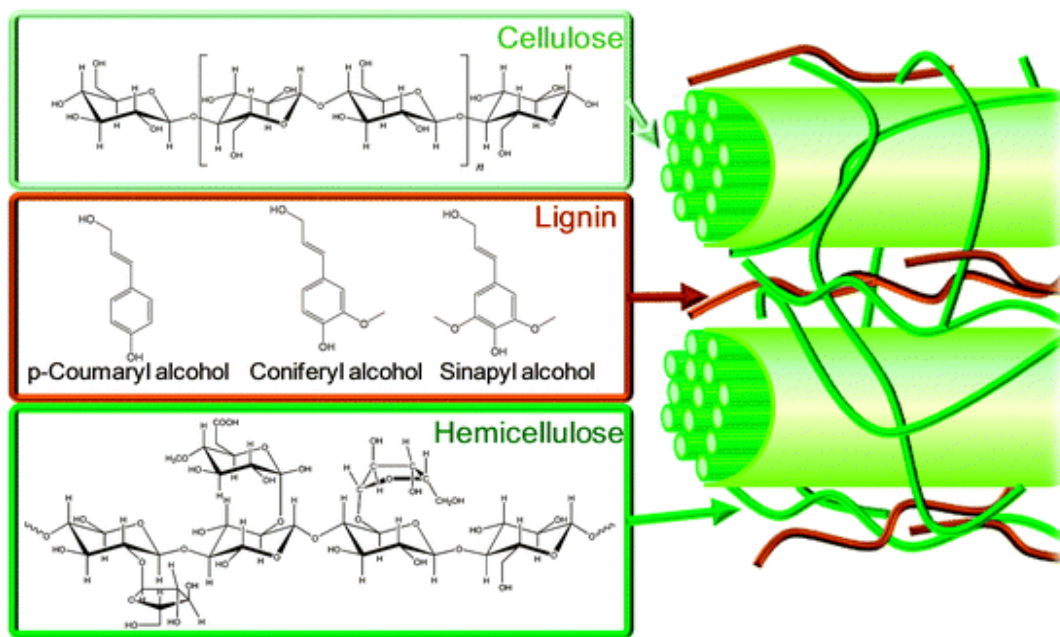


Figure 2-2. Structure of lignocellulosic biomass (Alonso et al., 2012)

The chemical composition of biomass (fractions of cellulose, hemicellulose, lignin, and extractives) can be determined using traditional methods, such as leaching with hot water and/or acid solvents for extractives, and sequential basic and acid washing for cellulose, hemicellulose

and lignin. However, these methods are not standardized, are not reproducible, and lack reliable accuracy. The fraction of extractives is often ignored or is reported as a fraction of cellulose or hemicellulose (Biagini and Tognotti, 2014).

Biomass pyrolysis consists of three main steps: hemicellulose decomposition, cellulose decomposition, and lignin decomposition (Yang et al., 2007). It has been suggested that the general pyrolysis of biomass is directly related to the independent kinetics of biomass components (Biagini and Tognotti, 2014). Based on this assumption, the devolatilization of lignocellulosic materials consists of a set of parallel reactions. These components react independently and may not have an impact on each other (Lewis and Fletcher, 2013; Biagini and Tognotti, 2014). However, other researchers have stipulated that biomass constituents have interactions throughout the pyrolysis process (Manya et al., 2003; Zhou et al., 2014a).

During thermal decomposition of a plant, the cell structure breaks down to its constituents. The devolatilization behavior of the biomass constituents depends on their molecular structures as well as their chemical compositions. The temperature range of pyrolysis for hemicellulose, cellulose, and lignin is 180-240, 230-310, and 300-500 °C, respectively, depending on the heating rate (Collard and Blin, 2014). At temperatures lower than 180 °C, biomass is primarily stable and pyrolysis does not occur (Xiao and Yang, 2013). Pyrolysis can be classified into three groups based on pyrolysis temperature and heating rate: (1) conventional or slow pyrolysis which is performed with a slow heating rate ($0.1-1 \text{ }^\circ\text{C s}^{-1}$), low temperature (300-400 °C), and long gas and solid residence time (more than 30 min); (2) fast pyrolysis which is operated with a fast heating rate ($1-100 \text{ }^\circ\text{C s}^{-1}$), high temperature (500-900 °C), and short gas and solid residence time (10-20 s); and (3) flash pyrolysis which is operated under a very high heating rate (more than $1000 \text{ }^\circ\text{C s}^{-1}$) and very short residence time (1 s) (Aysu and Kucuk, 2014; Liu et al., 2017).

Pyrolysis of biomass (as shown in Figure 2-3), which occurs after moisture removal, consists of two sequential steps: (1) primary pyrolysis (release of volatile compounds); and (2) secondary pyrolysis (where primary pyrolysis products undergo secondary reactions).

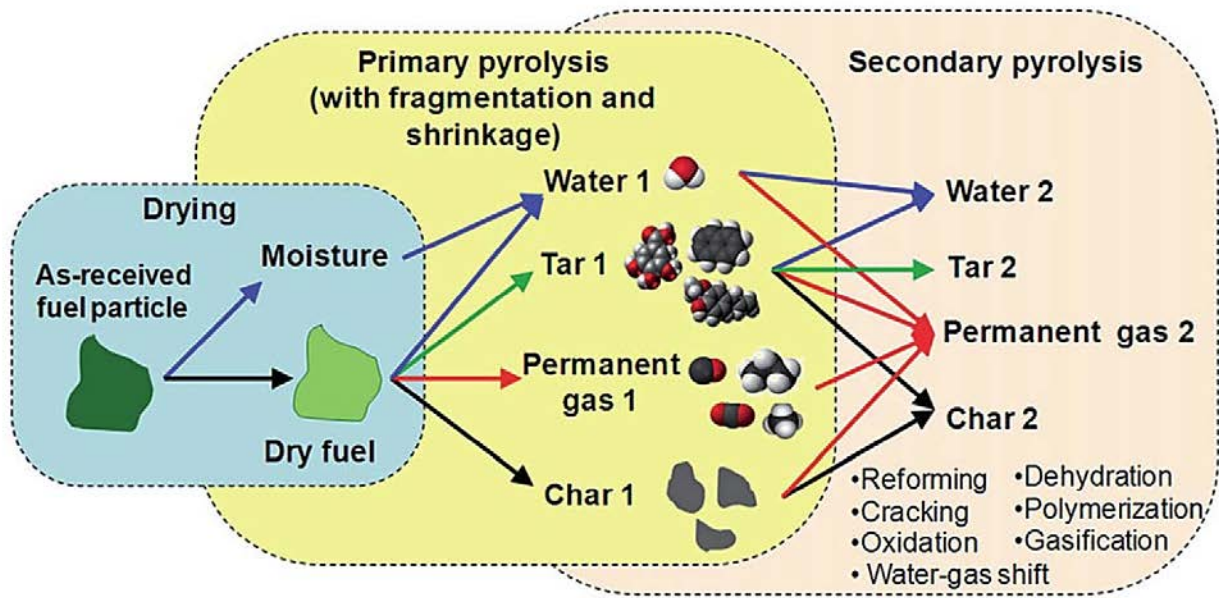


Figure 2-3. Mechanism of primary and secondary pyrolysis of biomass (Shen et al., 2016)

As the plant material is exposed to high temperature, first moisture content decreases, then during the primary reactions, the plant constituents (i.e., hemicellulose, cellulose, lignin, etc.) break down and form primary pyrolysis products. The primary pyrolysis products of biomass are light gases (e.g., CO, CO₂, H₂O, and H₂), light hydrocarbons (e.g., CH₄, C₂H₄), condensable gases (tars), solid residue (char), and mineral ash (see Equation (2-1)) (Gomez-Barea and Leckner, 2010).



The primary pyrolysis of biomass is complete at relatively low temperatures (<500 °C) (Neves et al., 2011; Shen et al., 2016). If the primary products undergo further reactions at higher temperatures and heating rates, or longer residence time, secondary pyrolysis occurs (Shen et al., 2017). Secondary pyrolysis includes processes such as cracking, polymerization, condensation, and carbon deposition, which can occur either homogeneously (when reactions occur in the gas phase), or heterogeneously (when the reactions occur at the surface of a solid fuel or char particle) (Collard and Blin, 2014).

Secondary pyrolysis is not as widely studied as primary pyrolysis. However, secondary reactions can have significant effects on the yields and the compositions of pyrolysis products. For example, during secondary pyrolysis, the tar compounds heat up in the flame and either decompose to lighter gases or polymerize to form soot. The orange color of flames is due to the radiation from the tiny soot particles in the fuel-rich part of the flame (DiBlasi, 1994). The secondary reactions include: (1) reactions between liquid/gaseous products and char; (2) reactions between tar compounds; (3) reactions between gases; and (4) reactions between tar compounds and gases.

2.3 Characterization of Pyrolysis Products

2.3.1 Effects of Temperature and Heating Rate on Product Yields

Pyrolysis temperature, heating rate, fuel type, reactor type, sweep gas flow rate, and fuel residence time in the reactor have been shown to have important impacts on the yields and the compositions of pyrolysis products of biomass (Aysu and Kucuk, 2014; Gao et al., 2015; Oudenhoven et al., 2015).

Lin et al. (2016) has reported that by increasing pyrolysis temperature and heating rate, char yield decreases, gas yield increases, and tar yield increases until it reaches its maximum value and then decreases due to the decomposition of tar compounds to light gases. Fast pyrolysis, which occurs at higher heating rates and lower residence time, may lead to higher gas and tar yields, while slow pyrolysis leads to higher char yield (Bridgwater, 2012; Choi et al., 2012). Higher yield of volatiles in fast pyrolysis is caused by further cracking of char as well as decomposition of tar compounds which undergo secondary reactions (Horne and Williams, 1996; Zanzi et al., 2002).

In another study, Sussott (1980) measured the char yields at 500 °C of foliage, wood, small stems, and bark at heating rates from 20 °C min⁻¹ to about 1000 °C min⁻¹. His samples were freeze-dried and ground to pass through a 20-mesh screen (0.84 mm) before pyrolysis. Sussott's results showed little difference in char yield as heating rate was increased. However, Zhao et al. (2018) studied the effects of temperature and heating rate on tar and char yields from the pyrolysis of rapeseed stem. Zhao's results indicated that by increasing the heating rate starting at 1 °C min⁻¹, char yield increased until it reached its maximum value at the heating rate of 5 °C min⁻¹, then char yield decreased continuously at higher heating rates. Other studies have shown that higher heating rates favor higher tar yield and lower char yield, higher temperatures provide higher light gas yield, but lower temperatures and heating rates favor higher char yield (Sharma and Hajaligol, 2003; Torikai et al., 2004; Haykiri-Acma et al., 2006).

In addition to the heating rate and temperature, fuel residence time in the reactor and sweep (carrier) gas flow rate can also affect the yields as well as the compositions of the products (Horne and Williams, 1996; Zanzi et al., 2002; Onay and Kockar, 2003; Bridgwater, 2012). Increasing the residence time enhances the gas yield due to the decomposition of tar and char.

The effect of residence time on the tar yield may be much stronger than that of the char yield due to the secondary reactions of the tar (Puy et al., 2011). Furthermore, higher sweep gas flow rate minimizes secondary pyrolysis reactions by reducing the residence time of the primary products in the reactor (Putun et al., 2007). In the field of bio-oil production from biomass, finding the optimum sweep gas flow rate and the best residence time of the volatiles in the reactor is very important (Maggi and Delmon, 1994; Pütün et al., 2005; Uzun et al., 2006; Putun et al., 2007).

2.3.2 Tar Analysis

Several definitions of tar have been proposed. Tar is commonly defined as any pyrolysis product that condenses at room temperature and pressure. Tar has also been defined as a mixture of condensable hydrocarbon compounds, including polycyclic aromatic hydrocarbons (PAHs) and oxygen-containing hydrocarbons (Ni et al., 2006). Tar was also defined as any hydrocarbons with a molecular weight greater than benzene (Maniatis and Beenackers, 2000).

Tar measurement can be either performed off-line by using a cold trap and subsequent solvent extraction or by on-line monitoring of the pyrolysis products (Moersch et al., 2000; Li and Suzuki, 2009). Tar components (called bio-oil in biomass pyrolysis) can be identified and measured by either a gas chromatograph-mass spectrometer (GC-MS) or a Fourier transform infrared spectrometer (FTIR) (Aysu and Kucuk, 2014; Gao et al., 2015).

As shown in Figure 2-4, tar can be classified based on two factors: (1) process conditions (Rios et al., 2018), and (2) solubility and condensability of tar compounds (Anis and Zainal, 2011). Based on process conditions, tar can be classified into primary, secondary, and tertiary tars. Primary tars including acids, alcohols, ketones, and aldehydes, are mainly formed at lower pyrolysis temperatures from the decomposition of plant constituents (i.e., cellulose, hemicellulose, and lignin). Secondary tars, such as phenols and olefins, form at higher

temperatures (above 500 °C) from the rearrangements of the primary tars. At higher temperatures (above 700 °C), tertiary tars, which include multi-ring aromatics such as naphthalene, anthracene, pyrene, etc., evolve from primary and secondary tars (Anis and Zainal, 2011; Rios et al., 2018).

Tars can also be classified into five subclasses based on their solubility and condensability: (1) heterocyclic aromatic compounds with high solubility (e.g. pyridine); (2) light single-ring aromatic compounds (e.g. toluene); (3) light polycyclic aromatic compounds with 2-3 rings (e.g. naphthalene); (4) heavy polycyclic aromatic compounds with 4-7 rings (e.g. pyrene); and (5) very heavy tars which are not detectable by gas chromatography (Li and Suzuki, 2009; Shen et al., 2016).

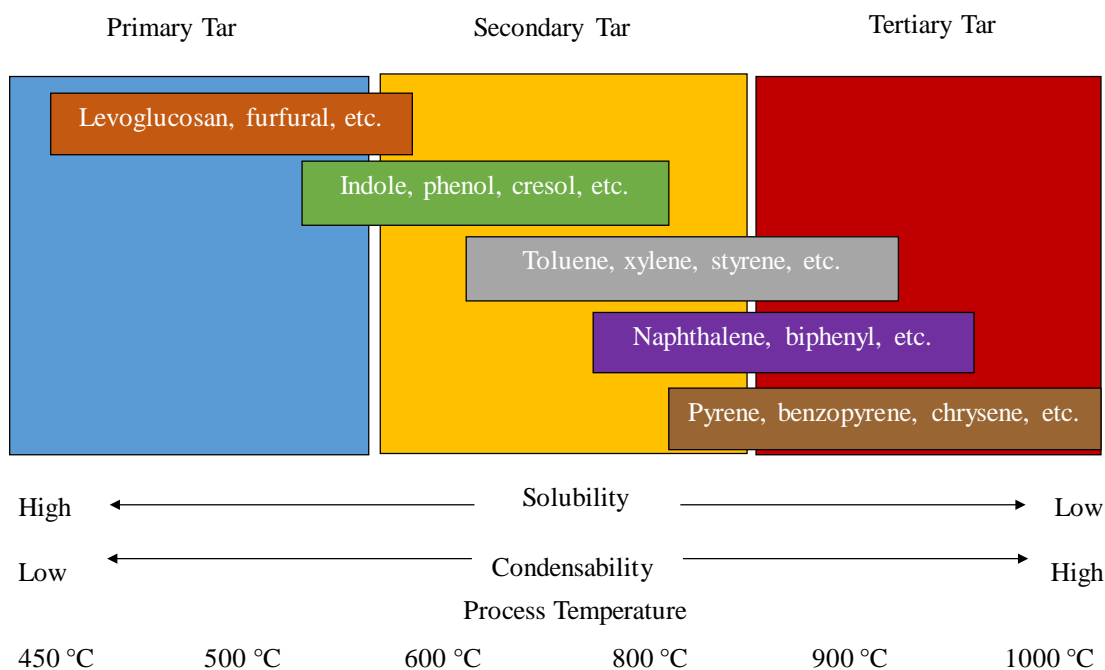


Figure 2-4. Tar classification (Shen et al., 2016)

As shown in Figure 2-5, it is believed that tar compounds mainly form from the decomposition of lignin, which has an aromatic nature (Amen-Chen et al., 2001; Shin et al., 2001;

Palma, 2013b; Wang et al., 2016; Rios et al., 2018). Lignin is highly reactive due to the presence of phenolic hydroxyl (OH) and methoxy (O-CH₃) groups in its chemical structure. Lignin decomposition leads to the formation of single-ring, low molecular weight aromatics (Xiao and Yang, 2013). Methoxyaromatics, such as phenol and guaiacol, are products of the decomposition of the lignin building blocks (Shen et al., 2016; Xu et al., 2016).

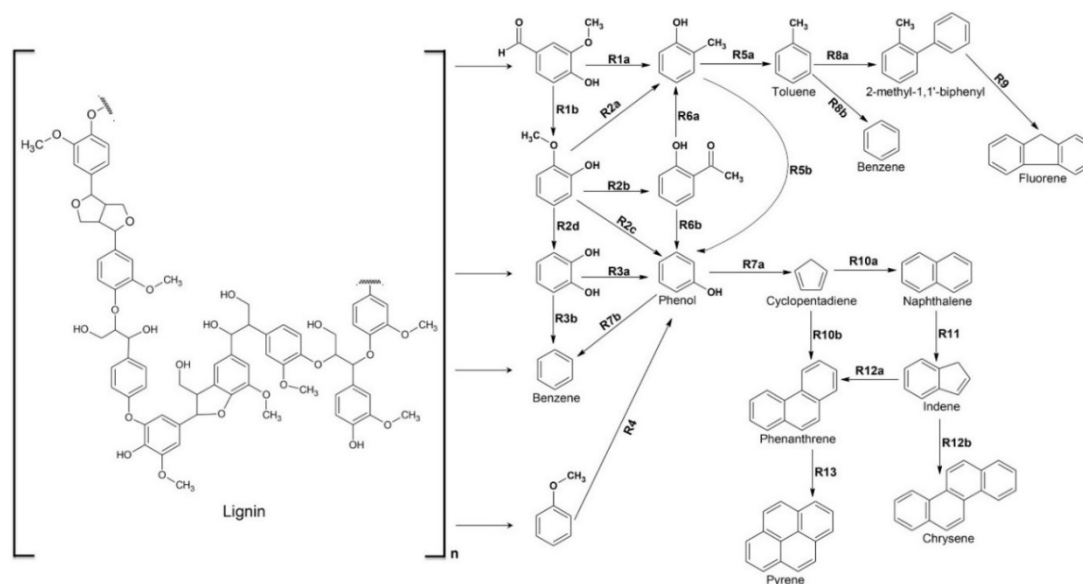


Figure 2-5. Lignin decomposition mechanism and formation of tar compounds (Rios et al., 2018)

The precursors of polycyclic aromatic hydrocarbons (PAHs), which are single-ring compounds, such as derivatives of benzene and styrene, are mainly formed by dehydroxylation and demethylation of tar compounds (Xiao and Yang, 2013). PAHs may form by hydrogen abstraction acetylene addition (HACA). For example, naphthalene can be formed from benzene with phenylacetylene as an intermediate (Zhou et al., 2015). The heavier PAHs of 3+ rings can form from naphthalene via various mechanisms. For example, acenaphthylene can evolve by the addition of acetylene to naphthalene (Palma, 2013a).

In energy production from the pyrolysis of biomass, tar is an undesirable material because it deposits in the gas line, blocks gas pathways, and causes corrosion of the downstream equipment (Li and Suzuki, 2009; Phuphuakrat et al., 2010). In the gasification of biomass, tar is a major problem that can cause the contamination of the producer gas and the failure of combustion engines. In these cases, gas cleaning is required to remove tars (Moersch et al., 2000).

2.3.3 Light Gas Analysis

Light gases can be analyzed either off-line or on-line. The major light gases during the pyrolysis of biomass and live plants are CO, CO₂, CH₄, H₂, and H₂O. Like tar, the composition of light gases depends on several factors, such as operating temperature, heating rate, fuel type, residence time, etc. Based on a study performed by Yang et al. (2007), during the pyrolysis of individual biomass constituents, higher CO yields were obtained from the pyrolysis of cellulose, while the pyrolysis of hemicellulose led to higher yields of CO₂. Furthermore, the pyrolysis of lignin caused higher yields of H₂ and CH₄.

Carbon monoxide is the main component in light gases at moderate and high pyrolysis temperatures (>500 °C). The high yields of CO at high temperatures is due to a decarbonylation reaction (Xu et al., 2016). By increasing pyrolysis temperature, CO yield increases while CO₂ yield decreases. At low temperatures (<500 °C), CO and CO₂ mainly form from the decomposition of cellulose and hemicellulose. However, at higher temperatures, the formations of CO and CO₂ are mainly caused by lignin degradation via the decomposition of COOH and C-O bonds. The formation of CO₂ is due to a decarboxylation reaction, especially at low pyrolysis temperatures (Gao et al., 2015).

By increasing pyrolysis temperature from 500 to 800 °C, CH₄ yield increases slightly due to the splitting of C-O bonds during lignin degradation, but with further temperature increase,

CH₄ content decreases. At high temperatures, CH₄ in the gas phase and phenolic groups in the liquid phase are formed by the removal of methoxy groups from aromatic rings (Xu et al., 2016).

H₂ yield increases by increasing pyrolysis temperature from 500 to 800 °C. At lower pyrolysis temperatures (<500 °C), the formation of H₂ is mainly caused by a dehydrogenation reaction. At higher temperatures (>500 °C), H₂ yield increases via two mechanisms. The first mechanism is the decomposition of phenolic groups in lignin. The second mechanism is the secondary reactions of heavy gaseous hydrocarbons at high temperatures. H₂ yield can increase at high temperatures due to the cracking and the rearrangement of aromatic bonds (Heo et al., 2010; Gao et al., 2015; Xu et al., 2016).

Fuel residence time is another important parameter in the yields of light gases. Increasing the fuel residence time decreases the yield of CO₂ (Gao et al., 2015). Longer residence time causes secondary cracking of macromolecules, leading to higher yields of CO. However, increasing the fuel residence time does not have as extreme an effect as temperature on the yields of H₂, CO₂ and C₂-C₃ content, but it still slightly increases the yields of these gases (Gao et al., 2015).

2.4 Differences between Live and Dead Plants

The pyrolysis of live plants has not been extensively studied. However, the pyrolysis of biomass (dead and dried plants) and wood as a promising technology for bio-char, bio-oil, and bio-gas production has been explored in detail during the past few decades (Bradbury et al., 1979; DiBlasi, 1994; Diebold, 1994; Rao and Sharma, 1998). This literature review provides significant background knowledge to form a basis for studies on the pyrolysis of live and dead plants.

Wildland fires are fueled by live and dead plants that have a variety of characteristics. The differences in the characteristics of these plants affect the behavior of the pyrolysis, ignition, and

spread of wildland fires (Weise and Wright, 2014; Gallacher, 2016; Yashwanth et al., 2016). Although the structures of live and dead plants (biomass) are similar, there are some differences in their characteristics, which may lead to different compositions of their pyrolysis products.

Dead plants have dry-basis moisture contents typically lower than 30 wt%, but this value can be as low as 4% (Viney, 1991). In contrast, the dry-basis moisture content of live plants may exceed 250 wt% resulting in significant amounts of water may remain in the fuel during ignition (Fletcher et al., 2007; McAllister et al., 2012). When the moisture content of wildland fuels exceeds 56 wt%, the majority of the water released during pyrolysis and combustion comes from the water contained in the fuel, not the combustion reaction (Byram, 1959). Liquid water in live plants is converted to water vapor during thermal heating of the plants. The evaporated moisture can then dilute the pyrolysis gases and slow down the burning rate (Ferguson et al., 2013).

The role of water throughout the process of heating live and dead plants may depend on how water is stored inside of the plants. Plants contain moisture in different forms: (1) bound water, which refers to the water in the structure of the plants; and (2) unbound water, which fills the voids inside of the plants (Gronli and Melaaen, 2000). The manner in which live plants burn varies visibly from that of dead plants (Dimitrakopoulos et al., 2010). Live plants have higher moistures of extinction (up to 140 wt%) compared to dead plants (between 12 and 30 wt%), which means that live plants are able to maintain fire spread at greater moisture contents than dead plants (Burgan and Rothermel, 1984; Dimitrakopoulos and Papaioannou, 2001). Wet dead fuels absorb water in their cell walls, and by heating the fuels, this vapor diffuses out. However, in live fuels, some of the unevaporated water expands rapidly causing the cell walls to burst (Fletcher et al., 2007; McAllister et al., 2012). In addition to moisture content, it has been suggested that components such as non-structural carbohydrates, fats, and other components may

impact the combustion behavior of live fuels, but are not usually found in dead fuels (Jolly et al., 2014; Jolly and Butler, 2015; Jolly and Johnson, 2018).

During the thermal drying of plants, two sequential mass transport mechanisms occur: (1) surface moisture evaporates due to an increase in temperature; and (2) internal moisture transfers to the surface of the plants and subsequently evaporates (Haghi, 2003). The moisture diffuses from a higher moisture content region in the plant to a lower moisture content region on the surface of the plant (Baronas and Ivanauskas, 2004).

For plants with high moisture content, significant amounts of heat are required to initiate drying and then pyrolysis of the plants (Yang et al., 2007). As moisture content in the plant structure increases, the temperature of the gases surrounding the plant decreases, which leads to a slower heat transfer rate to the surface of the plant and a lower surface temperature (Ferguson et al., 2013). This is important because pyrolysis has been shown to be a function of plant surface temperature (Leroy et al., 2010; Haseli et al., 2011). Gases around live plants with high moisture contents are diluted with evaporated water. Therefore, a higher rate of pyrolysis is required to sustain flame spread in a fuel bed (Catchpole et al., 1998; Ferguson et al., 2013). This explains why live plants have longer ignition times compared to that of dead plants (Xanthopoulos and Wakimoto, 1993; Dimitrakopoulos and Papaioannou, 2001). Ignition time is defined as the amount of elapsed time between plant exposure to a high temperature and the ignition of the plant. However, noticeable amounts of water still remain in the samples at the time of ignition, which is due to the pyrolyzing of different zones at different times (McAllister et al., 2012; Prince and Fletcher, 2014; Yashwanth et al., 2015).

Recent work has shown that the moisture content of plants changes over a growing season due to lack of precipitation and physiological changes in plant structure (McAllister et al., 2012;

Gallacher, 2016). Historical records show that large fires occurred in the Los Angeles and Santa Monica areas when the moisture content of live plants decreased below 79 and 77 wt%, respectively (Dennison and Moritz, 2009). It has been shown that live plants can sustain flame spread in fuel beds with moisture contents of over 100 wt% on a dry basis (Weise et al., 2005a), whereas dead plants cannot sustain flame spread in fuel beds with moisture contents of over 35 wt% (Weise et al., 2005b; Weise et al., 2016).

During the thermal decomposition of live plants, two peaks can be observed in the mass loss rate curve versus time. The first peak forms due to the evaporation of free water and an increase in the water concentration in the gas phase. At this moment, the surface temperature of the leaf is at the pyrolysis temperature, while the temperature inside of the leaf is close to the evaporation temperature, indicating a temperature gradient within the leaf. By continuous heating, the second peak appears due to the evaporation of bound water (Yashwanth et al., 2016).

2.5 Heat Transfer Mechanisms in Wildland Fires

Heat transfer during pyrolysis consists of two sequential steps: (1) external heat transfer from the surroundings of the plants to the surface of the plants; (2) internal heat transfer from the surface of the plants to the interior of the plants. If the external heat transfer is the determining step, the heat transfer regime is “thermally thin”. In contrast, if there are internal temperature gradients within the plants, the heat transfer regime is referred to as “thermally thick” (Di Blasi, 2000). Dimensionless numbers, such as the Biot number and the Pyrolysis number, have been defined to determine the heat transfer regime (Pyle and Zaror, 1984; DiBlasi and Lanzetta, 1997).

During wildland fires, both live and dead plants are burned through very complex heat transfer mechanisms (McAllister and Finney, 2017). As shown in Figure 2-6, heat transfer mechanisms in wildland fires are: (1) convective heat transfer from hot gases to plants, especially

for wind-driven fires; (2) radiative heat transfer from burning plant particles; and (3) radiative heat transfer from flames (Wagner, 1967). Radiative and convective heat transfer mechanisms are the two most dominant types of heat transfer mechanisms in wildland fires (Frankman et al., 2010a). Conductive heat transfer is only significant in thermally-thick fuels.



Figure 2-6. Heat transfer mechanisms in wildland fires (Stehle, 2017)

The convective heat transfer mechanism is essential for pyrolysis, ignition of plants, and wildland fire spread (Feng et al., 2017b). Convection occurs when heat is transferred by the movement of hot post-combustion gases into close contact with plants. As this happens, plants start to give off moisture and pyrolysis products. The pyrolysis products can later react with oxygen in the presence of an ignition source and burn the surrounding plants. This process repeats continuously and fire propagates to burn other nearby plants (Albini, 1985). Convective currents

are also a source of spotting, which is when small amounts of burning material float away from the main fire and settle in different areas to start smaller fires. Spotting can cause a fire to grow very quickly.

Radiation occurs as radiant heat energy is released from: (1) burning solid fuels such as leaves and branches; (2) pyrolysis and post-combustion gases, such as H₂ and CO; and (3) soot. Soot is mainly formed by the attachment of polycyclic aromatic compounds in tar. The evolution of smoke, along with the presence of water vapor in the air, may cause the attenuation of flame radiation. Water vapor has a moderate effect on the radiative heat transfer from the flames to the plants. Radiative heat flux decreases exponentially relative to the distance from the flames (Frankman et al., 2010b).

During wildland fires, plant species may be subject to both radiative and convective heat transfer mechanisms before ignition. In order to develop predictive models, it is important to understand how convection and radiation contribute to the pyrolysis and combustion of live and dead plants. The relative contribution of convective and radiative heat transfer mechanisms are complicated and not well understood (Frankman et al., 2010b). There is still a lack of consensus among the researchers regarding the dominant heat transfer mechanism in wildland fires. Some previous researchers believe that a combination of convective and radiative heat transfer mechanisms plays a role in fire spread (Asensio and Ferragut, 2002; McAllister and Finney, 2017), whereas others have demonstrated that radiation is only important in plant preheating (Albini, 1985; Demestre et al., 1989). More recent studies have indicated that radiative heat transfer, at the levels experienced in wildland fires, is not sufficient to ignite the plants (Gallacher, 2016). However, ignition of plant species can occur via convective heat transfer through hot gases without an ignition source (Pickett et al., 2010). Furthermore, it has been proposed that

convection or direct flame-fuel contact is important in fire spread, especially in windy conditions (Fang and Steward, 1969; Baines, 1990; Carrier et al., 1991; Weber, 1991; Wolff et al., 1991; Butler et al., 2004; Zhou et al., 2005; Yedinak et al., 2010; Prince, 2014; Gallacher, 2016).

The research by Rothermel (1972) has shown that radiation from both burning particles and hot gases is more important in pre-heating the plants during no-wind conditions and backing fires (when fire spreads against wind). In contrast, convection dominates in pre-heating plants in heading fires (when fire spreads with wind) (Frankman et al., 2010b; McAllister et al., 2012). The lack of consensus among researchers regarding the dominant heat transfer mechanism is likely caused by the different data sets that have been collected in various experimental conditions.

It has been proposed that the relative contribution of heat transfer mechanisms in wildland fires depends on a wide variety of factors, such as fuel type, wind speed, relative humidity, etc. (Tihay et al., 2009). In addition, weather conditions, such as rainfall, humidity, wind, and temperature, greatly influence fire behavior. Precipitation and humidity, which are determined by the air temperature, affect the moisture content of both live and dead plants. Plants tend to ignite more easily in hot, dry weather because of low moisture contents occurring frequently in these conditions. Wind can increase fire intensity and the rate of fire spread (Zhou et al., 2005; Dimitrakopoulos et al., 2010).

2.6 Summary of Literature Review

Many valuable studies have been performed during the past few decades regarding the pyrolysis and combustion of biomass (dead and dried plants). However, there is still a major gap in understanding the pyrolysis of live wildland fuels and characterization of their pyrolysis products under different heating modes. The research described in this dissertation helps to shed

light on the areas which have received little attention in this field. These areas include: (1) the effects of pyrolysis temperature, heating rate, fuel type, and fuel condition (i.e., live and dead) on the yields and the compositions of pyrolysis products from pyrolysis of wildland fuels; and (2) the effects of convective and radiative heat transfer mechanisms on the pyrolysis and the ignition of thin solid fuels especially live fuels with high moisture contents. The results of this dissertation will help to provide an understanding of the fundamental processes related to the pyrolysis and eventual combustion of wildland fuels.

3 OBJECTIVE AND TASKS

3.1 Objective

The objective of this research is to improve the understanding of the pyrolysis of live and dead plant species native to the forests of the southern United States. In this research, the effects of heating rate, operating temperature, heat transfer mechanisms, and fuel type on the yields and the compositions of pyrolysis products have been investigated. The results from this research are being used by other members of a large team (Weise et al., 2018) to determine heat release rates and model reactions that occur during the slow and fast pyrolysis of live and dead vegetation. Understanding of the reactions that occur during pyrolysis then can be used to develop more accurate pyrolysis models, which in turn can be used to improve the prediction of the conditions of prescribed burning, and to improve the prediction of fire propagation.

3.2 Tasks

The following tasks were identified to achieve the objectives:

1. Develop a system to heat intact live samples of vegetation at heating rates similar to those observed in wildland fires, including measurement of the sample mass and surface temperature as a function of time, as well as collection of gaseous pyrolysis products.
2. Develop a system to characterize major pyrolysis products, including measurement of yields and compositions of condensable (i.e., tar) and non-condensable (light gas) products.

3. Study the effects of heating rates and pyrolysis temperatures on the yields and the compositions of pyrolysis products using a flat-flame burner apparatus (for fast pyrolysis experiments) and a pyrolyzer apparatus (for slow pyrolysis experiments). The slow pyrolysis experiments were performed by Amini et al. (2019), so this task was led by me but published jointly.
4. Examine the effects of heat transfer mechanisms on the process of pyrolysis by running the flat-flame burner apparatus under three different heating modes: (1) convection-only, (2) radiation-only, and (3) a combination of convection and radiation.
5. Compare the pyrolysis behavior of various fuel types, which include 14 plant species native to the forests of the southern United States. The experiments were performed on both live and dead plants to determine the effects of the fuel type and the fuel condition on the yields and compositions of pyrolysis products.

In order to accomplish the aforementioned tasks, two experimental setups were used: a flat-flame burner apparatus (Safdari et al., 2018b) and a pyrolyzer apparatus (Amini et al., 2019) for the purpose of studying fast and slow pyrolysis, respectively. The flat-flame burner was operated under three different heating modes to evaluate the effects of heat transfer mechanisms on the yields and the compositions of pyrolysis products. The heating modes were: (1) convection-only: to study the effects of convective heat transfer; (2) radiation-only: to study the effects of radiative heat transfer; and (3) a combination of convection and radiation heat transfer mechanisms.

For each plant species, pre-burn measurements, such as proximate and ultimate analysis, as well as physical measurements, were performed. The pyrolysis of both live and dead plants was studied and factors such as temperature, heating rate, and change of mass over time were measured.

The pyrolysis products, including tars and light gases, were collected and analyzed using GC-MS and GC-TCD, respectively.

The following chapters are organized in the following manner. Chapter 4 describes the equipment and experimental procedure used. Chapter 5 provides the results of the convection-only experiments. Chapter 6 includes the comparison of the results from the slow and fast pyrolysis experiments. Chapter 7 presents the results of pyrolysis experiments performed using three heating modes. Finally, summary and conclusions are presented in Chapter 8.

4 DESCRIPTION OF EXPERIMENTS

4.1 Plants Tested

The plant species, as listed in Table 4-1, were nursery grown in Florida. These plant species were selected because they represent a range of common plants in the region where the prescribed burning has been performed. Live potted plants were then express-mailed to the combustion laboratory at Brigham Young University (BYU) and kept in a location with sufficient sunlight and water to keep the plants alive until they could be used in the experiments.

Among the plants, two of the plant species were grasses (little bluestem and wiregrass), 9 of the plant species were shrub species, and others were tree species. Longleaf pine litter (i.e., pine straw) was also studied and compared with the live and 1-week old dead longleaf pine foliage data to investigate the effects of aging on the composition of pyrolysis products. Longleaf pine litter is used as a ground cover in gardens in the southern U.S. A large box of longleaf pine litter was shipped to BYU for the pyrolysis experiments. Pictures of the plants and a brief description of their characteristics are shown in the Appendix A.

4.2 Proximate and Ultimate Analysis

Before running the pyrolysis experiments, for each plant species, pre-burn measurements including proximate and ultimate analysis as well as physical measurements were performed. Proximate analysis determines moisture, volatile matter, fixed carbon, and ash contents in a

sample. Ultimate analysis provides determination of weight percent of carbon, hydrogen, oxygen, nitrogen, and sulfur in a plant.

Table 4-1. List of plants used in pyrolysis experiments

Common name	Scientific name	Growth form	Leaf shape
Darrow's blueberry	<i>Vaccinium darrowii</i> Camp "Rosa's Blush"	Shrub	Elliptical
Dwarf palmetto	<i>Sabal minor</i> (Jacq.) Pers.	Shrub	Palmate
Fetterbush	<i>Lyonia lucida</i> (Lam.) K. Koch	Shrub	Elliptical
Inkberry	<i>Ilex glabra</i> (L.) A. Gray	Shrub	Elliptical
Little bluestem	<i>Schizachyrium scoparium</i> (Michx.) Nash	Grass	Linear
Live oak	<i>Quercus virginiana</i> Mill.	Tree	Elliptical
Longleaf pine foliage	<i>Pinus palustris</i> Mill.	Tree	Linear
Longleaf pine litter	<i>Pinus palustris</i> Mill.	Tree	Linear
Saw palmetto	<i>Serenoa repens</i> (W. Bartram) Small	Shrub	Palmate
Sparkleberry	<i>Vaccinium arboreum</i> Marshall	Shrub	Elliptical
Swamp bay	<i>Persea palustris</i> (Raf.) Sarg.	Shrub	Elliptical
Water oak	<i>Quercus nigra</i> L.	Tree	Elliptical
Wax myrtle	<i>Morella cerifera</i> (L.) Small	Shrub	Elliptical
Wiregrass	<i>Aristida stricta</i> Michx.	Grass	Linear
Yaupon	<i>Ilex vomitoria</i> Aiton "Schelling Dwarf"	Shrub	Elliptical

The moisture content of the plant samples was measured using a Computrac MAX 1000 moisture analyzer at the beginning and the end of each run. The average of these two values was taken and reported as the moisture content of the run. The proximate (Figure 4-1) and ultimate analysis were measured by the University of Wisconsin Forage Laboratory according to ASTM D7582 and ASTM D5291 procedures. In addition, high and low heating values were measured using the ASTM E711 procedure. Table 4-2 shows the results of proximate and ultimate analysis of the plants.

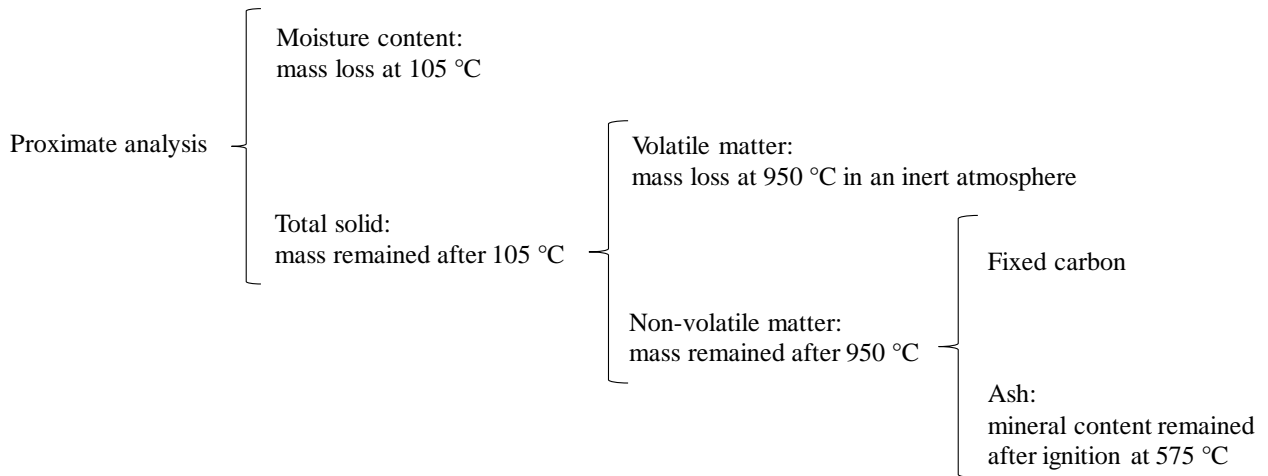


Figure 4-1. Proximate analysis of plants

The proximate analysis revealed that the foliage samples were generally similar. For the live plants, the moisture content ranged from 85 to 217 wt% (dry basis). The moisture content of the longleaf pine litter was only 15 wt%. Ash content (silica) ranged from a low of 1.77 wt% for longleaf pine litter to a high of 4.89 wt% for yaupon. While the two grasses (little bluestem grass and wiregrass) had similar ash content, other closely related species differed in ash content (e.g., inkberry and yaupon, saw palmetto and dwarf palmetto).

Volatile material content ranged from 76.4 to 89.8 wt%. The fixed carbon ranged from a low of 10.2 wt% for dwarf palmetto to a high of 23.6 wt% for saw palmetto. Proximate analysis of the palmettos were similar to the results for date palm (Sait et al., 2012). Ultimate analysis of the plants yielded no surprises meaning that the elemental composition of the foliage fell within the accepted ranges. The C and N content of the fetterbush and inkberry agreed well with published values (Burling et al., 2010).

Table 4-2. Proximate and ultimate analysis of plant species

Common name	MC ¹	Proximate analysis ²			Ultimate analysis ³						
		Ash	VM	FC	C	H	N	S	O	LHV	HHV
Darrow's blueberry	104	2.85	n.a. ⁴	n.a.	n.a.	n.a.	n.a.	n.a.	n.a.	n.a.	n.a.
Dwarf palmetto	164	3.26	89.8	10.2	47.36	5.93	2.14	0.66	43.91	19.04	20.61
Fetterbush	91	2.24	77.7	22.3	54.36	5.81	0.80	0.12	38.91	19.00	20.57
Inkberry	85	1.88	80.2	19.8	54.63	6.42	0.87	0.11	37.97	20.94	22.52
Live oak	103	2.71	80.9	19.1	49.57	6.01	2.30	0.15	41.97	18.21	19.81
Little bluestem	217	4.12	84.9	15.1	51.22	5.66	2.22	0.15	40.75	17.63	19.09
Longleaf pine foliage	207	2.02	79.7	20.3	51.37	3.00	1.21	0.11	44.31	19.26	20.11
Longleaf pine litter	15	1.77	78.3	21.7	52.31	6.09	2.31	0.06	39.23	19.59	21.10
Saw palmetto	112	3.19	76.4	23.6	49.49	5.48	0.90	0.17	43.96	19.09	20.56
Sparkleberry	103	3.10	79.0	21.0	52.49	7.71	0.74	0.16	38.90	18.96	20.90
Swamp bay	116	1.84	79.6	20.4	52.48	6.11	1.36	0.17	39.88	20.50	22.10
Water oak	170	4.18	80.6	19.4	50.06	5.57	1.47	0.10	42.80	18.23	19.96
Wax myrtle	118	2.41	77.4	22.6	50.65	5.44	2.31	0.14	41.46	19.98	21.36
Wiregrass	135	4.34	81.7	18.3	47.42	6.34	3.31	0.25	42.68	17.74	19.34
Yaupon	104	4.89	86.2	13.8	51.34	6.28	1.46	0.18	40.74	19.79	21.43

¹ MC (moisture content wt% dry basis) of samples used in experiments at BYU

² VM (volatile material), FC (fixed carbon). Values are wt% dry-ash free. ASTM D7582

³ C, H, N, S, O – values are % dry mass; LHV – low heating value, HHV – high heating value (kJ g⁻¹, dry-ash free basis). ASTM D5291, D4239, E711

⁴ n.a. means not available

4.3 Physical Measurement

Physical and chemical properties of the plants are important factors that can affect the behavior of wildland fires. These properties can later be used to develop more precise models. The blade thickness of the leaves (not including central vein) was measured using a caliper. The width of the leaves was measured at their widest point. In addition, the length of the leaves was measured, which included the leaf blade and the leaf petiole (Figure 4-2).

For plants with stems, the thickness of these stems was measured at various points along the stem except for the longleaf pine which was provided as a “plug seedling” and did not have a pronounced stem (Barnett and McGilvary, 1997). The results of the physical measurements are presented in Table 4-3. The results are the average of three measurements $\pm 95\%$ confidence interval.



Figure 4-2. Leaf length and width measurements

Table 4-3. Physical measurements of samples

Plant name	Thickness of leaves (mm)	Length of leaves (mm)	Width of leaves (mm)	Thickness of stem (mm)	Width/Length ratio
Darrow's blueberry	0.23* ± 0.06 [†]	22 ± 5	7 ± 4	0.7 ± 0.4	0.32
Dwarf palmetto	0.21 ± 0.04	120 ± 25	9 ± 3	-	0.08
Fetterbush	0.20 ± 0.08	27 ± 6	15 ± 4	1.2 ± 0.4	0.56
Inkberry	0.32 ± 0.06	29 ± 5	15 ± 3	2 ± 0.8	0.52
Live oak	0.33 ± 0.05	61 ± 9	29 ± 6	3 ± 1.2	0.48
Little bluestem grass	0.11 ± 0.03	175 ± 67	2.3 ± 0.6	-	0.01
Longleaf pine foliage	0.42 ± 0.04	106 ± 4	-	-	-
Longleaf pine litter	0.46 ± 0.03	104 ± 4	-	-	-
Saw palmetto	0.22 ± 0.06	95 ± 22	14 ± 4	-	0.15
Sparkleberry	0.24 ± 0.05	20 ± 4	8 ± 2	0.6 ± 0.2	0.40
Swamp bay	0.30 ± 0.06	104 ± 8	27 ± 4	3.4 ± 0.5	0.26
Water oak	0.18 ± 0.03	63 ± 17	16 ± 7	2.2 ± 0.8	0.25
Wax myrtle	0.19 ± 0.04	33 ± 4	12 ± 2	0.7 ± 0.2	0.36
Wiregrass	0.31 ± 0.04	154 ± 49	-	-	-
Yaupon	0.31 ± 0.09	11 ± 3	6 ± 2	1.4 ± 0.2	0.55

* Average

[†] ± 95% confidence interval

4.4 Experimental Setup and Procedure

In order to simulate the pyrolysis of live and dead plants in wildland fires, pyrolysis experiments were performed using a flat-flame burner (FFB) apparatus. The fast pyrolysis experiments were performed with three heating modes and the results are presented in Chapters 5-7. The results of fast pyrolysis experiments (under convective heat transfer only) then were compared with the results of slow pyrolysis experiments, which were performed using a pyrolyzer apparatus. These two pieces of apparatus enabled running experiments to compare the yields and the compositions of pyrolysis products during slow and fast pyrolysis. Experiments were performed both on live and dead samples. Samples were not dried prior to the pyrolysis experiments. To study the pyrolysis of live plants, which had high moisture contents as high as 217 wt% (dry basis), the samples were cut from their roots and the experiments were performed immediately. Dead plants consisted of live samples that were cut and then left in the lab at room temperature for about a week to dry out until their moisture content decreased to ~5 wt%.

4.4.1 Flat-Flame Burner (FFB) Apparatus

The FFB apparatus (Figure 4-3) provided high heating rate and moderate temperature to simulate fast pyrolysis of the plants. The FFB was operated under three different heating modes: (1) convection-only, where the FFB apparatus was operated at a high sample heating rate of $180\text{ }^{\circ}\text{C s}^{-1}$ (convective heat flux of 100 kW m^{-2}) and a maximum fuel surface temperature of $750\text{ }^{\circ}\text{C}$ to imitate pyrolysis under convective heat transfer; (2) radiation-only, where the plants were pyrolyzed under a moderate heating rate of $4\text{ }^{\circ}\text{C s}^{-1}$ (radiative heat flux of 50 kW m^{-2}) and a maximum fuel surface temperature of $550\text{ }^{\circ}\text{C}$. Nitrogen flowed from the burner as a carrier gas, but the burner was not ignited. The lower heating rate in the radiation-only mode was due to the convective cooling by N_2 ; and (3) a combination of radiation and convection, where the plants

were exposed to both convective and radiative heat transfer. The heating rate was $195\text{ }^{\circ}\text{C s}^{-1}$ and maximum fuel surface temperature was measured to be $800\text{ }^{\circ}\text{C}$.

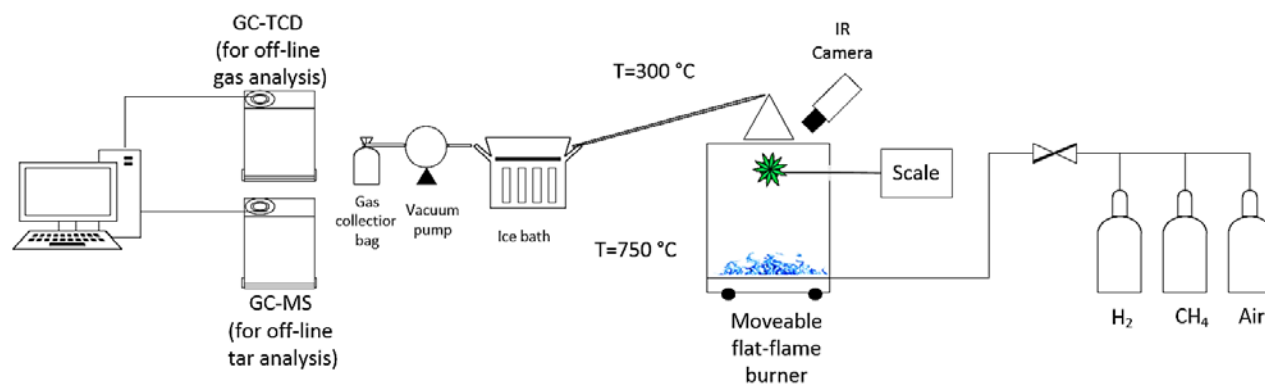


Figure 4-3. Flat-flame burner apparatus

Previous researchers used a similar setup at Brigham Young University to study: (1) the influence of seasonal change and heating mode on wildland fire behavior (Gallacher, 2016); (2) live plant combustion properties (Shen and Fletcher, 2015); (3) semi-empirical modeling for fire spread in shrub fuels (Prince et al., 2017); and (4) the differences in the burning behavior of live and dead leaves (Prince and Fletcher, 2014).

Modifications were made on the FFB apparatus to prepare it for the pyrolysis experiments as explained in the following sections. For modes (1) and (3) where the effects of convective heat were studied, in order to provide pyrolysis conditions and an oxygen-free environment (i.e., no sample combustion), the FFB was operated in a fuel-rich mode (equivalence ratio: $\Phi=1.13$). A mixture of CH_4 and H_2 with flow rates of 26.5 L min^{-1} and 16.6 L min^{-1} , respectively, comprised the burner fuel, which was oxidized with atmospheric air with a flow rate of 258.8 L min^{-1} . The samples were heated convectively by the post-flame burner products (CO_2 , H_2O , and CO). The major post-flame gases from the FFB were analyzed using the GC-TCD as N_2 (69.2 mole%),

H₂O (19.9 mole%), CO₂ (6.1 mole%), CO (3.1 mole%), and H₂ (1.7 mole%). No O₂ was detected in the post-flame gases. No flaming or smoldering of the plant samples was observed during the experiments since the FFB was operated in fuel-rich mode.

The burner cross-section was 20 cm by 27 cm, and gases were premixed before passing through the sintered bronze surface. The windows around the burner were made of ceramic glass (Neoceram) and were 30.5 cm high. Previous experiments in the flat-flame burner were combustion experiments, where the burner was operated under fuel-lean conditions (i.e., excess O₂). In these previous experiments, the sample could be pre-loaded onto the clip suspended horizontally from the balance on a rod, with the rod extending through a small 5 cm diameter hole in one window. The windows were stationary and not attached to the burner, so the burner was moved underneath the sample without forming a seal with the windows. This did not matter much in the combustion experiments, since a small amount of excess air from leaks around the burner did not impact the sample combustion rate. However, in the current pyrolysis experiments, no O₂ could be present in order to provide pyrolysis conditions and avoid combustion of the sample. Therefore, the windows were mounted to the burner surface, and a seal between the glass and the burner surface was made with zirconia felt. The gases within the FFB were analyzed by GC-TCD to insure there was no O₂ in the system.

About 2-3 g of previously-weighed leaves with little or no stem material were then loaded onto the horizontal rod with a clip connected to a Mettler Toledo XS204 scale which recorded the mass of the samples with a data rate of 50 Hz using LabVIEW software. In this experiment, leaves were positioned with the leaf face parallel to the burner surface. The FFB structure was designed to be moveable and was mounted on wheels and moved with a manual conveyor belt. To initiate pyrolysis experiments, the burner was pulled quickly into position under the sample

in approximately 1 s. The sample on the rod passed through a 3 cm diameter hole as the burner/window assembly was moved underneath the sample. The hole was large enough to permit the sample to pass through, but small enough to prevent significant entrainment of air into the center of the glass chimney. The hole was near the top of the window so the sample was located 24 cm above the burner surface. Under fuel-rich conditions, a faint blue diffusion flame was visible above the height of the glass chimney, where the fuel-rich gases contacted the ambient air. A small faint blue flame was also visible near the hole in the side window, but this flame rose quickly along the side window and did not extend to the center of the chimney where the sample was located. The FFB was equipped with a cooling water recirculation system to prevent overheating and potential damage, which kept the burner surface cool enough that radiation from the burner to the sample was negligible. The burner surface temperature, as measured by a thermocouple at various locations was 80 ± 5 °C.

As illustrated in Figure 4-4, a stainless steel funnel with a mouth diameter of 12.5 cm was placed above the pyrolyzed sample to collect pyrolysis gases using an oil-less Air Cadet vacuum pump. The distance between the sample and the top of the funnel was 10 cm. The velocity of the gases at the location of the plant sample was about 1 m s^{-1} (see Appendix C for calculations). The estimated residence time of pyrolysis gases between the sample and the top of the funnel was 100 ms. After entering the funnel, the pyrolysis gases flowed through a 1 m stainless steel transfer line (ID = 1.25 cm) that was held at a temperature of 300 °C using heating tape to avoid the condensation of heavy hydrocarbons in the line. Several thermocouples were placed along the heated transfer line to record the temperature.

In order to collect condensable pyrolysis products (tars), the pyrolysis gases then flowed through a series of test tubes which were filled with glass wool and placed inside an ice bath.

The remaining light gases (non-condensable gases) were then collected in 5 liter Tedlar[®] bags which were placed at the end of the process line.

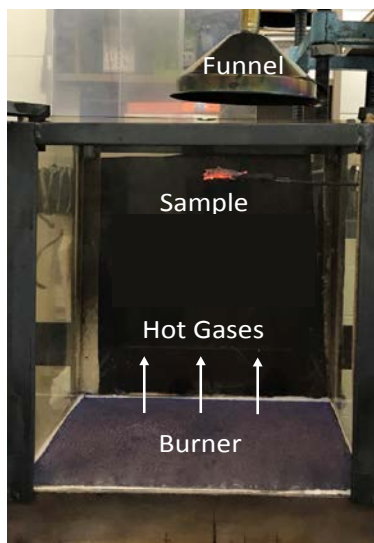


Figure 4-4. The flat-flame burner apparatus with flame and pyrolyzing sample

The average gas temperature within the FFB at the height where the sample was located was measured by an OMEGA K-type thermocouple (wire diameter of 0.38 mm, response time of 0.8 s, and maximum working temperature of 871 °C). This temperature, corrected for radiation losses, was 765 °C for the convection-only mode, 105 °C for the radiation-only mode, and 804 °C for the combined mode. The calculations to find the actual gas temperature are presented in Appendix B. In addition, plant surface temperature was recorded by an FLIR A-300 Series infrared camera, and the data analysis was performed using FLIR ResearchIR Max 4 software. Emissivity of the samples was considered to be 0.98 (Lopez et al., 2012). A heat flux meter (radiometer) was used to measure the radiative, convective, and total heat flux during the experiments. The heat flux meter was equipped with a Medtherm 64-series heat flux sensor to measure the radiative heat flux. For the convection-only mode, the total heat flux at the position

of the plants was estimated to be approximately 100 kW m^{-2} with less than 5% due to radiation. The total heating rate was estimated to be approximately $180 \text{ }^\circ\text{C s}^{-1}$ and $195 \text{ }^\circ\text{C s}^{-1}$ for the convection-only and the combined modes, respectively. These heating rates were calculated by finding the difference between the maximum fuel temperature (from IR temperature data) and room temperature ($25 \text{ }^\circ\text{C}$) divided by the corresponding time elapsed to reach the maximum temperature. These high heating rates provided conditions to investigate the fast pyrolysis of the plants similar to what has been measured in wildland fires. The total heat flux for the radiation-only mode was 50 kW m^{-2} . The total heating rate for the radiation-only mode was measured to be $4 \text{ }^\circ\text{C s}^{-1}$.

Gas chromatography is a common technique for the analysis and quantification of volatile compounds. The compounds are injected into a gas chromatograph (GC) and then vaporized in a GC column. This process can be done using either a packed column or a capillary column. The column and the gas are called the stationary and mobile phases, respectively. The injected compounds are separated within the column based on their interactions with the GC column (stationary phase) (Scott, 2017). Therefore, GC column selection is a very important process variable to properly separate the compounds. Absorbed gases are released from the column at different temperatures, so the column is heated in an oven at a prescribed temperature ramp, allowing different species to desorb at different times. Finally, the vaporized compounds can be detected by various detectors, such as a thermal conductivity detector (TCD), flame ionization detector (FID), mass spectrometer, etc. The detector type is selected by the user based on the particular measurement application and required detection limit (French, 2017).

The thermal conductivity detector (TCD) relies on the differences in the thermal conductivity between the gases that are leaving the GC column and a carrier gas (e.g., helium).

The TCD is an appropriate detector for the analysis of non-condensable gases, such as O₂, N₂, CO, CO₂, H₂, CH₄, etc. (Grob and Barry, 2004). Mass spectrometry (MS) is a powerful analytical technique which is used for the analysis of all kinds of chemicals. A mass spectrometer uses three key stages for the analysis of the compounds; ionization, acceleration and deflection, and detection (Hoffmann and Stroobant, 2007). First, the vaporized compounds are converted into gaseous ions by an ion source. The ions are then separated in the mass spectrometer based on their specific mass to charge ratio (m/z). Finally, the ions are detected and their relative abundances are recorded in the detector (French, 2017). Each species has an identifiable distribution of fragment ions, which is built in to a library accompanying the MS machine.

Upon the completion of the experiments, the light gases were analyzed off-line using a ThermoFisher Scientific Trace 1310 gas chromatograph equipped with Chrompack Molsieve5A (25 m × 0.32 mm × 30 μm) and TracePLOT TG-Bond Q (30 m × 0.32 mm × 10 μm) columns and a thermal conductivity detector (GC-TCD). The oven temperature was programmed to hold the sample at 40 °C for 3 min, then heated to 250 °C at 10 °C min⁻¹, and then held at 250 °C for 4 min. Ultra high purity (UHP) helium was the carrier gas and the size of the sample was 10.0 μL with a split ratio of 25.

The glass wool was then removed from the test tubes and placed in a beaker. Tars were extracted from the glass wool using CH₂Cl₂ as a solvent. About 2 g of anhydrous CaSO₄ powder was added to the CH₂Cl₂/tar solution to absorb any H₂O present. The decanted CH₂Cl₂/tar solution was then analyzed off-line by an HP 5890 gas chromatograph equipped with a Restek Rxi-1ms capillary column (60 m × 0.25 mm × 1 μm) and an HP 5972 mass spectrometer (GC-MS). The oven temperature was programmed to hold the sample at 50 °C for 5 min, then heated to 310 °C at 10 °C min⁻¹, and held at 310 °C for 5 min. Ultra high purity (UHP) helium was used

as a carrier gas, and the size of the sample was 1.0 μL with a split ratio of 10. After each experimental run, the line, test tubes, and the funnel were cleaned using acetone and dichloromethane as solvents in order to remove contaminants and prepare the setup for the next experiments.

For modes (2) and (3), where the effects of radiation heat transfer were studied, an OMEGALUX QH-101060 infrared radiant heating panel was used (Figure 4-5). The radiant heating panel used a fused quartz glass emitter face. The panel was connected to a temperature controller. By adjusting the set point to 600 $^{\circ}\text{C}$, the panel emitted radiation at an output wavelength between 2.5 and 6 μm and a heat flux of 50 kW m^{-2} until the temperature of the heater approached 600 $^{\circ}\text{C}$ and the heater was turned off. The maximum operating temperature of the panel was 1800 $^{\circ}\text{F}$ (981 $^{\circ}\text{C}$). The housing was made of rugged aluminized steel with the electrical terminal housing on the back. For mode (2), where the effects of only radiative heat transfer were studied, 16.6 L min^{-1} nitrogen at room temperature (25 $^{\circ}\text{C}$) flowed as a carrier gas through the burner to provide an oxygen-free environment in the system while the burner was not ignited. It should be noted that in the radiation-only experiments the leaf sample was positioned parallel to the surface of the radiation panel.

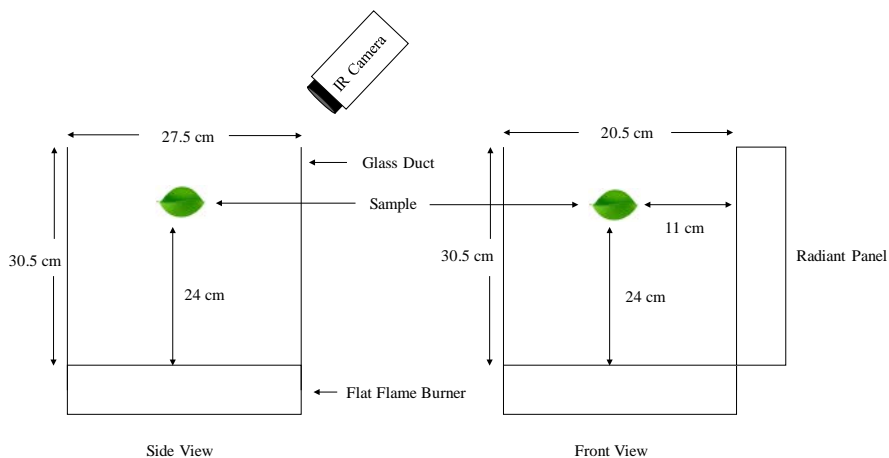


Figure 4-5. Schematic of the FFB

4.4.2 Pyrolyzer Apparatus

The pyrolyzer apparatus (as shown in Figure 4-6) was developed by Amini et al. (2019). The full description of the apparatus is presented elsewhere (Amini et al., 2019). This apparatus provided slow pyrolysis conditions with a carrier gas of 100 mL min^{-1} of N_2 . Before running the experiments, about 2-3 g of previously-weighed leaves with little or no stem material were loaded into a U-shaped stainless steel portion of the reactor. The reactor was placed in an electric furnace equipped with K-type thermocouple connected to a temperature controller. During the slow pyrolysis experiments, the temperature of the reactor was increased by $0.5 \text{ }^\circ\text{C s}^{-1}$ until reaching a gas phase temperature of $500 \text{ }^\circ\text{C}$, and then kept at this temperature for up to an hour until no further gas generation was observed.

The pyrolysis gases passed through an ice bath equipped with a series of test tubes filled with glass wool to collect condensable pyrolysis products (tars). The light gases were collected at the end of the process line using 5 L Tedlar[®] bags. The collected light gases were analyzed off-line using a ThermoFisher Scientific Trace 1310 gas chromatograph equipped with a thermal conductivity detector. The tars were removed using CH_2Cl_2 and analyzed with an HP 5890 gas chromatograph equipped an HP 5972 mass spectrometer (GC-MS).

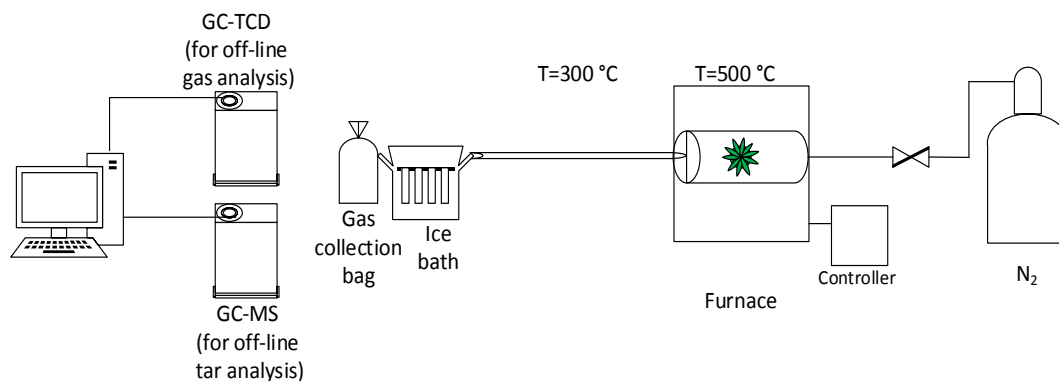


Figure 4-6. Pyrolyzer apparatus

4.5 Statistical Analysis

All the results which have been presented in this research are the average of three experiments. The error bars in the figures and tables represent the $\pm 95\%$ confidence intervals for three experiments (see Equation (4-1)). The average values (\bar{x}) and the standard deviations (s) for three replications were first calculated. The t-value, which is a function of the number of replications and the confidence interval, was found to be equal to 2.92 for three replications ($n = 3$) and 95% confidence intervals ($\alpha = 1 - 0.95$ then $\alpha = 0.05$) using the t-value table (Ramsey and Schafer, 2013), as follows:

$$\mu = \bar{x} \pm t \cdot \left(\frac{s}{\sqrt{n}} \right) \quad (4-1)$$

The ANOVA (Analysis of Variance) data analysis tool in Microsoft Excel 2017 was used to calculate the p-values for the statistical analysis. This statistical analysis technique can be used to determine whether the differences between the means of three or more independent groups are statistically significant. The null hypothesis is that the means of the independent groups are the same. The null hypothesis is rejected if the p-value is less than 0.05. If the p-value is found to be in the range 0-0.01, then it is considered to be convincing evidence that the null hypothesis should be rejected and the difference between the means of the independent groups is statistically significant. If the p-value is between 0.01 and 0.05, there is moderate evidence of difference between the means of the independent groups, and a p-value between 0.05 and 0.1 indicates that there is a difference between the means; however, it is inconclusive. If the p-value is greater than 0.1, the difference between the means is not significant (Ramsey and Schafer, 2013). This method of p-value interpretation has been used in this research for the statistical analysis.

5 FAST PYROLYSIS OF PLANTS BY CONVECTIVE HEAT TRANSFER²

In this chapter, the fast pyrolysis of live and dead plant species under convection-only mode is investigated. During the convection-only experiments, the samples were exposed to a high heating rate of $180\text{ }^{\circ}\text{C s}^{-1}$ and a gas temperature of $765\text{ }^{\circ}\text{C}$ to imitate typical wildland fire conditions. The maximum fuel surface temperature was measured to be $750\text{ }^{\circ}\text{C}$.

5.1 Pyrolysis Product Yields

Pyrolysis temperature and heating rate have significant impacts on the yields and the compositions of pyrolysis products (i.e., tar, light gases, and char). Figure 5-1 and Figure 5-2 illustrate the pyrolysis product yields for live and dead plant species, respectively. The char yield was obtained from the final mass of the solid residue. The tar yield was determined by finding the difference between the initial mass of the test tubes used in the cold trap and their final mass after subtracting the amount of moisture evolved from the pyrolysis of the sample. The moisture content of the sample was measured by a moisture content analyzer, before performing the pyrolysis experiments. The gas yield was determined by difference. The results are the average of three experiments and are expressed on a dry ash-free (daf) basis. For the live plants, the average relative confidence intervals (i.e., the confidence interval divided by the mean) were

² The results of this chapter were published in Fuel (Safdari et al., 2018b)

10%, 4%, and 19% for gas, tar, and char yields, respectively. Similar average confidence intervals were obtained for the dead plant species.

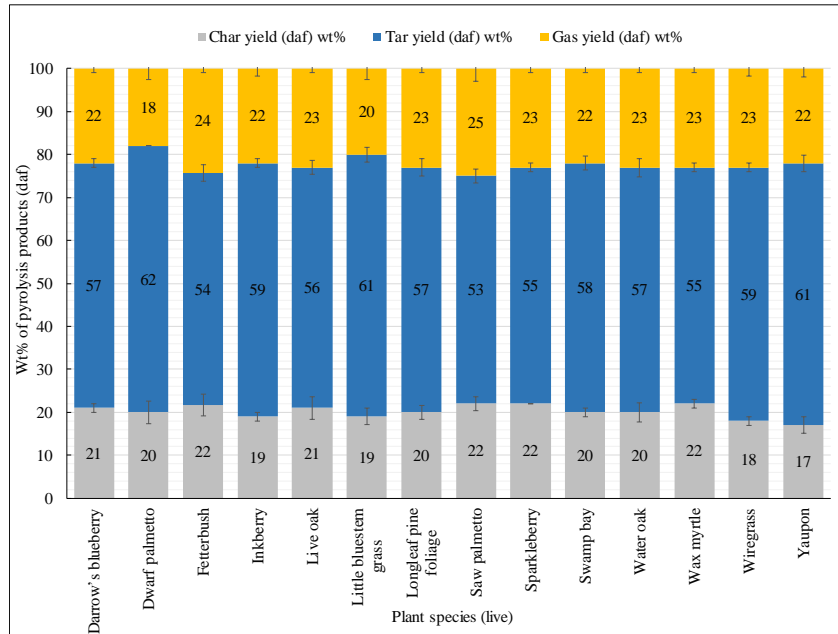


Figure 5-1. Product yields of live plant species on a dry, ash-free (daf) basis

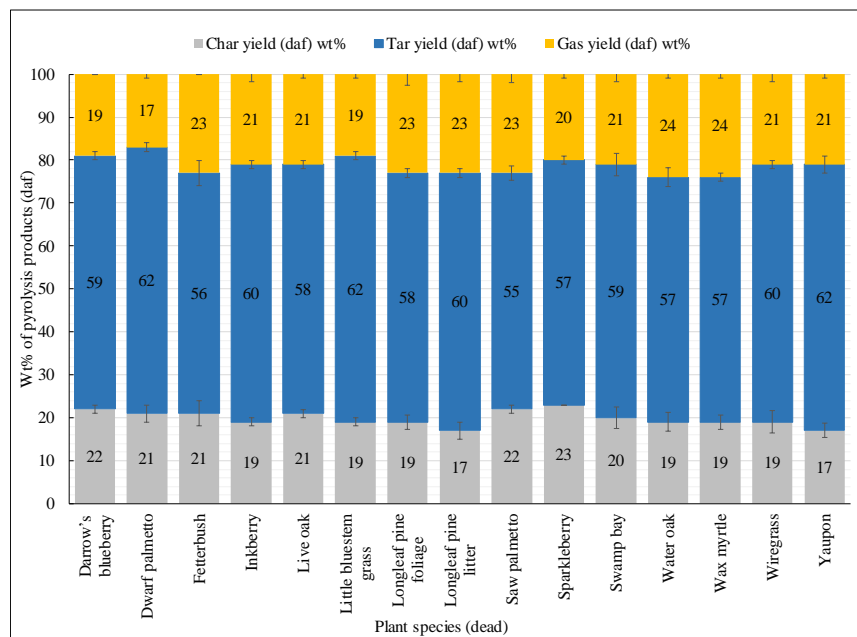


Figure 5-2. Product yields of dead plant species on a dry, ash-free (daf) basis

Table 5-1. Summary of pyrolysis product yields for convection-only experiments

Heating rate	Plants	Tar yield ^a	Light gas yield ^a	Char yield ^a
180 °C s ⁻¹	Live	53-62	18-25	17-22
	Dead	55-62	17-24	17-23

^a wt% on a dry, ash-free (daf) basis

The results of Figure 5-1 and Figure 5-2 are summarized in Table 5-1. The results from the ANOVA statistical tool indicate that the difference between the means of tar yields from the pyrolysis of live plant species was statistically significant (p-value = 1×10^{-6}). A similar observation was made for the light gas yields (p-value = 0.001). However, in contrast with the light gas and tar yield data, the difference between the char yields from the pyrolysis of live plant species was not significant (p-value = 0.27). Similar to the live plant species, there was a statistically significant difference between the means of both light gas and tar yields from the pyrolysis of different dead plant species (tar p-value = 5×10^{-5} , light gas p-value = 1×10^{-4}). A difference between the means of char yields from the pyrolysis of dead plant species was observed; however, this difference was inconclusive (p-value = 0.06). Therefore, the plant type had a statistically significant effect on the light gas and tar yields, but not the char yield during the fast pyrolysis of plant species under the convection-only mode.

Live and dead dwarf palmetto showed the highest tar yield (62 wt%). The highest gas yield was observed during pyrolysis of live saw palmetto (24 wt%). The largest differences in both tar yield (2 wt%) and char yield (2 wt%) for a single species were found between live and dead wax myrtle. Darrow's blueberry and sparkleberry showed the largest difference in the gas yield (3 wt%) between the live and dead samples. The statistical analysis indicates that there was a

moderate evidence of difference between the means of tar yields from the pyrolysis of live vs. dead plant species (p-value = 0.03). Similar to the tar yield statistical analysis, there was a moderate evidence of difference between the means of light gas yields from the pyrolysis of live vs. dead plant species (p-value = 0.02). However, there was not a statistically significant difference between the means of char yields from the fast pyrolysis of live and dead plant species under the convection-only mode (p-value = 0.78). Therefore, the fuel condition (live vs. dead) had a statistically moderate effect on the light gas and tar yields, but not a significant effect on the char yield.

The results indicate that the plants from the same family (i.e., (i) live oak and water oak, (ii) inkberry and yaupon, and (iii) sparkleberry and Darrow's blueberry) showed very similar tar and char yields during the fast pyrolysis experiments. For example, tar yields for live inkberry and live yaupon were 59 and 61 wt%, respectively.

Variation in the pyrolysis product yields between different plant species may be caused by changes in the composition of plants as well as the interactions of the plant constituents (i.e., cellulose, hemicellulose, and lignin) (Zhou et al., 2014a). For instance, it has been reported that the interaction between lignin and cellulose causes an increase in the decomposition temperature of the plants (Hilbers et al., 2015). In another study, Wang et al. (2011) observed that bio-oil yield was noticeably decreased when a mixture of components was studied compared to the summation of bio-oil obtained from the individual components. However, there is not a general consensus among the researchers on the interactions between the plant constituents during pyrolysis. Some researchers have reported that there are none or only negligible interactions (Raveendran et al., 1996; Xie et al., 2013).

5.2 Light Gas Analysis

The major post-flame gases from the FFB were analyzed using the GC-TCD as N₂ (69.2 mole%), H₂O (19.9 mole%), CO₂ (6.1 mole%), CO (3.1 mole%), and H₂ (1.7 mole%). The background gases were subtracted in order to find the actual concentration of light gases from the pyrolysis of plant species. The measured compositions of light gas species for live and dead plants are shown in Figure 5-3 and Figure 5-4 on a dry (H₂O-free) basis, respectively. All other gas species seemed to be below the detection limit of the GC-TCD. Light gas species data are presented on a wt% basis in order to correlate with the light gas yield, which is also on a mass basis. Weight fraction (wt%) here means the ratio of the mass of an individual gas species to the total mass of gases collected in the gas collection bag. The GC instrument shows the yields of light gas species on mole% basis. The mole fraction of each gas species can be calculated by dividing the area under the corresponding peak by the total area under the peaks. The results of light gas analysis are summarized in Table 5-2. The results are the average of three tests. The error bars in the graphs, represent the $\pm 95\%$ confidence intervals for three experiments.

Carbon monoxide was the main component in the light gases on a wt% dry basis, followed by CO₂, CH₄, and H₂. The highest CO yield (63 wt%) was obtained from the pyrolysis of live saw palmetto. The statistical analysis indicates that there was moderate evidence of a difference between the means of CO yields from the pyrolysis of live plant species (p-value = 0.025). For dead plants, the statistical analysis indicates that there was convincing evidence of a difference between the means of CO yields (p-value = 3×10^{-4}). Little bluestem grass demonstrated the highest difference in CO yield (5.2 wt%) between its live and dead samples. Darrow's blueberry exhibited the next highest live vs. dead differences in CO yield at 3.3 wt%. The high CO yield is attributed to a decarbonylation reaction at high heating rates and temperatures (Gao et al., 2015).

Carbon dioxide was the second most abundant light gas. The highest weight fraction of CO₂ (35 wt%) was observed from the pyrolysis of live swamp bay. The statistical analysis shows that there was convincing evidence of difference between the means of CO₂ yields from the pyrolysis of live plant species (p-value = 0.001) and of dead plant species (p-value = 3×10⁻⁶). The largest difference in the weight percent of CO₂ between live and dead samples was observed in Darrow's blueberry (3.7 wt%), followed by wiregrass (3 wt%). At high heating rates and temperatures, CO₂ is formed mainly by lignin degradation. Formation of CO₂ is also due to a decarboxylation reaction, especially at lower temperatures (Gao et al., 2015).

Methane comprised about 6 to 11 wt% (dry) of light gases in live plants. This range was 7 to 12 wt% for dead plants. The highest wt% of CH₄ belonged to the pyrolysis of dead little bluestem grass (12 wt%). The largest difference in CH₄ composition between live and dead samples was found in little bluestem grass (3.7 wt%) and fetterbush (2.7 wt%). At high pyrolysis temperatures, CH₄ mainly forms due to the splitting of C-O bonds during lignin degradation as well as removal of methoxy groups from the aromatic rings (Xu et al., 2016).

H₂ yield varied between 1 to 2 wt% (dry). Among all the plant species, dwarf palmetto exhibited the highest H₂ weight percent difference (0.46 wt%) between the live and dead samples. The formation of H₂ is caused by dehydrogenation during pyrolysis. Hydrogen can form by two mechanisms at high pyrolysis temperatures: first, the decomposition of phenolic groups in lignin; and second, the secondary reactions of heavy gaseous hydrocarbons, which causes cracking and the rearrangement of aromatic bonds (Gao et al., 2015; Xu et al., 2016).

In most of the cases, weight fractions of CO and H₂ were slightly higher in the pyrolysis of live plants than that of the dead plants. In contrast, weight fractions of CO₂ and CH₄ were slightly higher in the pyrolysis of dead plants.

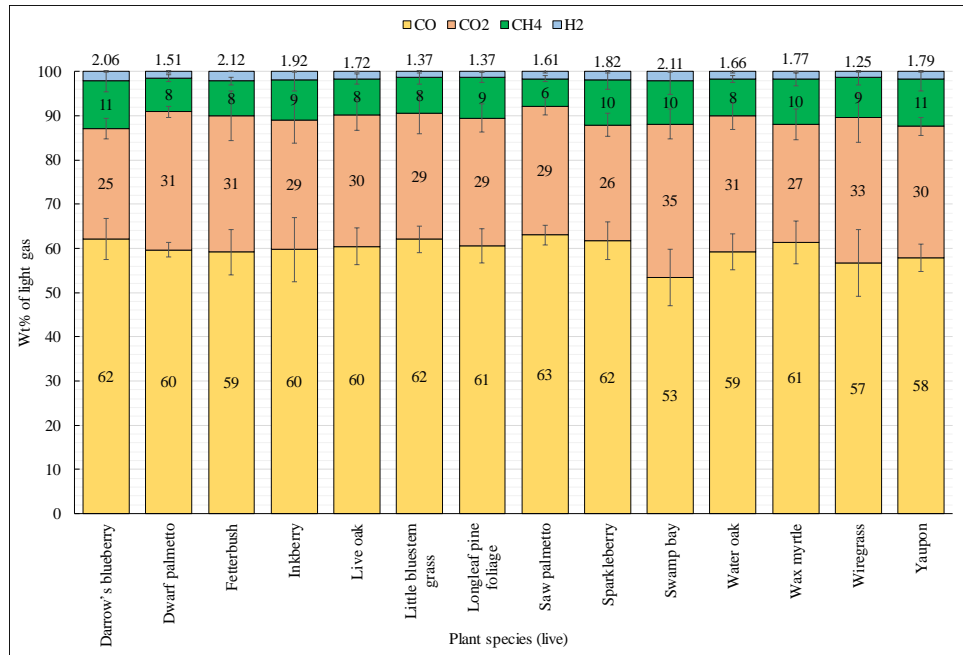


Figure 5-3. Light gas analysis for live plant species wt% on a dry basis

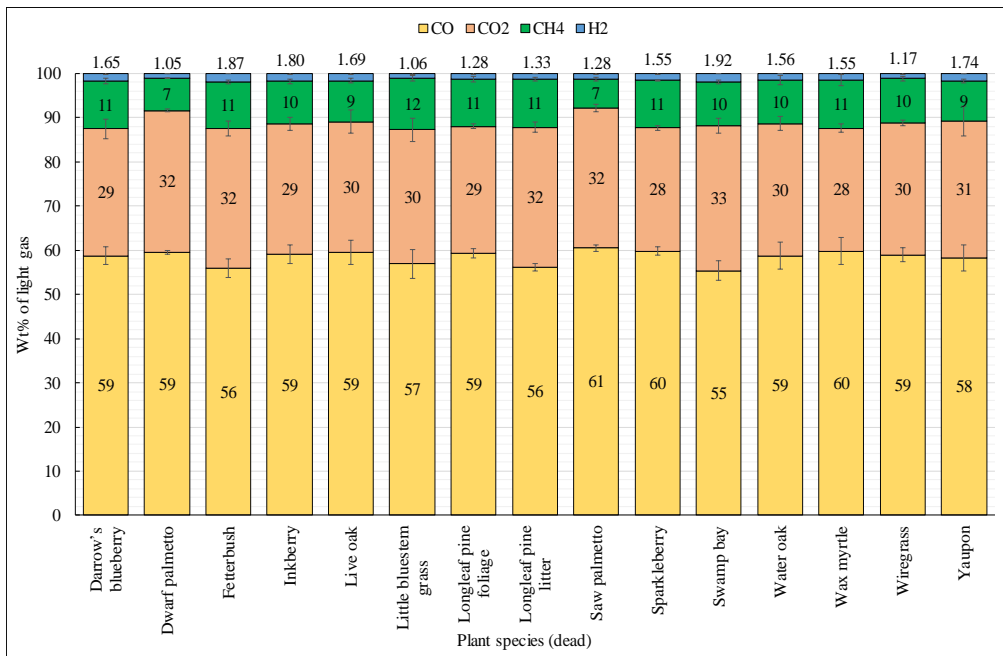


Figure 5-4. Light gas analysis for dead plant species wt% on a dry basis

The length of aging of longleaf pine needles did not have a large effect on any of the light gas yields (changes of less than 5 wt% for any major light gas species). From a combustion

perspective, the differences in the H₂ wt% among all species, live or dead, seemed minor. For the most part, it may be reasonable to assume an average composition of light gases (on a dry basis) for live or dead plant species.

Table 5-2. Summary of light gas analysis for convection-only (fast pyrolysis) experiments

Heating Rate	Plants	H ₂		CO		CO ₂		CH ₄	
		AVG ^a	RNG ^b	AVG	RNG	AVG	RNG	AVG	RNG
180 °C s ⁻¹	Live	1.7 ^c	1.3-2.1	59.8	53-63	29.5	25-35	8.9	6-11
	Dead	1.5	1.0-1.9	58.4	55-61	30.2	28-33	9.8	7-12

^a Average

^b Range

^c wt% on a dry light gas basis

5.3 Tar Analysis

Tar is defined here as the mixture of pyrolyzed hydrocarbons that condensed in the cold trap. Tar generally consists of a complex mixture of aliphatic and 1- to 5-ring aromatic compounds (Li and Suzuki, 2009; Phuphuakrat et al., 2010; Shen et al., 2016). During the fast pyrolysis experiments, the liquid products (tars) which were condensed and collected in the ice bath were brownish. The tars then were extracted by dichloromethane as a solvent and analyzed using GC-MS. The majority of the identified tar from high heating rate pyrolysis included compounds that were composed of 1- to 5-ring aromatics with very few attachments on their rings. Figure 5-5 illustrates the chromatogram of tar analysis for live inkberry that was pyrolyzed in the FFB apparatus and then analyzed by the GC-MS instrument. This is one example of more

than 90 tar analysis experiments that were performed for the pyrolysis of live and dead plants using the convection-only mode. Table D-1 shows a list of the tar compounds identified by GC-MS during the fast pyrolysis of live and dead plant species in the FFB apparatus. The results of the tar analysis from the fast pyrolysis of live versus dead plant species using convective heat transfer are shown in Figure 5-6. The identified tar compounds and their mole fractions are shown in the figures. Mole fractions of identified tar compounds were obtained by dividing their relative peak area to the total area of the peaks. Mole fractions are shown because there may be some compounds that were too heavy to detect in the GC-MS system. The results of tar analysis for live and dead longleaf pine foliage, along with longleaf pine litter (pine straw), are shown in Figure 5-6 (g). For brevity, tar species with less than 0.1 mole% are not shown in this figure.

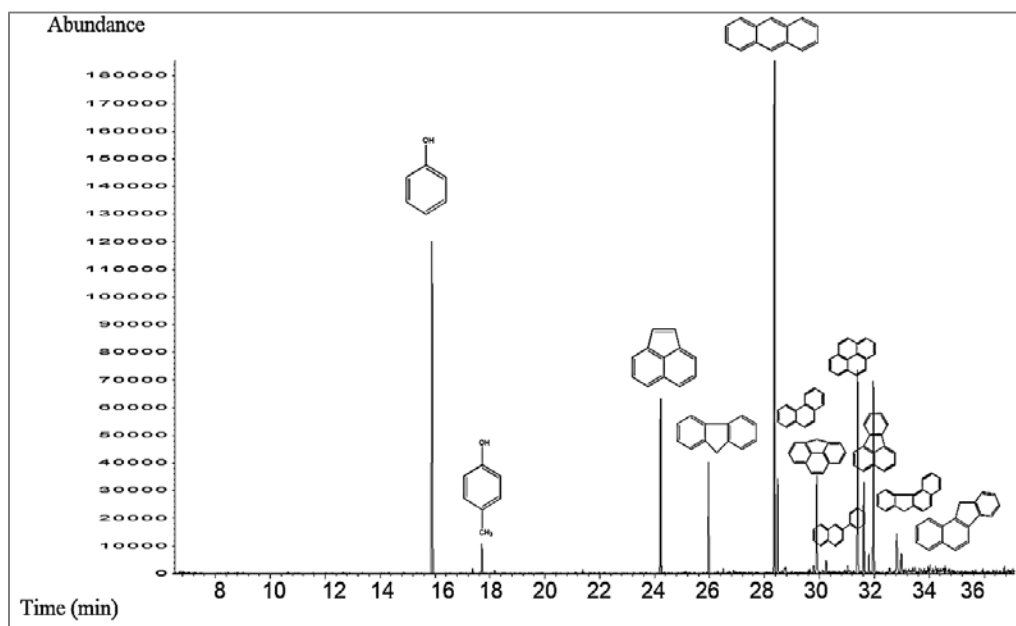
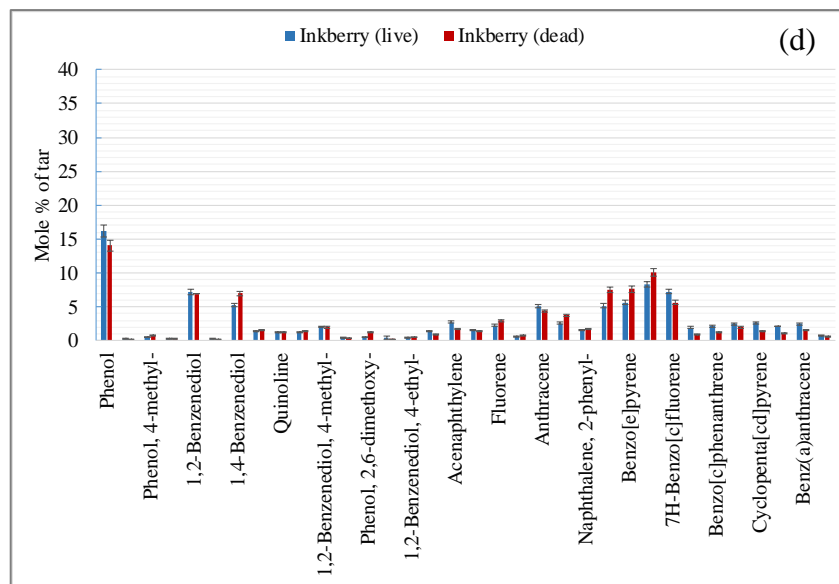
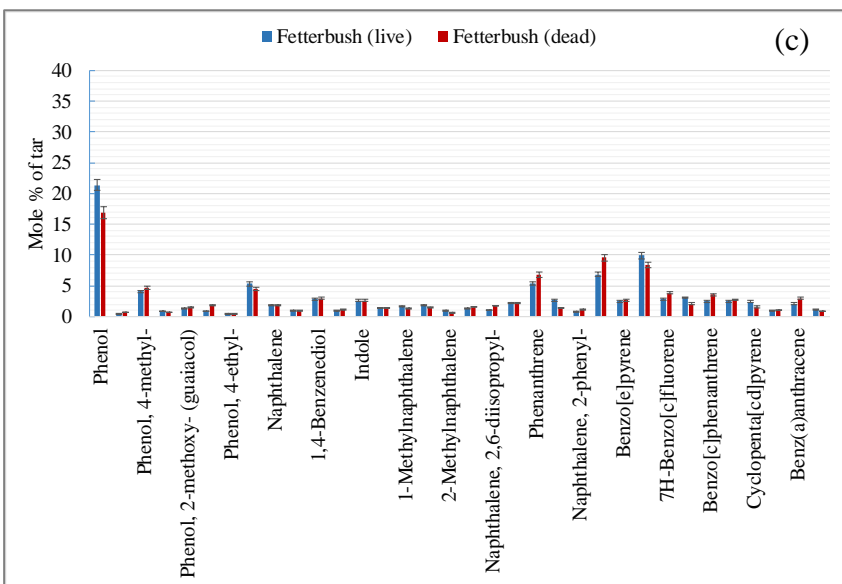
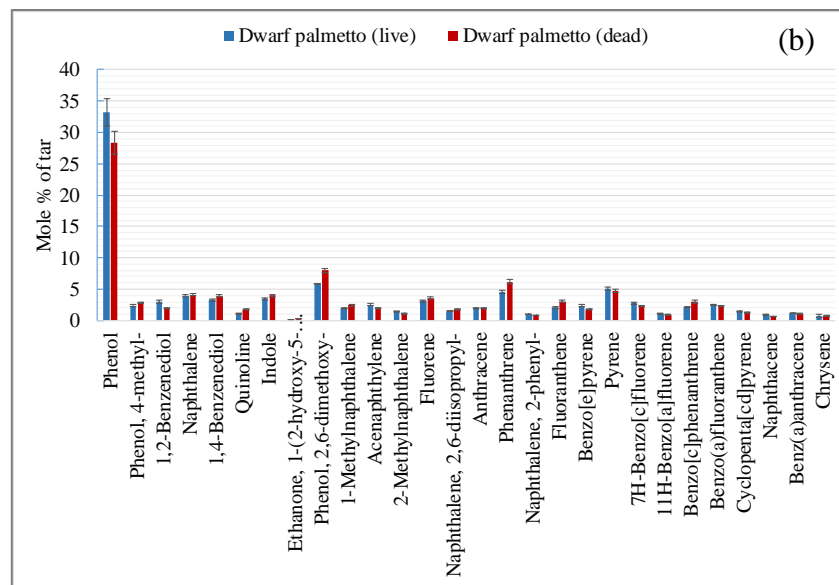
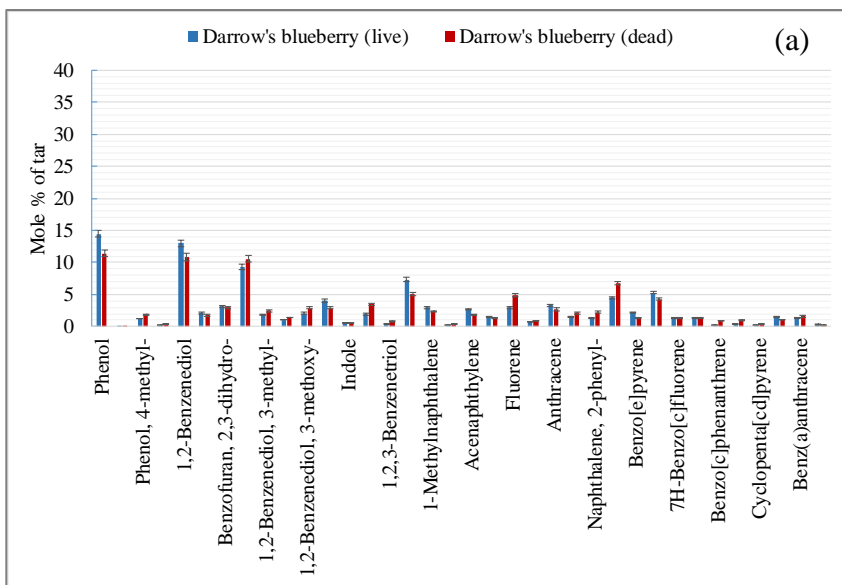
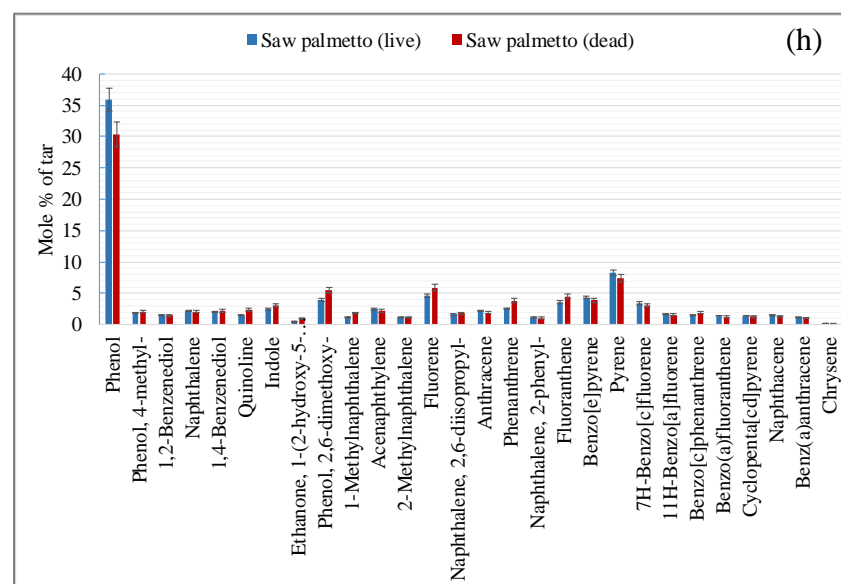
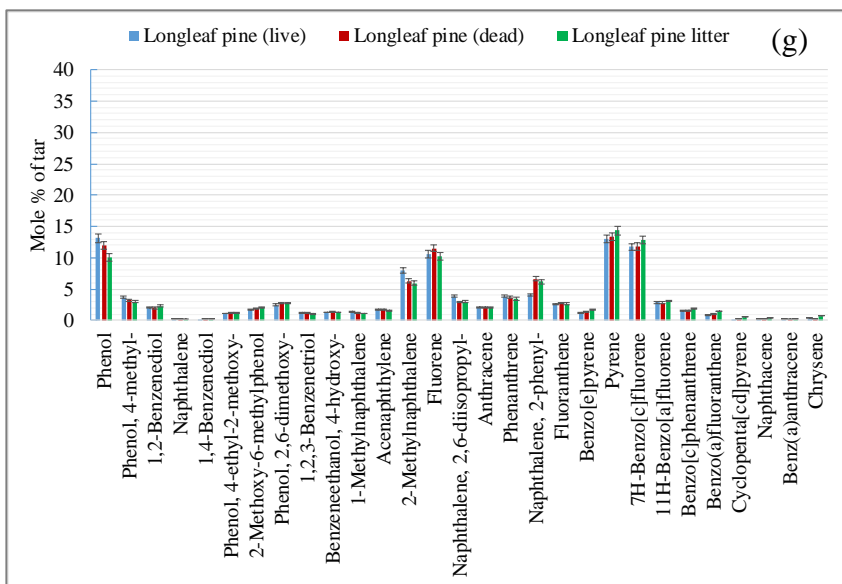
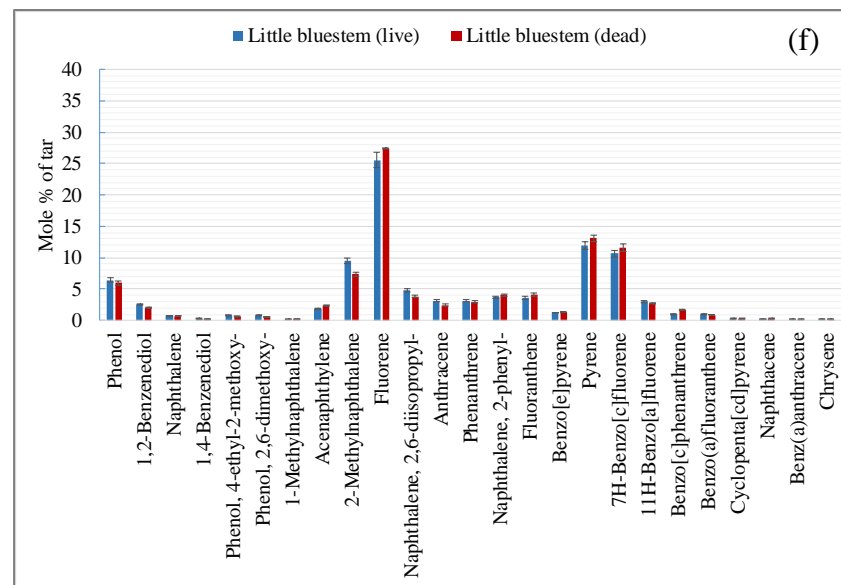
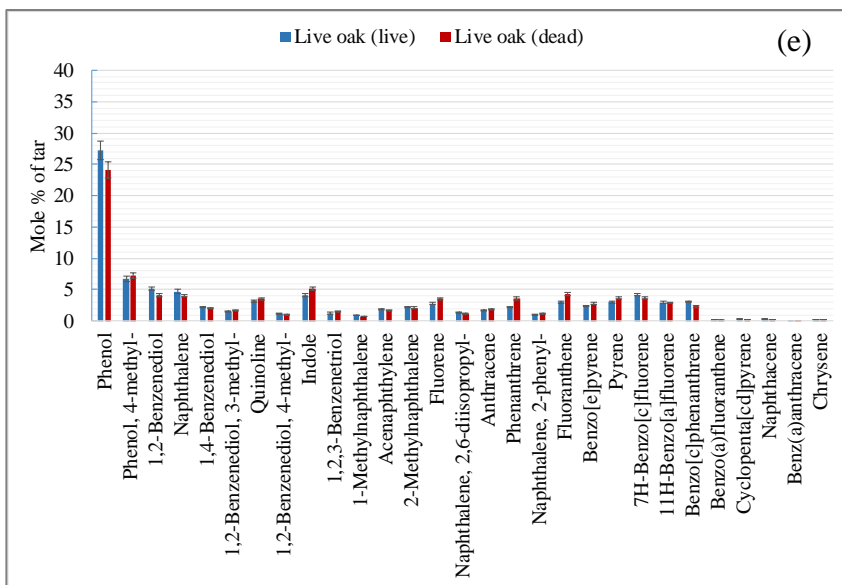
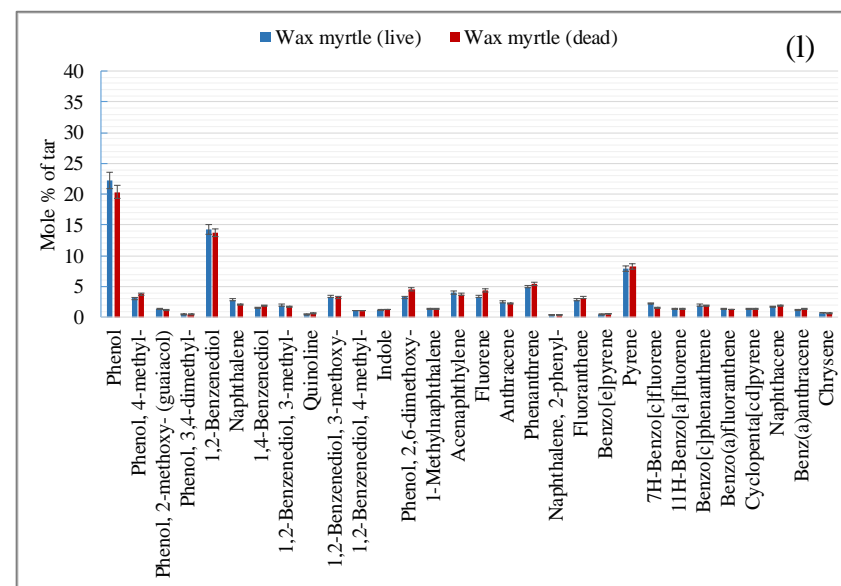
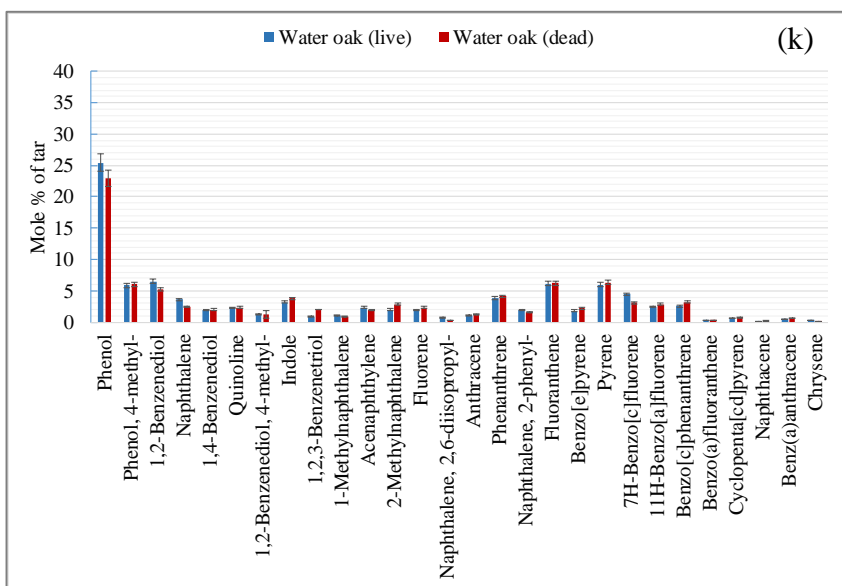
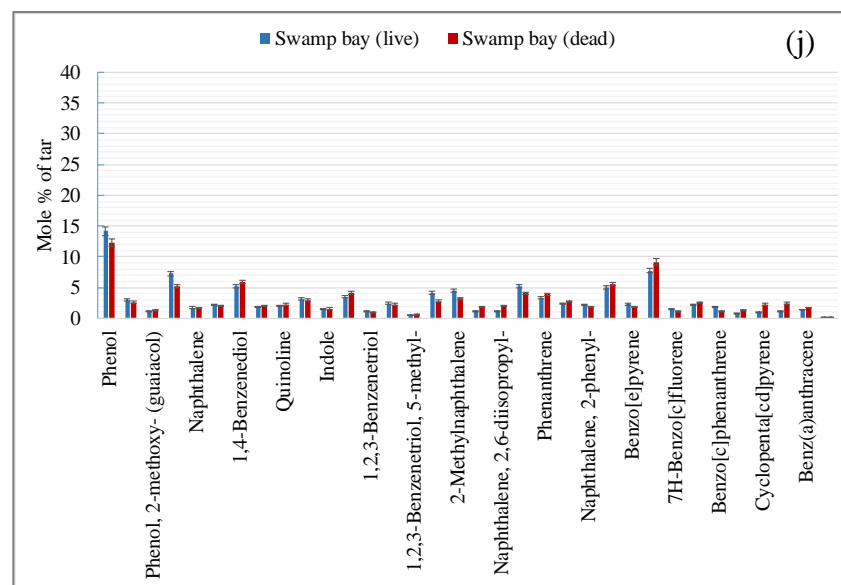
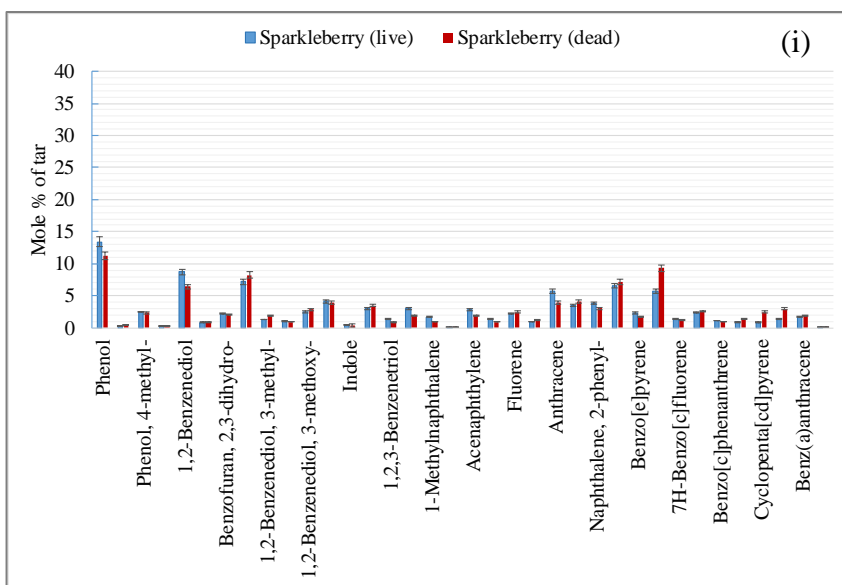


Figure 5-5. GC-MS chromatogram of tar from fast pyrolysis of live inkberry







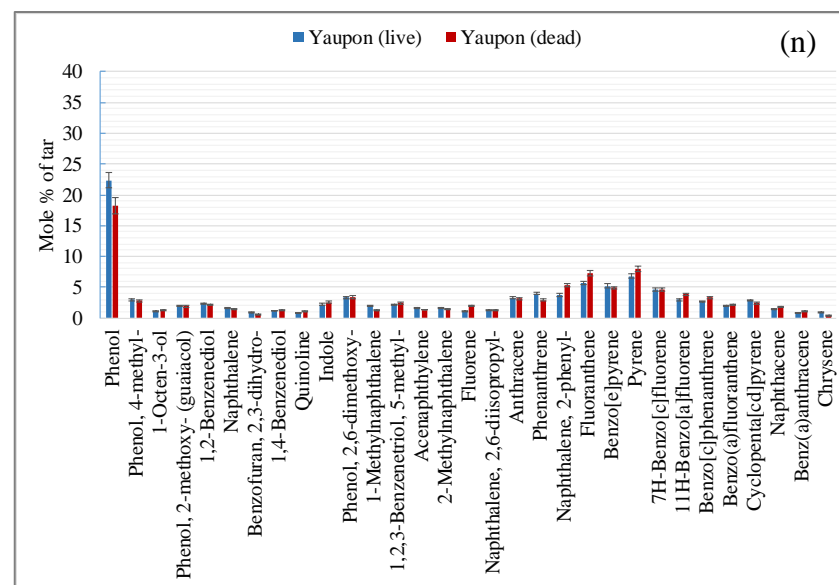
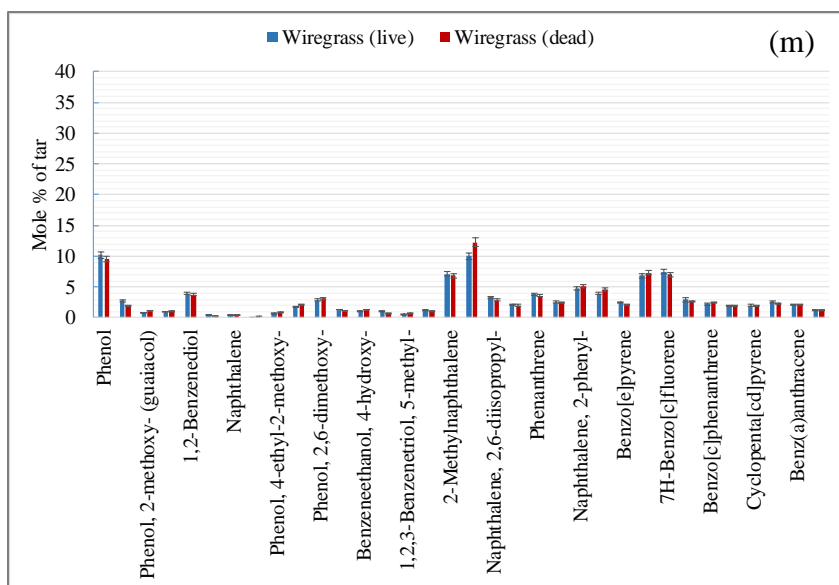


Figure 5-6. Analysis of tar compounds for convection-only (fast pyrolysis) experiments

During the fast pyrolysis of both live and dead plants, using convective heat transfer, 1- to 5-ring compounds were observed with very few attachments on their rings. Phenol, naphthalene, fluorene, anthracene, phenanthrene, fluoranthene, and pyrene were the major identified tar compounds. Differences in tar composition were observed for each plant species. For example, in tar analysis, phenol ranged from 6 mole% in dead little bluestem grass to 36 mole% in live saw palmetto. Saw palmetto and dwarf palmetto, showed the highest phenol formation at 36 and 33 mole%, respectively. The grasses (little bluestem and wiregrass) and needle-like species (i.e., longleaf pine) exhibited the lowest concentrations of phenol with 6, 10, and 13 mole%, respectively. In grasses, higher concentrations of fluorene (12 to 27 mole%) and pyrene (7 to 14%) were observed compared to the rest of the plant species.

Phenolic compounds were generally the main constituents of tar. Phenolic compounds, such as 4-methyl phenol, 2-methoxy phenol (guaiacol), and 3,4-dimethyl phenol, mainly form by the depolymerization of lignin building blocks (Wang et al., 2013; Xu et al., 2016). Lignin decomposition leads to the formation of single-ring, low molecular weight aromatics (Farak et al., 2014; Moore et al., 2015).

Figure 5-7 indicates a proposed mechanism of lignin decomposition and the formation of polycyclic aromatic hydrocarbon (PAH) precursors (Xiao and Yang, 2013; Henrich et al., 2016). This mechanism explains the presence of the many phenolic compounds observed in Figure 5-6.

The presence of multi-ring compounds in Figure 5-6 may be related to the formation of naphthalene from benzene (with phenylacetylene as an intermediate via hydrogen abstraction acetylene addition) as shown in Figure 5-8 (Zhou et al., 2015). This mechanism is usually important in combustion of light gases, such as methane. However, due to the low concentration of acetylene usually observed in biomass pyrolysis, and the presence of many 1-ring compounds,

the formation of naphthalene and higher ring compounds may be due to polymerization reactions, where a hydroxyl group is released, forming a radical which can then bond with another aromatic compound.

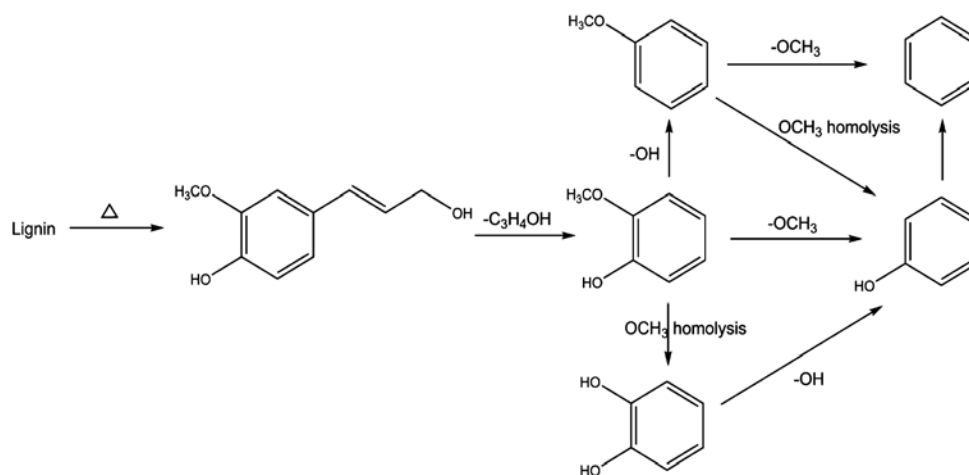


Figure 5-7. Mechanisms of PAH precursor formation from lignin decomposition

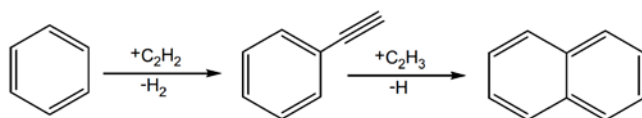


Figure 5-8. Mechanism of formation of naphthalene from benzene (Zhou et al., 2015)

The heavier polycyclic aromatic hydrocarbons (PAHs) of 3+ rings in Figure 5-6 can form from naphthalene via various mechanisms. For example, acenaphthylene can evolve by the addition of acetylene to naphthalene (Palma, 2013a). The presence of furans (and their derivatives) in tar is mainly believed to be from hemicellulose, and the evolution of carbonyl and carboxylic groups are from the pyrolysis of cellulose (Maggi and Delmon, 1994; Ku and Mun, 2006). These mechanisms may explain the presence of the tar species in Figure 5-6 with an oxygen in their ring or $\text{C}=\text{O}$ groups.

5.4 Distribution of Functional Groups in Tar

Figure 5-9 shows the distribution of functional groups in tar for four plant species as an example of more than 90 tar analysis experiments that were performed for the pyrolysis of live and dead vegetation. These plant species were chosen to be representative of palmetto-type, broadleaf, grass, and needle-like species.

There was only a small difference between the distribution of functional groups in the tar produced from the pyrolysis of live and dead plant species. For example, phenols comprised 48 and 45 mole% of the tar from live and dead dwarf palmetto, respectively. Three-ring aromatics comprise 13 mole% of the tar from live dwarf palmetto vs. about 15 mole% from dead dwarf palmetto. This trend of small differences in the yields of functional groups for live vs. dead samples was observed in all plant species.

For the majority of the live plants, slightly more phenol, anthracene, pyrene, and 1,2-benzenediol formed during pyrolysis. On the other hand, slightly more 1,4-benzenediol, fluorene, phenanthrene, and fluoranthene evolved during the pyrolysis of dead plants. In contrast, when comparing tar compounds from different plant species a statistically significant difference in the distribution of functional groups was observed. For live inkberry (a broad-leaf plant), the tar consisted of more than 35 mole% phenolic compounds and 60 mole% polycyclic aromatic hydrocarbons, which included about 4% 2-ring, 14% 3-ring, 32% 4-ring, and 10% 5-ring aromatics. For needle-like plants such as live longleaf pine, the functional group distribution was noticeably different from live broad-leaf plants. In live longleaf pine, about 26 and 73 mole% of the tar were phenols and polycyclic aromatics, respectively. In contrast, phenols and polycyclic aromatics were 11 and 89 mole% in little bluestem grass, which seems to be evidence of different distributions of functional groups in tars evolved from the pyrolysis of different plant species.

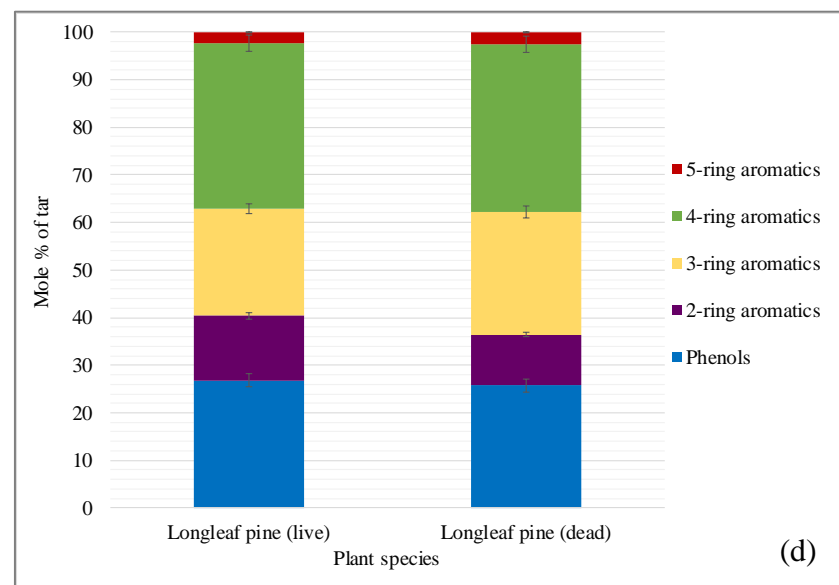
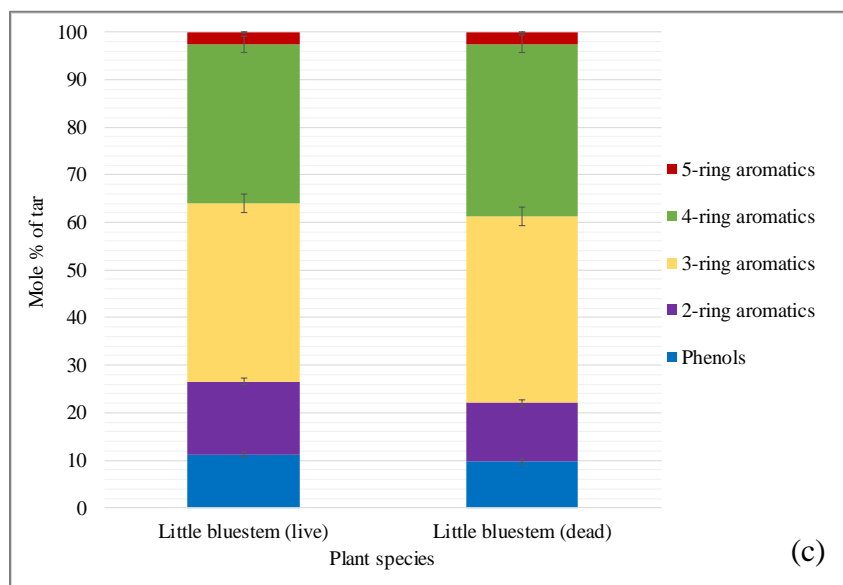
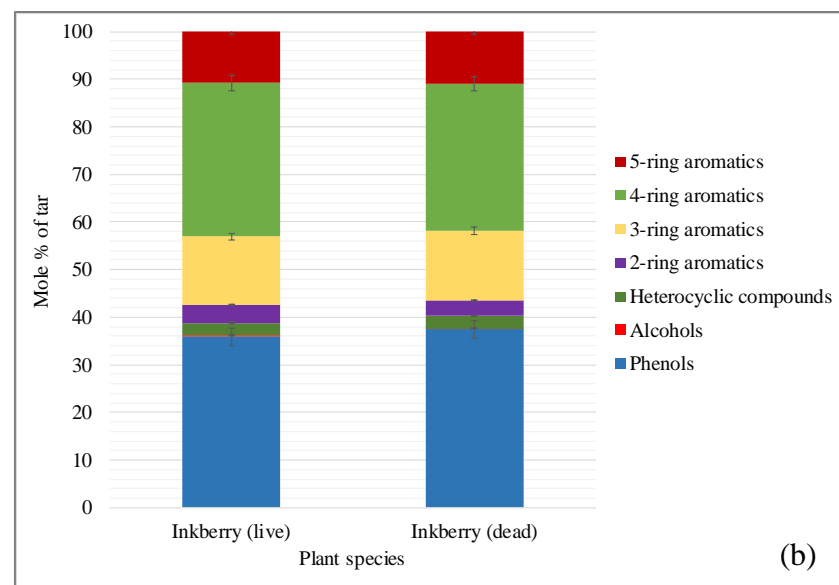
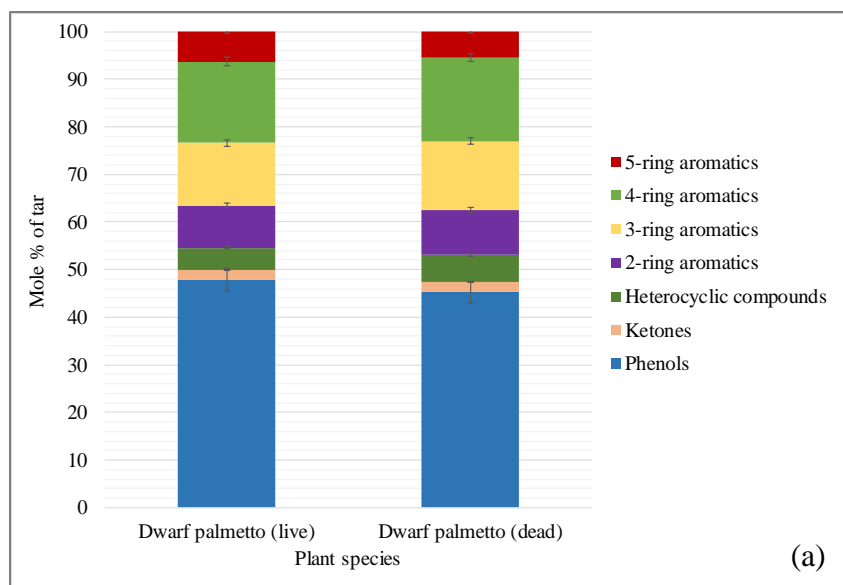


Figure 5-9. Distribution of functional groups in tar for live and dead plants

5.5 Mass Loss over Time

Figure 5-10 shows the change of the mass of live and dead inkberry over time. A similar trend was observed for the other plants (as shown in Appendix E). Live plants lost their initial mass with a slower rate and the process of pyrolysis took longer to complete when compared to dead plants. This difference in the rate of mass loss can be attributed to the presence of higher moisture in the structure of live plants. Significant amounts of moisture may still be in the leaf sample during pyrolysis at high heating rate (McAllister et al., 2012; Finney et al., 2013).

It has been proposed that in live plants, the complete release of water does not occur until the cellular structure has been broken down. In contrast with live plants, this water is not bound within the cells of dead plants, from which water is released much earlier (Prince and Fletcher, 2014).

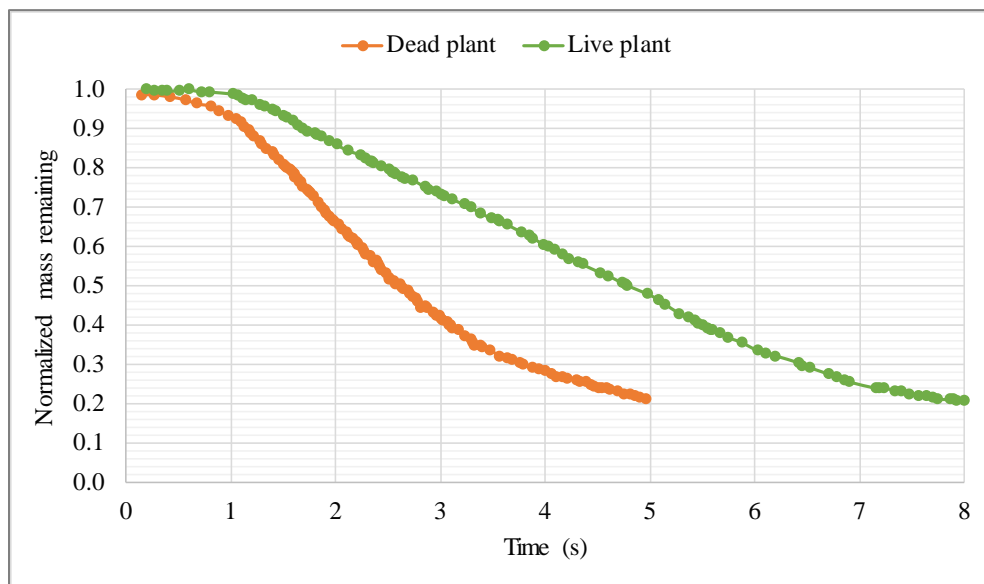


Figure 5-10. Mass loss over time during fast pyrolysis of live and dead inkberry

5.6 Fuel Surface Temperature

Infrared images taken using an IR camera during the pyrolysis of the leaves indicate that the leaves did not heat isothermally under convective heating (as shown in Figure 5-11). At the beginning of the experiments, there were temperature gradients within the leaves; the edges of the leaves had higher temperatures than the middle of the leaves. As time passed, the heat traveled from the edges towards the center until the temperature was uniform across the entire leaf.

Non-uniformity of the temperature within the leaves may be caused by: (1) the formation of a convective boundary layer across the surface of the leaves that reduces the heat transfer from the hot gases to the surface of the leaves; (2) characteristic differences between the edges and the centers of the leaves, such as moisture content and thickness. A similar observation has been reported by Prince and Fletcher (2014).

Live plants started to pyrolyze from the edges and proceed towards the center. The temperature of the center increased over a period of time until the temperature became uniform across the plant. Plants with smaller thickness and a lower moisture content reached a uniform temperature within a shorter time period. The live plants were found to have similar heating patterns during the pyrolysis experiments. The maximum fuel surface temperature during the convection-only experiments was measured to be 750 °C.

5.7 Summary and Conclusions

In this chapter, the fast pyrolysis of live and dead plant species was studied using a fuel-rich FFB apparatus operated under only convective heat transfer. The yields and the compositions of pyrolysis products were investigated using GC-MS for analysis of the tars, and GC-TCD for analysis of the light gases. The main conclusions are listed as follows:

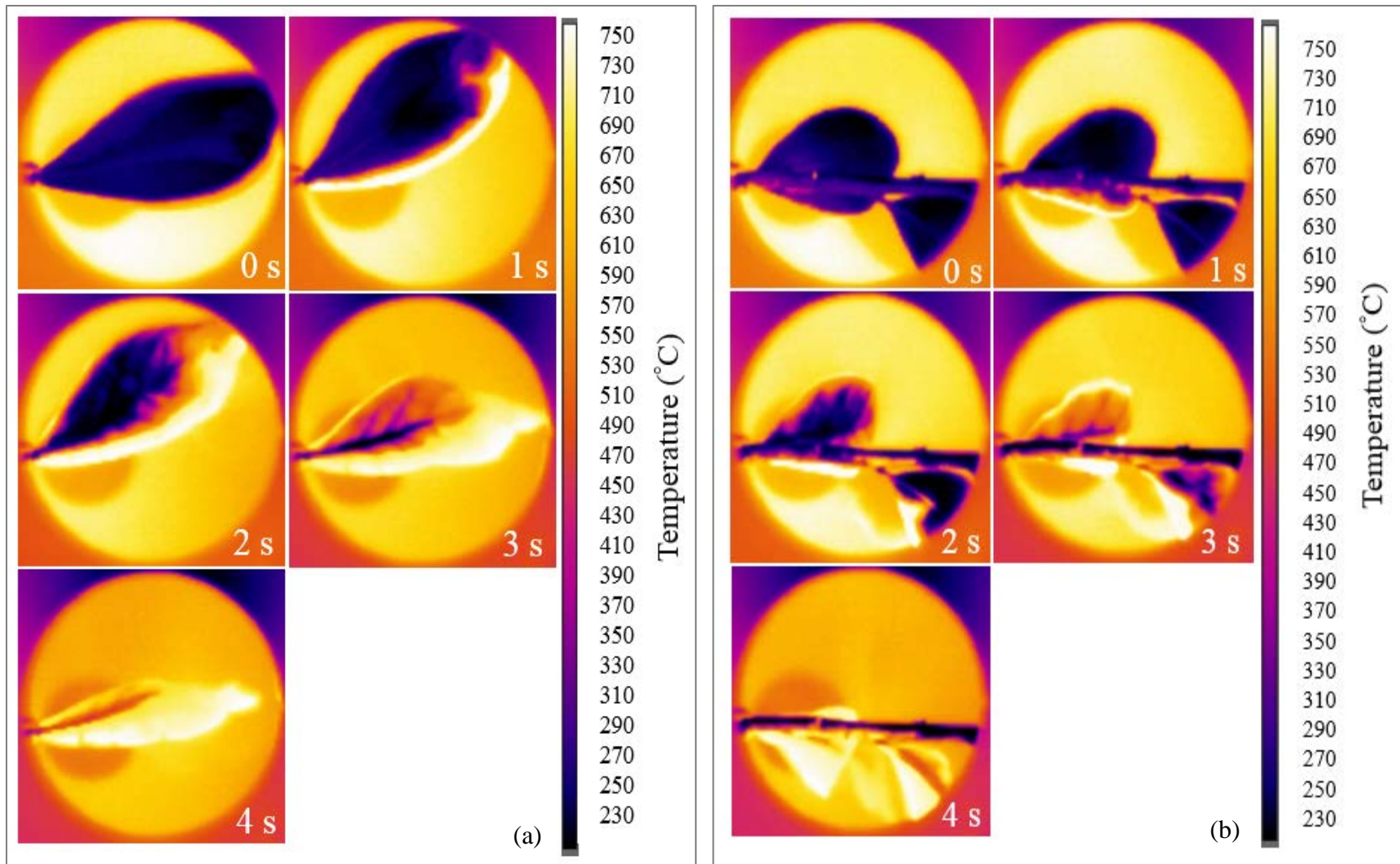


Figure 5-11. Fuel surface temperature over time for convection-only experiments: (a) single-leaf live inkberry, (b) multi-leaf live inkberry

- 1- Tar yields for live plants ranged from 53 to 62 wt% (dry basis), and corresponding light gas yields ranged from 18 to 25 wt%.
- 2- There was convincing statistical evidence of a difference between the means of tar and light gas yields from the pyrolysis of live plant species. However, in contrast with the light gas and tar yield data, the difference between the char yields from the pyrolysis of live plant species was not significant. Similar to the live plant species, there was convincing evidence of difference between the means of both light gas and tar yields from the pyrolysis of different dead plant species. A difference between the means of char yields from the pyrolysis of dead plant species was observed; however, this difference was statistically inconclusive. Therefore, the plant type had a statistically significant effect on the light gas and tar yields for both live and dead samples during fast pyrolysis under the convection-only mode, but not the char yield.
- 3- There was moderate evidence of a difference between the means of tar yields from the pyrolysis of live vs. dead plant species. Similar to the tar yield statistical analysis, there was moderate evidence of a difference between the means of light gas yields from the pyrolysis of live vs. dead plant species. However, there was not a statistically significant difference between the means of char yields from the fast pyrolysis of live vs. dead plant species under the convection-only mode.

The fuel condition (live vs. dead) had a statistically moderate effect on the light gas and tar yields, but not a significant effect on the char yield.
- 4- Carbon monoxide was the main component in the light gases on a wt% dry basis, followed by CO₂, CH₄, and H₂. For most plant species, weight fractions of CO and H₂ were slightly higher in the pyrolysis of live plants than in that of the dead plants.

In contrast, weight fractions of CO₂ and CH₄ were slightly greater in the pyrolysis of dead plants.

- 5- Most plant species from the same type of plant (broadleaf, grass, or needle-like) showed only small differences in the yields of the light gases (CO, CO₂, CH₄, and H₂).
- 6- The pyrolysis products observed at this temperature and heating rate appear to have experienced secondary pyrolysis. Tar compounds from high heating rate pyrolysis of both live and dead plants consisted of 1- to 5-ring compounds with very few attachments on the rings. Major tar species observed included phenol, naphthalene, fluorene, anthracene, phenanthrene, fluoranthene, and pyrene.
- 7- For a given plant species, there was only a small difference between the distribution of functional groups in the tar from live and dead plants. For the majority of the live plants, slightly more phenol, anthracene, pyrene, and 1,2-benzenediol formed during pyrolysis. On the other hand, slightly more 1,4-benzenediol, fluorene, phenanthrene, and fluoranthene evolved during the pyrolysis of dead plants.
- 8- Tar compounds from different plant species exhibited a significant difference in distribution of functional groups. The greatest concentrations of phenolic compounds were observed in the broadleaf species, with especially high concentrations in the palmetto species. However, for needle-like plants such as longleaf pine, fewer phenolic compounds were observed in the tar but more 3-ring compounds were observed.

The tars from grass species had very few phenolic compounds, but increased levels of 3- and 4-rings compounds.
- 9- The analysis of change of mass of fuel over time indicated that intact live plant samples lost their initial mass with a slower rate compared with dead plants, which caused the pyrolysis

of live plants takes longer to complete. The slower mass release for live plants is due to moisture evaporation.

10- The analysis of fuel surface temperature showed that the leaves do not heat isothermally under convective heating. There were temperature gradients within the leaves at the beginning of the experiments; the edges of the leaves had higher temperatures than the middle of the leaves. As time passed, the heat traveled from the edges towards the center until the temperature was uniform across the leaves.

6 COMPARISON OF SLOW AND FAST PYROLYSIS OF LIVE AND DEAD VEGETATION³

During wildland fires, slow heating rate pyrolysis occurs during preheating and/or smoldering of plant material. High heating rate pyrolysis exists in the flame region. Comparing slow and fast pyrolysis of the plants enables development of more accurate models over a wide range of temperatures and heating rates (Safdari et al., 2018a). The focus of this chapter is to conduct a comparative study of the slow and fast pyrolysis of live and dead plant species. The slow and fast pyrolysis experiments were performed using a pyrolyzer (Amini et al., 2019) and a flat-flame burner (FFB) (Safdari et al., 2018b) apparatus, respectively.

The pyrolyzer apparatus was operated at a slow heating rate of $0.5\text{ }^{\circ}\text{C s}^{-1}$ and an operating temperature of $500\text{ }^{\circ}\text{C}$. The FFB apparatus was operated at a high heating rate of $180\text{ }^{\circ}\text{C s}^{-1}$ and a temperature of $765\text{ }^{\circ}\text{C}$. The yields and compositions of the pyrolysis products during the slow and fast pyrolysis experiments were analyzed in detail using a gas chromatograph equipped with a mass spectrometer (GC-MS) for the analysis of tars and a gas chromatograph equipped with a thermal conductivity detector (GC-TCD) for the analysis of light (non-condensable) gases.

6.1 Pyrolysis Product Yields

Pyrolysis temperature, heating rate, fuel type, reactor type, sweep gas flow rate, and sample residence time in the reactor play important roles in the yields and the composition of pyrolysis

³ The results of this chapter have been submitted to Fuel (Safdari et al., 2018a)

products (Sensoz and Can, 2002; Debdoubi et al., 2006; Tsai et al., 2006; Putun et al., 2007; Ben and Ragauskas, 2013). The effects of these process conditions on the distribution of pyrolysis products have been investigated by previous researchers (Williams and Besler, 1992; Bilbao et al., 1994; Williams and Besler, 1996; Bridgwater et al., 1999; Cetin et al., 2005; Debdoubi et al., 2006; Tsai et al., 2006; Butterman and Castaldi, 2010; Demiral et al., 2012; Aho et al., 2013; Shen et al., 2015).

Table 6-1 shows the yields of pyrolysis products (i.e., tar, light gases, and char) for live and dead plant species in both slow and fast pyrolysis experiments. Furthermore, to have a better visual comparison of the yields of pyrolysis products, the data are also presented in Figure 6-1 (gas yield data), Figure 6-2 (tar yield data), and Figure 6-3 (char yield data) for live plants. A similar trend was observed for dead plant species (as shown in Appendix F). The results are the average of three experiments and the error bars represent $\pm 95\%$ confidence intervals.

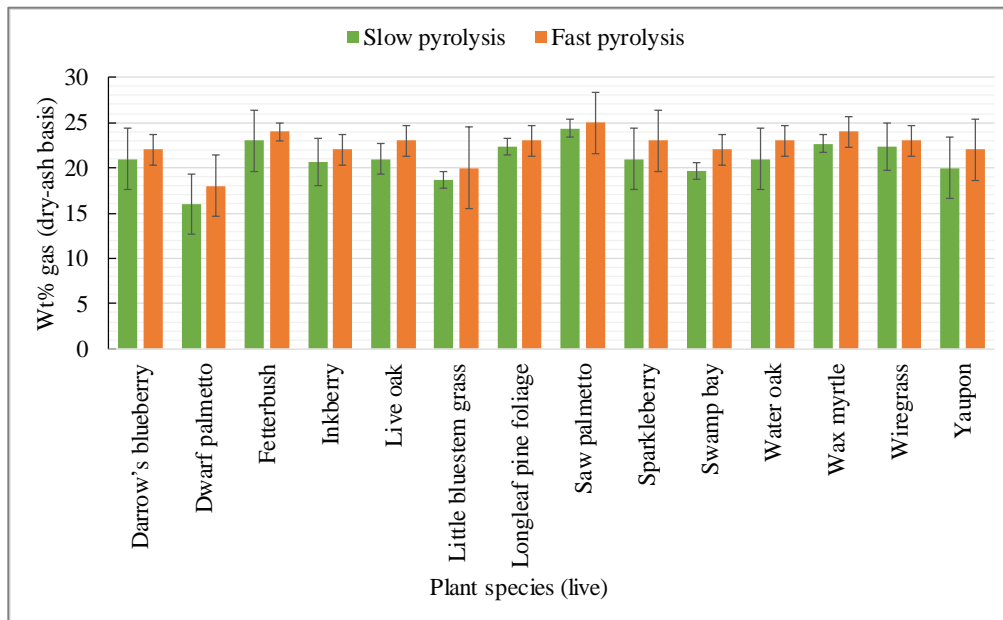


Figure 6-1. Gas yield of live plant species on a dry, ash free (daf) basis

Table 6-1. Pyrolysis product yields of live and dead plant species on a dry, ash-free (daf) wt% basis

Plant name	Live Plants						Dead Plants					
	Slow Pyrolysis			Fast Pyrolysis			Slow Pyrolysis			Fast Pyrolysis		
	Tar Yield ^a	Gas Yield ^a	Char Yield ^a	Tar Yield ^a	Gas Yield ^a	Char Yield ^a	Tar Yield ^a	Gas Yield ^a	Char Yield ^a	Tar Yield ^a	Gas Yield ^a	Char Yield ^a
Darrow's blueberry	47	21	32	57	22	21	48	18	35	59	19	22
Dwarf palmetto	54	16	30	62	18	20	55	16	25	62	17	21
Fetterbush	45	23	32	54	24	22	45	21	34	56	23	21
Inkberry	50	21	29	59	22	19	50	18	31	60	21	19
Little bluestem grass	52	19	29	61	20	19	54	18	28	62	19	19
Live oak	45	21	34	56	23	21	46	19	35	58	21	21
Longleaf pine foliage	51	22	27	57	23	20	51	22	27	58	23	19
Longleaf pine litter	n/a [*]	n/a	n/a	n/a	n/a	n/a	52	20	28	60	23	17
Saw palmetto	45	24	31	53	25	22	45	21	34	55	23	22
Sparkleberry	45	21	34	55	23	22	45	19	36	57	20	23
Swamp bay	50	20	31	58	22	20	50	19	31	59	21	20
Water oak	47	21	32	57	23	20	48	21	31	57	24	19
Wax myrtle	44	23	33	55	24	21	45	22	33	57	24	19
Wiregrass	51	22	27	59	23	18	51	18	31	60	21	19
Yaupon	52	20	28	61	22	17	54	20	26	62	21	17

^a wt% on a dry, ash-free (daf) basis

* n/a means not applicable

As shown in Figure 6-1, the gas yield from the fast pyrolysis was always higher for each species. The results from the ANOVA statistical analysis indicate that there was a suggestive, but inconclusive evidence of a difference between the means of light gas yields from the slow and fast pyrolysis experiments (p -value = 0.05). Saw palmetto showed the highest gas yield during both slow and fast pyrolysis experiments (24 and 25 wt%, respectively). Swamp bay showed the largest difference (2.3 wt%) between the gas yields from slow and fast pyrolysis experiments. Higher tar yields and lower char yields were obtained for all plant species from fast pyrolysis experiments, as shown in Figure 6-2 and Figure 6-3.

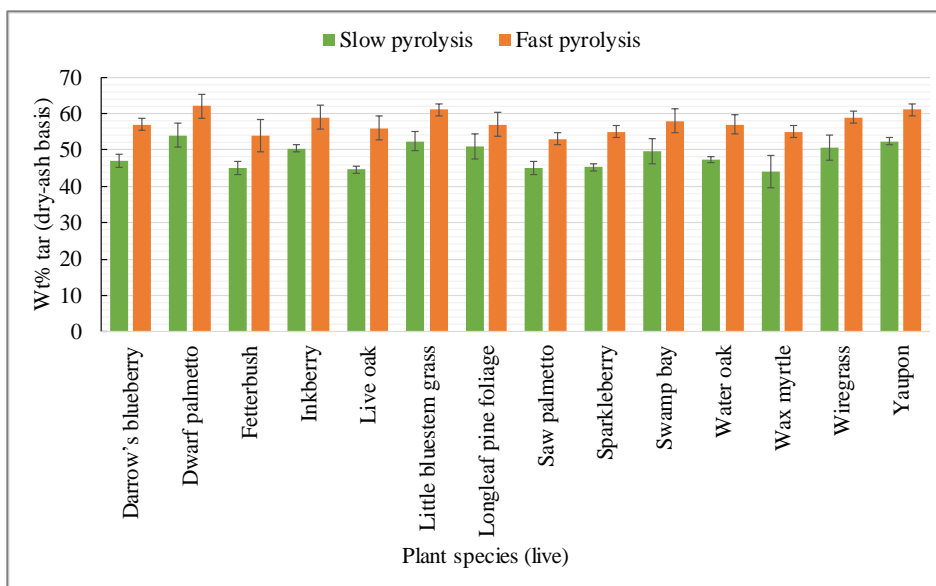


Figure 6-2. Tar yield of live plant species on a dry, ash free (daf) basis

In contrast with the light gas yield results, for most plant species, the tar and char yields measured for the two heating rates showed non-overlapping confidence intervals, indicating that there was convincing evidence of differences between the results from slow and fast pyrolysis experiments (tar p -value = 4×10^{-8} , char p -value = 3×10^{-13}). Dwarf palmetto showed the highest

tar yield during both slow and fast pyrolysis experiments (54 and 62 wt%, respectively). Wax myrtle showed the largest difference (11 wt%) between the tar yields from slow and fast pyrolysis experiments. Live oak and sparkleberry showed the highest char yield (34 wt%) in slow pyrolysis experiments, followed by wax myrtle (33 wt%) and water oak (32 wt%). These plant species also had the highest char yield during fast pyrolysis experiments. Like the tar yield results, wax myrtle showed there was convincing evidence of difference between the char yields (12 wt%) from slow and fast pyrolysis experiments. Furthermore, the results indicate that the plants from the same family (i.e., (i) live oak and water oak, (ii) inkberry and yaupon, and (iii) sparkleberry and Darrow's blueberry) showed very similar tar and char yields during both slow and fast pyrolysis experiments.

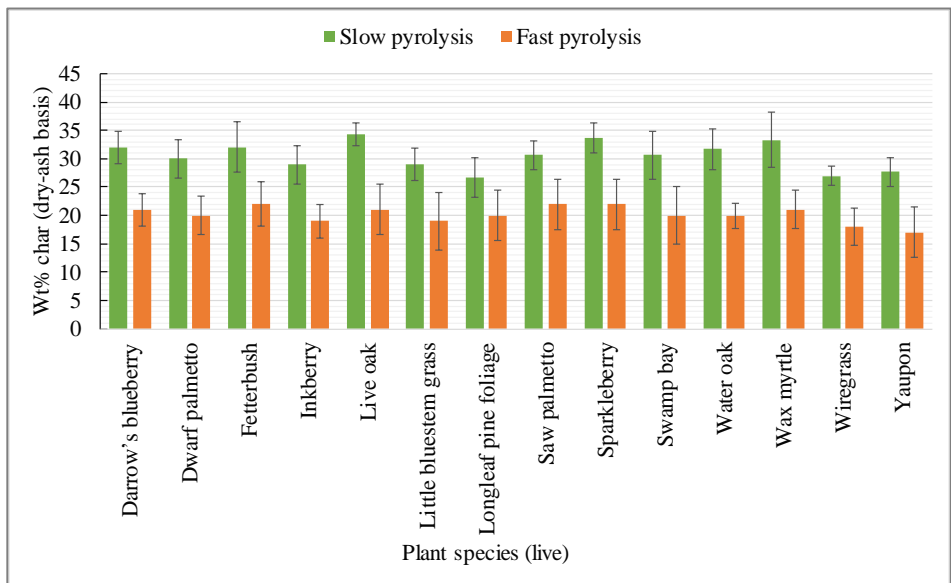


Figure 6-3. Char yield of live plant species on a dry, ash free (daf) basis

These results indicate that heating rate and operating temperature have a significant impact on the yields of pyrolysis products, especially the tar and char yields. Previous researchers who

have studied pyrolysis of biomass in various systems have reported similar observations (Prins et al., 2006; Bridgwater, 2012; Adrados et al., 2013; Agirre et al., 2013; Solar et al., 2016).

The ranges of pyrolysis product yields are shown in Table 6-2. The tar yields were 8 to 9 wt% higher in fast pyrolysis experiments, while the light gas yields were only 2 to 3 wt% higher in the high heating rate experiments. The increased tar and light gas yields at high heating rates resulted in lower char yields by 10 to 12 wt%. The average total volatile yields (i.e., tar plus light gas) for all live and dead plant species, increased from 69 wt% in the slow pyrolysis to 81 wt% for the fast pyrolysis.

Table 6-2. Summary of pyrolysis product yields for slow and fast pyrolysis experiments

Heating Rate	Plants	Tar yield ^a	Light gas yield ^a	Char yield ^a
0.5 °C s ⁻¹	Live	44-54	16-24	27-34
	Dead	45-55	16-22	25-36
180 °C s ⁻¹	Live	53-62	18-25	17-22
	Dead	55-62	17-24	17-23

^a wt% on a dry, ash-free basis

For the fast pyrolysis experiments, the increased heating rate was expected to increase the tar yield, but the increased temperature was expected to decrease the tar yield and increase the gas yield, due to further cracking of char and the occurrence of secondary pyrolysis reactions (Horne and Williams, 1996; Zanzi et al., 2002; Onay and Kockar, 2003; Bridgwater, 2012).

In addition to the heating rate and temperature, residence time of the fuel in the reaction zone also has a significant effect on the yields of pyrolysis products. However, the effect of the residence time was not included in the present research. Increasing the residence time enhances the gas yield, which is caused by the decomposition of tar and char. The effect of residence time on the tar yield may be much stronger than that of the char yield due to the secondary reactions of tar (Puy et al., 2011).

The differences shown in pyrolysis product yields in the data above may have been due to either the difference in heating rate or due to the difference in final temperature achieved. A study was performed on one plant species to separate the effects of temperature and heating rate. Longleaf pine litter was pyrolyzed at $0.5\text{ }^{\circ}\text{C s}^{-1}$ to a maximum gas temperature of $765\text{ }^{\circ}\text{C}$ to compare with the data from the FFB apparatus. The sample was held at $765\text{ }^{\circ}\text{C}$ for one hour, which is similar to the hold time for the low heating rate experiments.

Figure 6-4 indicates the yields of pyrolysis products from the longleaf pine litter for three different pyrolysis conditions. By keeping the heating rate constant ($0.5\text{ }^{\circ}\text{C s}^{-1}$) and increasing the pyrolysis temperature from $500\text{ }^{\circ}\text{C}$ to $765\text{ }^{\circ}\text{C}$, char yield decreased from 27 to 25 wt%, indicating a 2 wt% increase in the volatile yield. In addition, tar yield decreased by 2 wt% at the higher temperature (with low heating rate) due to the secondary reactions of tar compounds to increase the light gas yield. Furthermore, by keeping the pyrolysis temperature constant at $765\text{ }^{\circ}\text{C}$, and increasing the heating rate from $0.5\text{ }^{\circ}\text{C s}^{-1}$ to $180\text{ }^{\circ}\text{C s}^{-1}$, char yield decreases noticeably from 25 wt% to 17%, which led to higher tar and total volatile yields. These results seem to indicate that the heating rate affects tar yield more than the temperature, at least for this plant species.

6.2 Light Gas Analysis

The analysis of the yield of light gases; CO, CO₂, CH₄, and H₂, during the slow and fast pyrolysis experiments is shown in Table 6-3. Furthermore, the data for live plant species are shown in Figure 6-5 (CO yield data), Figure 6-6 (CO₂ yield data), Figure 6-7 (CH₄ yield data), and Figure 6-8 (H₂ yield data). A similar trend was observed for the pyrolysis of dead plant species (as shown in Appendix F). The results show that for both slow and fast pyrolysis experiments, CO was the main component in the light gases on a wt% dry basis, followed by CO₂, CH₄, and H₂. All other gas species, such as C₂H₆ and C₃H₈, were below the detection limit of the GC-TCD instrument (500 ppm). The statistical analysis indicates that there was convincing evidence of a difference between the yields of all light gas species comparing slow vs. fast pyrolysis of live plant species (CO p-value = 4×10^{-8} , CO₂ p-value = 4×10^{-10} , CH₄ p-value = 5×10^{-17} , and H₂ p-value = 1×10^{-3}).

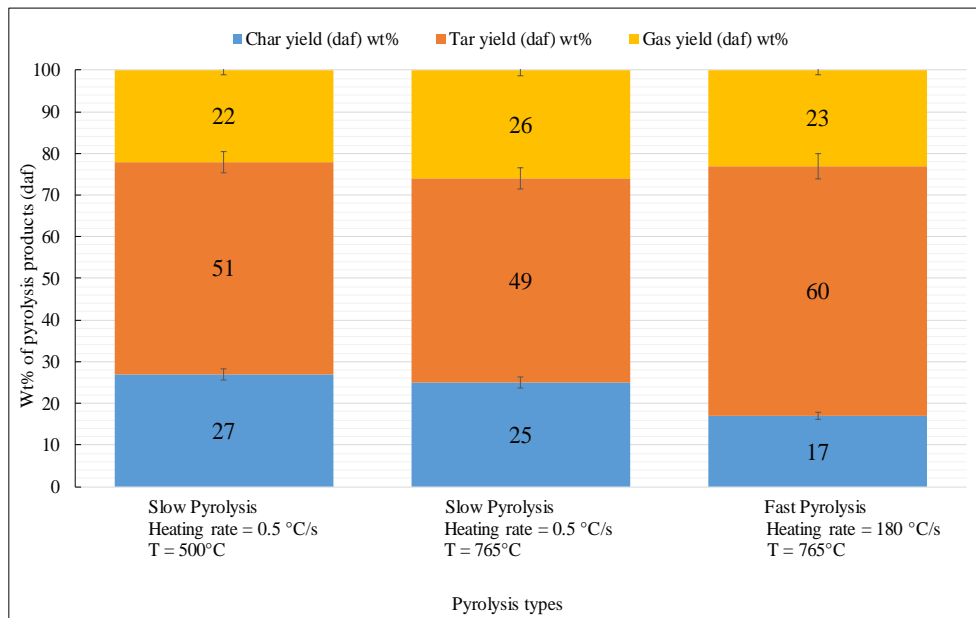


Figure 6-4. Pyrolysis product yields from pyrolysis of longleaf pine litter

As shown in Figure 6-5, for the fast pyrolysis experiments, compared with the slow pyrolysis experiments, a higher wt% of the total collected gases consisted of CO for both live and dead plant species. The live longleaf pine foliage showed the highest yield of CO (58 wt%) for slow pyrolysis experiments. The live saw palmetto indicated the highest yield of CO (63 wt%) for fast pyrolysis experiments. It is interesting that the plant species with the largest CO yield changed with heating rate. Large differences in the compositions of light gases were observed at the different heating rates. The live dwarf palmetto showed the largest difference in CO yield (12.5 wt%) between slow and fast pyrolysis experiments. The plant species with the second largest difference in CO yield was saw palmetto (11.4 wt%). However, the maximum difference in CO yield from experiments comparing live and dead plants did not exceed 5 wt% for either fast or slow pyrolysis.

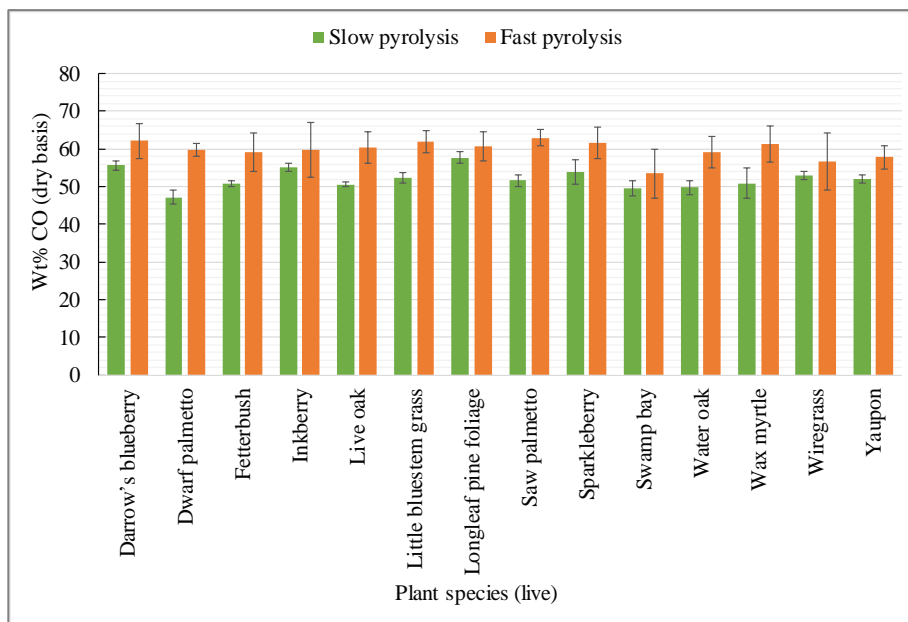


Figure 6-5. The yield of CO wt% (dry basis) obtained from pyrolysis of live plant species

Decarbonylation reactions at high heating rates and temperatures are thought to contribute to high yields of CO during the pyrolysis of live and dead plants (Duman et al., 2011; Gao et al., 2015). The variation in CO yields due to plant species seemed to be larger in the slow heating experiments than in the high heating rate experiments. A CO yield of 59 wt% would pass through all of the error bars in the high heating rate data, but no common CO yield would pass through all of the error bars for the slow heating rate data. Furthermore, the results show that the plants from the same family (e.g., yaupon and inkberry or live oak and water oak) had similar behavior when underwent pyrolysis.

The light gas with the second highest yield was CO₂. By increasing the pyrolysis temperature and the heating rate, CO₂ formation shows a different trend than CO; higher CO₂ yields were obtained from the slow pyrolysis of plant species regardless of the condition of the plant (live or dead). The average CO/CO₂ ratio increased from 1.29 (slow pyrolysis experiments) to 1.92 (fast pyrolysis experiments) by increasing the pyrolysis temperature and the heating rate. At high temperatures, CO₂ is thought to be mainly formed by the thermal decomposition of lignin (Gao et al., 2015). However, at low pyrolysis temperatures, CO₂ forms due to the decomposition of cellulose and hemicellulose by the cracking and reforming of C=O and COOH functional groups. CO₂ may also form due to decarboxylation reaction (Gautam et al., 2017). By increasing the operating temperature, the CO₂ yield decreases, which seems to contribute to the increased formation of CO. The dead little bluestem grass showed the highest CO₂ yield (43 wt%) for slow pyrolysis experiments. For fast pyrolysis experiments, the live swamp bay indicated the highest CO₂ yield (35 wt%). The dead wax myrtle showed the largest difference in the CO₂ yield (14 wt%) between slow and fast pyrolysis experiments.

Methane was the third most prevalent light gas observed in both the slow and fast pyrolysis of the samples. The yields of CH₄ were very similar for the slow and fast pyrolysis experiments. CH₄ is thought to form mainly due to the splitting of C-O bonds during lignin decomposition. In addition, CH₄ may also form due to removal of methoxy groups from the aromatic rings (Xu et al., 2016).

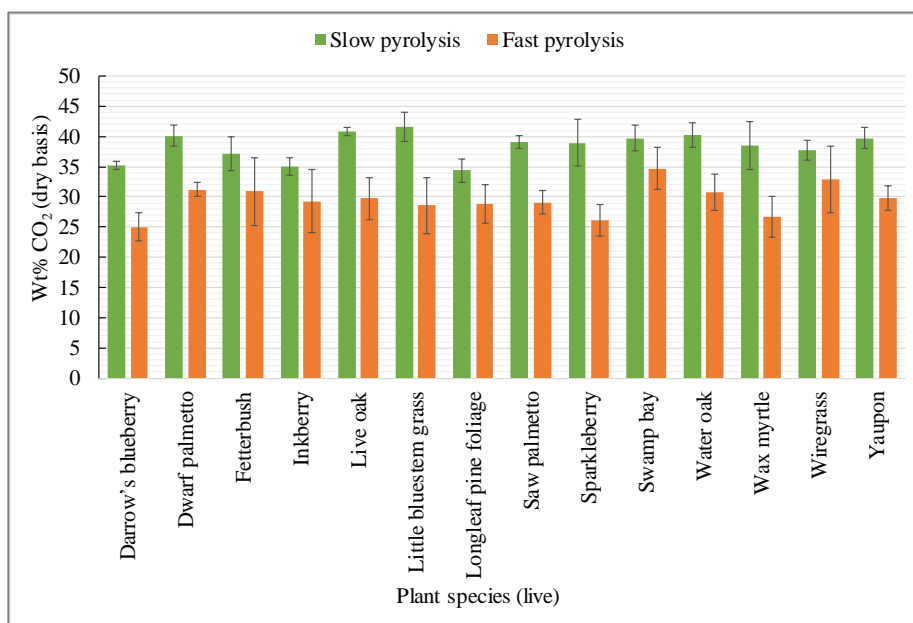


Figure 6-6. The yield of CO₂ wt% (dry basis) obtained from pyrolysis of live plant species

The dead fetterbush (13 wt%) and the dead little bluestem grass (12 wt%), showed the highest yields of CH₄ for the slow and fast pyrolysis experiments, respectively. In contrast with the yields of CO and CO₂, CH₄ did not show a consistent trend among the plant species when comparing slow and fast pyrolysis experiments. For example, yaupon showed a higher yield of CH₄ during fast pyrolysis experiments, while fetterbush indicated a higher yield of CH₄ during slow pyrolysis experiments. The largest difference in the CH₄ yield (5.1 wt%) between slow and fast pyrolysis experiments was observed during the pyrolysis of dwarf palmetto.

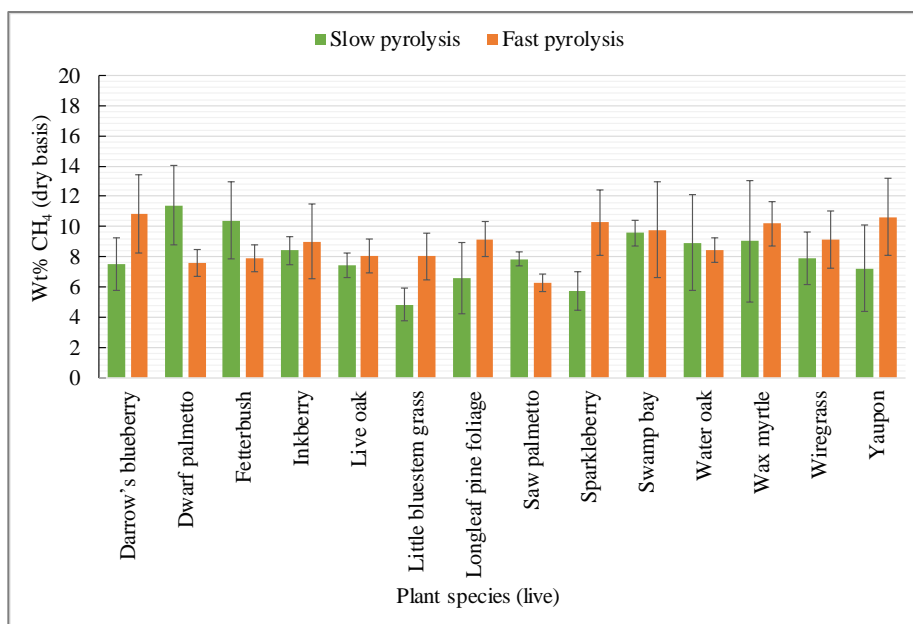


Figure 6-7. The yield of CH₄ wt% (dry basis) obtained from pyrolysis of live plant species

H₂ yields varied between 1 and 2 wt% for both the slow and fast pyrolysis experiments. In most of the cases, slightly higher wt% of H₂ was formed in the fast pyrolysis experiments compared to the slow pyrolysis experiments. Two main mechanisms lead to the formation of H₂ at high pyrolysis temperatures. The first mechanism is the formation of H₂ from the breaking of hydrogen bonds attached to the benzoic rings, which are present in the form of the phenolic groups in the lignin structure (Zhou et al., 2014b). The second mechanism is the decomposition of heavy gaseous hydrocarbons due to the secondary pyrolysis reactions, which leads to the formation of H₂ (Gao et al., 2015; Xu et al., 2016; Al Arni, 2018).

The live Darrow's blueberry showed the highest H₂ yields for both slow and fast pyrolysis experiments (1.7 and 2.1 wt%, respectively). The largest difference in H₂ yield between slow and fast pyrolysis experiments, was observed during the pyrolysis of swamp bay (0.9 wt%).

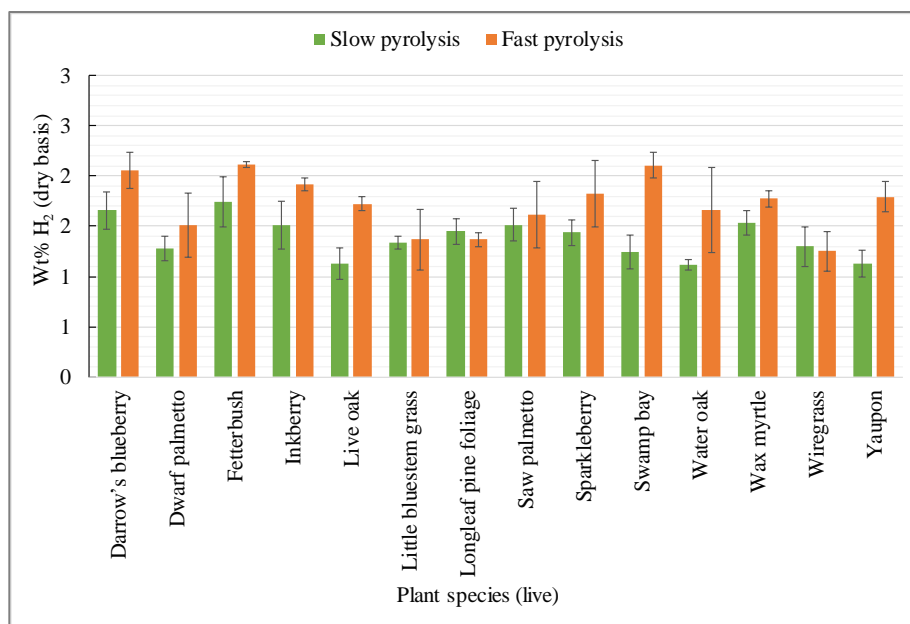


Figure 6-8. The yield of H₂ wt% (dry basis) obtained from pyrolysis of live plant species

The results of the yields of light gas species for these experiments are summarized in Table 6-4. These results indicate that higher wt% of CO and H₂ were obtained in the fast pyrolysis experiments. In contrast, higher weight fractions of CO₂ were observed in the slow pyrolysis experiments. The CH₄ yield did not show a consistent trend among the plants when comparing slow and fast pyrolysis experiments. The average wt% of CO from the fast pyrolysis of all plant species including live and dead plants was 57 wt%. However, this value was 49 wt% for the slow pyrolysis experiments. In contrast with CO, CO₂ showed a different trend; the average wt% of CO₂ from all the slow pyrolysis experiments including both live and dead plants was 38 wt%, while this value was 29 wt% for the fast pyrolysis experiments.

Table 6-3. Light gas analysis from pyrolysis of live and dead samples (wt% on dry light gas basis)

Plant name	Live Plants								Dead Plants							
	Slow Pyrolysis				Fast Pyrolysis				Slow Pyrolysis				Fast Pyrolysis			
	H ₂	CO	CO ₂	CH ₄	H ₂	CO	CO ₂	CH ₄	H ₂	CO	CO ₂	CH ₄	H ₂	CO	CO ₂	CH ₄
Darrow's blueberry	1.7 ^a	55.6	35.2	7.5	2.1	62.1	25.0	10.9	1.2	50.3	40.6	7.9	1.6	58.8	28.7	10.9
Dwarf palmetto	1.3	47.2	40.1	11.4	1.5	59.7	31.2	7.6	0.8	45.2	41.5	12.5	1.0	59.5	32.1	7.4
Fetterbush	1.7	50.7	37.1	10.4	2.1	59.1	30.9	7.9	1.4	46.1	39.1	13.4	1.9	55.9	31.6	10.6
Inkberry	1.5	55.1	35.0	8.4	1.9	59.8	29.3	9.0	1.3	52.4	37.8	8.5	1.8	59.1	29.5	9.6
Little bluestem grass	1.3	52.2	41.6	4.8	1.4	62.1	28.6	8.0	1.2	46.5	43.0	9.3	1.1	56.9	30.4	11.7
Live oak	1.1	50.6	40.9	7.4	1.7	60.4	29.8	8.1	0.9	48.4	41.8	8.9	1.7	59.4	29.7	9.2
Longleaf pine foliage	1.4	57.6	34.3	6.6	1.4	60.6	28.9	9.2	1.1	52.0	38.5	8.4	1.3	59.4	28.7	10.7
Longleaf pine litter	n/a ^b	n/a	n/a	n/a	n/a	n/a	n/a	n/a	1.1	51.0	39.0	8.9	1.3	56.2	31.6	10.9
Saw palmetto	1.5	51.6	39.1	7.8	1.6	63.0	29.1	6.3	1.1	46.9	42.7	9.3	1.3	60.5	31.7	6.5
Sparkleberry	1.4	53.9	38.9	5.7	1.8	61.7	26.2	10.3	1.2	50.2	41.1	7.5	1.5	59.8	27.8	10.8
Swamp bay	1.2	49.5	39.7	9.6	2.1	53.4	34.7	9.8	1.1	47.0	41.0	11.0	1.9	55.4	32.8	9.9
Water oak	1.1	49.7	40.2	8.9	1.7	59.2	30.7	8.4	1.0	46.4	41.9	10.7	1.6	58.7	29.9	9.8
Wax myrtle	1.5	50.9	38.5	9.0	1.8	61.3	26.7	10.2	1.2	47.9	41.8	9.1	1.5	59.8	27.8	10.8
Wiregrass	1.3	53.1	37.7	7.9	1.3	56.7	32.9	9.1	1.0	48.8	40.8	9.4	1.2	58.9	29.9	10.0
Yaupon	1.1	51.9	39.7	7.2	1.8	57.9	29.7	10.6	1.0	48.9	41.5	8.6	1.7	58.3	30.9	9.0

^a wt% on a dry light gas basis

^b n/a means not applicable

Table 6-4. Summary of light gas analysis for slow and fast pyrolysis experiments

Heating Rate	Plant type	H ₂		CO		CO ₂		CH ₄	
		Average ^a	Range ^a						
0.5 °C s ⁻¹	Live	1.3	1.1-1.7	48.6	47-58	35.9	34-42	7.5	5-11
	Dead	1.1	0.8-1.4	48.5	45-52	40.8	38-43	9.6	8-13
180 °C s ⁻¹	Live	1.7	1.3-2.1	59.8	53-63	29.5	25-35	8.9	6-11
	Dead	1.5	1.0-1.9	58.4	55-61	30.2	28-33	9.8	7-12

^a wt% on a dry light gas basis

6.3 Tar Analysis

Figure 6-9 and Figure 6-10 illustrate typical GC-MS chromatograms of tar, which were obtained from the slow and fast pyrolysis experiments, respectively. The chromatograms of the slow pyrolysis experiments illustrate that the majority of the identified tar compounds were C₅-C₂₀ aliphatic and 1-ring aromatic compounds.

The fast pyrolysis experiments led to formation of 1- to 5-ring aromatic compounds with very few hydroxyl (OH) or other attachments. The lists of identified tar compounds during slow and fast pyrolysis experiments are shown in Appendix D. Figure 6-11 and Figure 6-12 provide a typical comparison of the composition of tar compounds for the slow and fast pyrolysis experiments of longleaf pine. For brevity, the tar compounds with 0.1 mole% are not shown. Mole fractions of identified tar compounds were obtained by dividing their relative peak area to the total area of the peaks. The error bars in the graphs, represent the $\pm 95\%$ confidence intervals for three experiments.

As shown in Figure 6-11, primary tar compounds from the slow pyrolysis experiments were oxygenated 1-ring aromatic compounds, such as phenol, 1,2-benzendiol, 2-methoxy phenol, and 4-methyl phenol. The absence of multi-ring aromatic compounds and the presence of many alkyl and hydroxyl attachments seem to indicate that during these slow pyrolysis experiments, primary pyrolysis products did not undergo secondary pyrolysis reactions.

As shown in Figure 6-12, phenol was still a major constituent of the tar from the fast pyrolysis experiments. However, other major tar compounds observed from the fast pyrolysis experiments were multi-ring aromatic compounds, such as naphthalene, fluorene, anthracene, phenanthrene, fluoranthene, and pyrene.

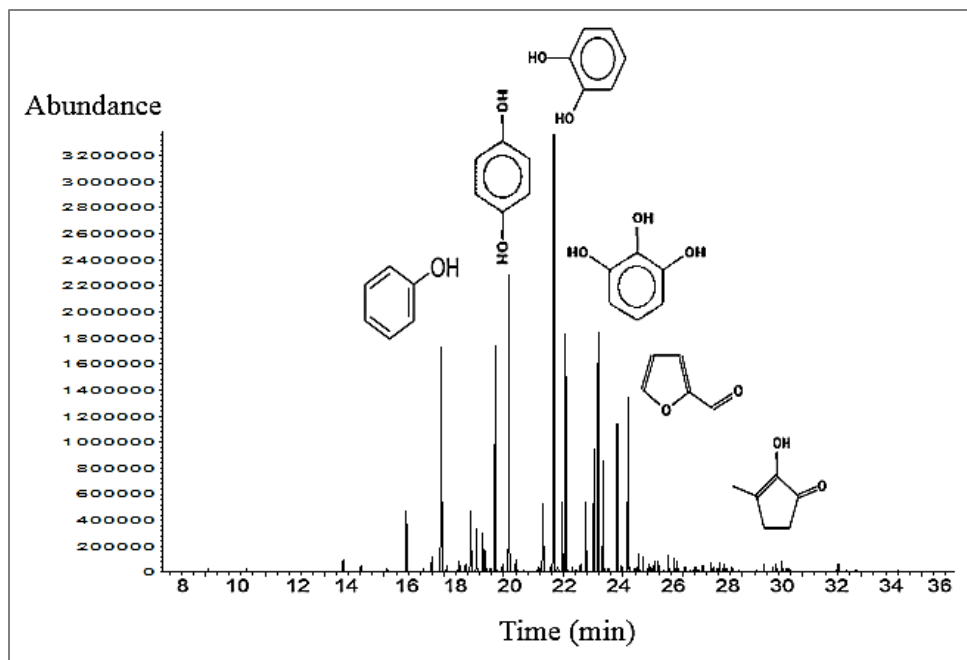


Figure 6-9. GC-MS chromatogram of tar from slow pyrolysis of live longleaf pine foliage

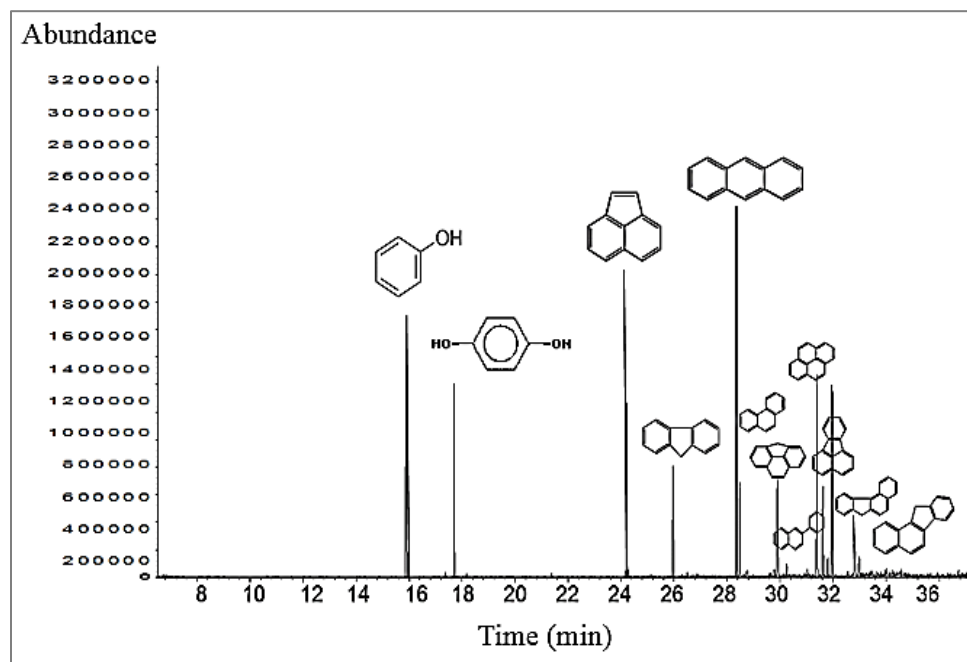


Figure 6-10. GC-MS chromatogram of tar from fast pyrolysis of live longleaf pine foliage

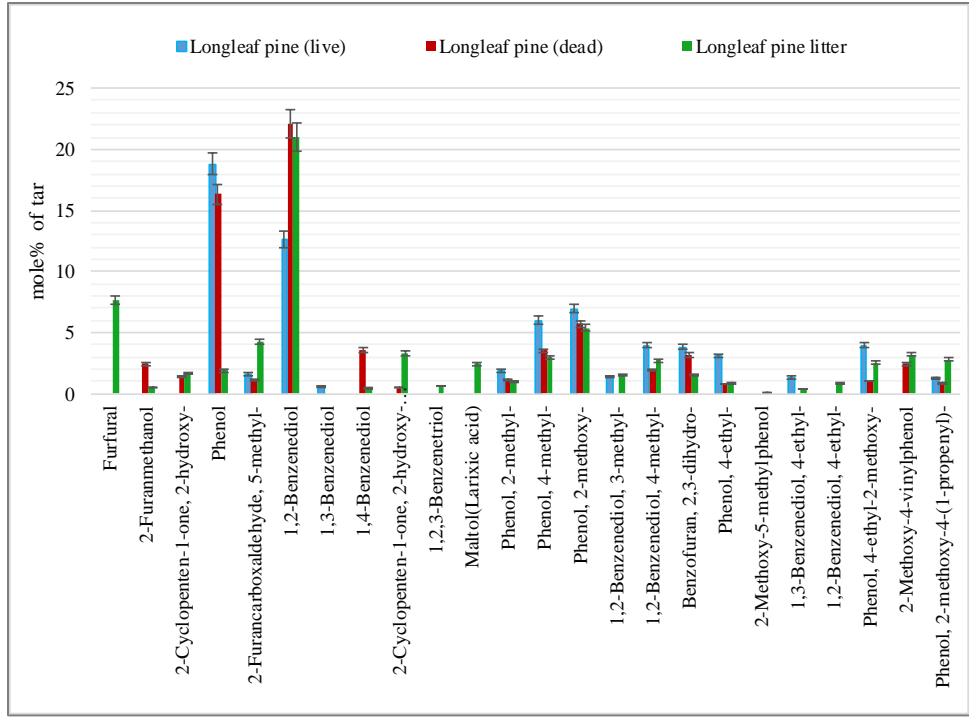


Figure 6-11. Distribution of tar compounds for the slow pyrolysis of longleaf pine

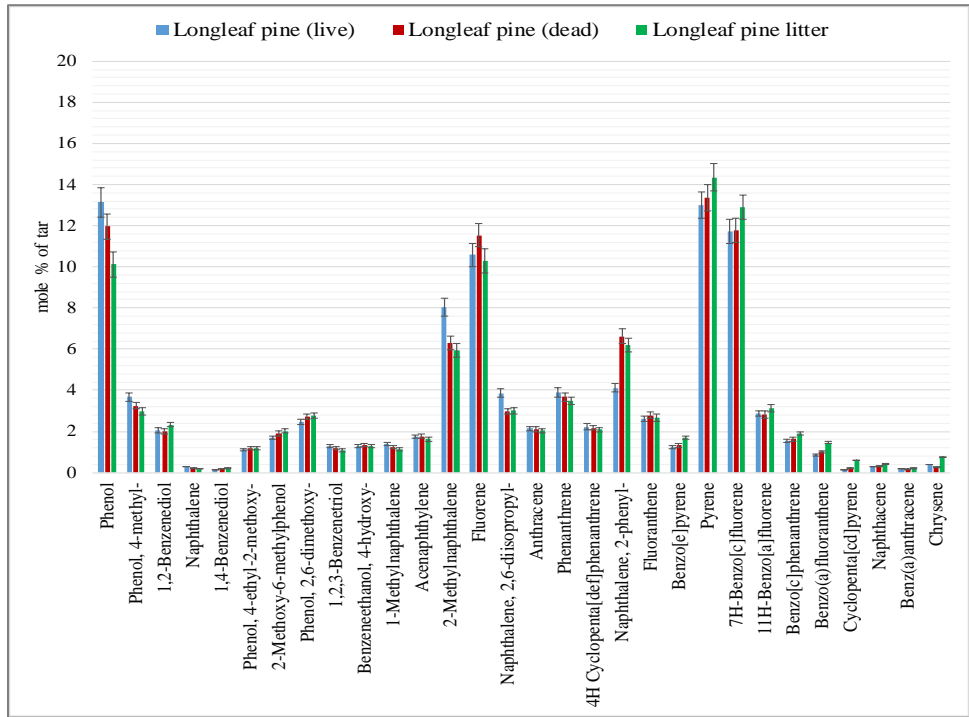


Figure 6-12. Distribution of tar compounds for the fast pyrolysis of longleaf pine

The presence of multi-ring compounds seems to indicate that the primary tars underwent secondary pyrolysis reactions and formed secondary and tertiary tars (i.e., heavy PAHs) in the fast pyrolysis experiments. The 1- and 2-ring tar species from the fast pyrolysis experiments still had some alkyl and hydroxyl groups, but not to the extent seen in the tars from the slow heating experiments. The aromatic compounds with 3 or more rings seen in the high heating rate experiments generally did not have attachments.

For the fast pyrolysis tars, the main constituents were generally phenolic compounds, such as 4-methyl phenol, 2-methoxy phenol (guaiacol), and 3,4-dimethyl phenol, which are mainly thought to evolve during the pyrolysis of plants due to the depolymerization of lignin building blocks (Wang et al., 2013; Xu et al., 2016).

Low molecular weight 1-ring aromatic compounds, such as benzene and phenol are thought to form during the decomposition of lignin (Farag et al., 2014). Larger molecules, such as naphthalene, seem to be formed from 1-ring aromatic compounds by hydrogen abstraction and acetylene at high temperatures and heating rates (fast pyrolysis). Multiple-ring aromatic compounds may form from naphthalene via more complex mechanisms. For instance, by the addition of acetylene to naphthalene, acenaphthylene can form (Maggi and Delmon, 1994; Ku and Mun, 2006; Palma, 2013a).

In addition, by increasing the pyrolysis temperature and heating rate, ketone, alcohol, and aldehyde content decreases due to the secondary reactions (Maggi and Delmon, 1994; Ku and Mun, 2006; Garcia-Perez et al., 2007; Gao et al., 2015; Stankovikj and Garcia-Perez, 2017).

There were a few compounds, such as phenol (Figure 6-13), 1,2-benzenediol (Figure 6-14), and 4-methyl phenol (Figure 6-15), present in both slow and fast pyrolysis tars. The results of these figures indicate that for most of the plant species, the hydroxyl (OH) and methyl (-CH₃)

attachments to the aromatic ring of phenols were removed during fast pyrolysis experiments, causing lower mole% of 1,2-benzenediol and 4-methyl phenol. The mole% of phenol in the tar generally increased for each plant species when the heating rate increased. Since the tar yield increased with heating rate, and the amount of multi-ring compounds increased in the fast pyrolysis tar, more phenol had to be formed in the fast pyrolysis experiments. The decrease in tar species such as 1,2-benzenediol and 4-methyl phenol coincided with the increase in phenol, indicating that some additional phenol is likely formed as alkyl and hydroxyl groups were lost from 1-ring compounds. Radical sites, which formed on aromatic rings when alkyl and hydroxyl moieties were released, may also be part of the mechanism for the formation of multi-ring compounds through polymerization reactions.

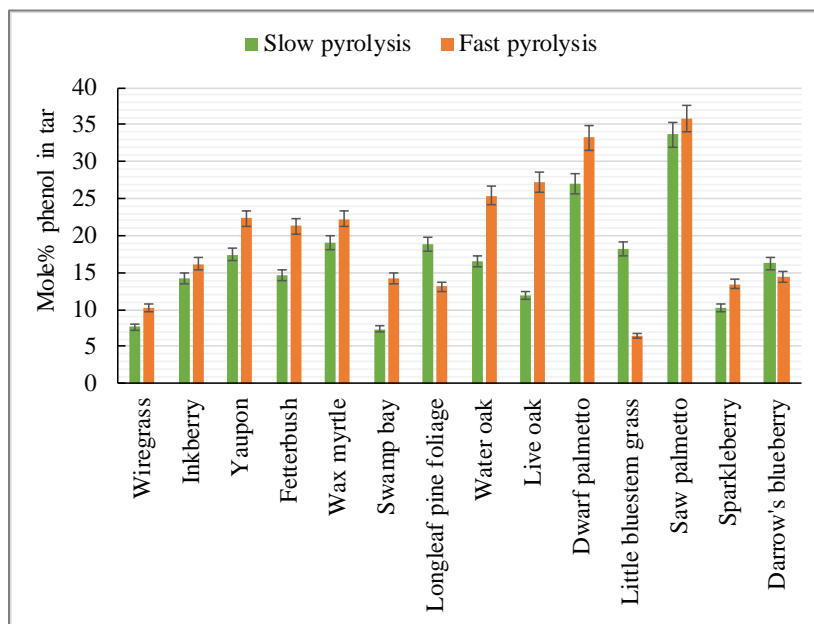


Figure 6-13. Mole% of phenol in tar during pyrolysis of live plant species

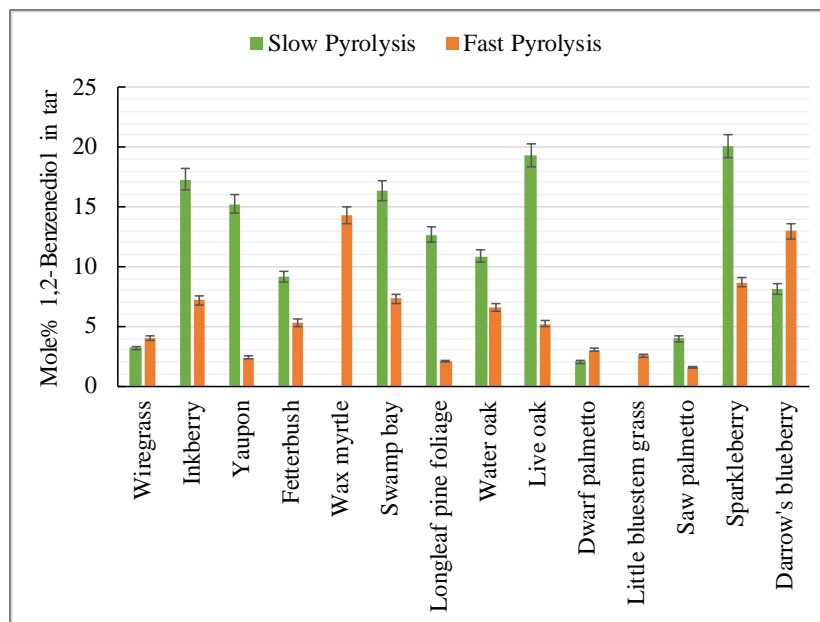


Figure 6-14. Mole% of 1,2-benzenediol in tar during pyrolysis of live plant species

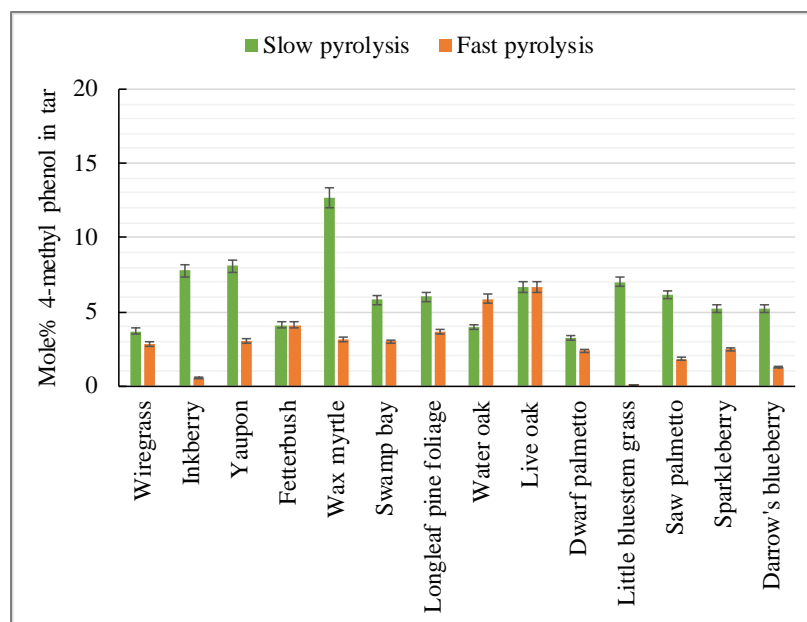


Figure 6-15. Mole% of 4-methyl phenol in tar during pyrolysis of live plant species

6.4 Summary and Conclusions

In this chapter, the results of the slow and fast pyrolysis of plant species were compared.

The main conclusions from this study are as follows:

- 1- The total volatiles yields were higher in the fast heating rate experiments than in the slow heating rate experiments. The average volatile yield observed for all plants (live and dead) was 69 wt% (daf basis) at the slow heating rate but 80 wt% (daf) for the high heating rate.
- 2- Higher tar yields were obtained from the fast pyrolysis experiments. The average tar yield was 58 wt% (daf) for the fast pyrolysis experiments compared to 49 wt% (daf) for the slow pyrolysis experiments, an increase of 9 wt%. The average gas yields for the slow and fast pyrolysis of the plants were 20 and 22 wt%, respectively.
- 3- By keeping the heating rate constant at $0.5\text{ }^{\circ}\text{C s}^{-1}$ and increasing the pyrolysis temperature from $500\text{ }^{\circ}\text{C}$ to $765\text{ }^{\circ}\text{C}$, char yield decreased from 27 to 25 wt%, indicating a 2 wt% increase in the volatile yield. In addition, tar yield decreased by 2 wt% at the higher temperature (with low heating rate) due to the secondary reactions of tar compounds to increase the light gas yield.
- 4- By keeping the pyrolysis temperature constant at $765\text{ }^{\circ}\text{C}$, and increasing the heating rate from $0.5\text{ }^{\circ}\text{C s}^{-1}$ to $180\text{ }^{\circ}\text{C s}^{-1}$, char yield decrease noticeably from 25 wt% to 17%, which led to 11 wt% higher tar yield and 8 wt% higher total volatile yield. The increase in heating rate seemed to have more of an effect on tar and total volatiles yield than final temperature for these experiments.
- 5- The major light gas species observed (on a wt% of dry gas basis) was CO, followed by CO₂, CH₄, and H₂, for both the slow and the fast pyrolysis experiments. Higher yields of CO were observed for all plants in the higher heating rate experiments. In contrast, higher yields

of CO₂ were observed in the slow pyrolysis of the plants compared to the fast pyrolysis. The yields of H₂ were all small on a basis of wt% of dry light gas. The CH₄ yields did not show the same trend with heating rate for all plant species; some plants showed higher CH₄ yields in the fast pyrolysis experiments, while other plants showed higher CH₄ yields in the slow pyrolysis experiments.

- 6- There was a convincing evidence of difference in the distribution of tar compounds during the slow and fast pyrolysis of the plants (p-value < 0.05). During the slow pyrolysis of the plants, primary tar compounds are thought to be formed largely from the decomposition of lignin. Primary tar compounds from the slow heating experiments were some aliphatic hydrocarbons in addition to 1-ring aromatics with a large number of attachments. However, tar compounds from the fast pyrolysis of the plants included phenol and a few other 1-ring compounds, but also included a significant amount of 3- to 5-ring aromatic compounds with very few attachments on the rings. Formation of heavy polycyclic aromatic hydrocarbons (PAHs) during fast pyrolysis experiments seems to indicate that primary tar compounds underwent secondary reactions in the gas phase.
- 7- Examination of common tar species observed in the slow and fast pyrolysis experiments showed that phenol was created in the fast pyrolysis experiments as other one-ring species lost hydroxyl and alkyl groups. Loss of hydroxyl and alkyl groups may also have formed radical sites on aromatic rings that contributed to polymerization that formed multi-ring compounds.

7 THE EFFECT OF HEATING MODE ON DISTRIBUTION OF PYROLYSIS PRODUCTS

During wildland fires, both live and dead plants are burned through very complex heat transfer mechanisms (McAllister and Finney, 2017). Heat transfer mechanisms in wildland fires are: (1) convective heat transfer from hot gases to plants, especially for wind-driven fires; (2) radiative heat transfer from burning plant particles; and (3) radiative heat transfer from flames (Wagner, 1967). Radiative and convective heat transfer mechanisms are the two most dominant types of heat transfer mechanisms in wildland fires (Frankman et al., 2010a). Conductive heat transfer is only significant in thermally-thick fuels.

In this chapter, the results of the pyrolysis experiments in the FFB operated under three heating modes are compared. The modes were: (1) convection-only, where the FFB apparatus was operated at a high heating rate of $180\text{ }^{\circ}\text{C s}^{-1}$ (convective heat flux of 100 kW m^{-2}) to imitate pyrolysis under convective heat transfer; (2) radiation-only, where the plants were pyrolyzed at a moderate heating rate of $4\text{ }^{\circ}\text{C s}^{-1}$ (radiative heat flux of 50 kW m^{-2}); and (3) a combination of convection and radiation, where the plants were exposed to both convective and radiative heat fluxes. In the combined mode, the heating rate was calculated to be approximately $195\text{ }^{\circ}\text{C s}^{-1}$. The average gas temperature (corrected for radiation) within the FFB at the height where the sample was located was measured to be $765\text{ }^{\circ}\text{C}$ for the convection-only mode, $105\text{ }^{\circ}\text{C}$ for the radiation-only mode, and $804\text{ }^{\circ}\text{C}$ for the combined mode. The maximum fuel surface temperature was $750\text{ }^{\circ}\text{C}$ for the convection-only mode, $550\text{ }^{\circ}\text{C}$ for the radiation-only mode, and $800\text{ }^{\circ}\text{C}$ for

the combined mode. The lower heating rate in the radiation-only mode was affected by the convective cooling by N₂. Table 7-1 summarizes the operating conditions of three heating modes.

Table 7-1. Operating temperature and heat flux in the experiments

Heating modes	Radiative heat flux	Convective heat flux	Heating rate	Average gas temperature	Fuel surface temperature
Radiation-only	50 kW m ⁻²	0 kW m ⁻²	4 °C s ⁻¹	105 °C	550 °C
Convection-only	0 kW m ⁻²	100 kW m ⁻²	180 °C s ⁻¹	765 °C	750 °C
Convection and Radiation	50 kW m ⁻²	100 kW m ⁻²	195 °C s ⁻¹	804 °C	800 °C

7.1 Fuel Surface Temperature

The results from the changes of fuel surface temperature with respect to time during the pyrolysis of a live inkberry sample under the convection-only heating was shown in Figure 5-11. Figure 7-1 and Figure 7-2 indicate the typical changes of fuel surface temperature in the radiation-only and the combined modes. The maximum fuel surface temperature for the radiation-only mode, the convection-only mode, and the combined mode, was 550, 750, and 800 °C, respectively. The results for all three heating modes show that the leaves did not heat isothermally. There were temperature gradients within the leaves. First, the edges of the leaf reached higher temperatures and began to pyrolyze. As time passed, the heat traveled from the edges towards the center until the temperature was uniform across the entire leaf. For the radiation-only mode, a uniform temperature across the entire leaf was observed after 120 s. However, this time was only 4 s for the convection-only and the combined modes.

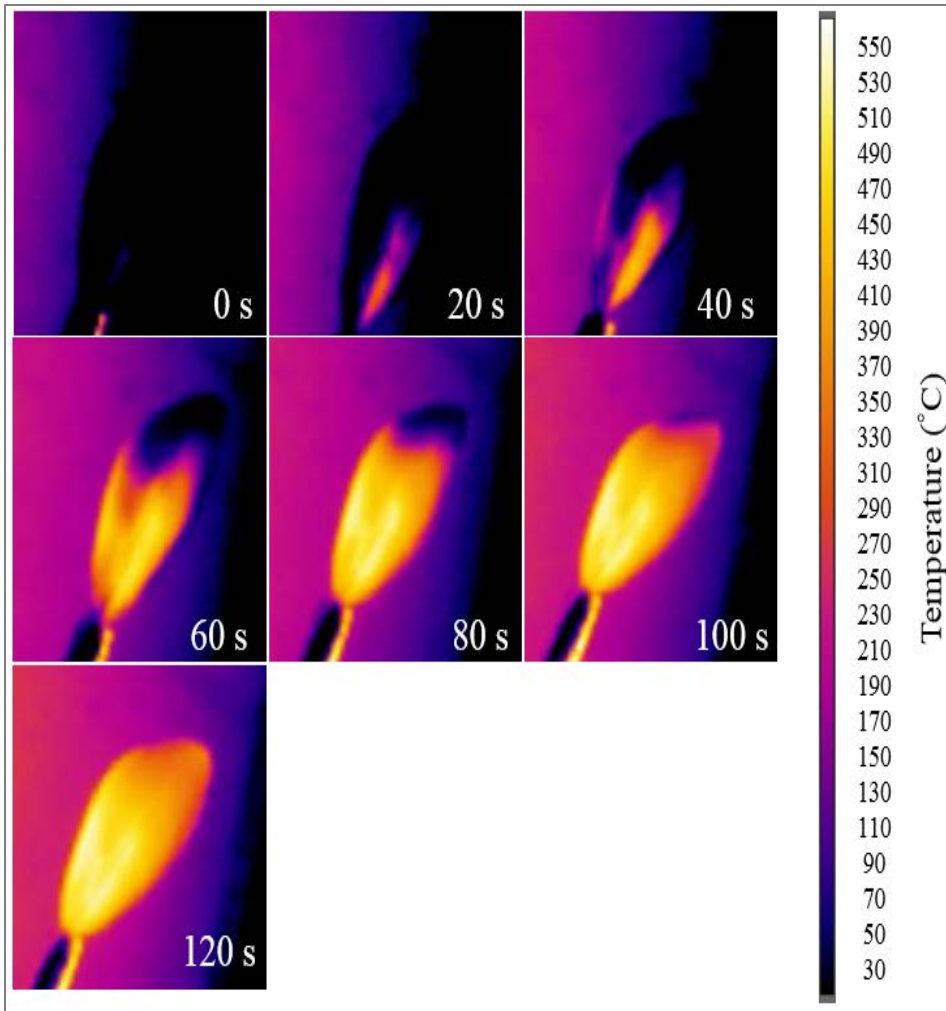


Figure 7-1. Fuel surface temperature changes over time for the radiation-only experiments (live inkberry)

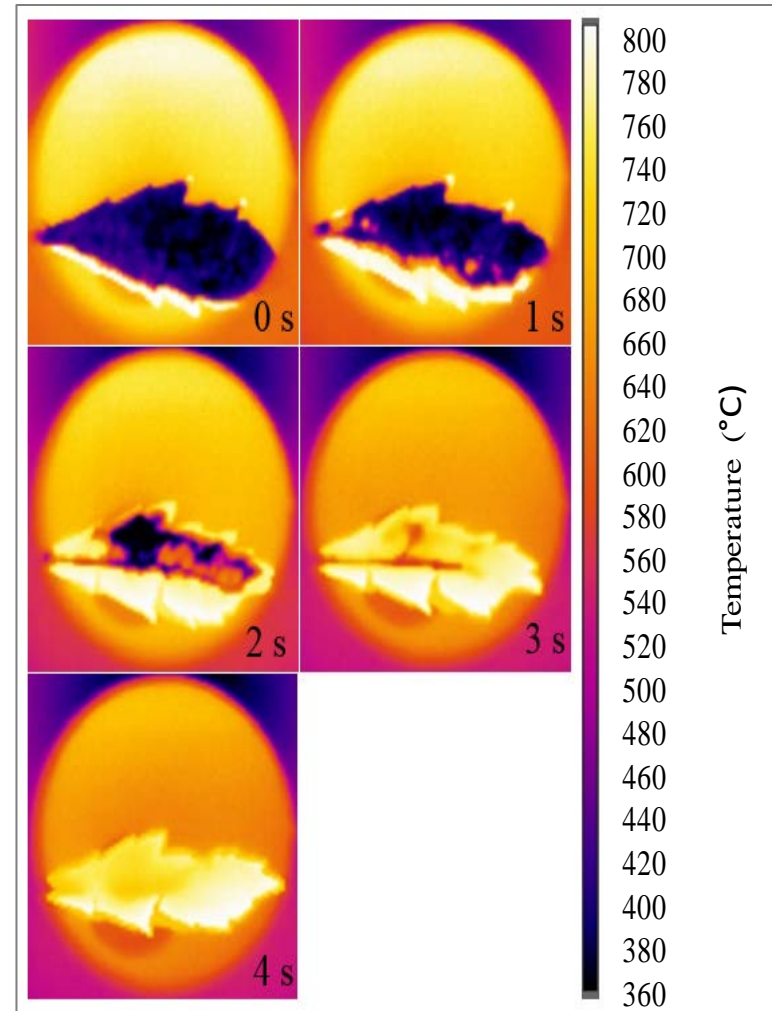


Figure 7-2. Fuel surface temperature changes over time for the combined convection and radiation (live wax myrtle)

7.2 Pyrolysis Product Yields

As discussed in Chapters 5 and 6, pyrolysis temperature and heating rate play important roles in determining the yields and compositions of pyrolysis products. The yields of pyrolysis products (i.e., tar, light gases, and char) for the pyrolysis experiments operated under three heating modes were measured using the same techniques as explained in Chapters 4-6. The gas yield data, tar yield data, and char yield data for the live plant species are presented in Figure 7-3, Figure 7-4, and Figure 7-5, respectively. A similar trend was observed for dead plant species (as shown in Appendix G). The presented results are the average of three experiments and the error bars in the figures represent the $\pm 95\%$ confidence intervals.

As shown in Figure 7-3, the gas yields obtained from the combined mode were higher than the gas yields from the radiation-only and convection-only modes. The radiation-only mode, which was performed at a lower pyrolysis temperature and a lower heating rate showed the lowest gas yields. The statistical analysis shows that there was convincing evidence of a difference between the means of light gas yields from the radiation-only mode vs. two other heating modes (p -value = 6×10^{-8}). However, there was suggestive, but inconclusive difference between the gas yield data from the convection-only vs. the combined mode (p -value = 0.1). For most of the plants, the confidence intervals of the gas yield data from the convection-only mode overlap the data from the combined mode, showing that the difference between these heating modes was not statistically significant. The highest gas yields for each heating mode were observed during the pyrolysis of: (1) live saw palmetto in the radiation-only mode (23 wt%); (2) live saw palmetto in the convection-only mode (23 wt%); and (3) live and dead fetterbush (27 wt%) followed by live saw palmetto (26 wt%) in the combined mode. Wax myrtle showed the largest difference between the gas yields for the radiation-only and the combined modes (5 wt%). The high gas yield seen

in the convection-only and the combined modes was partially due to the further pyrolysis of char and partially due to the secondary reactions of tar compounds at higher pyrolysis temperatures and heating rates.

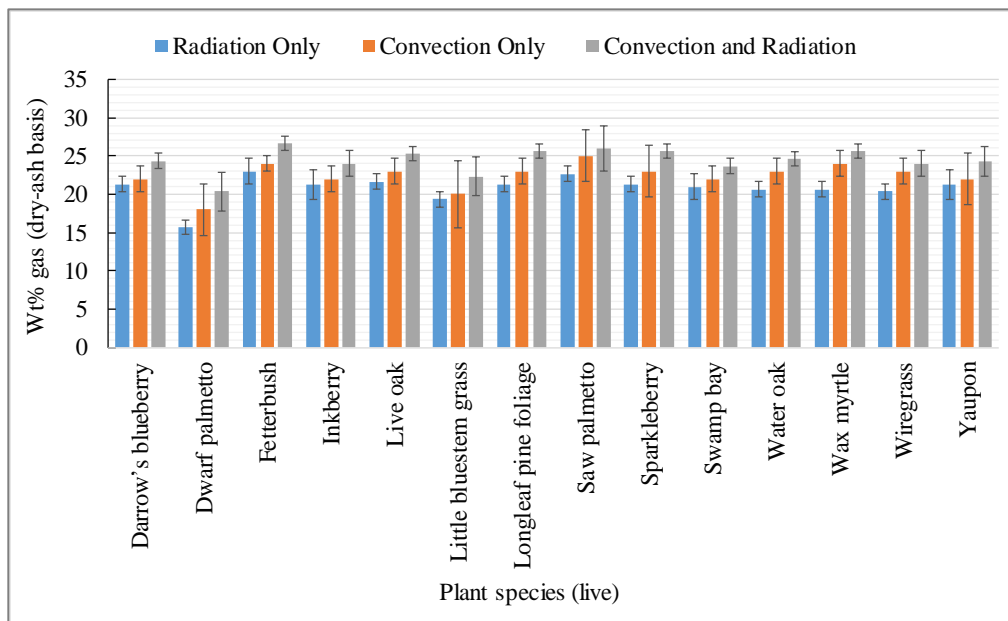


Figure 7-3. Gas yield of live plant species on a dry, ash free (daf) basis

The results of the tar yield analysis for the three heating modes are shown in Figure 7-4. Similar to the results observed in the gas yield data, by increasing the pyrolysis temperature and heating rate, higher tar yields were obtained. The statistical analysis indicate that there is convincing evidence of a difference between the tar yields when three heating modes were compared ($p\text{-value} = 8 \times 10^{-6}$). Among the plant species, dwarf palmetto showed the highest tar yield for all three heating modes: (1) 57 wt% in the radiation-only mode; (2) 62 wt% in the convection-only mode; and (3) 63 wt% in the combined mode. The largest difference between tar yield data sets was observed during the pyrolysis of live longleaf pine foliage with a difference of 9 wt% in tar yields from the radiation-only and the combined modes.

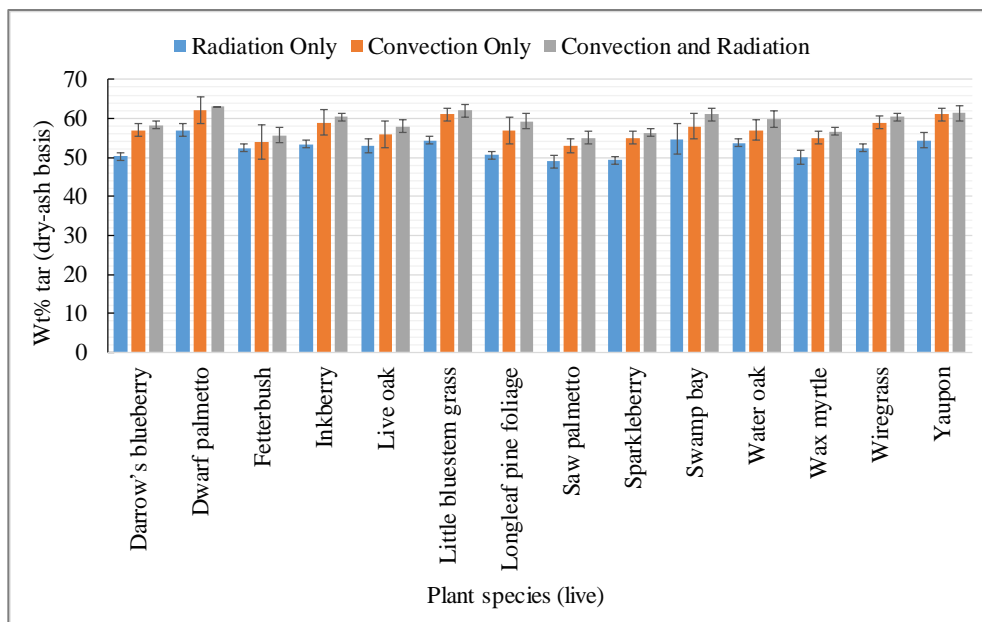


Figure 7-4. Tar yield of live plant species on a dry, ash free (daf) basis

The tar yield data indicate that the plants from the same family (i.e., (i) live oak and water oak, (ii) inkberry and yaupon, and (iii) sparkleberry and Darrow's blueberry) produced very similar tar yields in the experiments. For example, tar yields for water oak and live oak were 53 and 54 wt% in the radiation-only mode, 56 and 57 wt% in the convection-only mode, and 58 and 60 wt% in the combined mode.

As shown in Figure 7-5, consistent with the gas and tar yield data, the char yield decreased by increasing the pyrolysis temperature and the heating rate. For all the plant species, the statistical analysis showed that there was convincing evidence of a difference between the char yields from the radiation-only mode, the convection-only mode, and the combined mode ($p\text{-value} = 3 \times 10^{-19}$).

The highest char yields for each heating mode were observed during the pyrolysis of: (1) live and dead sparkleberry (29 wt%) in the radiation-only mode; (2) dead sparkleberry

(23 wt%) in the convection-only mode; and (3) live saw palmetto (19 wt%) in the combined mode. The largest statistically significant difference between the char yield data was observed during the pyrolysis of longleaf pine foliage in the radiation-only and the combined modes (13 wt%).

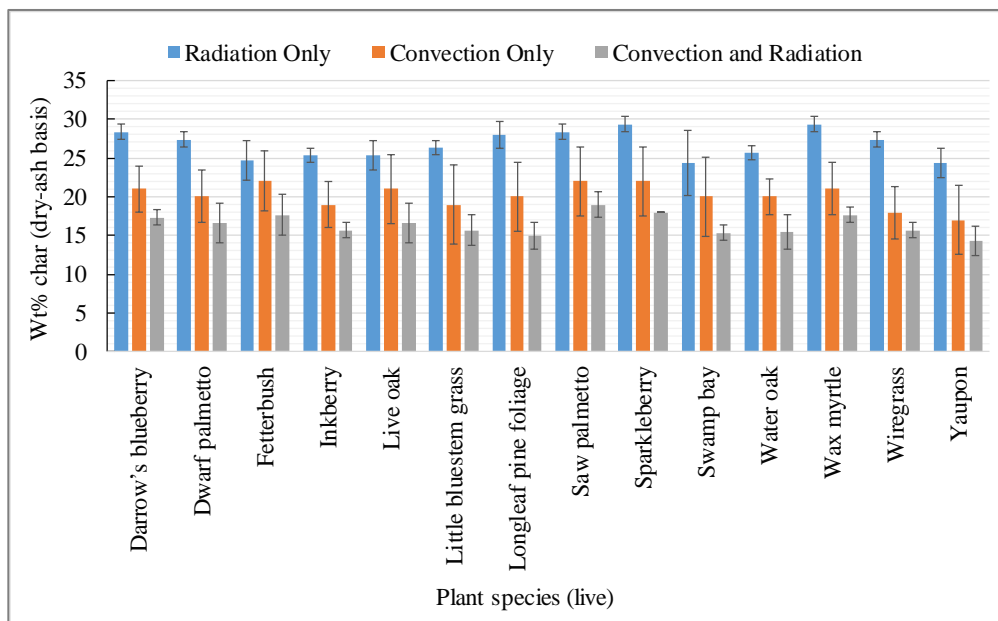


Figure 7-5. Char yield of live plant species on a dry, ash free (daf) basis

The ranges of pyrolysis product yields for the three heating modes are shown in Table 7-2. The results indicate that the lowest tar and gas yields, but highest char yields, were obtained in the radiation-only mode, which was performed at a lower pyrolysis temperature and a lower heating rate. In contrast, the convection-only and the combined modes, which were performed at higher pyrolysis temperatures and heating rates, exhibited higher gas, tar, and total volatile (light gas plus tar) yields, but lower char yields. Higher gas and tar yields in the convection-only and the combined modes were due to the further pyrolysis of char and secondary pyrolysis reactions at higher temperatures and heating rates. These pyrolysis product yield data showed that pyrolysis

temperature and heating rate have significant impacts on the yields of pyrolysis products. Higher pyrolysis temperatures and heating rates generally lead to further cracking of char and secondary reactions in tar, causing an increase in light gas yield. Previous researchers who have studied the pyrolysis of biomass in various systems have reported similar observations (Prins et al., 2006; Bridgwater, 2012; Adrados et al., 2013; Agirre et al., 2013; Solar et al., 2016).

Table 7-2. Summary of pyrolysis product yields for three heating modes

Heating mode	Plants	Tar yield ^a	Light gas yield ^a	Char yield ^a
Radiation-only	Live	49-57	16-23	24-29
	Dead	50-57	16-23	23-29
Convection-only	Live	53-62	18-25	17-22
	Dead	55-62	17-24	17-23
Combined mode	Live	55-63	20-27	14-19
	Dead	56-63	21-27	15-18

^a wt% on a dry, ash-free (daf) basis

7.3 Light Gas Analysis

The measured yields of light gas species for live plants in the three heating mode experiments are shown in Figure 7-6 (the yield of CO), Figure 7-7 (the yield of CO₂), Figure 7-8 (the yield of CH₄), and Figure 7-9 (the yield of H₂), all on a dry (H₂O-free) basis. The results of light gas analysis for dead plants are shown in Appendix G. The results are the average of three

experiments. The error bars in the graphs, represent the $\pm 95\%$ confidence intervals. The results indicate that for all three heating modes, CO was the main light gas species on a wt% basis, followed by CO₂, CH₄, and H₂. The statistical analysis indicates that there was convincing evidence of a difference between the yields of all light gas species comparing radiation-only, convection-only, and combined modes during pyrolysis of live plant species (CO p-value = 2×10^{-16} , CO₂ p-value = 4×10^{-14} , CH₄ p-value = 5×10^{-5} , and H₂ p-value = 7×10^{-6}).

As shown in Figure 7-6, the lowest and the highest CO yields were observed during the radiation-only mode and the combined mode, respectively. This trend suggests that by increasing the temperature and heating rate, higher yields of CO can be obtained. The highest CO yields for each heating mode were observed during the pyrolysis of: (1) live Darrow's blueberry (56 wt%) in the radiation-only mode; (2) live saw palmetto (63 wt%) in the convection-only mode; and (3) live inkberry (66 wt%) in the combined mode. The little bluestem sample showed the largest difference in CO yield (13 wt%) between different heating modes. At low pyrolysis temperatures, CO is formed mostly by the decomposition of hemicellulose and cellulose. However, at high pyrolysis temperatures, CO yield can be increased due to the cracking of carbonyl (C=O) and carboxyl (C(=O)OH) groups (Yang et al., 2007).

Carbon dioxide was the second most abundant light gas in all three heating modes. As shown in Figure 7-7, CO₂ showed a different trend compared to CO when increasing the temperature and heating rate. The radiation-only mode produced the highest CO₂ yields, while the convection-only and the combined modes resulted in lower yields of CO₂. The highest weight fractions of CO₂ for each heating mode experiments were observed during the pyrolysis of: (1) dead wax myrtle (43 wt%) in the radiation-only mode; (2) live swamp bay (35 wt%) in the convection-only mode; and (3) dwarf palmetto (31 wt%) in the combined mode. The little

bluestem sample showed the largest difference in the weight percent of CO₂ between different heating modes (12 wt%), followed by the water oak (11 wt%).

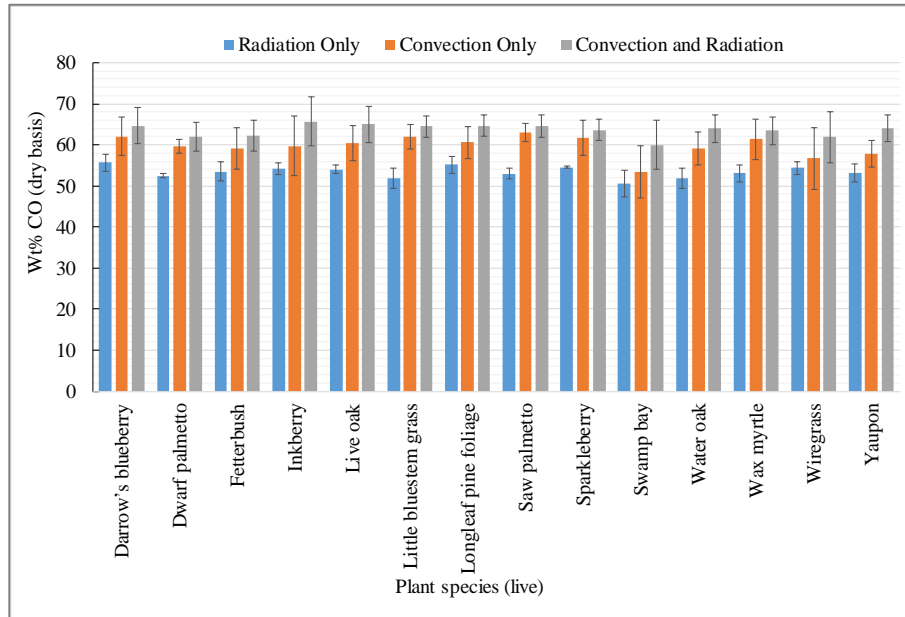


Figure 7-6. The yield of CO wt% (dry basis) from pyrolysis of live plant species

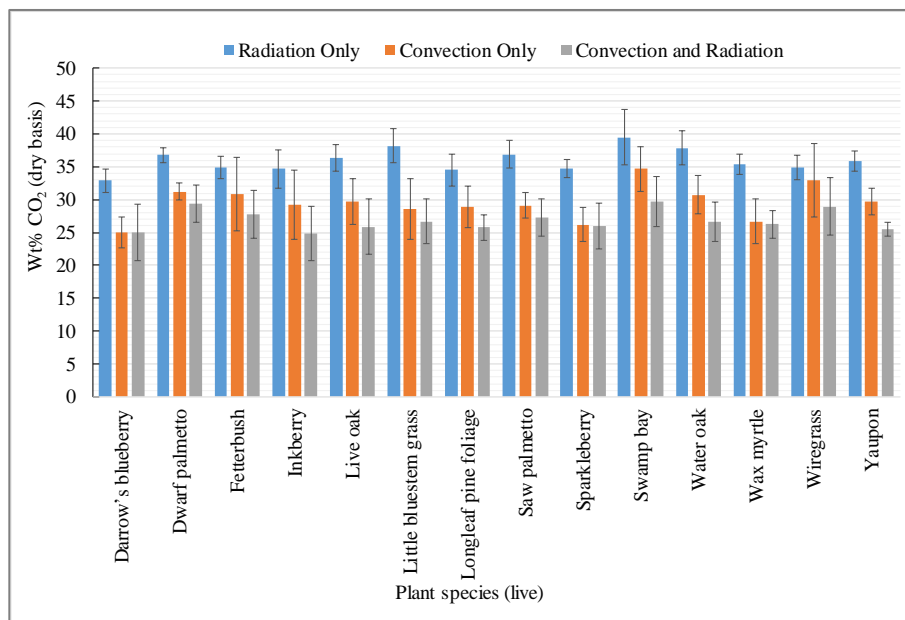


Figure 7-7. The yield of CO₂ wt% (dry basis) from pyrolysis of live plant species

CO₂ is mainly formed by the degradation of hemicellulose at low temperatures (<500 °C) (Chen et al., 2012). Only a small portion of CO₂ is thought to be formed due to the decomposition of cellulose. At higher temperatures (>500 °C), CO₂ is mainly formed by the cracking and reforming of oxygen-containing functional groups in lignin structure, such as carbonyl groups (C=O) and carboxyl groups (C(=O)OH) (Yang et al., 2007; Park et al., 2010; Gao et al., 2015).

The average ratio of CO/CO₂ was 1.36 for the radiation-only mode, 1.92 for the convection-only mode, and 2.38 for the combined mode. These results indicate that by increasing the pyrolysis temperature and heating rate, the CO₂ yield constantly decreased with a corresponding increase in the CO yield.

Methane was the third most prevalent light gas species in all three heating modes. The results of the CH₄ yields are shown in Figure 7-8. For most of the plants, higher yields of CH₄ were observed during the pyrolysis experiments performed under the radiation-only mode. However, for a few plant species, such as Darrow's blueberry and swamp bay, higher yields of CH₄ were obtained in the convection-only mode. The highest wt% of CH₄ belonged to the pyrolysis of dead little bluestem grass (12 wt%) under the convection-only mode. All the main structural components of plants can contribute to the formation of CH₄ during pyrolysis at all temperature ranges. However, lignin is thought to be the main contributor to CH₄ formation, which may be due to its high methoxy (O-CH₃) content (Yang et al., 2007).

As shown in Figure 7-9, the yields of H₂ varied from 1 to 2 wt% during all heating mode experiments. For all plant species, the greatest H₂ yields were observed during the combined mode. Live swamp bay showed the highest H₂ yield (2.4 wt%) in the combined mode. Among all plant species, live swamp bay exhibited the highest H₂ weight percent difference (0.9 wt%) between the radiation-only mode and the combined mode. H₂ can be formed due to either the

dehydrogenation reactions or the degradation of phenyl groups during the polycondensation reactions (Yang et al., 2007; Park et al., 2010).

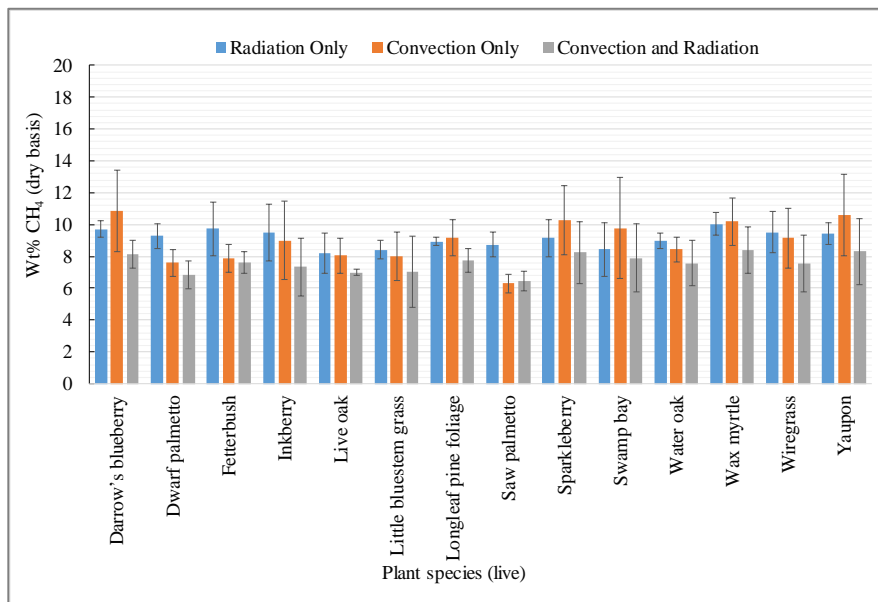


Figure 7-8. The yield of CH₄ wt% (dry basis) from pyrolysis of live plant species

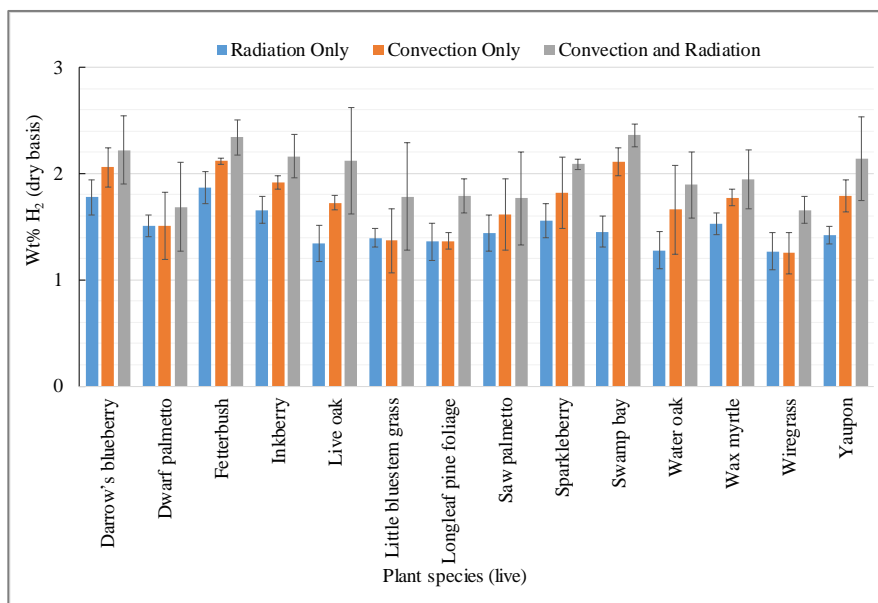


Figure 7-9. The yield of H₂ wt% (dry basis) from pyrolysis of live plant species

The results of the light gas yield are summarized in Table 7-3. In most cases, weight fractions of CO and H₂ increased by increasing the pyrolysis temperature and heating rate. The highest yields of CO and H₂ were observed during the pyrolysis experiments performed under the combined mode. In contrast, weight fractions of CO₂ and CH₄ exhibited a different behavior. The yields of CO₂ and CH₄ decreased by increasing the pyrolysis temperature and heating rate. Therefore, the highest yields of CO₂ and CH₄ were observed during the radiation-only mode and were slightly higher in the pyrolysis of dead plants. The yields of light gas species did not vary much between live and dead plant species.

Figure 7-10 shows the effects of pyrolysis temperature and heating rate on the distribution of pyrolysis products from the pyrolysis of live longleaf pine foliage in different heating modes. Among all the heating modes, the slow pyrolysis of longleaf pine foliage, which was performed in the pyrolyzer apparatus at the lowest pyrolysis temperature and the lowest heating rate, led to the highest char yield, but the lowest tar yield. By increasing the pyrolysis temperature and heating rate, char yield was observed to decrease constantly until it reached its minimum value in the combined mode. The continuous decrease in the char yield, coincided with an increase in the tar and gas yields.

The lowest yield of CO was observed in the low temperature and heating rate experiments, such as the slow pyrolysis experiment in the pyrolyzer apparatus and the radiation-only experiment in the FFB apparatus. By increasing the temperature and heating rate, the CO yield increased until it reached its maximum value in the combined mode. CO₂, as mentioned before, showed the opposite trend. The maximum CO₂ yield was observed during the slow pyrolysis experiment in the pyrolyzer apparatus and the radiation-only experiment in the FFB. CO₂ yield decreased continuously with the temperature and heating rate and reached its minimum value in

the combined mode. However, CH₄ and H₂ trends were different than those of CO and CO₂. CH₄ yield increased by increasing the temperature and heating rate initially and then decreased. The results of Figure 7-10 indicate that the yields of pyrolysis products were very similar for the slow pyrolysis experiment in the pyrolyzer apparatus and the radiation-only experiment in the FFB apparatus since the pyrolysis temperatures and the heating rates of these two set of experiments were similar.

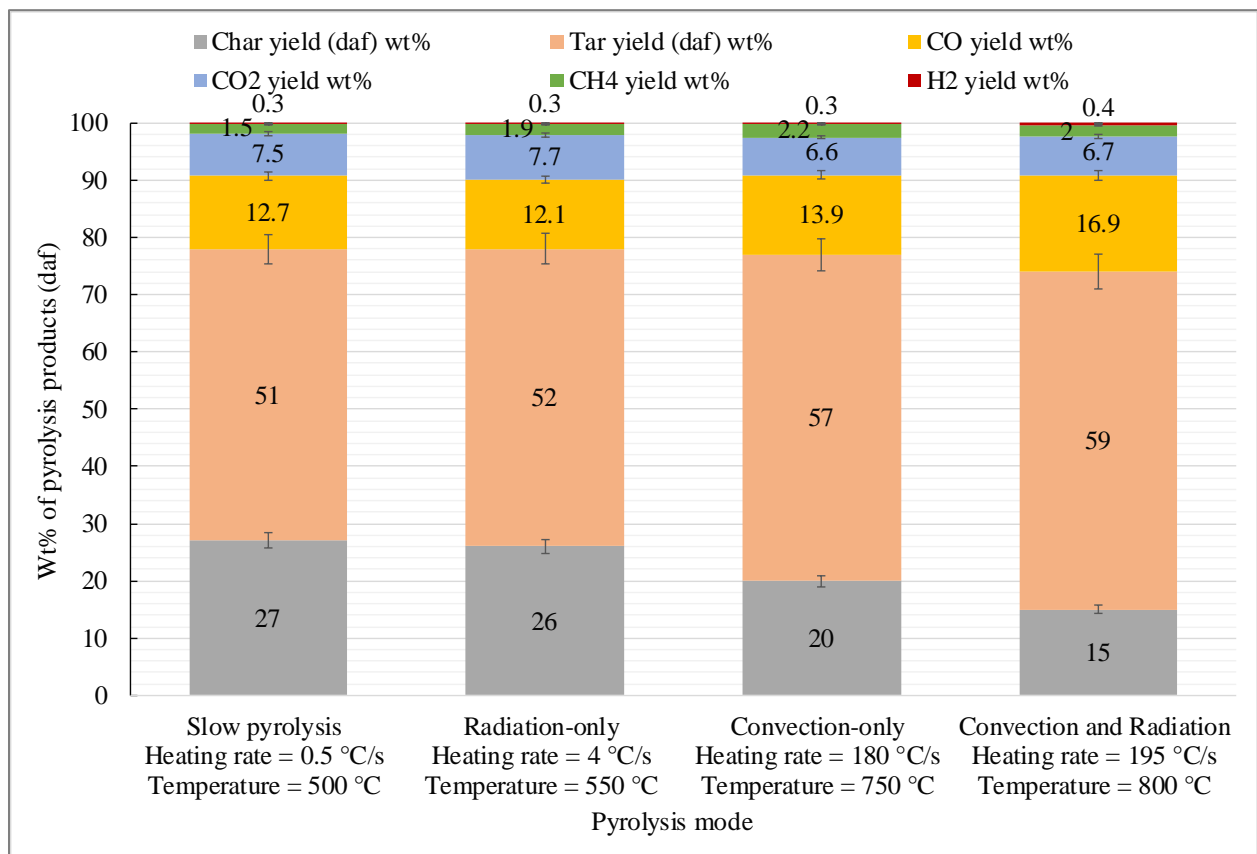


Figure 7-10. Distribution of pyrolysis products from pyrolysis of live longleaf pine foliage

Table 7-3. Summary of light gas analysis for three heating modes

Heating mode	Plants	H ₂		CO		CO ₂		CH ₄	
		Average ^a	Range ^a						
Radiation-only	Live	1.5	1.3-1.9	53.4	51-56	36.0	33-39	9.1	8-10
	Dead	1.3	1.1-1.6	50.4	48-54	40.1	36-43	8.2	7-9
Convection-only	Live	1.7	1.3-2.1	59.8	53-63	29.5	25-35	8.9	6-11
	Dead	1.5	1.0-1.9	58.4	55-61	30.2	28-33	9.8	7-12
Combination of convection and radiation	Live	2.0	1.7-2.4	63.6	60-66	26.8	25-30	7.6	6-8
	Dead	1.7	1.4-2.1	61.6	59-64	28.1	26-31	8.6	8-9

^awt% on a dry light gas basis

7.4 Tar Analysis

The tar analysis data for the convection-only mode were presented in Figure 5-6. The corresponding tar data for the radiation-only and the combined modes are presented in Figure G-8 and Figure G-9, respectively (see Appendix F). Milne and Evans (1998) classified tar into four groups depending on pyrolysis temperature: primary, secondary, alkyl-tertiary, and condensed-tertiary. Primary tars are formed by the decomposition of the plant building blocks (i.e., hemicellulose, cellulose, lignin, etc.) and consist of acids, ketones, aldehydes, alcohols, and phenols (Farag et al., 2014). Primary pyrolysis reactions are completed at approximately 500 °C. Secondary tars, such as heavier phenols and olefins, are formed as the primary tars undergo secondary reactions at temperatures above 500 °C (Shen et al., 2016). Alkyl-tertiary tars are aromatic compounds with alkyl attachments on their rings, such as toluene, methyl naphthalene, etc. Condensed-tertiary tars include PAHs without substituents, such as pyrene, phenanthrene, etc. However, sometimes the distinctions between the types of tars are not completely clear upon product analysis, such as the distinction between secondary and tertiary tar compounds (Rios et al., 2018).

Free-radical reactions are important factors in the formation of the heavier tars (secondary and tertiary tars) from the primary tars. First, the chemical bonds in the primary tars are broken to form free radicals via homolysis reactions. Next, the radicals can react with other tar compounds to form new radicals and heavier tar compounds via ring crosslinking reactions. Then heavier PAHs can form via a series of reactions, such as hydrogen transfer reactions, isomerization reactions, etc. Finally, two radicals can react to form a stable heavy PAH via a termination reaction (Zhou et al., 2015; Feng et al., 2017a).

The tar analysis data indicate that the majority of the tar compounds formed in the radiation-only mode (as shown in Figure 7-11), like the tar compounds in the slow pyrolysis experiments, were primary tars including C₅-C₂₀ aliphatic and 1-2 ring aromatic compounds with multiple attachments (e.g., hydroxyl (OH), methoxy (O-CH₃), etc.) on their rings. The main tar compounds in the radiation-only mode were phenol, 1,2-benzenediol, 1,4-benzenediol, 2-methyl phenol, 4-methyl phenol, 2,6-dimethoxy phenol. These tar compounds, which are known as primary tars, were mainly formed from the degradation of lignin, and have single aromatic rings with hydroxyl, alkyl, and methoxy attachments.

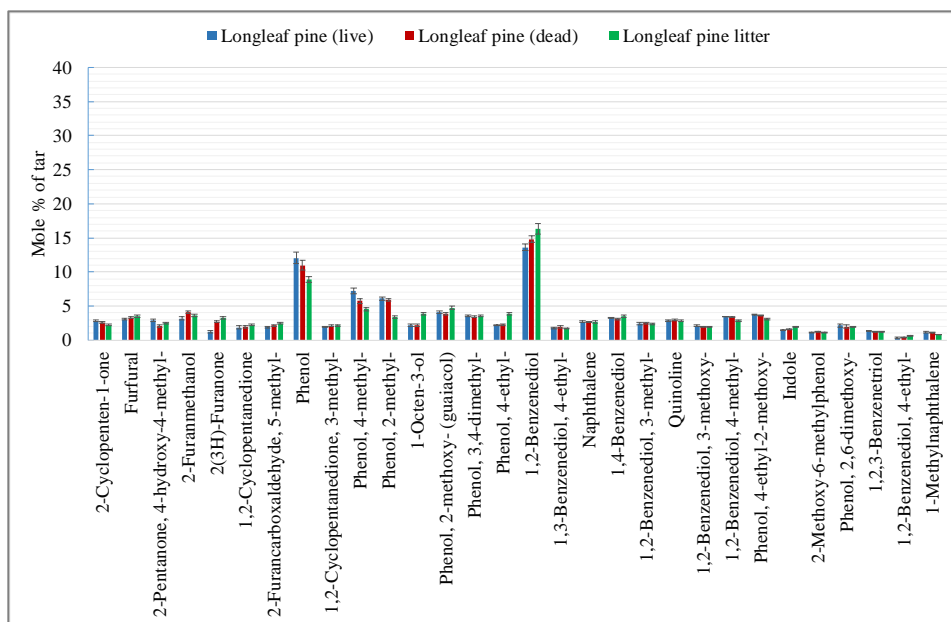


Figure 7-11. Analysis of tar compounds from the pyrolysis of longleaf pine in the radiation-only mode

This distribution of tar compounds exhibits that there were no or little possibilities for the secondary pyrolysis reactions in the radiation-only mode similar to what observed in the slow pyrolysis experiments. As shown in Figure 7-12 and Figure 7-13, in contrast with the tar analysis

in the radiation-only mode, some of the main tar compounds in the convection-only and combined modes were fluorene, anthracene, phenanthrene, flouranthene, pyrene, and benzopyrene. These tar compounds, which are known as secondary and tertiary tars, were mainly formed from the secondary reactions. However, phenol was still a major constituent of the tar in these heating modes. In the convection-only and the combined modes, tar compounds with attachments on their aromatic rings, such as 2,6-dimethoxy phenol, 1,2,3-benzenetriol, 4-methyl phenol, and 1,2, benzenediol were observed, but in lower quantities than those of the radiation-only mode. The tar analysis data shows that as the pyrolysis temperature and heating rate increased during the convection-only and the combined modes, more complex tar compounds including 1- to 5-ring aromatic compounds with few attachments on their rings (known as secondary and tertiary tars) were formed.

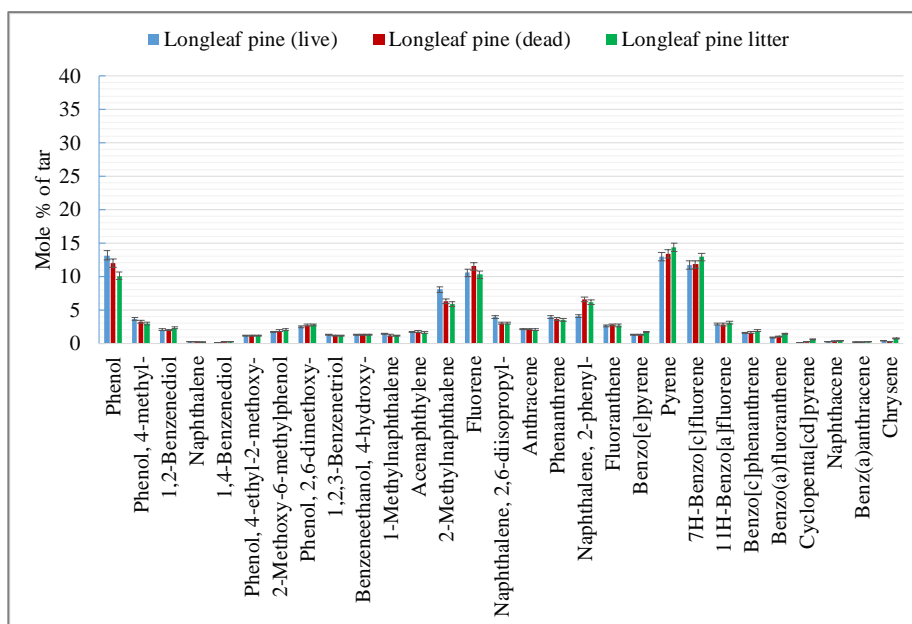


Figure 7-12. Analysis of tar compounds from the pyrolysis of longleaf pine in the convection-only mode

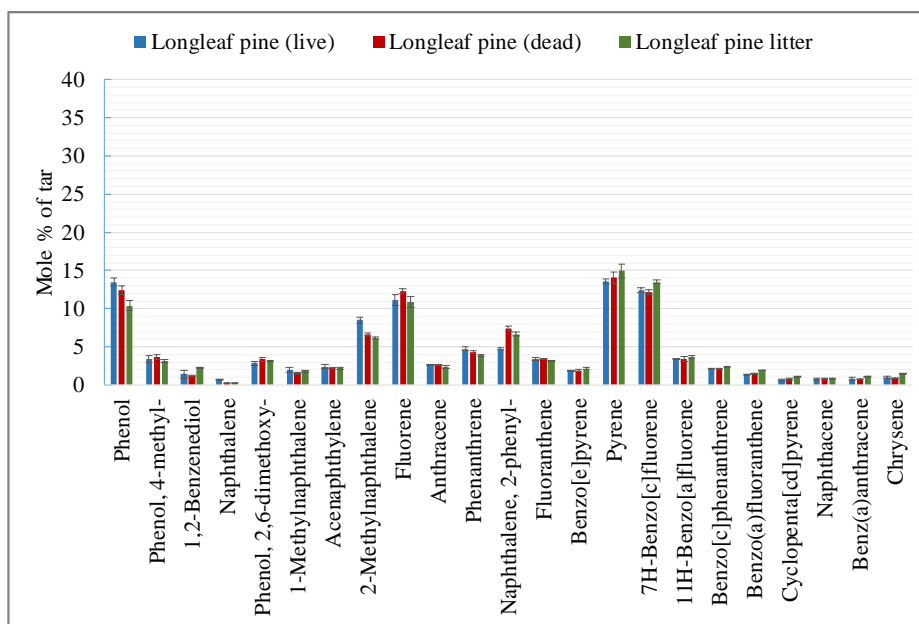


Figure 7-13. Analysis of tar compounds from the pyrolysis of longleaf pine in the combined mode

Figure 7-14 shows the distribution of tar compounds for the pyrolysis of live longleaf pine foliage in the different heating modes. The tar compounds were classified into five groups based on their molecular weight and chemical structure as follows: (1) phenol; (2) derivatives of phenol, including 1,2-benzenediol, 1,4-benzenediol, 2,6-dimethylphenol, etc.; (3) 2-ring aromatic compounds, including naphthalene, 1-methylnaphthalene, etc.; (4) 3- to 5-ring aromatic compounds, including fluoranthene, anthracene, phenanthrene, etc.; and (5) other hydrocarbons, including alcohols, ethers, esters, furans, etc. It is interesting that the distributions of tar compounds were similar for the slow pyrolysis and the radiation-only experiments, where the pyrolysis temperatures and heating rates were closer. In addition, a similarity between the tar distributions were observed in the convection-only and the combined modes. The results indicate that an increase in the pyrolysis temperature and heating rate had a statistically significant effect on the distribution of the functional groups present in the collected tars (p-value < 0.05).

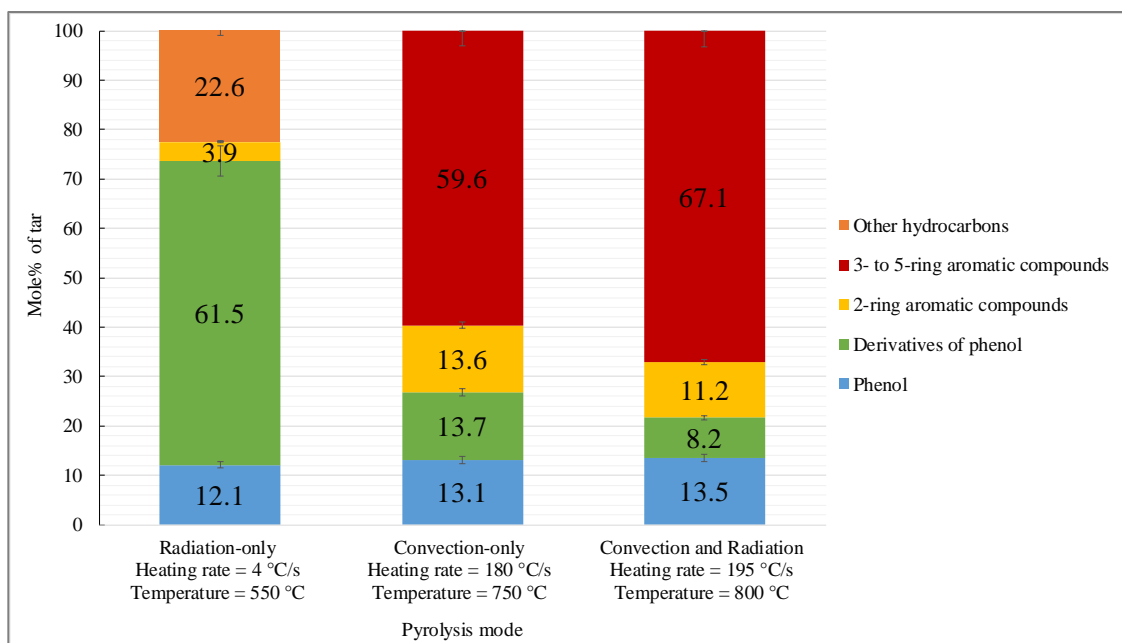


Figure 7-14. Distribution of functional groups in tar for pyrolysis of live longleaf pine

Oxygenated compounds, such as phenol with 10.4 mole% in the slow pyrolysis and 12.1 mole% in the radiation-only mode, and phenol derivatives with 62 mole% in the slow pyrolysis and 61.5 mole% in the radiation-only mode, made up the largest portion of tar produced in the low temperature and heating rate experiments. The remaining species in the slow pyrolysis tar were 2-ring aromatic compounds (only 0.9 mole%) and other oxygenated hydrocarbons (26.7 mole%), such as alcohols, furans, ketones, etc. The radiation-only mode led to a higher mole% of 2-ring aromatic compounds (3.9 mole%), but a lower mole% of other compounds (22.6 mole%) compared to the slow pyrolysis, indicating that the tar from the radiation-only mode underwent more secondary reactions. However, the primary pyrolysis tars underwent relatively few secondary reactions in the radiation-only mode compared to the convection-only and the combined modes. By increasing the temperature and heating rate, the yield of phenol derivatives decreased noticeably to 13.7 and 8.2% for the convection-only mode and the

combined mode, respectively. Lower mole% of phenol derivatives in the high temperature and heating rate experiments indicate that the attachments to the phenol ring were removed, leading to a higher yield of phenol and also contributing to the formation of heavier PAHs. The yield of 2-ring aromatic compounds increased noticeably from 3.9 mole% (in the radiation-only) to 13.6 and 11.2 mole% in the convection-only and the combined modes, respectively. No other oxygenated hydrocarbons, such as alcohols, ketones, esters, etc. were observed in tar at high temperatures and heating rates. Zhang et al. (2015) has reported that the oxygenated tars are completely decomposed and are not found at temperatures higher than 1000 °C. The largest portions of the tar were 3- to 5- ring aromatic compounds for the convection-only mode (59.6 mole%) and the combined mode (67.1 mole%); indicating that the primary tars underwent were significantly affected by secondary reactions. The combined mode, which was performed at a higher pyrolysis temperature and heating rates compared to the convection-only mode, showed that higher fractions of heavy PAHs may be caused by the further secondary reactions of tar compounds.

In a related study, Zhang et al. (2015) noted that by increasing pyrolysis temperature from 700 to 900 °C, the measured concentration of condensed PAHs (condensed means that the aromatic rings have one side in common) in pyrolysis tar during pyrolysis of rice straw increased from 7 to 41%. However, this concentration then slightly decreased to 37% as temperature was increased to 1000 °C. It was also reported that the concentration of alkyl aromatics noticeably decreased at temperatures higher than 800 °C. Cracking and polymerization reactions, which are simultaneous parallel reactions, play important roles in the conversion and formation of tar compounds, especially at higher temperatures and heating rates (Jess, 1996). Among the identified tar compounds during the experiments, as shown in Figure 7-15 and Figure 7-16,

phenol and 1,2-benzenediol were present with noticeable abundance in all three heating mode experiments. The results indicate that by increasing the temperature and heating rate, a higher mole% of phenol, but a lower mole% of 1,2-benzenediol were obtained. During the convection-only and the combined modes, the hydroxyl attachment on the aromatic phenol ring was removed from the chemical structure of 1,2-benzenediol, which led to lower quantity of 1,2-benzenediol at the higher temperature and higher heating rate experiments. Therefore, higher quantities of phenol formed due to the removal of attachments from the aromatic rings in the convection-only and the combined modes. The formation of multiple-ring aromatic compounds at higher temperatures and heating rates may be due to the availability of radical sites due to the removal of attachments from the aromatic rings and then polymerization reactions (Palma, 2013b; Zhang et al., 2015). PAHs may also form due to: (i) the transformation of methoxyphenols to phenol by cleaving the C-O bond, (ii) then phenol may be converted to cyclopentadiene as an intermediate via the decarbonylation reactions, and (iii) finally, PAHs may form from the intermediate through the Diels-Alder reactions (Jess, 1996; Nowakowska et al., 2014).

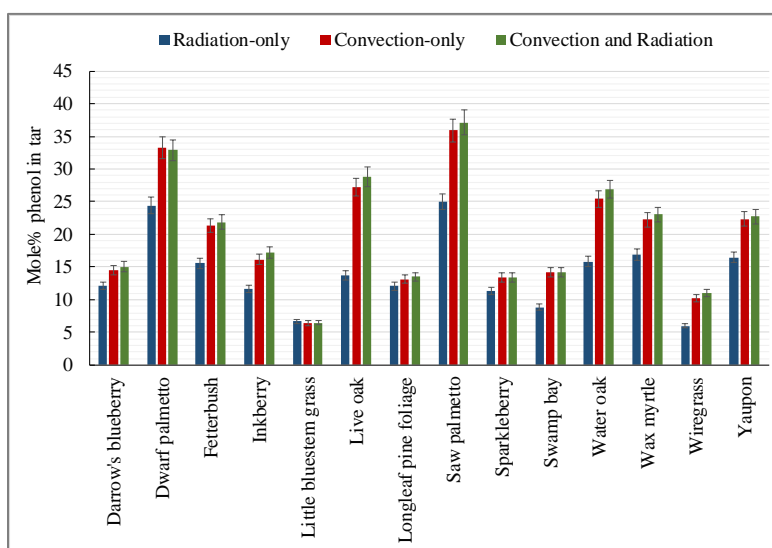


Figure 7-15. Mole% of phenol in tar during pyrolysis of live plant species

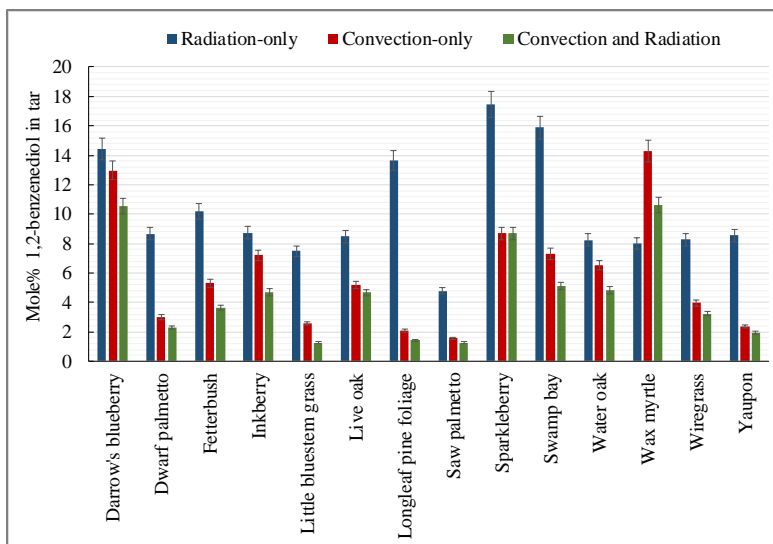


Figure 7-16. Mole% of 1,2-benzenediol in tar during pyrolysis of live plant species

7.5 Summary and Conclusions

In this chapter, the results of the radiation-only mode, the convection-only mode, and the combined mode were compared. The main conclusions from this study are as follows:

- 1- The analysis of pyrolysis product yields showed that the highest gas yields were obtained from the combined mode. The radiation-only mode, which was performed at a lower temperature and a lower heating rate, led to the lowest gas yields for all plant species. The average gas yield obtained from the pyrolysis of all plants (live and dead) was 20 wt% (daf) for the radiation-only mode, 22 wt% for the convection-only mode, and 24% for the combined mode.
- 2- Similar to the gas yield data, by increasing the pyrolysis temperature and heating rate, higher tar yields were obtained. The average tar yield from the pyrolysis of all plants (live and dead) was 53 wt% (daf) for the radiation-only mode. However, this value was 58 and 59 wt% (daf) for the convection-only mode and the combined mode, respectively.

The higher gas and tar yields at higher pyrolysis temperatures and heating rates were due to a combination of the further pyrolysis of char and secondary pyrolysis reactions of tar.

- 3- For all three heating modes, CO was the main light gas species on a wt% basis, followed by CO₂, CH₄, and H₂. The lowest and the highest CO yields were observed during the radiation-only mode and the combined mode, respectively. The average CO yield from the pyrolysis of all plants (live and dead) was 52 wt% (dry light gas basis) for the radiation-only mode, 59 wt% for the convection-only mode, and 63% for the combined mode. In contrast, higher yields of CO₂ were observed in the radiation-only mode compared to the two other heating modes. The average CO₂ yield from the pyrolysis of all plants (live and dead) was 38 wt% (dry light gas basis) for the radiation-only mode, 30 wt% for the convection-only mode, and 27% for the combined mode.
- 4- For most of the plants, higher yields of CH₄ were observed in the radiation-only mode. However, for a few plant species, such as Darrow's blueberry and swamp bay, higher yields of CH₄ were obtained in the convection-only mode. However, higher H₂ yields were obtained in the mode.
- 5- The distribution of tar compounds in the radiation-only mode was completely different than that of the convection-only and the combined modes. During the radiation-only mode, which was performed at a lower temperature and a lower heating rate, primary tar compounds were the most prevalent compounds in tar, which formed from the decomposition of lignin. However, during the convection-only and the combined modes, tar included phenol and a few other 1-ring compounds, but also included a significant amount of 3- to 5-ring aromatic compounds with very few attachments on the rings.
The presence of these heavy polycyclic aromatic hydrocarbons (PAHs) at high

temperatures and heating rates indicate that the primary tar compounds underwent secondary reactions.

- 6- Comparing the yields of tar compounds, such as phenol and 1,2-benzenediol, present in all heating modes, showed that a higher mole% of 1,2-benzenediol was obtained in radiation-only mode, but a higher mole% of phenol in the convection-only and the combined modes. It seems that at higher temperatures and heating rates, the hydroxyl attachment on the phenol aromatic ring was removed, which led to a higher mole% of phenol, and provided radical sites on the aromatic rings that contributed to the polymerization of smaller PAHs and formation of larger multi-ring compounds.
- 7- In this work, the differences between the yields and the compositions of pyrolysis products from different heating modes are thought to be mainly due to the different operating temperatures and heating rates regardless of the heat transfer mechanism. However, it is likely that a difference between the radiation-only and convection-only modes will still be observed if the radiation-only experiments were to be operated at a heating rate and a temperature similar to those of the convection-only experiments due to the further secondary reactions that occur in the gas phase during the convection-only mode. In radiation-only experiments, the gas phase temperature is not high enough for these secondary reactions to occur.

8 SUMMARY AND CONCLUSIONS

In this research, fast pyrolysis of 14 plant species native to the forests of the southern United States was studied using heating rates typical of wildland fires. The fast pyrolysis experiments were performed in a flat-flame burner (FFB) apparatus using three heating modes: convection-only, radiation-only, and a combination of radiation and convection. During the experiments, pyrolysis products were collected and analyzed using a GC-MS instrument for the analysis of tars and a GC-TCD instrument for the analysis of light gases. In addition, the results of fast pyrolysis experiments were compared with the results of slow pyrolysis experiments, which were performed in a pyrolyzer apparatus by Amini et al. (2019).

8.1 Pyrolysis Product Yield

Analysis of the pyrolysis products indicated that pyrolysis temperature, heating rate, and fuel type have significant impacts on the yields and the compositions of pyrolysis products. However, fuel condition (live vs. dead) had a moderate effect on the yields of pyrolysis products (on a dry basis).

For a specific pyrolysis temperature and heating rate, the variation in pyrolysis product yields between different plant species may be caused by changes in the composition of plants as well as the interactions of the plant constituents (i.e., cellulose, hemicellulose, and lignin). The results indicated that the plants from the same family (i.e., (i) live oak and water oak, (ii) inkberry

and yaupon, and (iii) sparkleberry and Darrow's blueberry) showed very similar tar and char yields during the experiments.

For all plant species, higher light gas, tar, and total volatile (tar plus gas) yields were obtained by increasing pyrolysis temperature and heating rate. Therefore, the highest light gas, tar, and total volatile yields were observed during the combined convection and radiation experiments. The high gas yield seen in the convection-only and the combined convection and radiation experiments was due to the further cracking of char and secondary reactions of tar compounds at higher pyrolysis temperatures and heating rates. In contrast, the radiation-only and the slow pyrolysis experiments, which were performed at lower temperatures and heating rates, led to the lower light gas, tar, and total volatile yields, but higher char yields.

8.2 Light Gas Analysis

Carbon monoxide was the main component in the light gases on a wt% dry basis, followed by CO₂, CH₄, and H₂ for all pyrolysis experiments. Like the product yield results, the light gas yields were observed to be highly dependent on pyrolysis temperature and heating rate. For most plant species, the light gas yields were not significantly different between live and dead samples for a specific plant species.

CO yield continuously increased by increasing the temperature and heating rate during the experiments. Therefore, the highest CO yield was observed during the combined convection and radiation experiments. In contrast, by increasing the pyrolysis temperature and heating rate, CO₂ formation showed a different trend than CO; higher CO₂ yields were obtained from the radiation-only and the slow pyrolysis experiments. For most of the plants, higher yields of CH₄ were observed at a lower pyrolysis temperature and heating rate (radiation-only mode). However, for a few plant species, higher yields of CH₄ were obtained during the high temperature and heating

rate experiments (convection-only mode). For all the plant species, H₂ yield enhanced by increasing the temperature and heating rate. Therefore, the highest H₂ yields were observed during the combined convection and radiation experiments.

8.3 Tar Analysis

The results of tar analysis showed that the majority of the identified tar compounds during the radiation-only and the slow pyrolysis experiments were C₅-C₂₀ aliphatic and 1-2 ring aromatic compounds, such as phenol, 1,2-benzendiol, 2-methoxy phenol, and 4-methyl phenol. These aromatic compounds had multiple attachments, such as hydroxyl, alkyl, and methoxy groups, to the rings. In contrast, the tar analysis from the convection-only and the combined convection and radiation experiments, which were performed at higher pyrolysis temperatures and heating rates, exhibited 1- to 5-ring aromatic compounds with very few attachments on the rings were formed during these experiments. Major tar species observed included phenol, naphthalene, fluorene, anthracene, phenanthrene, fluoranthene, and pyrene. The presence of heavier PAHs at higher pyrolysis temperature and heating rate showed that the primary tars underwent secondary reactions to form secondary and tertiary tars.

8.4 Recommended Future Work

A list of recommendations for future research on the pyrolysis of live and dead vegetation is given below:

- Study the effects of fuel orientation in relation to gas and heat flow and its effects on pyrolysis behavior and products.
- Investigate the difference between single-leaf and multi-leaf pyrolysis experiments.
- Conduct research on the effects of residence time of pyrolysis products at high temperatures

on the yields and the compositions of pyrolysis products.

- Create correlations between the compositions of pyrolysis products and the weight fractions of plant constituents such as hemicellulose, cellulose, lignin, etc.
- Compare the product analysis performed by GC-TCD with the results from an analysis by FTIR.
- Conduct a carbon balance using the compositions of pyrolysis products and the composition of the fuel.
- Compare the results measured in laboratory experiments with results measured in outdoor field experiments.
- Determine simplified product yield and species expressions for use in landscape simulations of fires.
- Measure the rates of pyrolysis in a TGA for these species and see if those rates can be used to explain the pyrolysis rates at the high heating rates in the FFB apparatus.

REFERENCES

- Adrados, A., A. Lopez-Urionabarrenechea, J. Solar, J. Requies, I. De Marco and J. F. Cambra, "Upgrading of pyrolysis vapours from biomass carbonization," *Journal of Analytical and Applied Pyrolysis*, **103**, 293-299 (2013).
- Agirre, I., T. Griessacher, G. Rosler and J. Antrekowitsch, "Production of charcoal as an alternative reducing agent from agricultural residues using a semi-continuous semi-pilot scale pyrolysis screw reactor," *Fuel Processing Technology*, **106**, 114-121 (2013).
- Aho, A., N. DeMartini, A. Pranovich, J. Krogell, N. Kumar, K. Eranen, B. Holmbom, T. Salmi, M. Hupa and D. Y. Murzin, "Pyrolysis of pine and gasification of pine chars - Influence of organically bound metals," *Bioresource Technology*, **128**, 22-29 (2013).
- Al Arni, S., "Comparison of slow and fast pyrolysis for converting biomass into fuel," *Renewable Energy*, **124**, 197-201 (2018).
- Albini, F. A., "A model for fire spread in wildland Fuels by radiation," *Combustion Science and Technology*, **42**(5-6), 229-258 (1985).
- Alonso, D. M., S. G. Wettstein and J. A. Dumesic, "Bimetallic catalysts for upgrading of biomass to fuels and chemicals," *Chemical Society Reviews*, **41**, 8075-8098 (2012).
- Amen-Chen, C., H. Pakdel and C. Roy, "Production of monomeric phenols by thermochemical conversion of biomass: a review," *Bioresource Technology*, **79**(3), 277-299 (2001).
- Amini, E., M.-S. Safdari, J. T. DeYoung, D. R. Weise and T. H. Fletcher, "Characterization of pyrolysis products from slow pyrolysis of live and dead vegetation native to the southern United States," *Fuel*, **235**, 1475-1491 (2019).
- Anis, S. and Z. A. Zainal, "Tar reduction in biomass producer gas via mechanical, catalytic and thermal methods: A review," *Renewable & Sustainable Energy Reviews*, **15**(5), 2355-2377 (2011).
- Asensio, M. I. and L. Ferragut, "On a wildland fire model with radiation," *International Journal for Numerical Methods in Engineering*, **54**(1), 137-157 (2002).

- Aysu, T. and M. M. Kucuk, "Biomass pyrolysis in a fixed-bed reactor: effects of pyrolysis parameters on product yields and characterization of products," *Energy*, **64**, 1002-1025 (2014).
- Baines, P. G., "Physical mechanisms for the propagation of surface fires," *Mathematical and Computer Modelling*, **13**(12), 83-94 (1990).
- Barnett, J. P. and J. M. McGilvary, "Practical guidelines for producing longleaf pine seedlings in containers," *U.S. Department of Agriculture, Forest Service, Southern Research Station*, (1997).
- Baronas, R. and F. Ivanauskas, "Reducing spatial dimensionality in a model of moisture diffusion in a solid material," *International Journal of Heat and Mass Transfer*, **47**(4), 699-705 (2004).
- Ben, H. X. and A. J. Ragauskas, "Comparison for the compositions of fast and slow pyrolysis oils by NMR characterization," *Bioresource Technology*, **147**, 577-584 (2013).
- Biagini, E. and L. Tognotti, "A generalized procedure for the devolatilization of biomass fuels based on the chemical components," *Energy & Fuels*, **28**(1), 614-623 (2014).
- Bilbao, R., M. L. Salvador and J. Arauzo, "Influence of the heating rate on the temperature profiles and on the conversion rate of powdery cellulose and pine sawdust," *Journal of Analytical and Applied Pyrolysis*, **30**(2), 145-159 (1994).
- Boerjan, W., J. Ralph and M. Baucher, "Lignin biosynthesis," *Annual Review of Plant Biology*, **54**, 519-546 (2003).
- Bradbury, A. W., Y. Sakai and F. Shafizadeh, "A kinetic model for pyrolysis of cellulose," *Journal of applied polymer science*, **23**(11), 3271-3280 (1979).
- Bridgwater, A. V., D. Meier and D. Radlein, "An overview of fast pyrolysis of biomass," *Organic Geochemistry*, **30**(12), 1479-1493 (1999).
- Bridgwater, A. V., "Review of fast pyrolysis of biomass and product upgrading," *Biomass & Bioenergy*, **38**, 68-94 (2012).
- Burgan, R. E. and R. C. Rothermel, "Behave: fire behavior prediction and fuel modeling system," General Technical Report INT-167. Ogden, UT: U. S. Department of Agriculture, Forest Service, Intermountain Forest and Range Experiment Station. 126 p. (1984).
- Burling, I. R., R. J. Yokelson, D. W. T. Griffith, T. J. Johnson, P. Veres, J. M. Roberts, C. Warneke, S. P. Urbanski, J. Reardon, D. R. Weise, W. M. Hao and J. de Gouw, "Laboratory measurements of trace gas emissions from biomass burning of fuel types from the southeastern and southwestern United States," *Atmospheric Chemistry and Physics*, **10**(22), 11115-11130 (2010).

- Butler, B. W., J. Cohen, D. J. Latham, R. D. Schuette, P. Sopko, K. S. Shannon, D. Jimenez and L. S. Bradshaw, "Measurements of radiant emissive power and temperatures in crown fires," *Canadian Journal of Forest Research-Revue Canadienne De Recherche Forestiere*, **34**(8), 1577-1587 (2004).
- Butterman, H. C. and M. J. Castaldi, "Biomass to suels: impact of reaction medium and heating rate," *Environmental Engineering Science*, **27**(7), 539-555 (2010).
- Byram, G. M., "Combustion of forest fuels: forest fire: control and use," Eds., McGraw-Hill: 61-89 (1959).
- Carrier, G. F., F. E. Fendell and M. F. Wolff, "Wind-aided firespread across arrays of discrete fuel-elements .1. theory," *Combustion Science and Technology*, **75**(1-3), 31-51 (1991).
- Catchpole, W. R., E. A. Catchpole, B. W. Butler, R. C. Rothermel, G. A. Morris and D. J. Latham, "Rate of spread of free-burning fires in woody fuels in a wind tunnel," *Combustion Science and Technology*, **131**(1-6), 1-37 (1998).
- Cesarino, I., P. Araujo, A. P. Domingues and P. Mazzafera, "An overview of lignin metabolism and its effect on biomass recalcitrance," *Brazilian Journal of Botany*, **35**(4), 303-311 (2012).
- Cetin, E., R. Gupta and B. Moghtaderi, "Effect of pyrolysis pressure and heating rate on radiata pine char structure and apparent gasification reactivity," *Fuel*, **84**(10), 1328-1334 (2005).
- Chen, Y. Q., H. P. Yang, X. H. Wang, S. H. Zhang and H. P. Chen, "Biomass-based pyrolytic polygeneration system on cotton stalk pyrolysis: Influence of temperature," *Bioresource Technology*, **107**, 411-418 (2012).
- Choi, H. S., Y. S. Choi and H. C. Park, "Fast pyrolysis characteristics of lignocellulosic biomass with varying reaction conditions," *Renewable Energy*, **42**, 131-135 (2012).
- Collard, F. X. and J. Blin, "A review on pyrolysis of biomass constituents: Mechanisms and composition of the products obtained from the conversion of cellulose, hemicelluloses and lignin," *Renewable & Sustainable Energy Reviews*, **38**, 594-608 (2014).
- Cosgrove, D. J., "Assembly and enlargement of the primary cell wall in plants," *Annual Review of Cell and Developmental Biology*, **13**, 171-201 (1997).
- Cosgrove, D. J., "Growth of the plant cell wall," *Nature Reviews Molecular Cell Biology*, **6**(11), 850-861 (2005).
- Debdoubi, A., A. El Amarti, E. Colacio, M. J. Blesa and L. H. Hajjaj, "The effect of heating rate on yields and compositions of oil products from esparto pyrolysis," *International Journal of Energy Research*, **30**(15), 1243-1250 (2006).

- Debiagi, P. E. A., C. Pecchi, G. Gentile, A. Frassoldati, A. Cuoci, T. Faravelli and E. Ranzi, "Extractives extend the applicability of multistep kinetic scheme of biomass pyrolysis," *Energy & Fuels*, **29**(10), 6544-6555 (2015).
- Demestre, N. J., E. A. Catchpole, D. H. Anderson and R. C. Rothermel, "Uniform propagation of a planar fire front without wind," *Combustion Science and Technology*, **65**(4-6), 231-244 (1989).
- Demiral, I., A. Eryazici and S. Sensoz, "Bio-oil production from pyrolysis of corncob (*Zea mays* L.)," *Biomass & Bioenergy*, **36**, 43-49 (2012).
- Dennison, P. E. and M. A. Moritz, "Critical live fuel moisture in chaparral ecosystems: a threshold for fire activity and its relationship to antecedent precipitation," *International Journal of Wildland Fire*, **18**(8), 1021-1027 (2009).
- Di Blasi, C., "The state of the art of transport models for charring solid degradation," *Polymer International*, **49**(10), 1133-1146 (2000).
- DiBlasi, C., "Numerical simulation of cellulose pyrolysis," *Biomass and Bioenergy*, **7**, 87-98 (1994).
- DiBlasi, C. and M. Lanzetta, "Intrinsic kinetics of isothermal xylan degradation in inert atmosphere," *Journal of Analytical and Applied Pyrolysis*, **40-1**, 287-303 (1997).
- Diebold, J. P., "A unified, global model for the pyrolysis of cellulose," *Biomass & Bioenergy*, **7**(1-6), 75-85 (1994).
- Dimitrakopoulos, A. P. and K. K. Papaioannou, "Flammability assessment of Mediterranean forest fuels," *Fire Technology*, **37**(2), 143-152 (2001).
- Dimitrakopoulos, A. P., I. D. Mitsopoulos and K. Gatoulas, "Assessing ignition probability and moisture of extinction in a Mediterranean grass fuel," *International Journal of Wildland Fire*, **19**(1), 29-34 (2010).
- Duman, G., C. Okutucu, S. Ucar, R. Stahl and J. Yanik, "The slow and fast pyrolysis of cherry seed," *Bioresource Technology*, **102**(2), 1869-1878 (2011).
- Elder, T., "A computational study of pyrolysis reactions of lignin model compounds," *Holzforschung*, **64**(4), 435-440 (2010).
- Fang, J. B. and F. R. Steward, "Flame spread through randomly packed fuel particles," *Combustion and Flame*, **13**(4), 392-& (1969).
- Farag, S., D. B. Fu, P. G. Jessop and J. Chaouki, "Detailed compositional analysis and structural investigation of a bio-oil from microwave pyrolysis of kraft lignin," *Journal of Analytical and Applied Pyrolysis*, **109**, 249-257 (2014).

- Feng, D. D., Y. J. Zhao, Y. Zhang and S. Z. Sun, "Effects of H₂O and CO₂ on the homogeneous conversion and heterogeneous reforming of biomass tar over biochar," *International Journal of Hydrogen Energy*, **42**(18), 13070-13084 (2017a).
- Feng, Y., Y. G. Jiang, X. Li, S. L. Zhang, J. Qin, Y. Cao and H. Y. Huang, "Numerical study on the influences of heat and mass transfers on the pyrolysis of hydrocarbon fuel in mini-channel," *Applied Thermal Engineering*, **119**, 650-658 (2017b).
- Ferguson, S. C., A. Dahale, B. Shotorban, S. Mahalingam and D. R. Weise, "The role of moisture on combustion of pyrolysis gases in wildland fires," *Combustion Science and Technology*, **185**(3), 435-453 (2013).
- Finney, M. A., J. D. Cohen, S. S. McAllister and W. M. Jolly, "On the need for a theory of wildland fire spread," *International Journal of Wildland Fire*, **22**(1), 25-36 (2013).
- Fletcher, T. H., B. M. Pickett, S. G. Smith, G. S. Spittle, M. M. Woodhouse, E. Haake and D. R. Weise, "Effects of moisture on ignition behavior of moist California chaparral and Utah leaves," *Combustion Science and Technology*, **179**(6), 1183-1203 (2007).
- Fourty, T., F. Baret, S. Jacquemoud, G. Schmuck and J. Verdebout, "Leaf optical properties with explicit description of its biochemical composition: Direct and inverse problems," *Remote Sensing of Environment*, **56**(2), 104-117 (1996).
- Frankman, D., B. W. Webb and B. W. Butler, "Time-resolved radiation and convection heat transfer in combusting discontinuous fuel beds," *Combustion Science and Technology*, **182**(10), 1391-1412 (2010a).
- Frankman, D., B. W. Webb, B. W. Butler and D. J. Latham, "Fine fuel heating by radiant flux," *Combustion Science and Technology*, **182**(2), 215-230 (2010b).
- Frankman, D., B. W. Webb and B. W. Butler, "Measurements of convective and radiative heating in wildland fires," *International Journal of Wildland Fire*, **22**, 157-167 (2012).
- French, D., Chapter five - advances in clinical mass spectrometry, (2017).
- Gallacher, J., "The influence of season, heating mode and slope angle on wildland fire behavior," PhD Dissertation, Chemical Engineering, Brigham Young University (2016).
- Gao, N. B., B. L. Liu, A. M. Li and J. J. Li, "Continuous pyrolysis of pine sawdust at different pyrolysis temperatures and solid residence times," *Journal of Analytical and Applied Pyrolysis*, **114**, 155-162 (2015).
- Garcia-Perez, M., A. Chaala, H. Pakdel, D. Kretschmer and C. Roy, "Characterization of bio-oils in chemical families," *Biomass & Bioenergy*, **31**(4), 222-242 (2007).

- Gautam, R., A. K. Varma and R. Vinu, "Apparent kinetics of fast pyrolysis of four different microalgae and product analyses using pyrolysis-FTIR and pyrolysis-GC/MS," *Energy & Fuels*, **31**(11), 12339-12349 (2017).
- Gomez-Barea, A. and B. Leckner, "Modeling of biomass gasification in fluidized bed," *Progress in Energy and Combustion Science*, **36**(4), 444-509 (2010).
- Grob, R. L. and E. F. Barry, *Modern practice of gas chromatography*, (2004).
- Gronli, M. G. and M. C. Melaaen, "Mathematical model for wood pyrolysis - comparison of experimental measurements with model predictions," *Energy & Fuels*, **14**(4), 791-800 (2000).
- Guo, X., S. Wang, K. Wang and Q. Liu, "Influence of extractives on mechanism of biomass pyrolysis," *Journal of Fuel Chemistry and Technology*, **38**, 42-46 (2010).
- Haghi, A. K., "Thermal analysis of drying process - a theoretical approach," *Journal of Thermal Analysis and Calorimetry*, **74**(3), 827-842 (2003).
- Hartman, G., "Forest land management guide: use of prescribed fire," Missouri Department of Conservation (2005).
- Haseli, Y., J. A. van Oijen and L. P. H. de Goey, "Modeling biomass particle pyrolysis with temperature-dependent heat of reactions," *Journal of Analytical and Applied Pyrolysis*, **90**(2), 140-154 (2011).
- Haykiri-Acma, H., S. Yaman and S. Kucukbayrak, "Effect of heating rate on the pyrolysis yields of rapeseed," *Renewable Energy*, **31**(6), 803-810 (2006).
- Henrich, E., N. Dahmen, F. Weirich, R. Reimert and C. Kornmayer, "Fast pyrolysis of lignocellulosics in a twin screw mixer reactor," *Fuel Processing Technology*, **143**, 151-161 (2016).
- Heo, H. S., H. J. Park, Y. K. Park, C. Ryu, D. J. Suh, Y. W. Suh, J. H. Yim and S. S. Kim, "Bio-oil production from fast pyrolysis of waste furniture sawdust in a fluidized bed," *Bioresource Technology*, **101**, S91-S96 (2010).
- Hilbers, T. J., Z. H. Wang, B. Pecha, R. J. M. Westerhof, S. R. A. Kersten, M. R. Pelaez-Samaniego and M. Garcia-Perez, "Cellulose-Lignin interactions during slow and fast pyrolysis," *Journal of Analytical and Applied Pyrolysis*, **114**, 197-207 (2015).
- Hoffmann, E. D. and V. Stroobant, *Mass spectrometry: principles and applications*, (2007).
- Horne, P. A. and P. T. Williams, "Influence of temperature on the products from the flash pyrolysis of biomass," *Fuel*, **75**(9), 1051-1059 (1996).

- Howell, J. R., M. P. Megnuc and R. Siegel, Thermal radiation heat transfer, 6th edition, CRC Press (2015).
- Jess, A., "Mechanisms and kinetics of thermal reactions of aromatic hydrocarbons from pyrolysis of solid fuels," *Fuel*, **75**(12), 1441-1448 (1996).
- Jolly, W. M., A. M. Hadlow and K. Huguet, "De-coupling seasonal changes in water content and dry matter to predict live conifer foliar moisture content," *International Journal of Wildland Fire*, **23**(4), 480-489 (2014).
- Jolly, W. M. and B. Butler, "Linking photosynthesis and combustion characteristics in live fuels: the role of soluble carbohydrates in fuel preheating," Joint Fire Science Program (2015).
- Jolly, W. M. and D. M. Johnson, "Pyro-ecophysiology: shifting the paradigm of live wildland fuel research," *Fire*, **1**(1), 8 (2018).
- Ku, C. S. and S. P. Mun, "Characterization of pyrolysis tar derived from lignocellulosic biomass," *Journal of Industrial and Engineering Chemistry*, **12**(6), 853-861 (2006).
- Leroy, V., D. Cancellieri, E. Leoni and J. L. Rossi, "Kinetic study of forest fuels by TGA: model-free kinetic approach for the prediction of phenomena," *Thermochimica Acta*, **497**(1-2), 1-6 (2010).
- Lewis, A. D. and T. H. Fletcher, "Prediction of sawdust pyrolysis yields from a flat-flame burner using the CPD model," *Energy & Fuels*, **27**(2), 942-953 (2013).
- Li, C. S. and K. Suzuki, "Tar property, analysis, reforming mechanism and model for biomass gasification - an overview," *Renewable & Sustainable Energy Reviews*, **13**(3), 594-604 (2009).
- Lin, Y. H., W. Yan and K. C. Sheng, "Effect of pyrolysis conditions on the characteristics of biochar produced from a tobacco stem," *Waste Management & Research*, **34**(8), 793-801 (2016).
- Liu, W. J., W. W. Li, H. Jiang and H. Q. Yu, "Fates of chemical elements in biomass during its pyrolysis," *Chemical Reviews*, **117**(9), 6367-6398 (2017).
- Lopez, A., F. D. Molina-Aiz, D. L. Valera and A. Pena, "Determining the emissivity of the leaves of nine horticultural crops by means of infrared thermography," *Scientia Horticulturae*, **137**, 49-58 (2012).
- Maggi, R. and B. Delmon, "Comparison between slow and flash pyrolysis oils from biomass," *Fuel*, **73**(5), 671-677 (1994).
- Maniatis, K. and A. A. C. M. Beenackers, "Tar protocols: IEA bioenergy gasification task," *Biomass & Bioenergy*, **18**(1), 1-4 (2000).

- Manya, J. J., E. Velo and L. Puigjaner, "Kinetic of biomass pyrolysis: a reformulated three parallel reactions model," *Industrial & Engineering Chemistry Research*, **42**(3), 434-441 (2003).
- McAllister, S., I. Grenfell, A. Hadlow, W. M. Jolly, M. Finney and J. Cohen, "Piloted ignition of live forest fuels," *Fire Safety Journal*, **51**, 133-142 (2012).
- McAllister, S. and M. Finney, "Autoignition of wood under combined convective and radiative heating," *Proceedings of the Combustion Institute*, **36**(2), 3073-3080 (2017).
- Melvin, M. A., "National prescribed fire use survey report. coalition of prescribed fire councils," T. R. 02-15: 17 (2015).
- Milne, T. A. and R. J. Evans, "Biomass gasifier "tars": their nature, formation, and conversion," TP-570-25357, NREL (1998).
- Moersch, O., H. Spliethoff and K. R. G. Hein, "Tar quantification with a new online analyzing method," *Biomass & Bioenergy*, **18**(1), 79-86 (2000).
- Mohnen, D., "Pectin structure and biosynthesis," *Current Opinion in Plant Biology*, **11**(3), 266-277 (2008).
- Moore, A., S. Park, C. Segura and M. Carrier, "Fast pyrolysis of lignin-coated radiata pine," *Journal of Analytical and Applied Pyrolysis*, **115**, 203-213 (2015).
- Neves, D., H. Thunman, A. Matos, L. Tarelho and A. Gomez-Barea, "Characterization and prediction of biomass pyrolysis products," *Progress in Energy and Combustion Science*, **37**(5), 611-630 (2011).
- Ni, M., D. Y. C. Leung, M. K. H. Leung and K. Sumathy, "An overview of hydrogen production from biomass," *Fuel Processing Technology*, **87**(5), 461-472 (2006).
- Nowakowska, M., O. Herbinet, A. Dufour and P.-A. Glaude, "Detailed kinetic study of anisole pyrolysis and oxidation to understand tar formation during biomass combustion and gasification," *Combustion and Flame*, **161**(6), 1474-1488 (2014).
- Onay, O. and O. M. Kockar, "Slow, fast and flash pyrolysis of rapeseed," *Renewable Energy*, **28**(15), 2417-2433 (2003).
- Oudenhoven, S. R. G., R. J. M. Westerhof and S. R. A. Kersten, "Fast pyrolysis of organic acid leached wood, straw, hay and bagasse: improved oil and sugar yields," *Journal of Analytical and Applied Pyrolysis*, **116**, 253-262 (2015).
- Palma, C. F., "Model for biomass gasification including tar formation and evolution," *Energy & Fuels*, **27**(5), 2693-2702 (2013a).

- Palma, C. F., "Modelling of tar formation and evolution for biomass gasification: a review," *Applied Energy*, **111**, 129-141 (2013b).
- Park, W. C., A. Atreya and H. R. Baum, "Experimental and theoretical investigation of heat and mass transfer processes during wood pyrolysis," *Combustion and Flame*, **157**(3), 481-494 (2010).
- Phuphuakrat, T., T. Namioka and K. Yoshikawa, "Tar removal from biomass pyrolysis gas in two-step function of decomposition and adsorption," *Applied Energy*, **87**(7), 2203-2211 (2010).
- Pickett, B. M., C. Isackson, R. Wunder, T. H. Fletcher, B. W. Butler and D. R. Weise, "Experimental measurements during combustion of moist individual foliage samples," *International Journal of Wildland Fire*, **19**(2), 153-162 (2010).
- Prince, D., C. Shen and T. Fletcher, "Semi-empirical model for fire spread in shrubs with spatially defined fuel elements and flames," *Fire Technology*, **53**(3), 1439-1469 (2017).
- Prince, D. R., "Measurement and modeling of fire behavior in leaves and sparse shrubs," PhD Dissertation, Chemical Engineering, Brigham Young University (2014).
- Prince, D. R. and T. H. Fletcher, "Differences in burning behavior of live and dead leaves, part 1: measurements," *Combustion Science and Technology*, **186**(12), 1844-1857 (2014).
- Prins, M. J., K. J. Ptasiński and F. J. J. G. Janssen, "Torrefaction of wood - Part 1. weight loss kinetics," *Journal of Analytical and Applied Pyrolysis*, **77**(1), 28-34 (2006).
- Putun, A. E., E. Onal, B. B. Uzun and N. Ozbay, "Comparison between the "slow" and "fast" pyrolysis of tobacco residue," *Industrial Crops and Products*, **26**(3), 307-314 (2007).
- Pütün, A. E., N. Özbay, E. P. Önal and E. Pütün, "Fixed-bed pyrolysis of cotton stalk for liquid and solid products," *Fuel Processing Technology*, **86**(11), 1207-1219 (2005).
- Puy, N., R. Murillo, M. V. Navarro, J. M. Lopez, J. Rieradevall, G. Fowler, I. Aranguren, T. Garcia, J. Bartroli and A. M. Mastral, "Valorisation of forestry waste by pyrolysis in an auger reactor," *Waste Management*, **31**(6), 1339-1349 (2011).
- Pyle, D. L. and C. A. Zaror, "Heat transfer and kinetics in the low temperature pyrolysis of solids," *Chemical Engineering Science*, **39**(1), 147-158 (1984).
- Ramsey, S. and D. Schafer, *The statistical sleuth: a course in methods of data analysis* 3rd edition, (2013).
- Rao, T. R. and A. Sharma, "Pyrolysis rates of biomass materials," *Energy*, **23**(11), 973-978 (1998).
- Raveendran, K., A. Ganesh and K. C. Khilar, "Pyrolysis characteristics of biomass and biomass components," *Fuel*, **75**(8), 987-998 (1996).

- Rios, M. L. V., A. M. Gonzalez, E. E. S. Lora and O. A. A. del Olmo, "Reduction of tar generated during biomass gasification: a review," *Biomass & Bioenergy*, **108**, 345-370 (2018).
- Rothermel, R. C., "A mathematical model for predicting fire spread in wildland fuels," Intermountain Forest and Range Experiment Station, Ogden, UT, USDA Forest Service (1972).
- Rubin, E. M., "Genomics of cellulosic biofuels," *Nature*, **454**(7206), 841-845 (2008).
- Safdari, M. S., E. Amini, D. R. Weise and T. H. Fletcher, "Heating rate and temperature effects on pyrolysis products (submitted)," *Fuel*, (2018a).
- Safdari, M. S., M. Diitenberger, D. R. Weise and T. H. Fletcher, "Characterization of pyrolysis products from fast pyrolysis of live and dead vegetation native to the Southern United States," *Fuel*, **229**, 151-166 (2018b).
- Sait, H. H., A. Hussain, A. A. Salema and F. N. Ani, "Pyrolysis and combustion kinetics of date palm biomass using thermogravimetric analysis," *Bioresource Technology*, **118**, 382-389 (2012).
- Scott, R., Introduction to analytical gas chromatography, (2017).
- Sensoz, S. and M. Can, "Pyrolysis of pine (*Pinus Brutia* Ten.) chips: 1. Effect of pyrolysis temperature and heating rate on the product yields," *Energy Sources*, **24**(4), 347-355 (2002).
- Sharma, R. K. and M. R. Hajaligol, "Effect of pyrolysis conditions on the formation of polycyclic aromatic hydrocarbons (PAHs) from polyphenolic compounds," *Journal of Analytical and Applied Pyrolysis*, **66**(1-2), 123-144 (2003).
- Shen, C. and T. H. Fletcher, "Fuel element combustion properties for live wildland Utah shrubs," *Combustion Science and Technology*, **187**(3), 428-444 (2015).
- Shen, D. K., W. Jin, J. Hu, R. Xiao and K. H. Luo, "An overview on fast pyrolysis of the main constituents in lignocellulosic biomass to valued-added chemicals: structures, pathways and interactions," *Renewable & Sustainable Energy Reviews*, **51**, 761-774 (2015).
- Shen, Y. F., J. F. Wang, X. L. Ge and M. D. Chen, "By-products recycling for syngas cleanup in biomass pyrolysis - an overview," *Renewable & Sustainable Energy Reviews*, **59**, 1246-1268 (2016).
- Shen, Y. F., D. C. Ma and X. L. Ge, "CO₂-looping in biomass pyrolysis or gasification," *Sustainable Energy & Fuels*, **1**(8), 1700-1729 (2017).
- Shin, E. J., M. R. Nimlos and R. J. Evans, "A study of the mechanisms of vanillin pyrolysis by mass spectrometry and multivariate analysis," *Fuel*, **80**(12), 1689-1696 (2001).

- Solar, J., I. de Marco, B. M. Caballero, A. Lopez-Uriónabarrenechea, N. Rodríguez, I. Agirre and A. Adrados, "Influence of temperature and residence time in the pyrolysis of woody biomass waste in a continuous screw reactor," *Biomass & Bioenergy*, **95**, 416-423 (2016).
- Stankovikj, F. and M. Garcia-Perez, "TG-FTIR method for the characterization of bio-oils in chemical families," *Energy & Fuels*, **31**(2), 1689-1701 (2017).
- Stehle, T., "Knysna's Great Fire of 2017," SA Forestry Magazine (2017).
- Sussott, R. A., "Effect of heating rate on char yield from forest fuels," U. F. S. Research Note INT-295, Intermountain Forest and Range Experiment Station, Ogden, UT (1980).
- Tansey, K., J. M. Gregoire, D. Stroppiana, A. Sousa, J. Silva, J. M. C. Pereira, L. Boschetti, M. Maggi, P. A. Brivio, R. Fraser, S. Flasse, D. Ershov, E. Binaghi, D. Graetz and P. Peduzzi, "Vegetation burning in the year 2000: global burned area estimates from SPOT VEGETATION data," *Journal of Geophysical Research-Atmospheres*, **109**(D14) (2004).
- Thammasouk, K., D. Tandjo and M. H. Penner, "Influence of extractives on the analysis of herbaceous biomass," *Journal of Agricultural and Food Chemistry*, **45**(2), 437-443 (1997).
- Tihay, V., A. Simeoni, P. A. Santoni, L. Rossi, J. P. Garo and J. P. Vantelon, "Experimental study of laminar flames obtained by the homogenization of three forest fuels," *International Journal of Thermal Sciences*, **48**(3), 488-501 (2009).
- Torikai, K., S. Yoshida and H. Takahashi, "Effects of temperature, atmosphere and pH on the generation of smoke compounds during tobacco pyrolysis," *Food and Chemical Toxicology*, **42**(9), 1409-1417 (2004).
- Tsai, W. T., M. K. Lee and Y. M. Chang, "Fast pyrolysis of rice straw, sugarcane bagasse and coconut shell in an induction-heating reactor," *Journal of Analytical and Applied Pyrolysis*, **76**(1-2), 230-237 (2006).
- Turumtay, H., "Cell wall engineering by heterologous expression of cell wall - degrading enzymes for better conversion of lignocellulosic biomass into biofuels," *Bioenergy Research*, **8**(4), 1574-1588 (2015).
- Uzun, B. B., A. E. Putun and E. Putun, "Fast pyrolysis of soybean cake: product yields and compositions," *Bioresource Technology*, **97**(4), 569-576 (2006).
- Viney, N. R., "A review of fine fuel moisture modelling," *International Journal of Wildland Fire*, **1**(4), 215-235 (1991).
- Wagner, C. E. V., "Calculations on forest fire spread by flame radiation," 6th World Forestry Congress, Madrid, Spain (1967).

- Wang, M., C. Liu, X. X. Xu and Q. Li, "Theoretical study of the pyrolysis of vanillin as a model of secondary lignin pyrolysis," *Chemical Physics Letters*, **654**, 41-45 (2016).
- Wang, S., Q. Wang, X. M. Jiang, X. X. Han and H. S. Ji, "Compositional analysis of bio-oil derived from pyrolysis of seaweed," *Energy Conversion and Management*, **68**, 273-280 (2013).
- Wang, S. R., X. J. Guo, K. G. Wang and Z. Y. Luo, "Influence of the interaction of components on the pyrolysis behavior of biomass," *Journal of Analytical and Applied Pyrolysis*, **91**(1), 183-189 (2011).
- Weber, R. O., "Modeling fire spread through fuel beds," *Progress in Energy and Combustion Science*, **17**(1), 67-82 (1991).
- Weise, D. R., R. H. White, F. C. Beall and M. Etlinger, "Use of the cone calorimeter to detect seasonal differences in selected combustion characteristics of ornamental vegetation," *International Journal of Wildland Fire*, **14**(3), 321-338 (2005a).
- Weise, D. R., X. Y. Zhou, L. L. Sun and S. Mahalingam, "Fire spread in chaparral - 'go or no-go?'," *International Journal of Wildland Fire*, **14**(1), 99-106 (2005b).
- Weise, D. R. and C. S. Wright, "Wild land fire emissions, carbon and climate: characterizing wildland fuels," *Forest Ecology and Management*, **317**, 26-40 (2014).
- Weise, D. R., E. Koo, X. Y. Zhou, S. Mahalingam, F. Morandini and J. H. Balbi, "Fire spread in chaparral - a comparison of laboratory data and model predictions in burning live fuels," *International Journal of Wildland Fire*, **25**(9), 980-994 (2016).
- Weise, D. R., T. H. Fletcher and T. J. Johnson, "A project to measure and model pyrolysis to improve prediction of prescribed fire behavior," Coimbra University Press, Portugal (2018).
- Williams, P. T. and S. Besler, "The pyrolysis of municipal solid waste," *Journal of the Institute of Energy*, **65**(465), 192-200 (1992).
- Williams, P. T. and S. Besler, "The influence of temperature and heating rate on the pyrolysis of biomass," *Renewable Energy*, **7**(3), 233-250 (1996).
- Wolff, M. F., G. F. Carrier and F. E. Fendell, "Wind-aided firespread across arrays of discrete fuel elements .2. experiment," *Combustion Science and Technology*, **77**(4-6), 261-289 (1991).
- Xanthopoulos, G. and R. H. Wakimoto, "A Time to Ignition - temperature moisture relationship for branches of 3 Western conifers," *Canadian Journal of Forest Research-Revue Canadienne De Recherche Forestiere*, **23**(2), 253-258 (1993).
- Xiao, C. W. and C. T. Anderson, "Roles of pectin in biomass yield and processing for biofuels," *Frontiers in Plant Science*, **4** (2013).

- Xiao, R. R. and W. Yang, "Influence of temperature on organic structure of biomass pyrolysis products," *Renewable Energy*, **50**, 136-141 (2013).
- Xie, H. Q., Q. B. Yu, Q. Qin, H. T. Zhang and P. Li, "Study on pyrolysis characteristics and kinetics of biomass and its components," *Journal of Renewable and Sustainable Energy*, **5**(1) (2013).
- Xu, J., A. Tahmasebi and J. L. Yu, "An experimental study on the formation of methoxyaromatics during pyrolysis of *Eucalyptus pulverulenta*: Yields and mechanisms," *Bioresource Technology*, **218**, 743-750 (2016).
- Yang, H. P., R. Yan, H. P. Chen, D. H. Lee and C. G. Zheng, "Characteristics of hemicellulose, cellulose and lignin pyrolysis," *Fuel*, **86**(12-13), 1781-1788 (2007).
- Yashwanth, B. L., B. Shotorban and S. Mahalingam, "A computational investigation of the role of moisture in live fuels subject to pyrolysis and ignition through convective heat transfer," 9th US National Meeting (2015).
- Yashwanth, B. L., B. Shotorban, S. Mahalingam, C. W. Lautenberger and D. R. Weise, "A numerical investigation of the influence of radiation and moisture content on pyrolysis and ignition of a leaf-like fuel element," *Combustion and Flame*, **163**, 301-316 (2016).
- Yedinak, K. M., J. D. Cohen, J. M. Forthofer and M. A. Finney, "An examination of flame shape related to convection heat transfer in deep-fuel beds," *International Journal of Wildland Fire*, **19**(2), 171-178 (2010).
- Zanzi, R., K. Sjostrom and E. Bjornbom, "Rapid pyrolysis of agricultural residues at high temperature," *Biomass & Bioenergy*, **23**(5), 357-366 (2002).
- Zhang, Y. I., W. G. Wu, S. H. Zhao, Y. F. Long and Y. H. Luo, "Experimental study on pyrolysis tar removal over rice straw char and inner pore structure evolution of char," *Fuel Processing Technology*, **134**, 333-344 (2015).
- Zhao, B., D. O'Connor, J. Zhang, T. Peng, Z. Shen, D. C. W. Tsang and D. Hou, "Effect of pyrolysis temperature, heating rate, and residence time on rapeseed stem derived biochar," *Journal of Cleaner Production*, **174**, 977-987 (2018).
- Zhou, H., C. F. Wu, A. H. Meng, Y. G. Zhang and P. T. Williams, "Effect of interactions of biomass constituents on polycyclic aromatic hydrocarbons (PAH) formation during fast pyrolysis," *Journal of Analytical and Applied Pyrolysis*, **110**, 264-269 (2014a).
- Zhou, H., C. F. Wu, J. A. Onwudili, A. H. Meng, Y. U. Zhang and P. T. Williams, "Polycyclic aromatic hydrocarbons (PAH) formation from the pyrolysis of different municipal solid waste fractions," *Waste Management*, **36**, 136-146 (2015).

Zhou, S., B. Pecha, M. van Kuppevelt, A. G. McDonald and M. Garcia-Perez, "Slow and fast pyrolysis of Douglas-fir lignin: importance of liquid-intermediate formation on the distribution of products," *Biomass and Bioenergy*, **66**, 398-409 (2014b).

Zhou, X. Y., S. Mahalingam and D. Weise, "Modeling of marginal burning state of fire spread in live chaparral shrub fuel bed," *Combustion and Flame*, **143**(3), 183-198 (2005).

APPENDIX

- A. Plants Tested
- B. Temperature Correction for Radiation Losses
- C. Calculations of Mass Flow rates and Gas Velocity
- D. Identified Tar Compounds
- E. Mass Loss Over Time
- F. Results of Slow vs. Fast Pyrolysis Experiments
- G. Results of Different Heating Modes

APPENDIX A. PLANTS TESTED

The plant species which were studied are listed as follows:

- 1- Darrow's blueberry: a small shrub that typically grows between 1 to 3 feet tall. It is native to the coastal plain from Georgia to Southeast Texas.
- 2- Dwarf palmetto: a small shrub that typically grows between 5 to 10 feet tall. It ranges from North Carolina to East Texas to Northern Mexico. It thrives in moist environments such as swamps and floodplains. Due to its evergreen nature, it is cold resistant. Moist soil and shady locations are best for this palm.
- 3- Fetterbush: a shrub that typically grows between 3 to 5 feet tall. It ranges from southeast Virginia to Florida and then west to Louisiana. Fetterbush prefer moist, acidic soil and shady locations. It is easily identified because of its pink blooms.
- 4- Inkberry: a colony-forming shrub that typically grows between 6 to 12 feet tall. It ranges from Nova Scotia in Canada down to Florida and then west to Louisiana. Inkberry plants live in the moist forests of coastal plains. They prefer sandy, acidic soil with slightly shady locations. Inkberry plants can be toxic if ingested by humans.
- 5- Live oak: a tree that grows between 40 to 80 feet in height and 60 to 100 feet in width. It ranges from southeast Virginia down to Florida and west to Texas. Live oak can live in dryer, rockier soils, but it still requires a healthy amount of water to live. Due to its extensive root system, live oak can withstand strong winds.

- 6- Little bluestem grass: a grass that forms mounds that typically grow between 18 to 24 inches tall. During the spring season, bluestem grasses have blue-green stems, which is how it got its name. It ranges across the entire contiguous United States and many parts of Canada. It is found in plains, prairies, meadows, and other flatlands where the soil is dry. It cannot tolerate large amounts of water.
- 7- Longleaf pine: a tree that typically grows between 80 to 100 feet tall. It ranges along the coastal plains of southeast Virginia down to central Florida. Longleaf pines prefer dryer soils with lots of sun. These trees are used for turpentine and resin as well construction lumber.
- 8- Saw palmetto: an evergreen shrub that typically grows between 10 to 12 feet tall and can be up to 3 feet across. It ranges along the grasslands of the southern United States from South Carolina to Florida and Louisiana. The saw palmetto requires large quantities of water with well-drained soils.
- 9- Sparkleberry: a deciduous shrub that typically grows between 12 to 15 feet tall but can reach 25 feet. It is also known as a huckleberry. It ranges along the banks of streams and rivers of the southern United States. Sparkleberries require an average amount of water and sandy, acidic soils.
- 10- Swamp bay: a smaller evergreen tree that typically grows between 45 to 65 feet tall. It is found in the swamps and marshes of the southern United States. The swamp bay requires long exposure to the Sun. It requires large quantities of water, making moist, acidic soils more favored for the swamp bay.
- 11- Water Oak: a deciduous tree that typically grows between 50 to 100 feet tall. It is found in damp woodlands in the southeastern United States as well as New Jersey, Delaware, and

Maryland. Water oaks live in partly shady areas and require large amounts of water. The best soils are moist, acidic soils.

12- Wax myrtle: a large evergreen shrub that typically grows between 6 to 12 feet but can reach up to 20 feet. It is found in marshes in the eastern and southern United States. The wax myrtle requires decent exposure to the sun as well as large quantities of water. Wet, acidic soils provide the best environment for the wax myrtle.

13- Wiregrass: a grass that grows in clumps up to 2 feet tall and is found in the grasslands from Mississippi to North Carolina. Wiregrass requires less than average amounts of water and prefers highly acidic, dryer soils. It is fire-dependent, meaning it seeds after being burned.

14- Yaupon: an evergreen shrub that typically grows between 12 to 25 feet tall. It grows in forests in the southern United States. The yaupon requires low amounts of water and prefers long exposure to the Sun, but can live in shadier locations. Dry, gravelly soils provide the best environment for the yaupon.

Table A-1. List of plants used in pyrolysis experiments

Common name	Scientific name	Picture
Darrow's blueberry	<i>Vaccinium darrowii</i> Camp "Rosa's Blush"	
Dwarf palmetto	<i>Sabal minor</i> (Jacq.) Pers.	

Table A-1: Continued

Common name	Scientific name	Picture
Fetterbush	<i>Lyonia lucida</i> (Lam.) K. Koch	
Inkberry	<i>Ilex glabra</i> (L.) A. Gray	
Live oak	<i>Schizachyrium scoparium</i> (Michx.) Nash	
Little bluestem	<i>Quercus virginiana</i> Mill.	
Longleaf pine	<i>Pinus palustris</i> Mill.	

Table A-1: Continued

Common name	Scientific name	Picture
Pine straw (Longleaf pine litter)	<i>Pinus palustris</i> Mill.	
Saw palmetto	<i>Serenoa repens</i> (W. Bartram) Small	
Sparkleberry	<i>Vaccinium arboreum</i> Marshall	
Swamp bay	<i>Persea palustris</i> (Raf.) Sarg.	
Water oak	<i>Quercus nigra</i> L.	

Table A-1: Continued

Common name	Scientific name	Picture
Wax myrtle	<i>Morella cerifera</i> (L.) Small	 A photograph of a Wax myrtle plant, showing its dense, green, waxy leaves and small, light-colored flowers.
Wiregrass	<i>Aristida stricta</i> Michx.	 A photograph of a Wiregrass plant, showing its thin, upright, and densely packed blades.
Yaupon	<i>Ilex vomitoria</i> Aiton 'Schelling Dwarf'	 A photograph of a Yaupon plant, showing its dense, green, rounded foliage.

APPENDIX B. TEMPERATURE CORRECTION FOR RADIATION LOSSES

The temperature of the post-flame gases was measured using a thermocouple positioned in the flat-flame burner apparatus at the height where the sample was located. The recorded temperature was a result of the combination of radiation, convection, and conduction through the thermocouple.

For the convection-only mode, the actual gas temperature was calculated from the temperature measured by the thermocouple using equation (B-1). At steady state conditions, the energy balance equation for the thermocouple can be expressed as follows:

$$Q_{conv} + Q_{rad} = hA_{bead}(T_{gas} - T_{bead}) + \sigma\epsilon A_{bead}(T_{bead}^4 - T_{sur}^4) = 0 \quad (B-1)$$

The bead of the thermocouple had a diameter of 0.127 mm. The properties of gases, such as thermal conductivity and viscosity, were found from the DIPPR database. The gas velocity was calculated in to order to determine the convective heat transfer. Uncorrected rotameter flow rates of the gases were 220 Lmin⁻¹ air, 20 L min⁻¹ H₂, and 60 L min⁻¹ CH₄.

After corrections, the actual flow rates were calculated as 258.8 L min⁻¹ air, 16.6 L min⁻¹ H₂, and 26.5 L min⁻¹ CH₄. The total volumetric flow rate of the gases into the burner was calculated to be 301.99 L min⁻¹. The cross-sectional area of the burner was calculated to be 0.054 m². The flow path had a measured cross-sectional area of 0.049 m² and the hot gas velocity was

calculated as the cold velocity multiplied by the hot (post-combustion) gas temperature divided by 300 K. For the convection-only mode, the average temperature of the post-combustion gases was calculated to be about 765 °C.

For the experiments utilizing a combination of convection and radiation, the bead temperature was measured to be 800 °C. At steady state conditions, the energy balance equation for the thermocouple can be expressed as follows:

$$Q_{conv} + Q_{r1} + Q_{r2} = 0 \quad (B-2)$$

Where Q_{conv} , Q_{r1} , and Q_{r2} are the convective heat from the hot gases to the thermocouple, the radiative heat from the radiation panel to the thermocouple, and the radiative heat from the thermocouple to the surroundings, respectively. The equation (B-2) can be rewritten as follows:

$$hA_{bead}(T_{gas} - T_{bead}) + \sigma\epsilon F_{b-panel}A_{bead}(T_{panel}^4 - T_{bead}^4) + \sigma\epsilon F_{b-sur}A_{bead}(T_{sur}^4 - T_{bead}^4) = 0 \quad (B-3)$$

The view factor (F) for this configuration can be obtained using the following equation (Howell et al., 2015):

$$F_{b-panel} = \frac{1}{2\pi} \left\{ \sin^{-1} \left[\frac{2B_1^2 - (1-B_1^2)(B_1^2+B_2^2)}{(1+B_1^2)(B_1^2+B_2^2)} \right] + \sin^{-1} \left[\frac{2B_2^2 - (1-B_2^2)(B_1^2+B_2^2)}{(1+B_2^2)(B_1^2+B_2^2)} \right] \right\} \quad (B-4)$$

Where $B_1 = b_1/a$ and $B_2 = b_2/a$ as shown in Figure B-1. $F_{b-panel}$ and F_{b-sur} were calculated to be 0.20 and 0.80, respectively.

Finally, the actual gas temperature at the level where the sample was loaded was calculated to be about 804 °C.

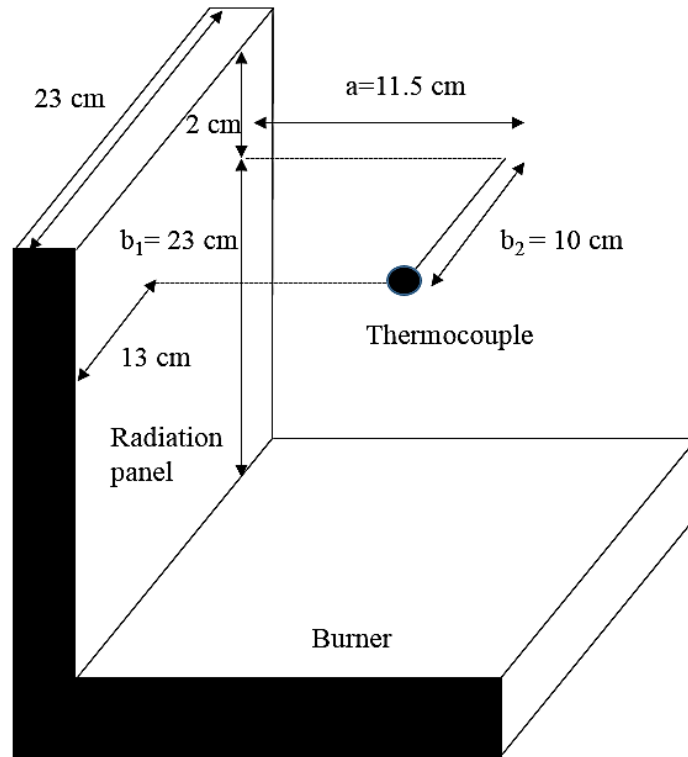


Figure B-1. Schematic of the flat-flame burner and the location of radiation panel relative to the burner

APPENDIX C. CALCULATIONS OF MASS FLOW RATES AND GAS VELOCITY

The purpose of this section is to: (1) find the post-flame gas velocity (v) at the level where the sample was loaded in the flat-flame burner (as shown in Figure C-1); and (2) compare the total mass flow rate of the reactants entered the flat flame burner (m_1) with the mass flow rate measured after the products of the reaction passed through the vacuum pump (m_2).

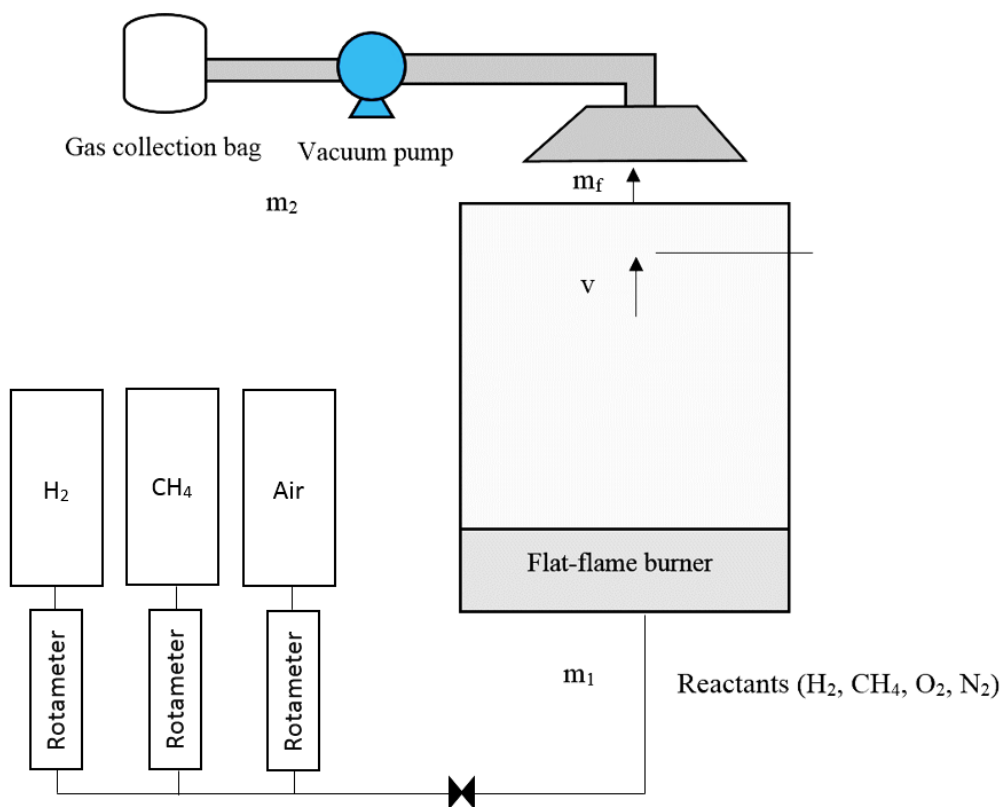


Figure C-1. Schematic of gas flow direction in the flat-flame burner apparatus

In order to find the total amount of mass entering the flat-flame burner (m_1), the volumetric flow rates of the reactants entered the burner were measured by rotameters. The measured flow rates were then corrected using the equation below to find the actual volumetric flow rates.

$$Q_{exp}^{act} = Q_{cal}^{act} \sqrt{\frac{P_{cal} T_{exp} MW_{cal}}{P_{exp} T_{cal} MW_{exp}}} \quad (C-1)$$

The rotameters were calibrated at $P_{cal} = 14.7$ psi and $T_{cal} = 21.1$ °C. The experimental temperature and pressures of the reactant gases H₂, CH₄, and air were $T_{exp} = 27$ °C, $P_{exp, H_2} = 74.7$ psi, $P_{exp, CH_4} = 74.7$ psi, $P_{exp, Air} = 104.7$ psi, respectively. The corrected volumetric flow rates (Q_i) were then multiplied by the respective densities (ρ_i) of the reactant gases to find the mass flow rate of each gas (m_i), which were then added together to find the total mass flow rate entering the burner (m_1) (see equations C-2 and C-3). These results are summarized in Table C-1.

$$m_i = \rho_i Q_i \quad (C-2)$$

$$m_1 = \sum \rho_i Q_i \quad (C-3)$$

Table C-1. Mass flow rates of the reactant entered the burner

Reactants	Q_{cal} (L min ⁻¹)	Q_{exp} (L min ⁻¹)	Q_{exp} (m ³ s ⁻¹)	ρ (kg m ⁻³)	m (kg s ⁻¹)
H ₂	16.60	36.50	0.0006	0.09	0.00005
CH ₄	26.50	58.27	0.0009	0.71	0.00069
O ₂	54.35	142.09	0.0024	1.43	0.00338
N ₂	204.45	534.53	0.0089	1.25	0.01114

The total mass flow rate entering the burner (m_1) was calculated to be $1.52 \times 10^{-2} \text{ kg s}^{-1}$ or 15.2 g s^{-1} . To find the gas velocity (v) at the point where the sample was exposed to convective heat transfer, the following equations were used:

$$\overline{MW} = \sum y_i MW_i = 26.54 \text{ (g} \cdot \text{mol}^{-1}) \quad (\text{C-4})$$

$$\rho = \frac{P \cdot \overline{MW}}{R \cdot T} = 0.26 \text{ (} \frac{\text{kg}}{\text{m}^3} \text{)} \quad (\text{C-5})$$

$$v = \frac{m_1}{\rho \cdot A} = 1.07 \text{ (} \frac{\text{m}}{\text{s}} \text{)} \quad (\text{C-6})$$

ρ is the total density of the post-combustion gases, T is the temperature of the gases at the level where the sample is loaded (1038 K), and A is the cross-sectional area of the burner. The wind (mixture of gases at the location of the samples) velocity was calculated to be 1.07 m s^{-1} .

The amount of mass flow rate entering the funnel (m_f) was determined by multiplying the mass flow rate entering the burner (m_1) by the ratio (R) of the funnel area to the burner area as shown below. The dimension of the burner was 20 cm by 27 cm, and the diameter of the funnel was measured to be 12.5 cm. Therefore, the R ratio can be calculated as follows:

$$R = \frac{\pi r^2}{lw} \approx 0.23 \quad (\text{C-7})$$

$$m_f = m_1 \times \frac{\pi r^2}{lw} = 0.00351 \text{ (} \frac{\text{kg}}{\text{s}} \text{)} \quad (\text{C-8})$$

This means that about 23%, or 3.51 g s^{-1} of the incoming mass from the burner is captured by the overhead funnel. The law of conservation of mass necessitates that all the mass that enters

the funnel (m_f) will exit from the end of process line (m_2). If there is a difference between these two measured mass flow rates, it means that either some gases escaped the system without entering the funnel ($m_f > m_2$) or some gases entered from outside of the system ($m_f < m_2$).

A rotameter was used to obtain the volumetric flow rate of the gases after the vacuum pump. Then the ideal gas law was used and the mass flow rate at the end of the process line (m_2) was measured to be 3.4 g s^{-1} . The mass flow rate at the end of the process line, m_2 and m_f ideally would be the same, but since the FFB system is not a closed system, m_f was found to be greater than m_2 . This means that approximately 3% of the gases directly below the funnel escaped the system without entering the funnel.

APPENDIX D. IDENTIFIED TAR COMPOUNDS

Table D-1. Identified tar compounds using GC-MS in high heating rate pyrolysis

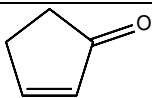
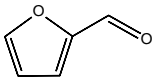
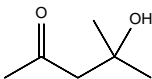
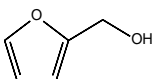
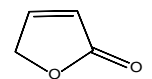
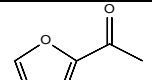
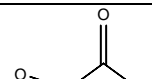
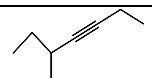
#	Peak R.T. (min)	Compound name	Molecular formula	Compound type	Structure
1	12.636	2-Cyclopenten-1-one	C_5H_6O	Oxygenated	
2	12.697	Furfural	$C_5H_4O_2$	Monocyclic aromatic	
3	12.986	2-Pentanone, 4-hydroxy-4-methyl-	$C_6H_{12}O_2$	Oxygenated	
4	13.260	2-Furanmethanol	$C_5H_6O_2$	Monocyclic aromatic	
5	14.050	2(3H)-Furanone	$C_4H_4O_2$	Monocyclic aromatic	
6	14.540	Ethanone, 1-(2-furanyl)-	$C_6H_6O_2$	Monocyclic aromatic	
7	14.730	1,2-Cyclopentanedione	$C_5H_6O_2$	Oxygenated	
8	15.132	3-Heptyne, 5-methyl-	C_8H_{14}	Aliphatic	

Table D-1: Continued

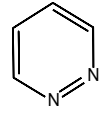
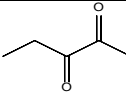
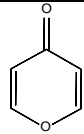
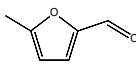
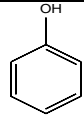
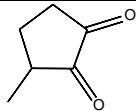
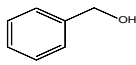
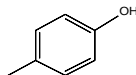
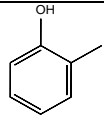
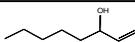
#	Peak R.T. (min)	Compound name	Molecular formula	Compound type	Structure
9	15.218	Pyridazine	C ₄ H ₄ N ₂	Heterocyclic aromatic	
10	15.296	2,3-Pentanedione	C ₅ H ₈ O ₂	Aliphatic	
11	15.563	4H-Pyran-4-one	C ₅ H ₄ O ₂	Heterocyclic aromatic	
12	15.585	2-Furancarboxaldehyde, 5-methyl-	C ₆ H ₆ O ₂	Monocyclic aromatic	
13	15.876	Phenol	C ₆ H ₆ O	Monocyclic aromatic	
14	16.183	2-Penten-1-ol, 2-methyl-	C ₆ H ₁₂ O	Oxygenated	
15	16.868	1,2-Cyclopentanedione, 3-methyl-	C ₆ H ₈ O ₂	Oxygenated	
16	17.076	Benzyl Alcohol	C ₇ H ₈ O	Monocyclic aromatic	
17	17.712	Phenol, 4-methyl-	C ₇ H ₈ O	Monocyclic aromatic	
18	17.383	Phenol, 2-methyl-	C ₇ H ₈ O	Monocyclic aromatic	
19	17.805	1-Octen-3-ol	C ₈ H ₁₆ O	Oxygenated	

Table D-1: Continued

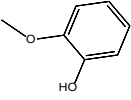
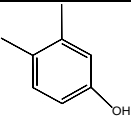
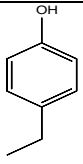
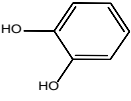
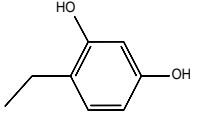
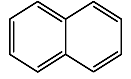
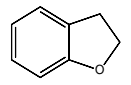
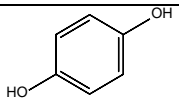
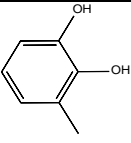
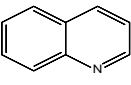
#	Peak R.T. (min)	Compound name	Molecular formula	Compound type	Structure
20	18.172	Phenol, 2-methoxy- (guaiacol)	$C_7H_8O_2$	Monocyclic aromatic	
21	19.071	Phenol, 3,4-dimethyl-	$C_8H_{10}O$	Monocyclic aromatic	
22	19.312	Phenol, 4-ethyl-	$C_8H_{10}O$	Monocyclic aromatic	
23	19.635	1,2-Benzenediol	$C_6H_6O_2$	Monocyclic aromatic	
24	19.948	1,3-Benzenediol, 4-ethyl-	$C_8H_{10}O_2$	Monocyclic aromatic	
25	20.047	Naphthalene	$C_{10}H_8$	Polycyclic aromatic	
26	20.058	Benzofuran, 2,3-dihydro-	C_8H_8O	Monocyclic aromatic	
27	20.611	1,4-Benzenediol	$C_6H_6O_2$	Monocyclic aromatic	
28	20.726	1,2-Benzenediol, 3-methyl-	$C_7H_8O_2$	Monocyclic aromatic	
29	20.891	Quinoline	C_9H_7N	Heterocyclic aromatic	

Table D-1: Continued

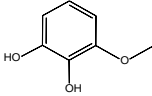
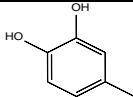
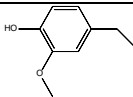
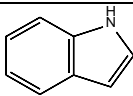
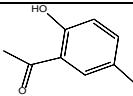
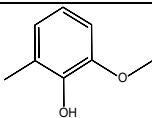
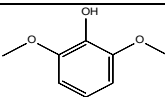
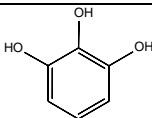
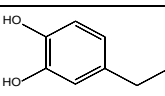
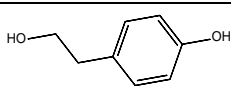
#	Peak R.T. (min)	Compound name	Molecular formula	Compound type	Structure
30	21.004	1,2-Benzenediol, 3-methoxy-	C ₇ H ₈ O ₃	Monocyclic aromatic	
31	21.132	1,2-Benzenediol, 4-methyl-	C ₇ H ₈ O ₂	Monocyclic aromatic	
32	21.322	Phenol, 4-ethyl-2-methoxy-	C ₉ H ₁₂ O ₂	Monocyclic aromatic	
33	21.429	Indole	C ₈ H ₇ N	Heterocyclic aromatic	
34	21.786	Ethanone, 1-(2-hydroxy-5-methylphenyl)-	C ₉ H ₁₀ O ₂	Monocyclic aromatic	
35	21.940	2-Methoxy-6-methylphenol	C ₈ H ₁₀ O ₂	Monocyclic aromatic	
36	22.146	Phenol, 2,6-dimethoxy-	C ₈ H ₁₀ O ₃	Monocyclic aromatic	
37	22.366	1,2,3-Benzenetriol	C ₆ H ₆ O ₃	Monocyclic aromatic	
38	22.535	1,2-Benzenediol, 4-ethyl-	C ₈ H ₁₀ O ₂	Monocyclic aromatic	
39	23.025	Benzene ethanol, 4-hydroxy-	C ₈ H ₁₀ O ₂	Monocyclic aromatic	
40	23.495	1-Methylnaphthalene	C ₁₁ H ₁₀	Polycyclic aromatic	

Table D-1: Continued

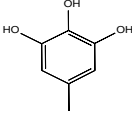
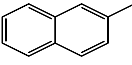
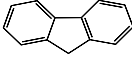
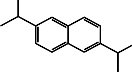
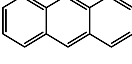
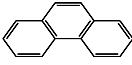
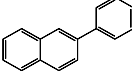
#	Peak R.T. (min)	Compound name	Molecular formula	Compound type	Structure
41	23.736	1,2,3-Benzenetriol, 5-methyl-	$C_7H_8O_3$	Monocyclic aromatic	
42	24.196	Acenaphthylene	$C_{12}H_8$	Polycyclic aromatic	
43	24.559	2-Methylnaphthalene	$C_{11}H_{10}$	Polycyclic aromatic	
44	25.941	Fluorene	$C_{13}H_{10}$	Polycyclic aromatic	
45	26.877	Naphthalene, 2,6-diisopropyl-	$C_{16}H_{20}$	Polycyclic aromatic	
46	28.352	Anthracene	$C_{14}H_{10}$	Polycyclic aromatic	
47	28.473	Phenanthrene	$C_{14}H_{10}$	Polycyclic aromatic	
48	29.898	4H Cyclopenta[def]phenanthrene	$C_{15}H_{10}$	Polycyclic aromatic	
49	30.237	Naphthalene, 2-phenyl-	$C_{16}H_{12}$	Polycyclic aromatic	
50	31.378	Fluoranthene	$C_{16}H_{10}$	Polycyclic aromatic	
51	31.762	Benzo[e]pyrene	$C_{20}H_{12}$	Polycyclic aromatic	

Table D-1: Continued

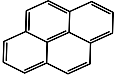
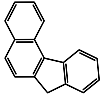
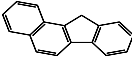
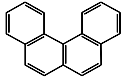
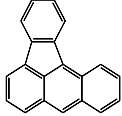
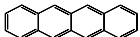
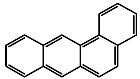
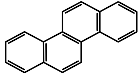
#	Peak R.T. (min)	Compound name	Molecular formula	Compound type	Structure
52	31.992	Pyrene	C ₁₆ H ₁₀	Polycyclic aromatic	
53	32.935	7H-Benzo[c]fluorene	C ₁₇ H ₁₂	Polycyclic aromatic	
54	32.979	11H-Benzo[a]fluorene	C ₁₇ H ₁₂	Polycyclic aromatic	
55	34.732	Benzo[c]phenanthrene	C ₁₈ H ₁₂	Polycyclic aromatic	
56	34.889	Benzo(a)fluoranthene	C ₂₀ H ₁₂	Polycyclic aromatic	
57	34.941	Cyclopenta[cd]pyrene	C ₁₈ H ₁₀	Polycyclic aromatic	
58	35.430	Naphthacene	C ₁₈ H ₁₂	Polycyclic aromatic	
59	35.517	Benz(a)anthracene	C ₁₈ H ₁₂	Polycyclic aromatic	
60	35.988	Chrysene	C ₁₈ H ₁₂	Polycyclic aromatic	

Table D-2. Identified tar compounds using GC-MS in slow heating rate pyrolysis

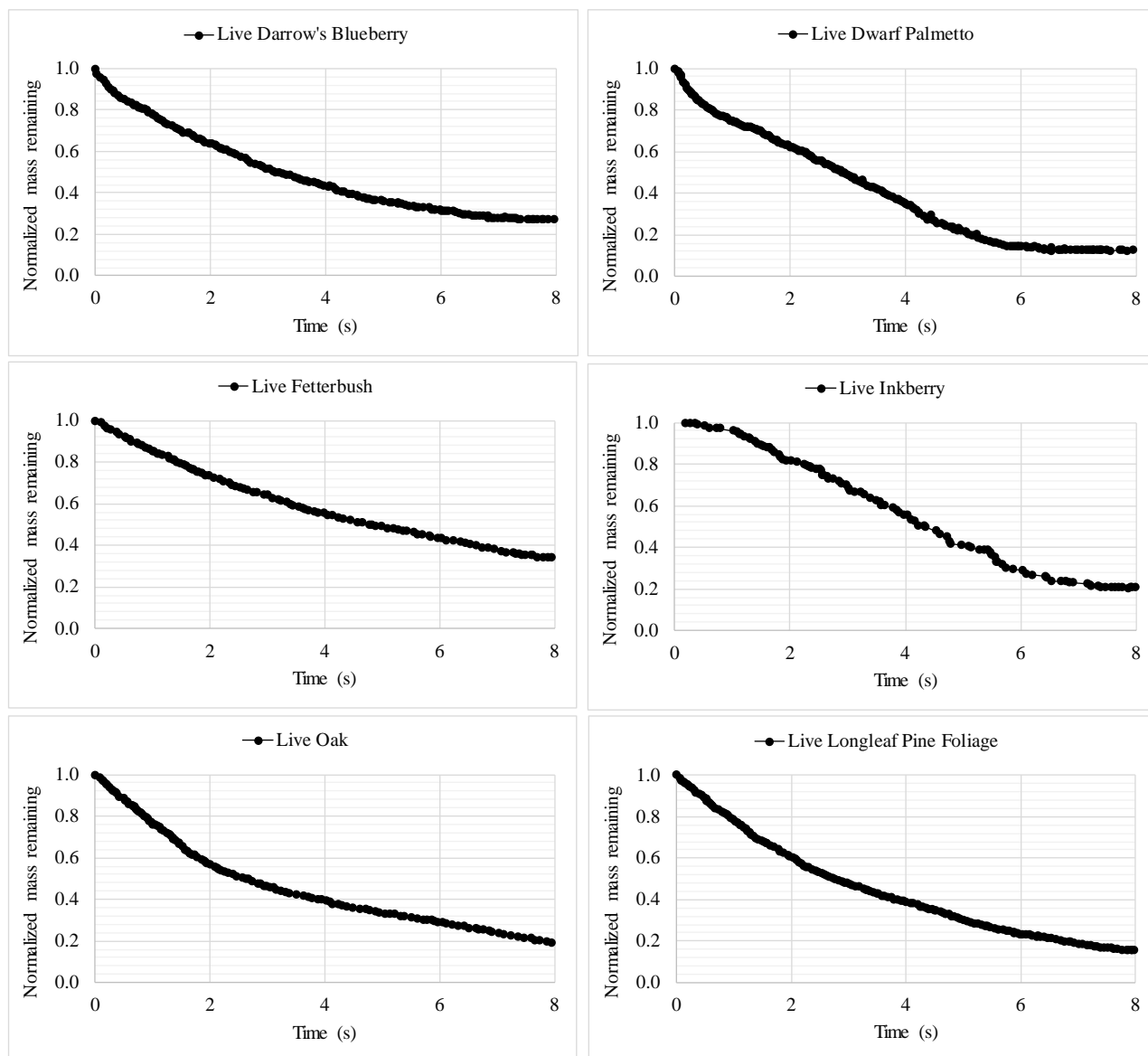
#	Peak R.T. (min)	Compound name	Molecular formula	Compound type	Structure
1	13.665	2(5H)-Furanone	C ₄ H ₄ O ₂	Ketone	
2	12.681	Furfural	C ₅ H ₄ O ₂	Aldehyde	
3	13.251	2-Furanmethanol	C ₅ H ₆ O ₂	Alcohol	
4	14.72	2-Cyclopenten-1-one	C ₅ H ₆ O ₂	Ketone	
5	15.893	Phenol	C ₆ H ₆ O	Phenol	
6	15.597	2-Furancarboxaldehyde, 5-methyl-	C ₆ H ₆ O ₂	Aldehyde	
7	19.29	1,2-Benzenediol	C ₆ H ₆ O ₂	Phenol	
8	20.599	1,3-Benzenediol	C ₆ H ₆ O ₂	Phenol	
9	20.632	1,4-Benzenediol	C ₆ H ₆ O ₂	Phenol	
10	14.147	Ethanone, 1-(2-furanyl)-	C ₆ H ₆ O ₂	Ketone	
11	16.872	2-Cyclopenten-1-one, 2-hydroxy-3-methyl-	C ₆ H ₈ O ₂	Ketone	
12	17.415	Propanoic acid, 2-propenyl ester	C ₆ H ₁₀ O ₂	Acid	
13	22.397	1,2,3-Benzenetriol	C ₆ H ₆ O ₃	Phenol	
14	18.461	Maltol (Larixic acid)	C ₆ H ₆ O ₃	Acid	
15	17.387	Phenol, 2-methyl-	C ₇ H ₈ O	Phenol	
16	16.971	Phenol, 3-methyl-	C ₇ H ₈ O	Phenol	
17	17.327	Phenol, 4-methyl-	C ₇ H ₈ O	Phenol	

Table D-2: Continued

#	Peak R.T. (min)	Compound name	Molecular formula	Compound type	Structure
18	16.779	2-Cyclopenten-1-one, 2,3-dimethyl-	C ₇ H ₁₀ O	Ketone	
19	17.739	Phenol, 2-methoxy-	C ₇ H ₈ O ₂	Phenol	
20	20.312	1,2-Benzenediol, 3-methyl-	C ₇ H ₈ O ₂	Phenol	
21	20.721	1,2-Benzenediol, 4-methyl-	C ₇ H ₈ O ₂	Phenol	
22	20.579	1,2-Benzenediol, 3-methoxy-	C ₇ H ₈ O ₃	Phenol	
23	21.001	Indole	C ₈ H ₇ N	Benzenoid	
24	19.666	Benzofuran, 2,3-dihydro-	C ₈ H ₈ O	Furans	
25	18.909	Phenol, 4-ethyl-	C ₈ H ₁₀ O	Phenol	
26	19.949	2-Methoxy-5-methylphenol	C ₈ H ₁₀ O ₂	Phenol	
27	19.534	Phenol, 2-methoxy-4-methyl-	C ₈ H ₁₀ O ₂	Phenol	
28	19.515	1,3-Benzenediol, 4-ethyl-	C ₈ H ₁₀ O ₂	Phenol	
29	22.551	1,2-Benzenediol, 4-ethyl-	C ₈ H ₁₀ O ₂	Phenol	
30	19.251	1,3-Benzodioxole, 2-methoxy-	C ₈ H ₈ O ₃	Phenyl	
31	21.727	Phenol, 2,6-dimethoxy-	C ₈ H ₁₀ O ₃	Phenol	
32	20.894	Phenol, 4-ethyl-2-methoxy-	C ₉ H ₁₂ O ₂	Phenol	
33	21.387	2-Methoxy-4-vinylphenol	C ₉ H ₁₀ O ₂	Alcohol	

APPENDIX E. MASS LOSS VS. TIME

The mass loss vs. time data in pyrolysis of live plant species in the convection-only and the combined modes are shown in Figure E-1 and Figure E-2, respectively.



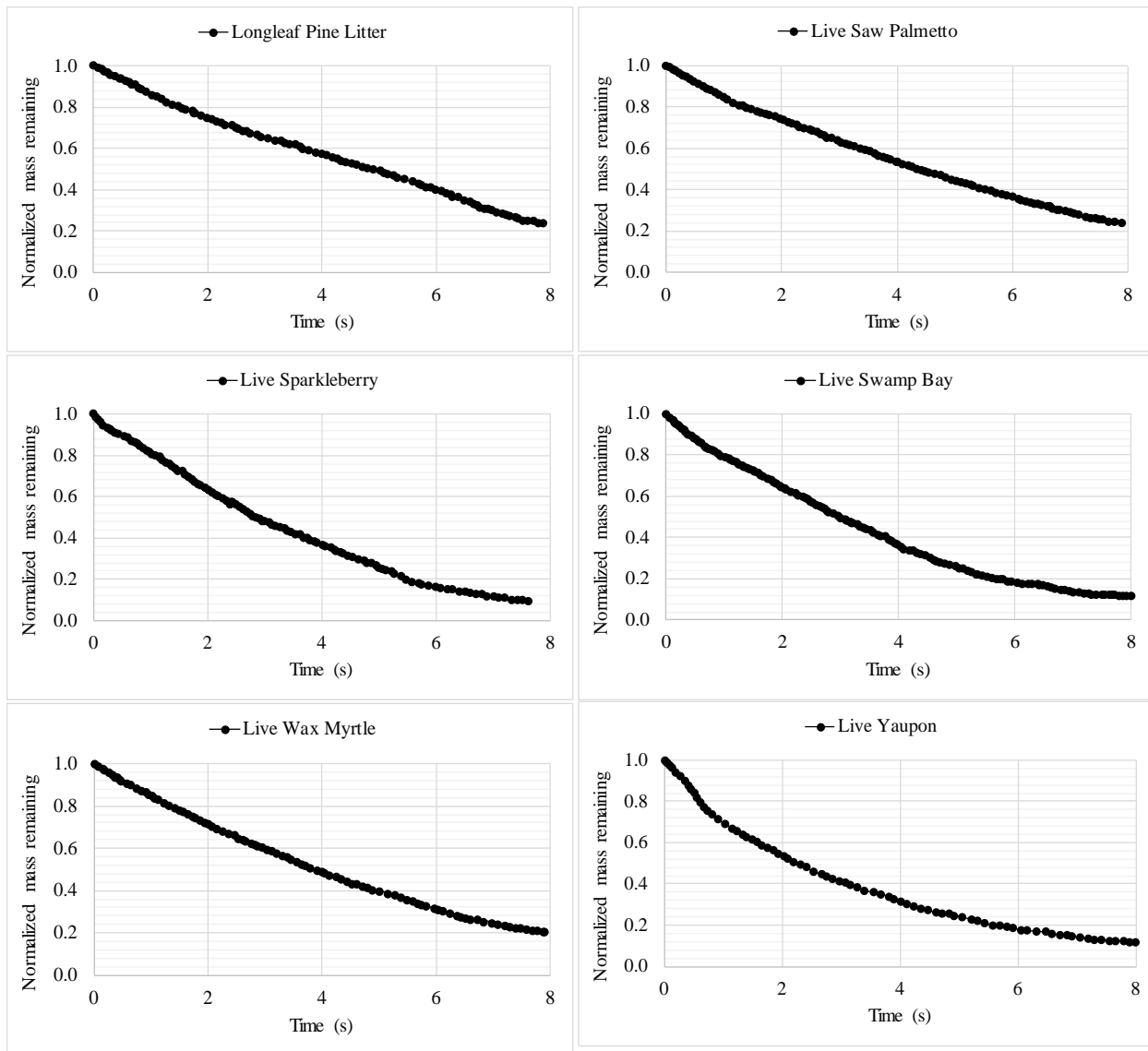
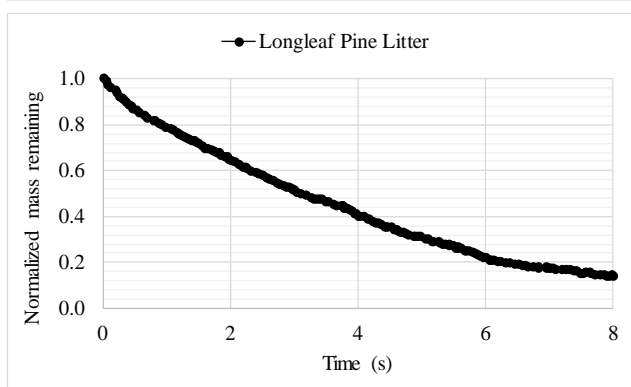
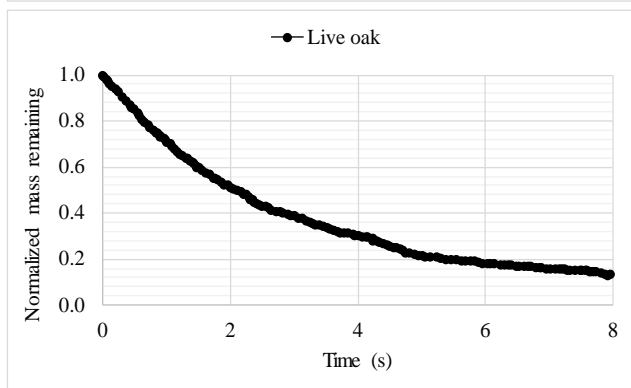
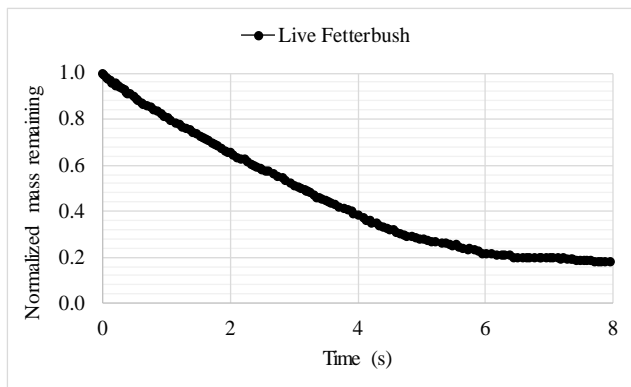
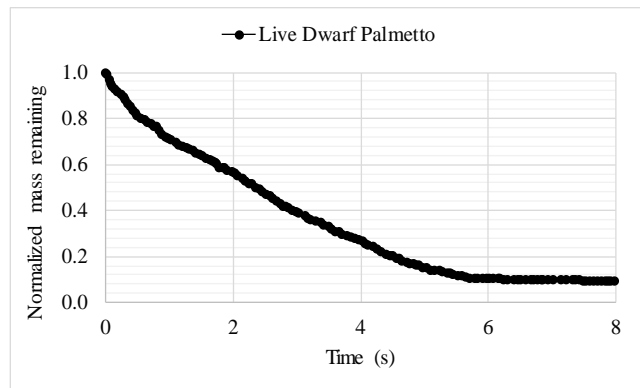
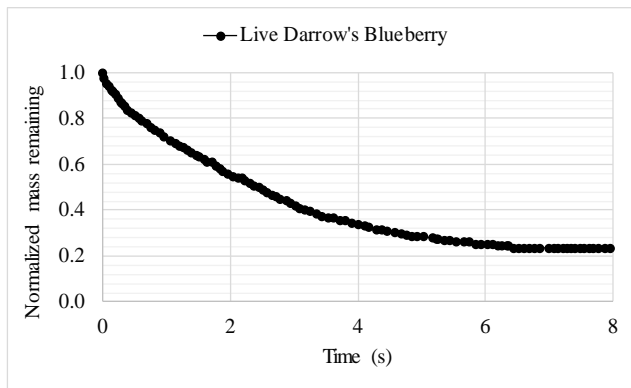


Figure E-1. Mass loss over time for live plant species in the convection-only experiments



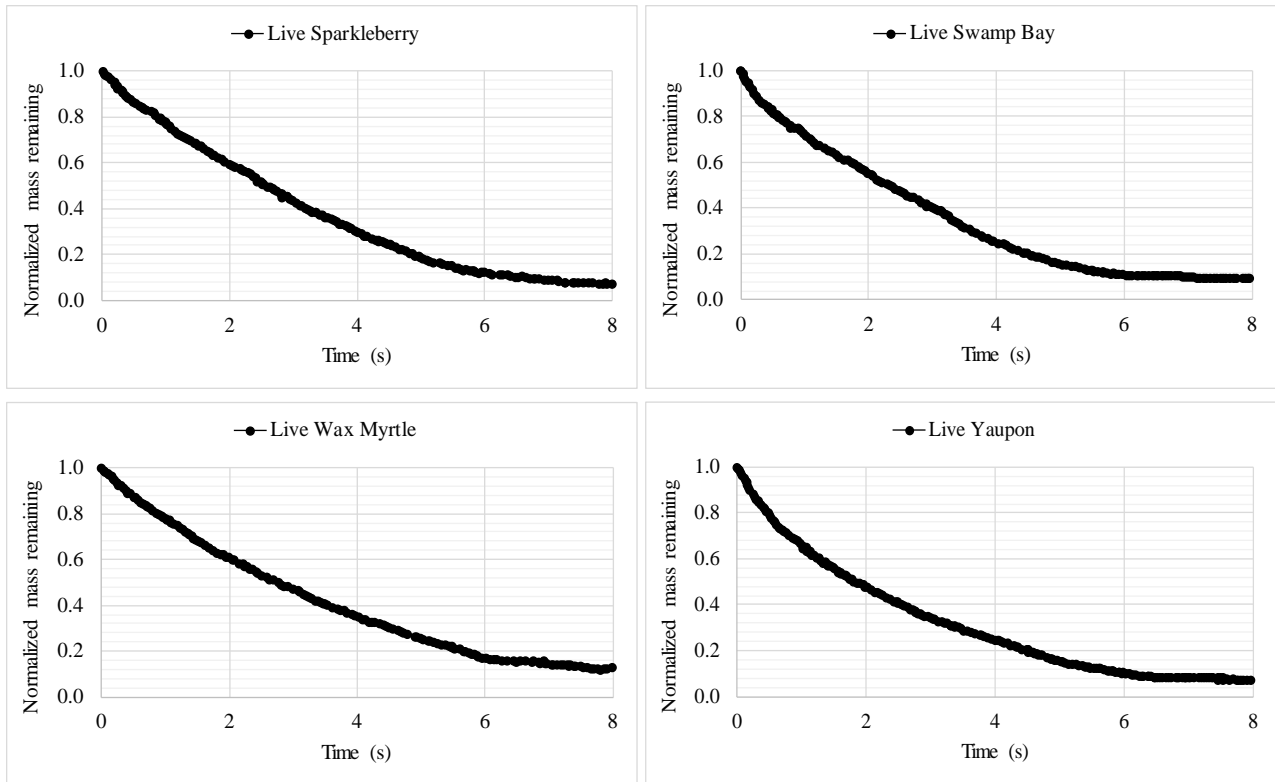


Figure E-2. Mass loss over time for live plant species in the combined mode

APPENDIX F. RESULTS OF SLOW AND FAST PYROLYSIS EXPERIMENTS

Figure F-1, Figure F-2, and Figure F-3 show the yields of pyrolysis products (i.e., tar, light gases, and char) for dead plant species for slow and fast pyrolysis experiments

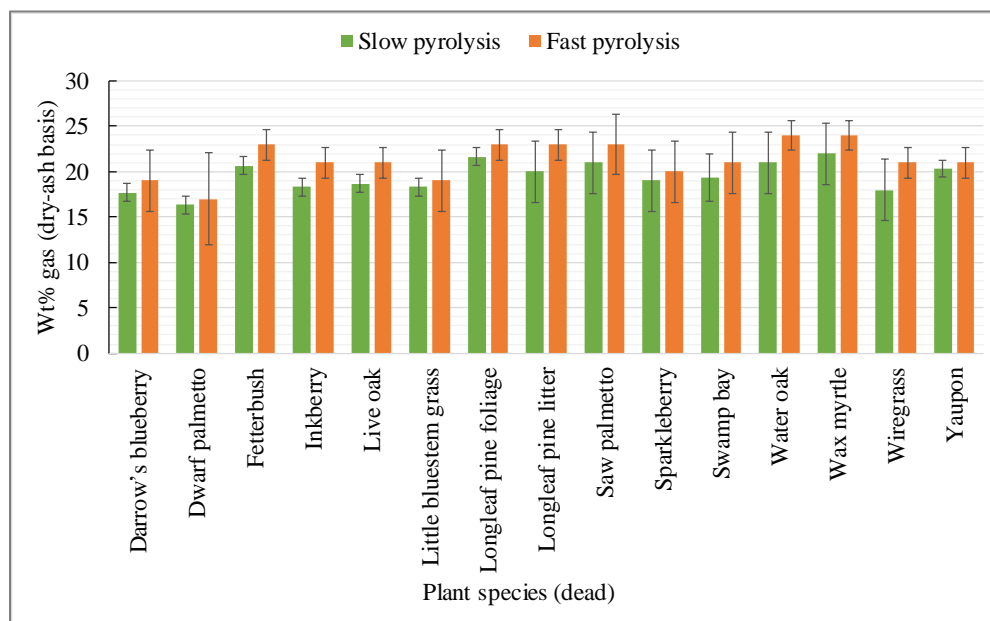


Figure F-1. Gas yield of dead plant species on a dry, ash free (daf) basis

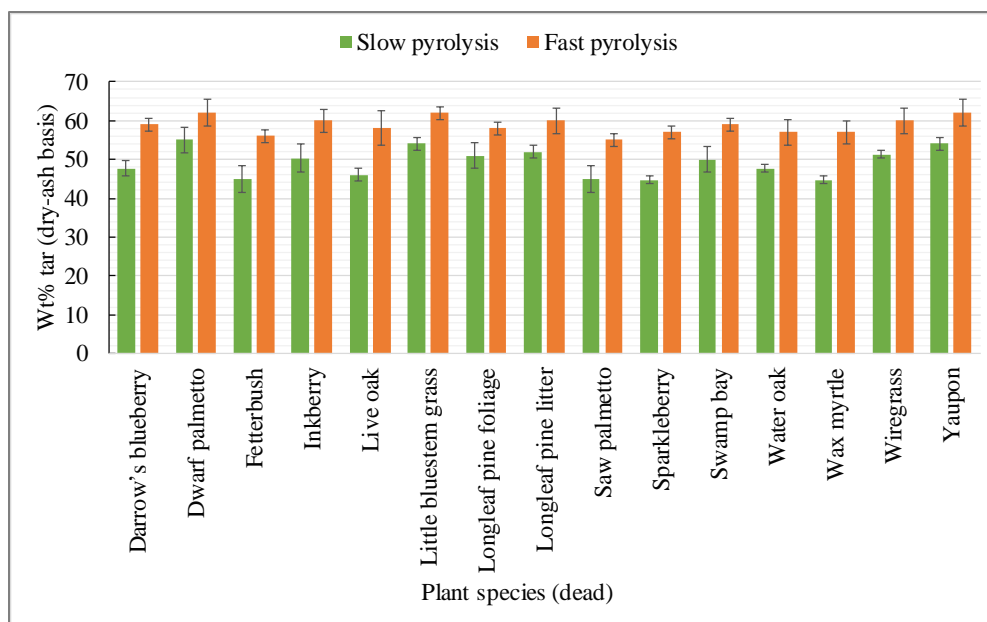


Figure F-2. Tar yield of live plant species on a dry, ash free (daf) basis

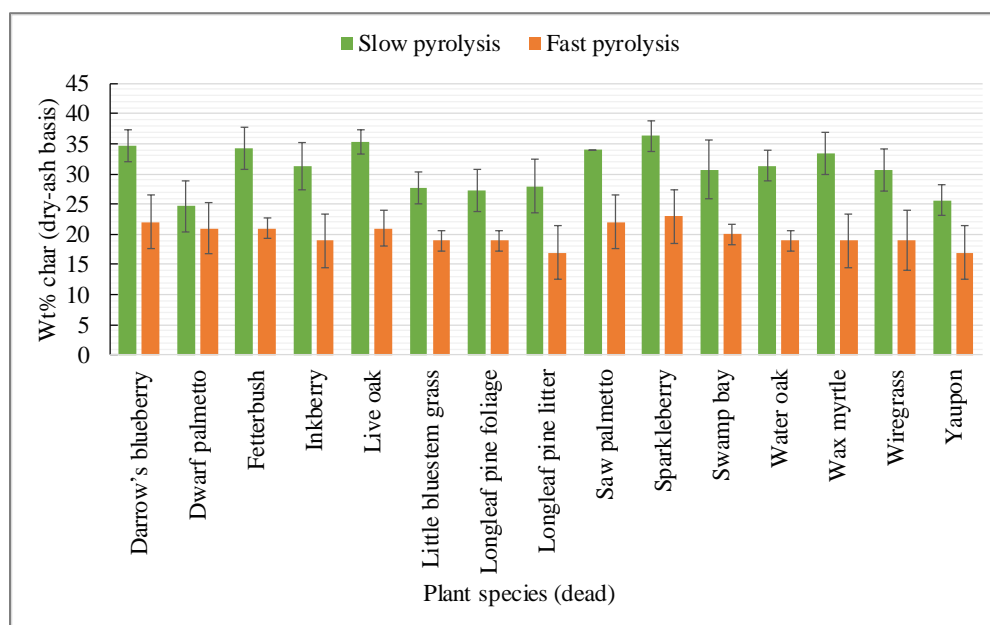


Figure F-3. Char yield of dead plant species on a dry, ash free (daf) basis

The analysis of yield of light gases; CO, CO₂, CH₄, and H₂, during the slow and fast pyrolysis experiments of dead plant species are shown in Figure F-4 (CO yield data), Figure F-5

(CO₂ yield data), Figure F-6 (CH₄ yield data), and Figure F-7 (H₂ yield data).

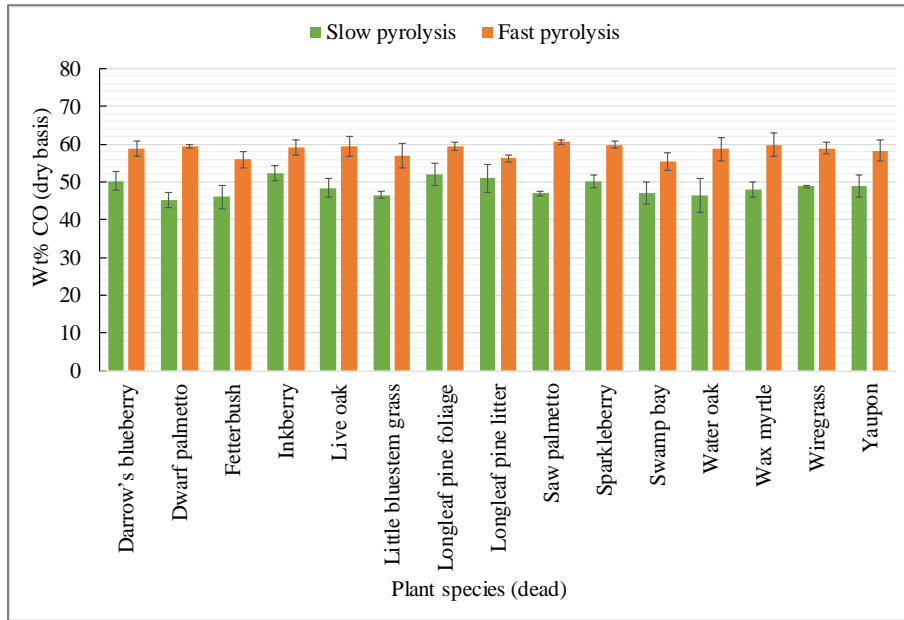


Figure F-4. The yield of CO wt% (dry basis) obtained from pyrolysis of dead plant species

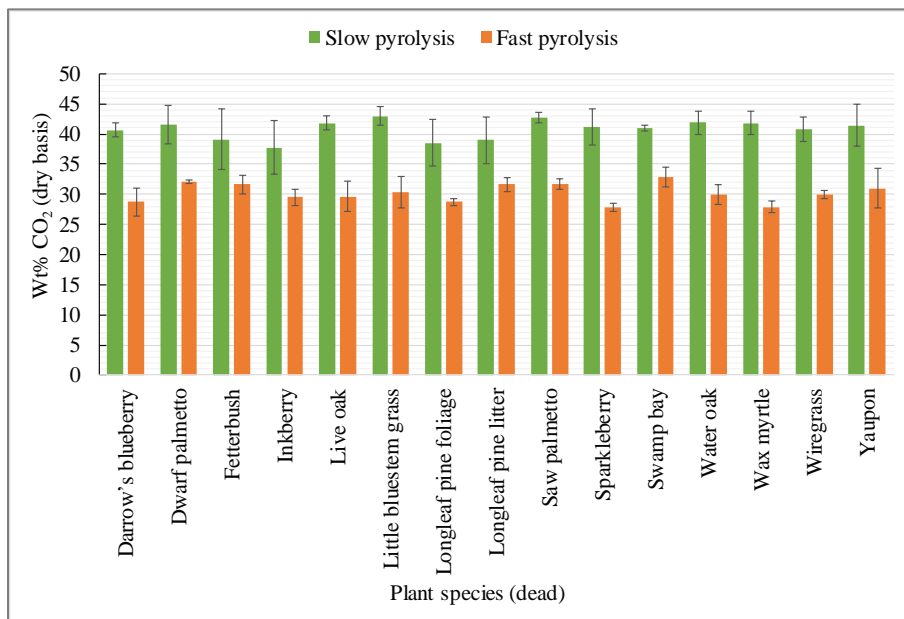


Figure F-5. The yield of CO₂ wt% (dry basis) obtained from pyrolysis of dead plant species

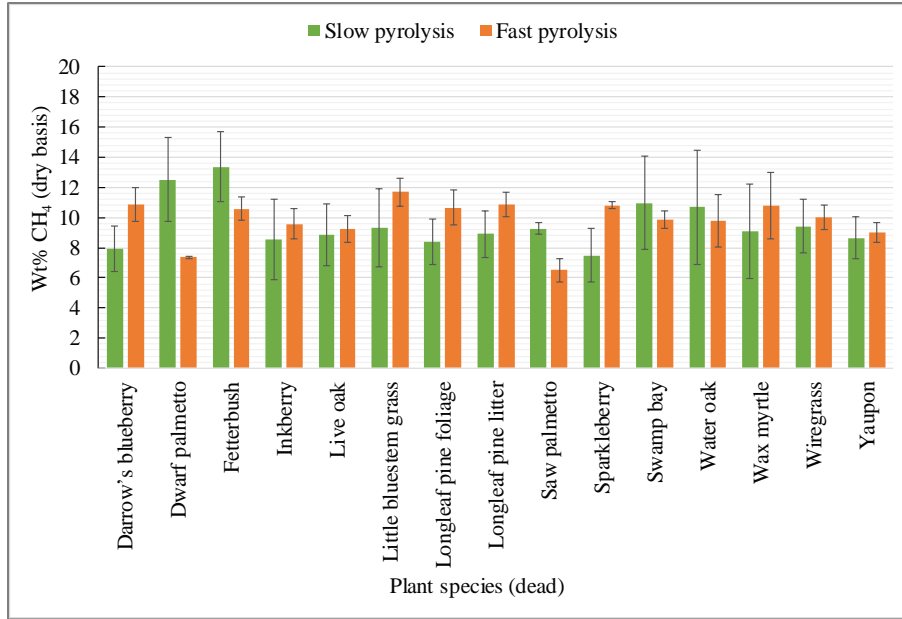


Figure F-6. The yield of CH₄ wt% (dry basis) obtained from pyrolysis of dead plant species

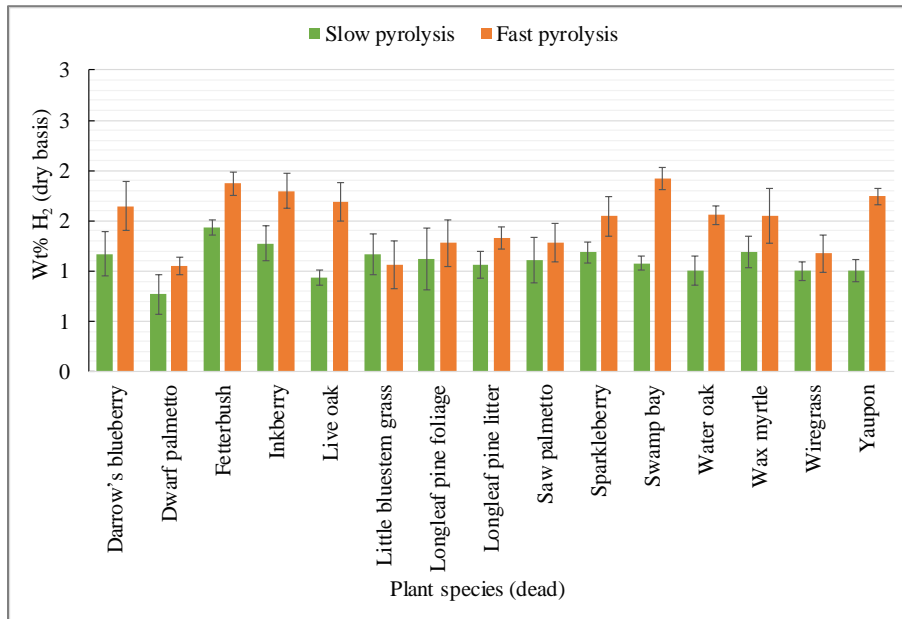


Figure F-7. The yield of H₂ wt% (dry basis) obtained from pyrolysis of dead plant species

APPENDIX G. RESULTS OF DIFFERENT HEATING MODES

The gas yield data, tar yield data, and char yield data for dead plant species during three heating modes are presented in Figure G-1, Figure G-2, and Figure G-3, respectively.

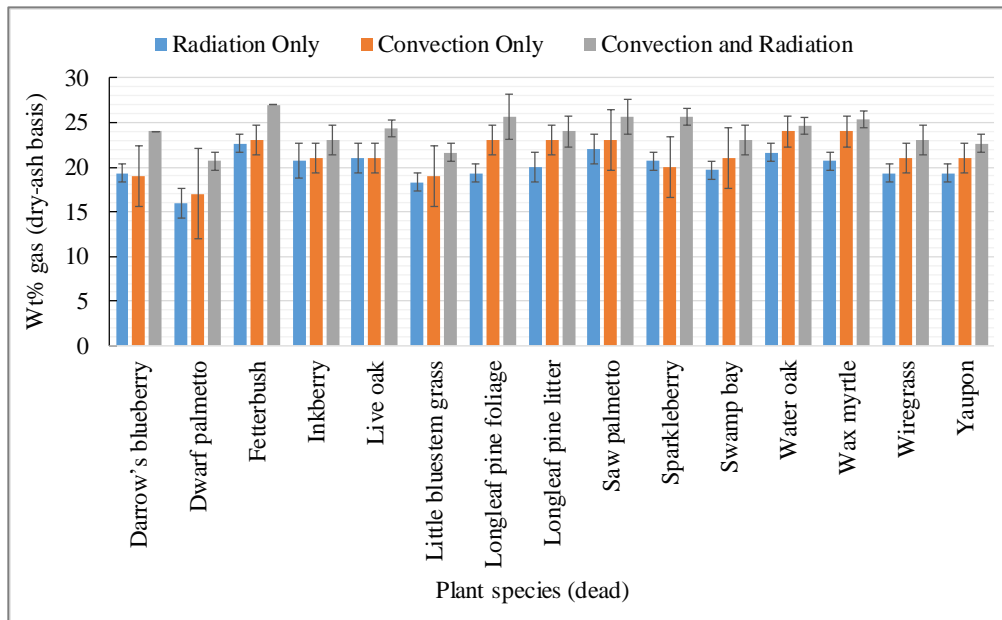


Figure G-1. Gas yield of dead plant species on a dry, ash free (daf) basis

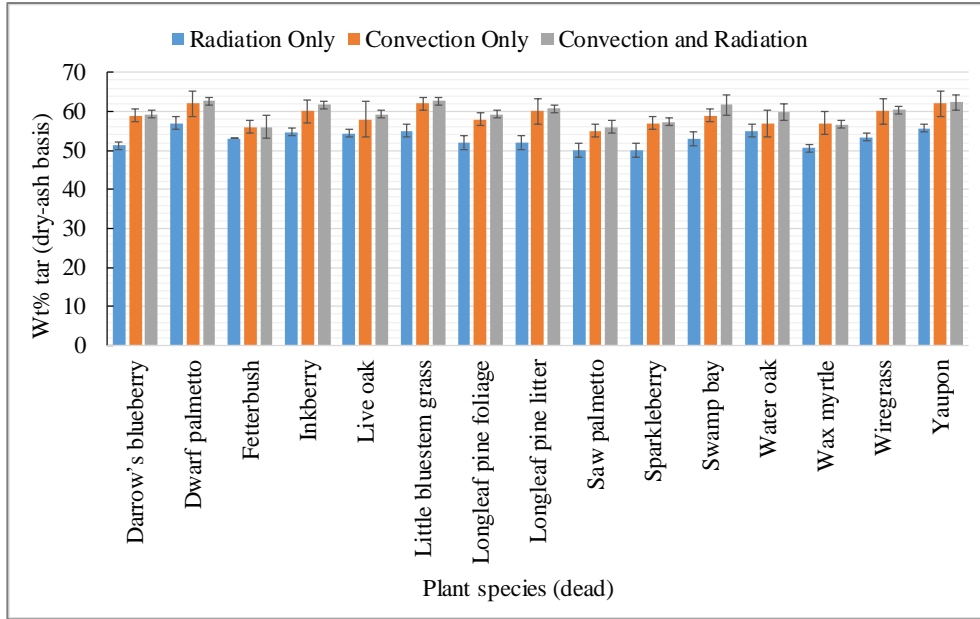


Figure G-2. Tar yield of dead plant species on a dry, ash free (daf) basis

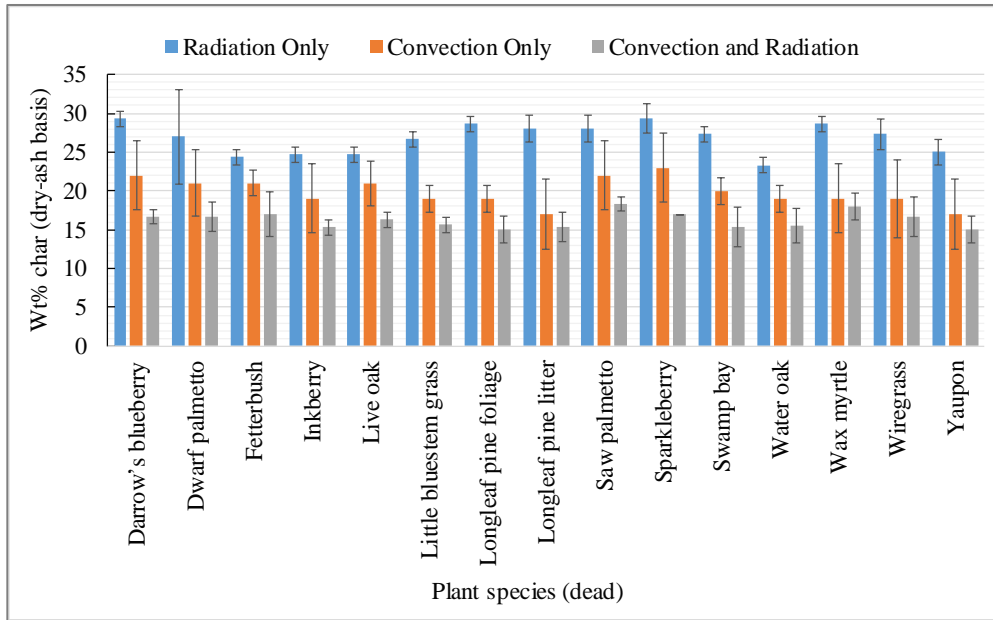


Figure G-3. Char yield of dead plant species on a dry, ash free (daf) basis

The light gas data for dead plant species are shown in Figure G-4 (CO yield data), Figure G-5 (CO₂ yield data), Figure G-6 (CH₄ yield data), and Figure G-7 (H₂ yield data).

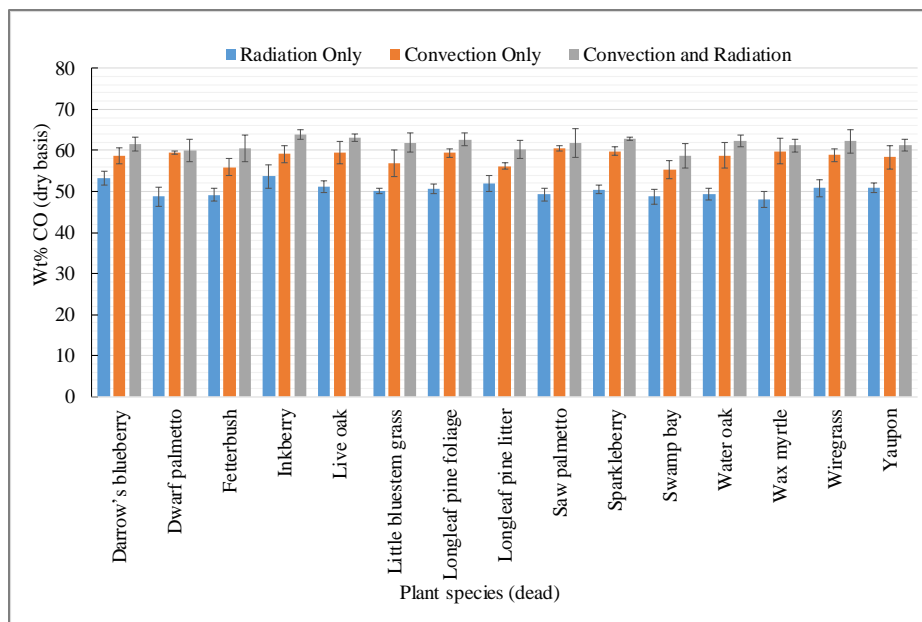


Figure G-4. The yield of CO wt% (dry basis) from pyrolysis of dead plant species

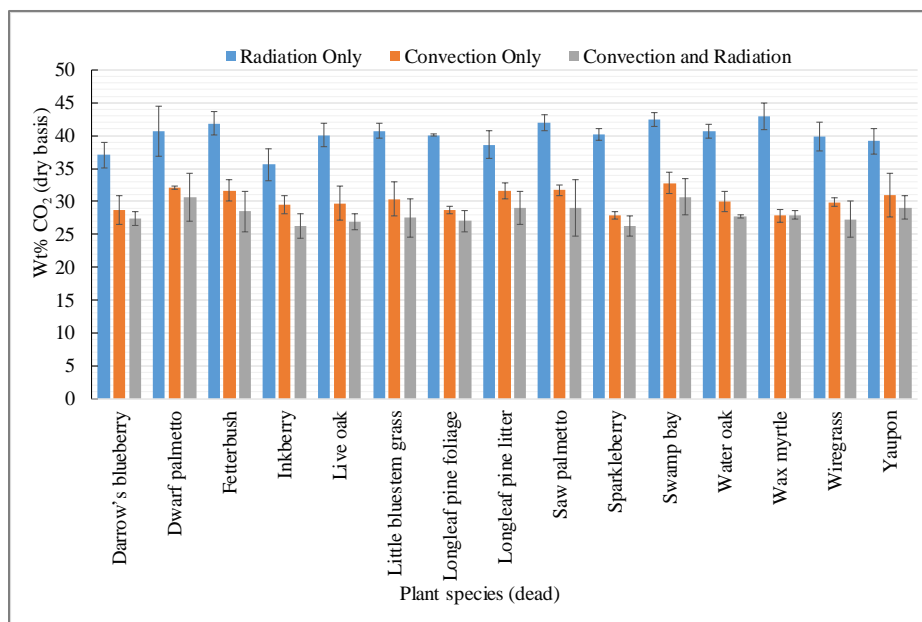


Figure G-5. The yield of CO₂ wt% (dry basis) from pyrolysis of dead plant species

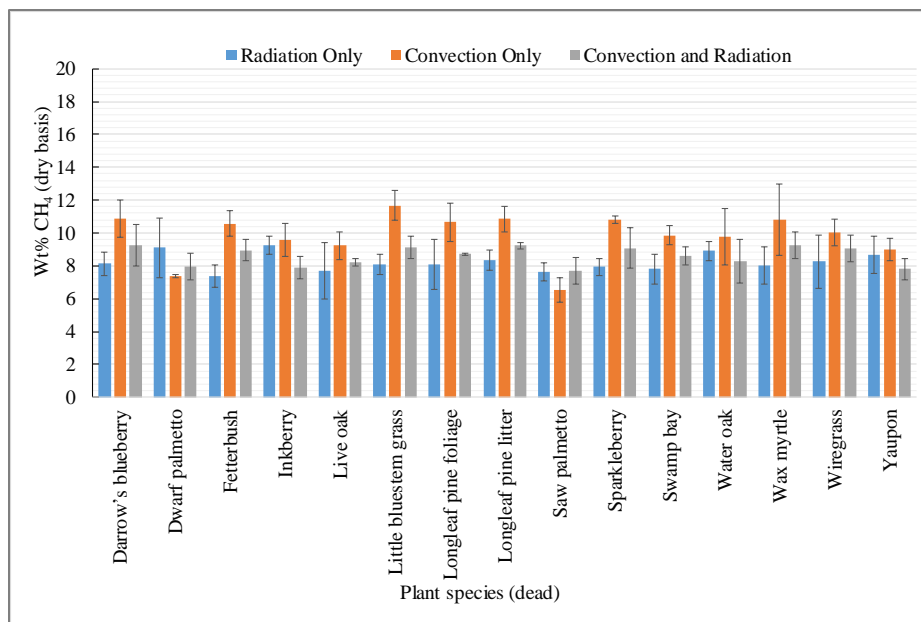


Figure G-6. The yield of CH₄ wt% (dry basis) from pyrolysis of dead plant species

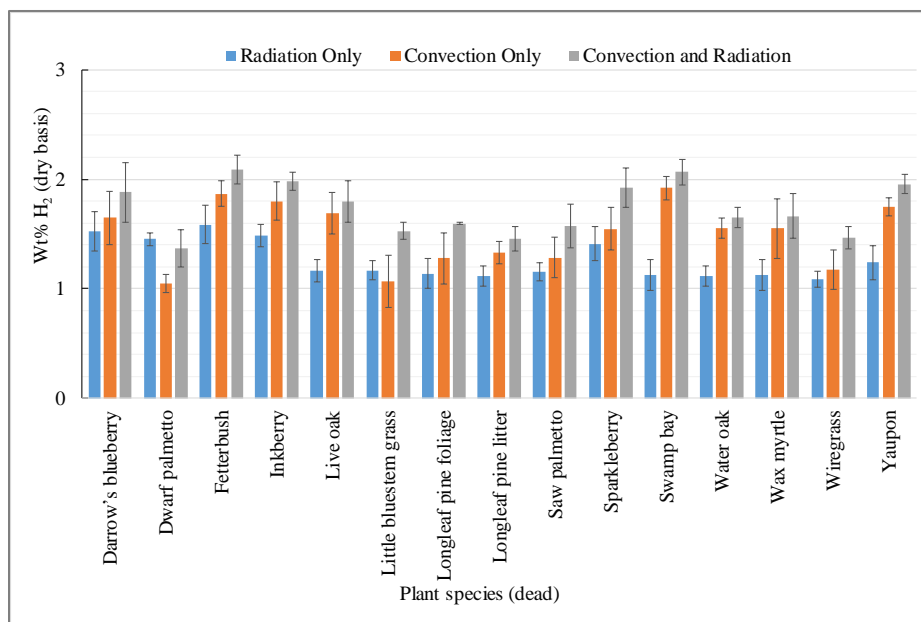
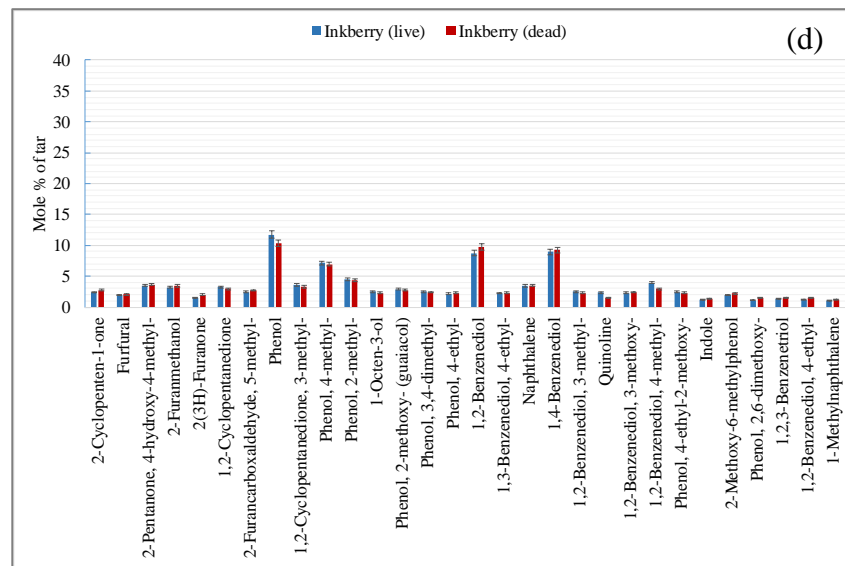
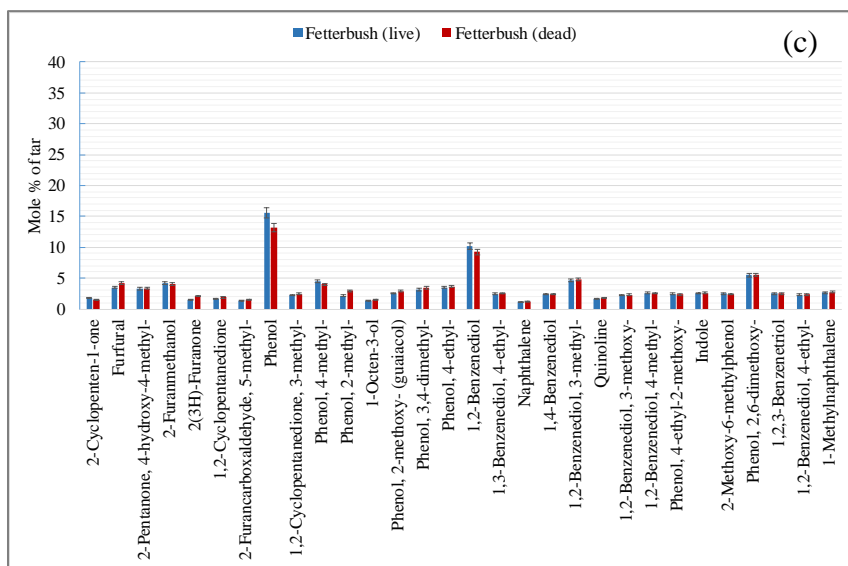
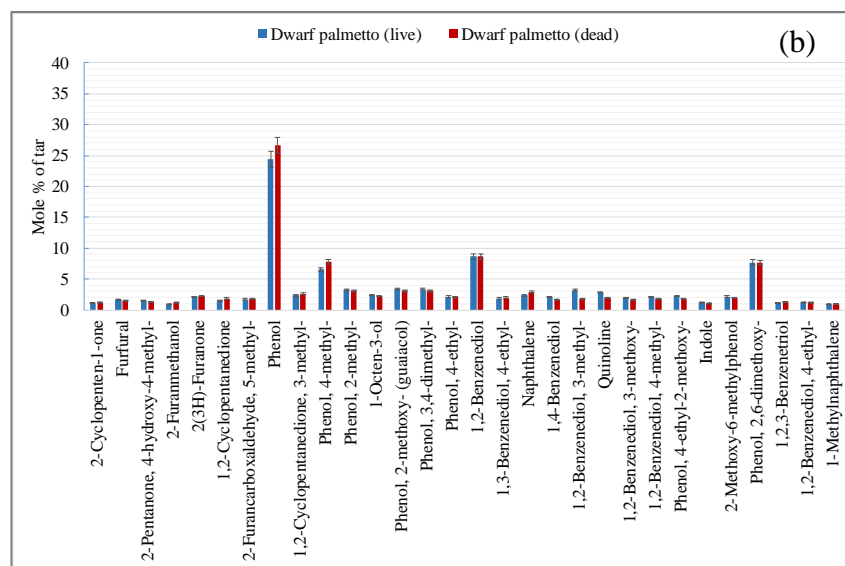
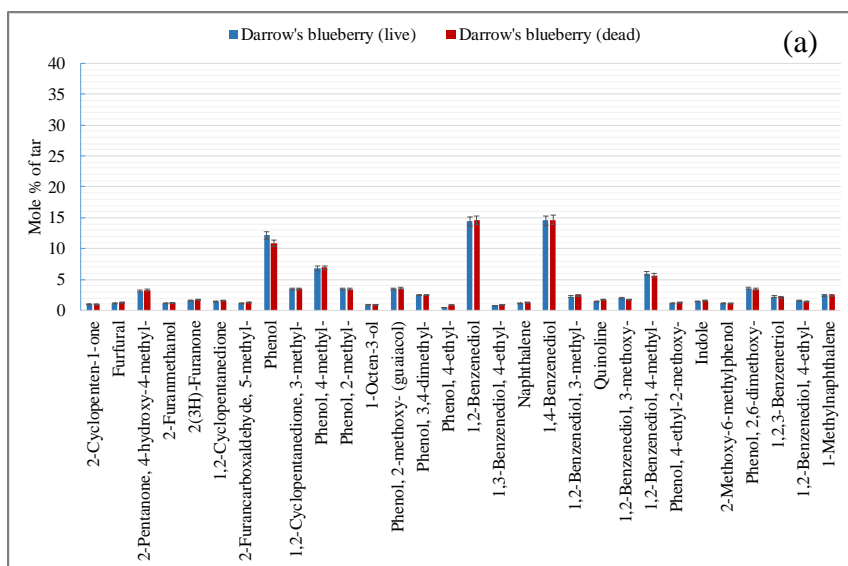
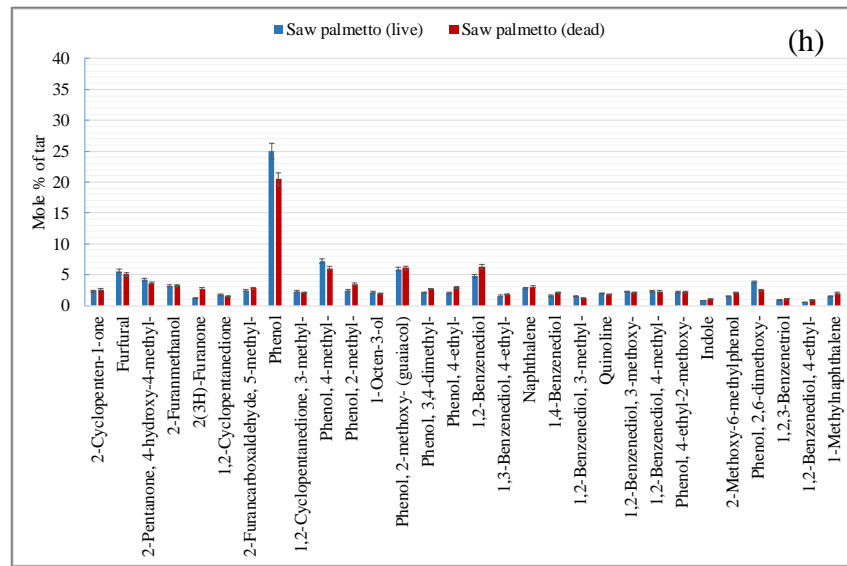
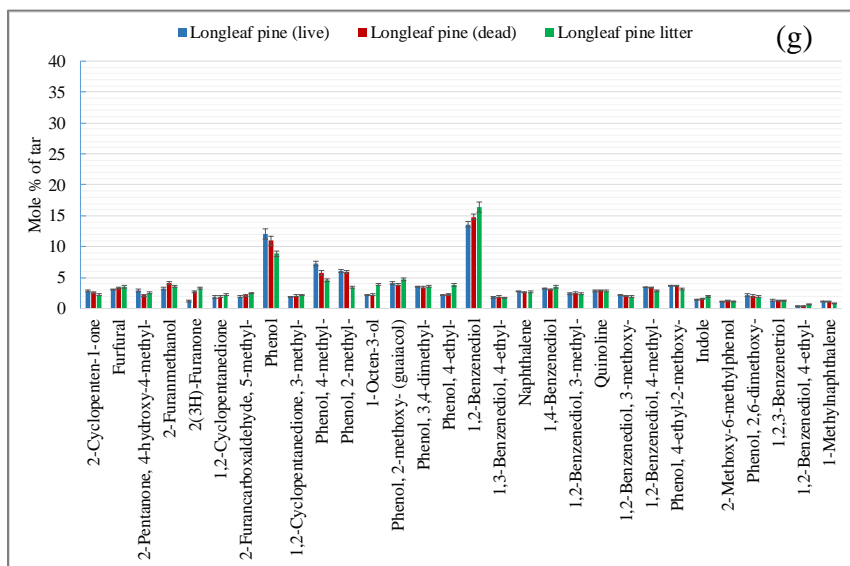
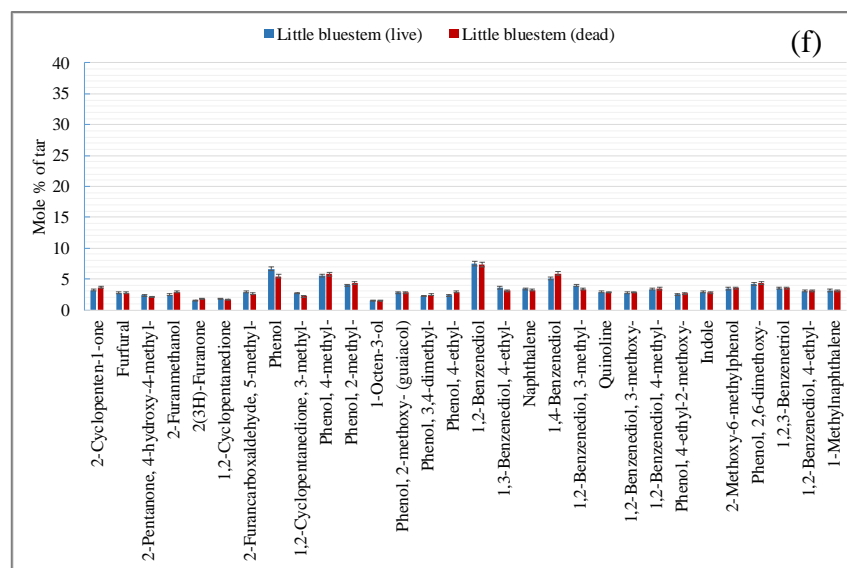
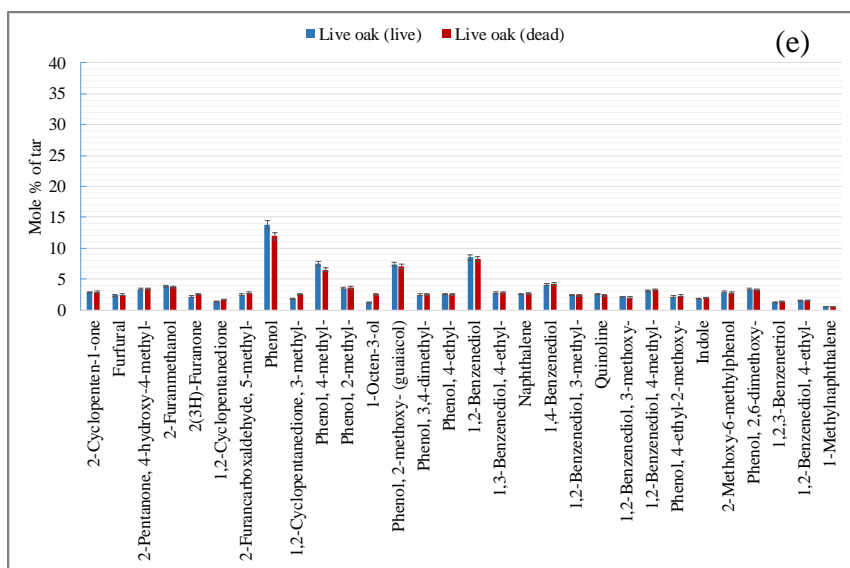
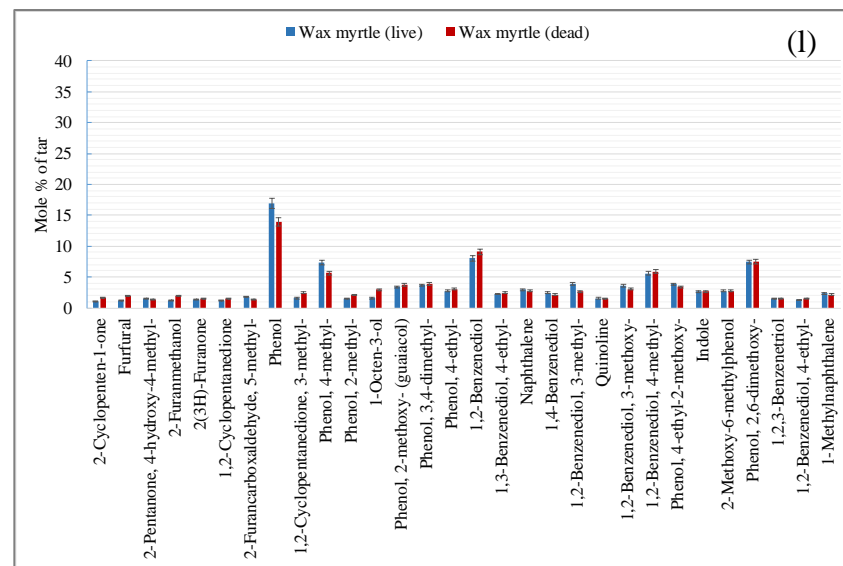
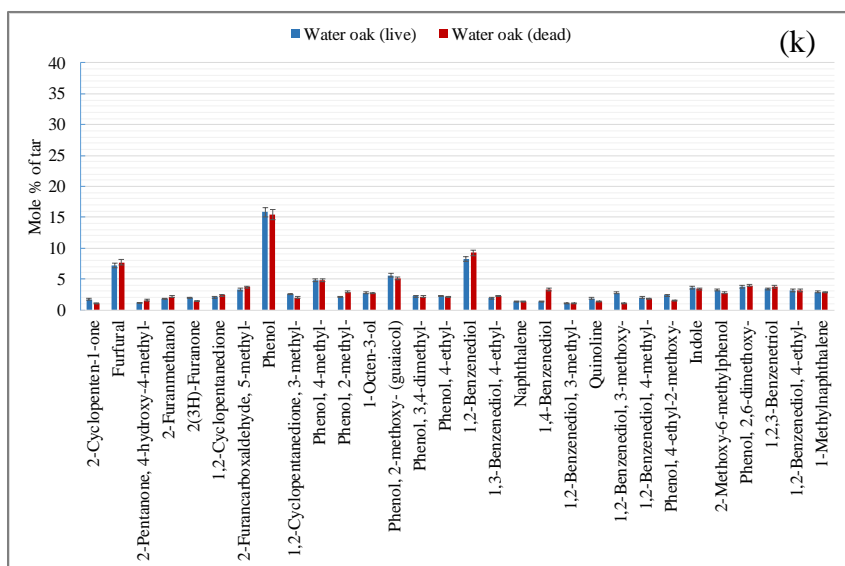
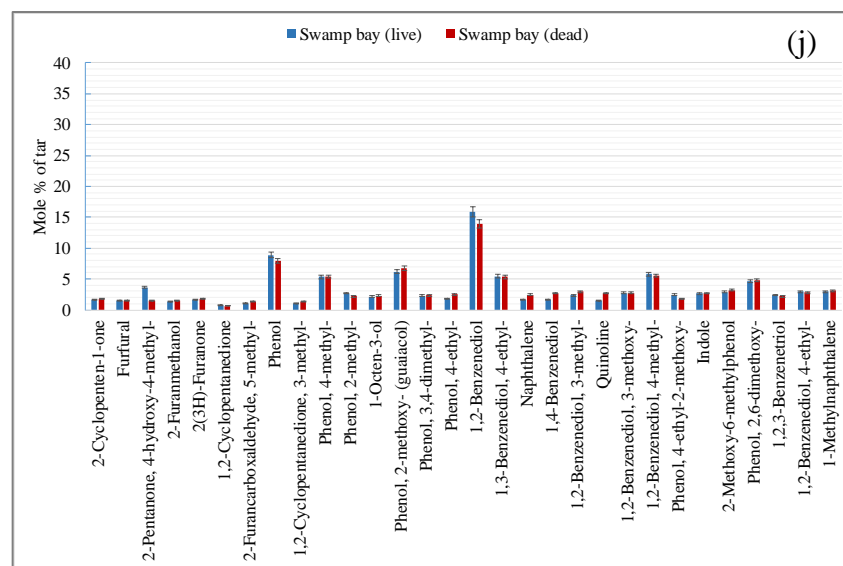
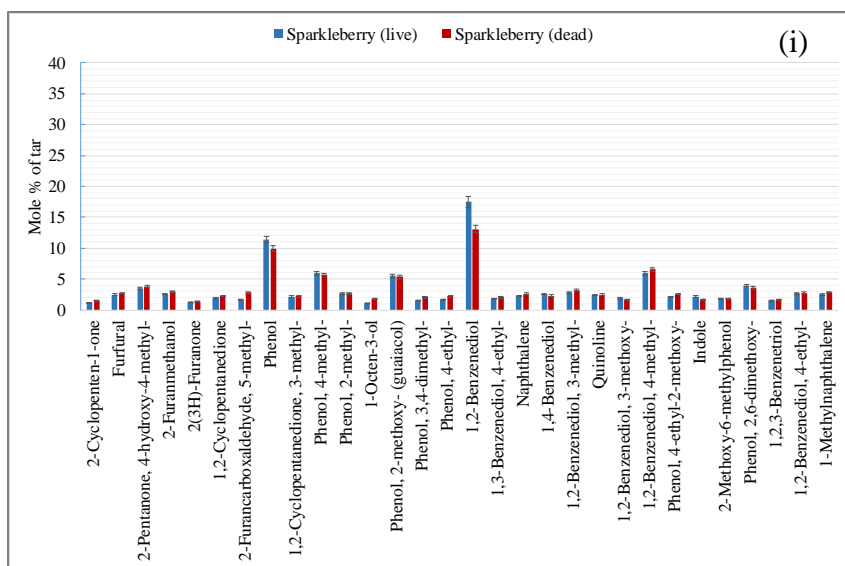


Figure G-7. The yield of H₂ wt% (dry basis) from pyrolysis of dead plant species







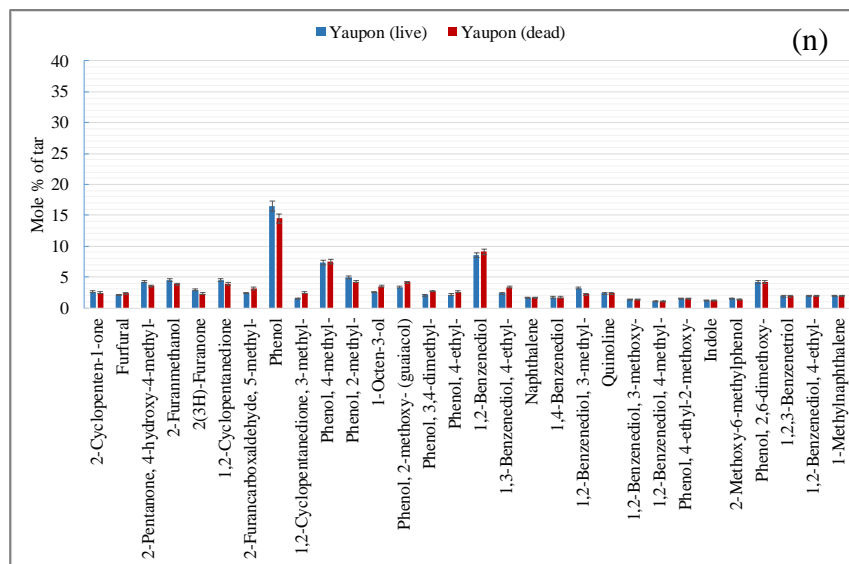
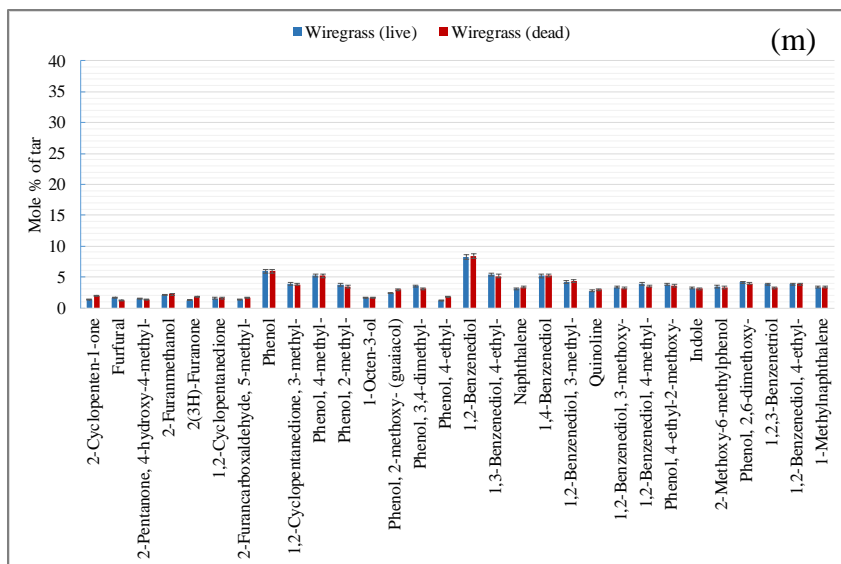
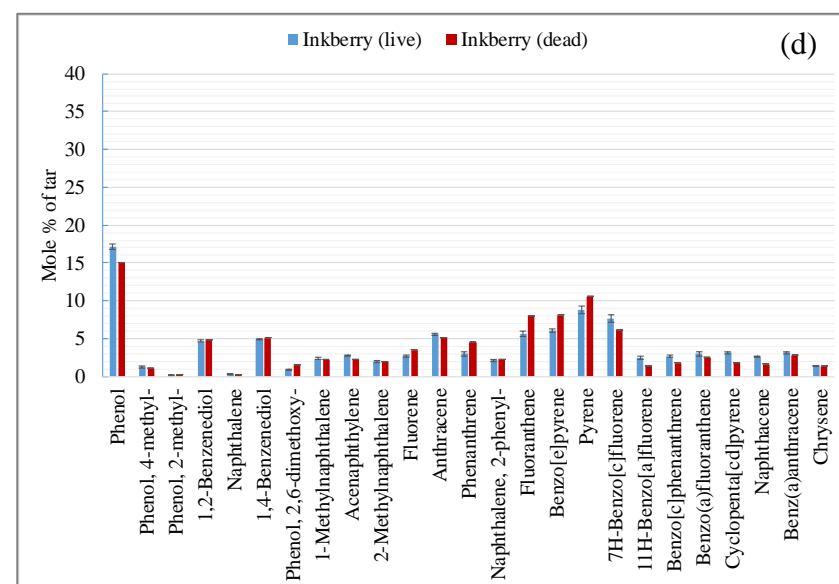
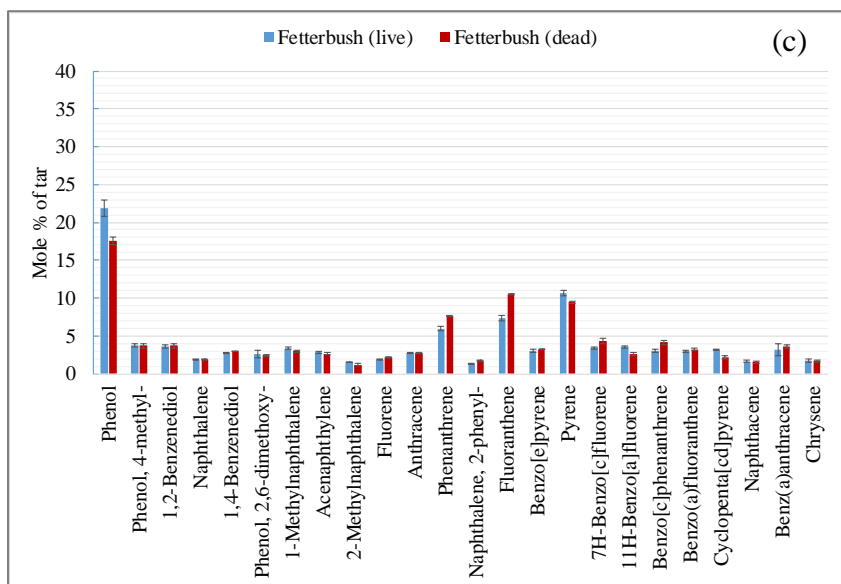
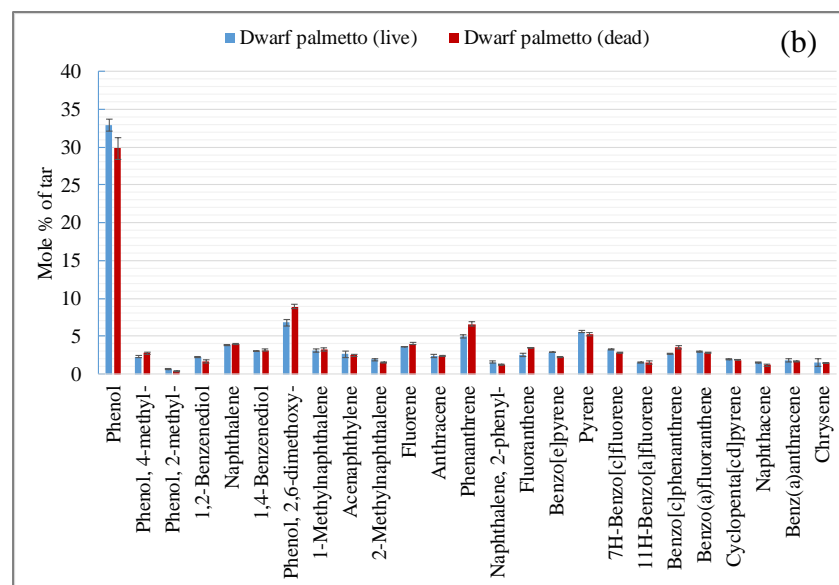
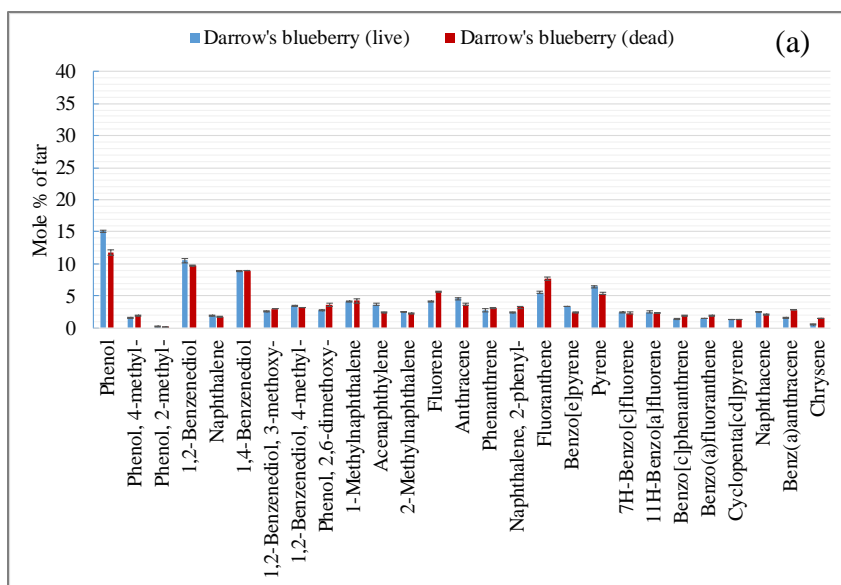
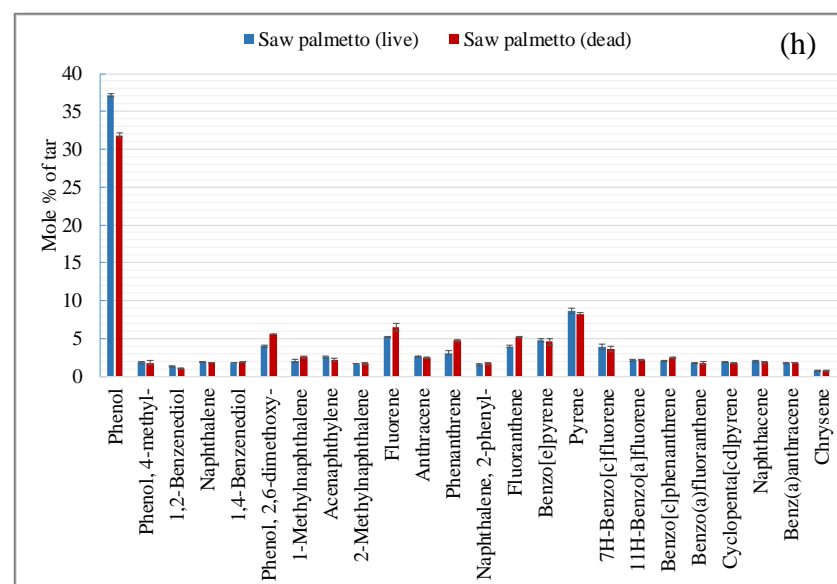
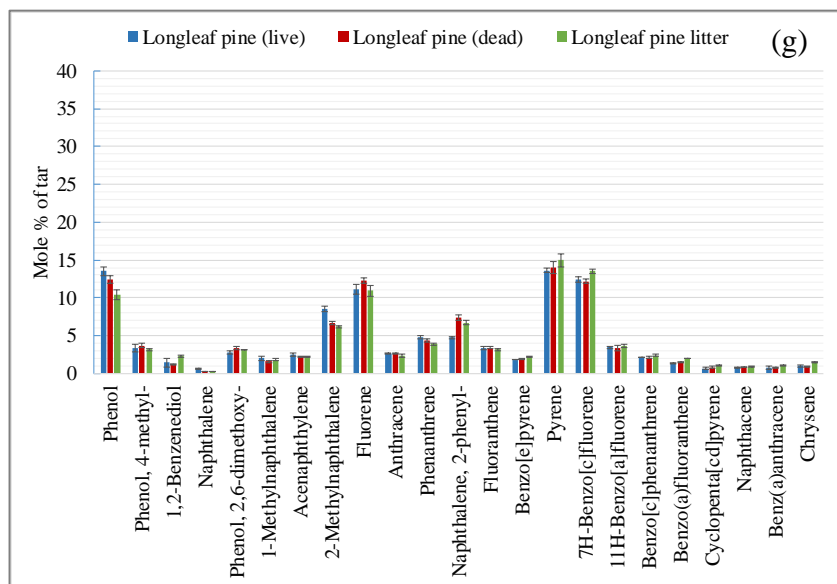
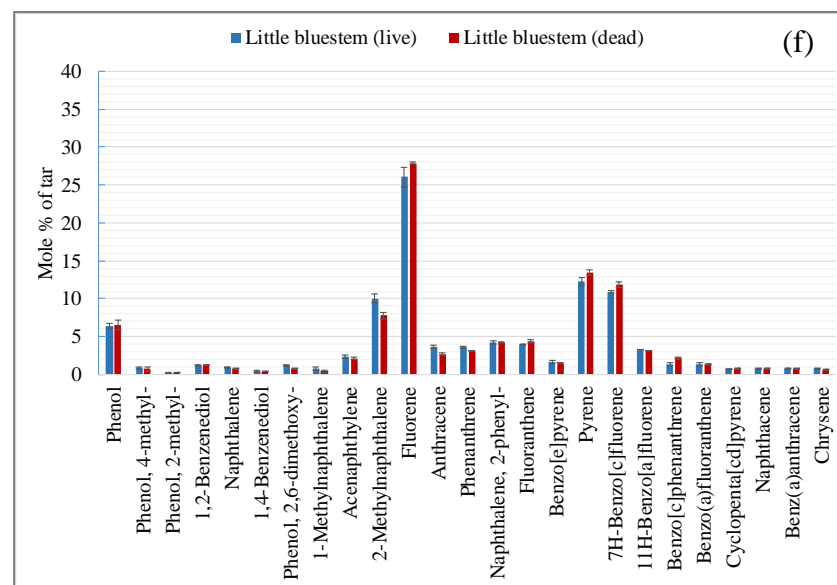
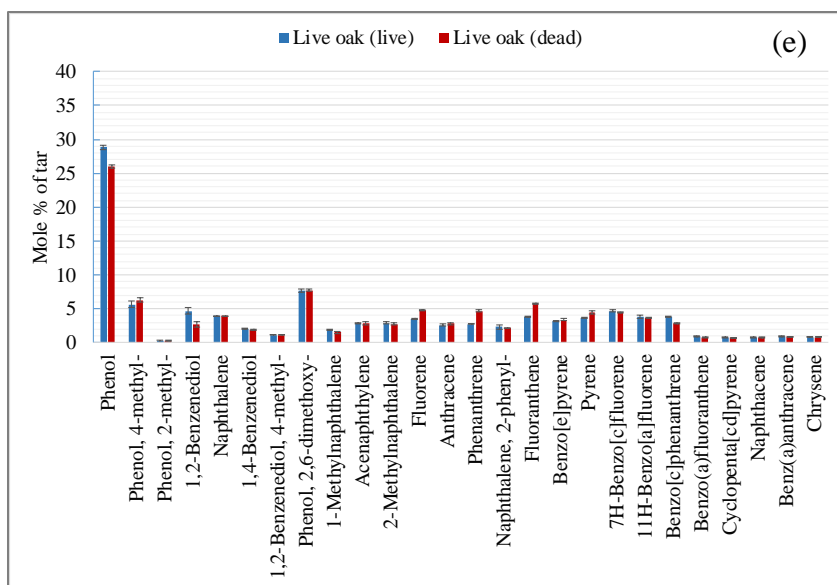
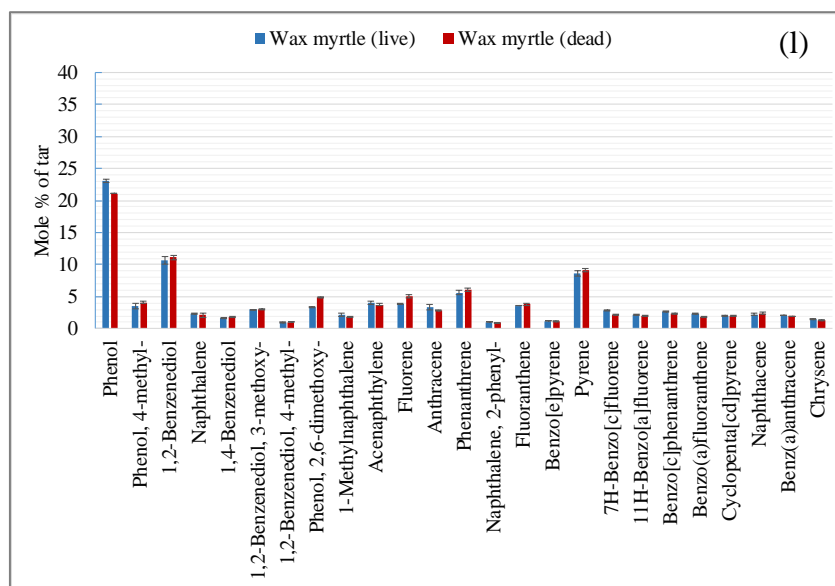
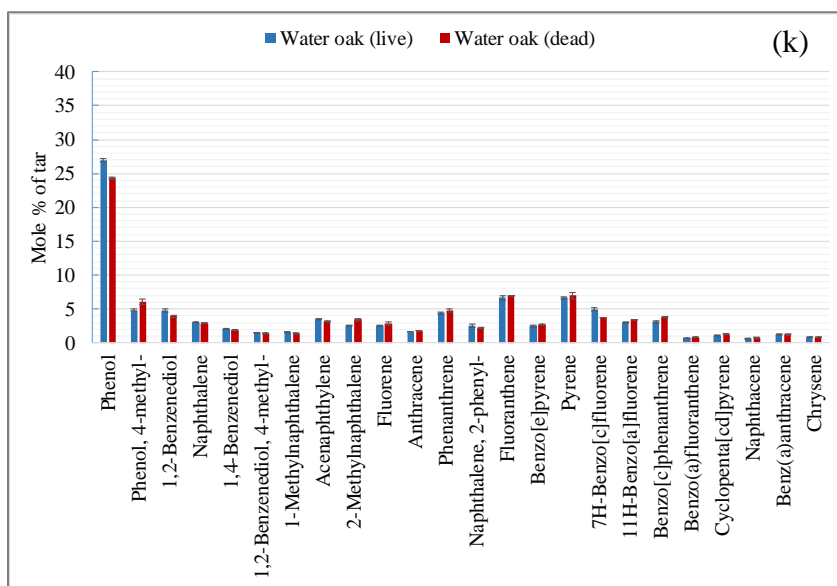
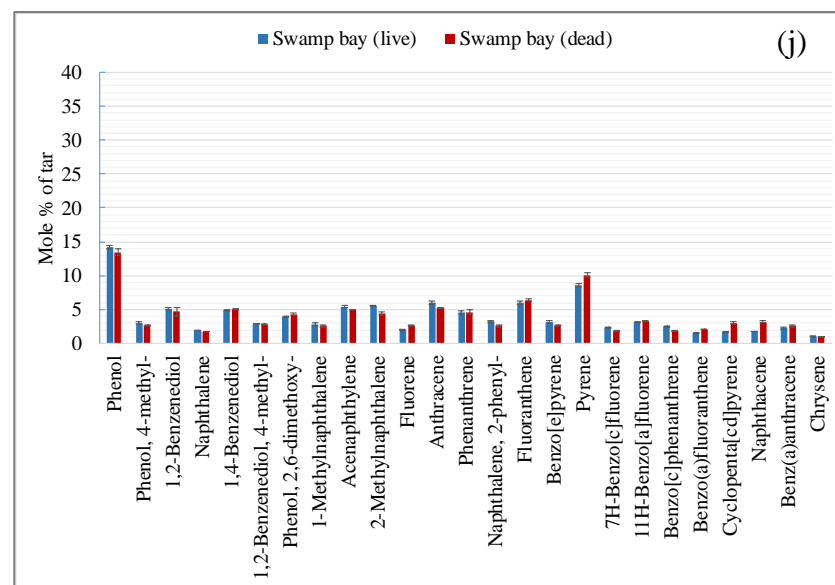
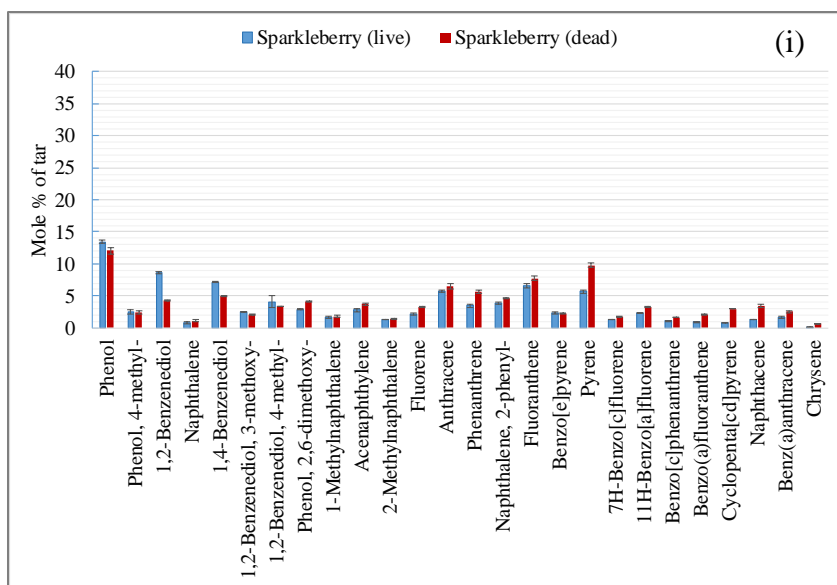


Figure G-8. Analysis of tar compounds for radiation-only experiments







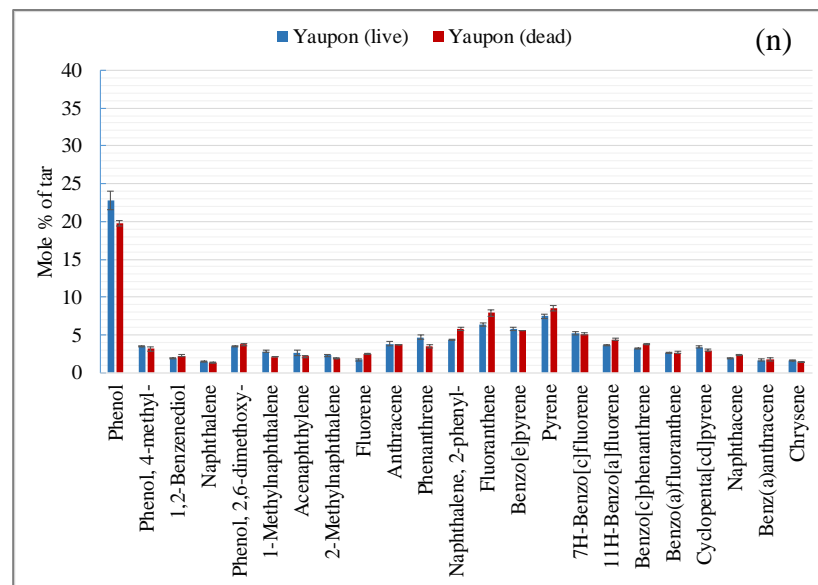
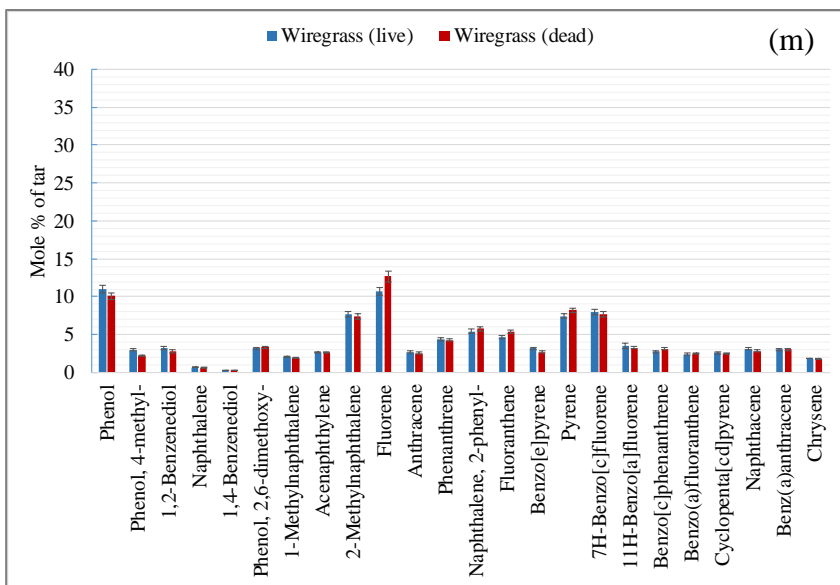


Figure G-9. Analysis of tar compounds for the combined convection and radiation experiments